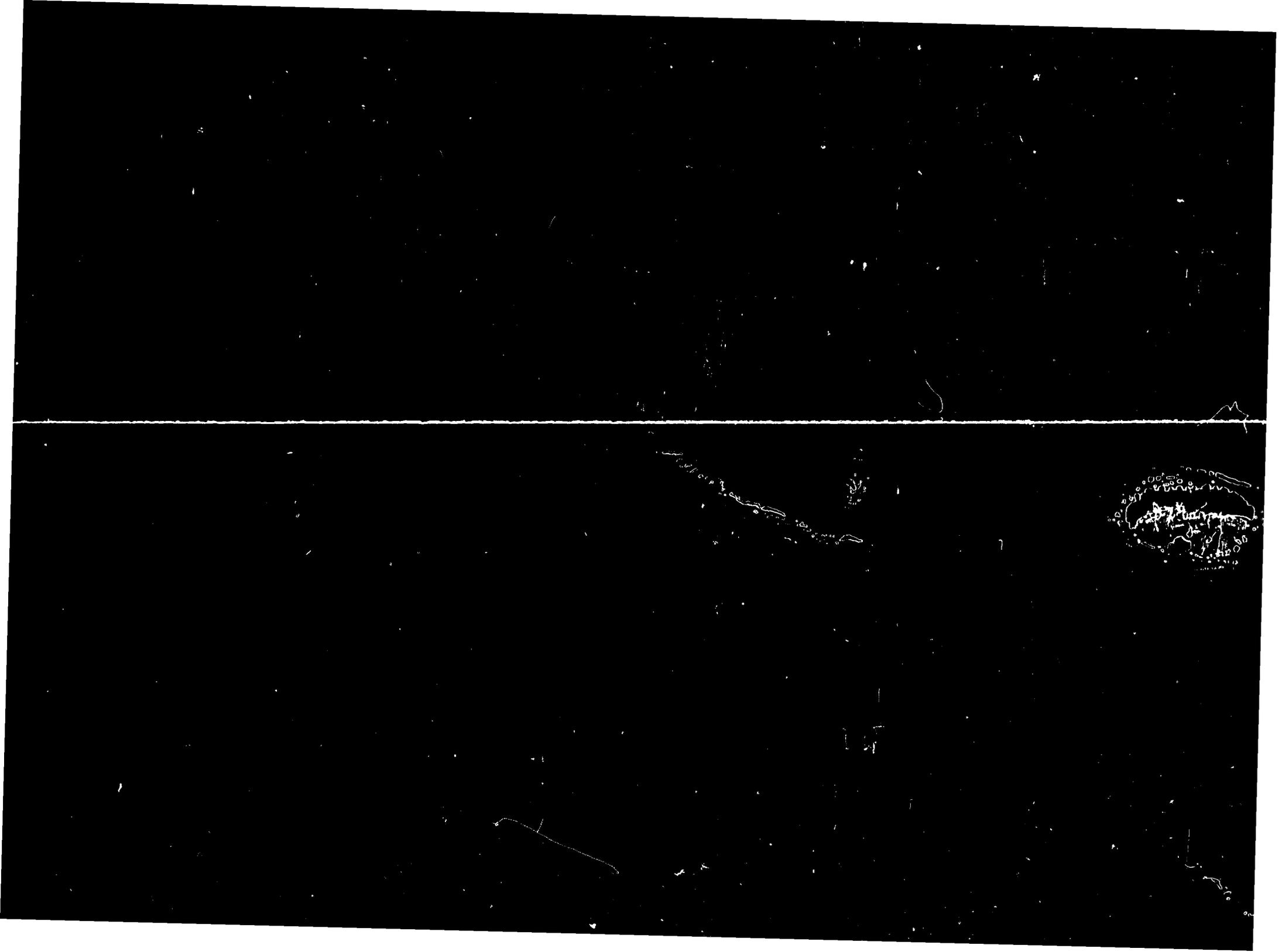




65

355

This dissertation has been 65–8355
microfilmed exactly as received

HASHEMI, Hadi Tafreshi, 1933–
HEAT CONDUCTION WITH CHANGE OF PHASE.

The University of Oklahoma, Ph.D., 1965
Engineering, chemical

University Microfilms, Inc., Ann Arbor, Michigan

THE UNIVERSITY OF OKLAHOMA

GRADUATE COLLEGE

HEAT CONDUCTION WITH CHANGE OF PHASE

A DISSERTATION

SUBMITTED TO THE GRADUATE FACULTY

in partial fulfillment of the requirements for the

degree of

DOCTOR OF PHILOSOPHY

BY

HADI TAFRESHI HASHEMI

Norman, Oklahoma

1965

HEAT CONDUCTION WITH CHANGE OF PHASE

APPROVED BY

C. M. Sliepcevich

C. N. Cooper

Charles Colvert

James [illegible]

C. W. Bert

DISSERTATION COMMITTEE

Please Note:
This is not original
copy. Small and in-
distinct type on several
pages. Filmed as received.
University Microfilms, Inc.

ABSTRACT

The object of this study was to find the practical methods for solving the two-dimensional temperature distribution in a locally isotropic medium whose state changes with temperature. A proposed numerical method and an experimental analog method appeared to offer greatest promise in solving such problems. To formulate the numerical solution it was first assumed that the changes of state of the medium under consideration occur in a finite temperature interval. By making this assumption the problem was reduced to solving a quasi-linear, parabolic differential equation subjected to some natural initial and boundary conditions. A generalized method was devised to study the behavior of the various numerical techniques for solving such problems. As a result, a predictor-corrector, alternating-direction, implicit (ADI) method was proposed. It was shown that the proposed solution is unconditionally stable and second order correct. The important features of this solution are: a) except for a nonlinear coefficient which should be evaluated by a suitable predictor formula, the proposed solution is similar to the solution of any ordinary heat conduction problem by an ADI method, b) the problems of composite media and more than one transition temperature can be solved without undue effort.

The proposed numerical method was employed to obtain the temperature field in a semi-infinite plane external to a square. The plane is initially at its transition temperature and its boundary is at a fixed, uniform temperature. This problem was solved for a uniform mesh spacing and a non-uniform mesh spacing. The computer results indicated a high degree of accuracy and uniform stability of the numerical solution. Prior to analyzing this example problem, several one-dimensional problems were solved numerically to study the influence of the transition temperature range and other parameters on the accuracy of the proposed numerical method.

The experimental analog method was based on the analogy between heat transfer by pure conduction accompanied by a single change of state and mass transfer by pure chemical diffusion in a partially miscible, liquid-liquid, binary system. Several diffusion cells were tested under a variety of conditions to establish the feasibility of such an analog method. It was found that a pure two-dimensional diffusion field can only be produced in a suitable porous medium. The binary system of phenol and water was used in all the diffusion experiments. Using Whatman filter paper Number 52 as the porous medium, several successful experiments were carried out with the two-dimensional diffusion cell. One shape of the moving interface obtained corresponded to a semi-infinite region external to a rectangle whose boundary was maintained at a fixed, uniform concentration. Another shape was a wedge-like region external to a circle.

As a result of these studies, it was concluded that the diffusion analog can be used for obtaining the shape of the moving interface at which a change of state occurs as well as the heat flux at the boundary of geometrically-complex, composite, two-dimensional regions. As an alternative to the diffusion analog, the numerical solution developed herein is recommended where a high degree of accuracy and a knowledge of the temperature distribution are desired, particularly for regions having simple geometries.

ACKNOWLEDGEMENT

The author wishes to express his sincere appreciation and gratitude to Dr. C. M. Sliepcevich for guidance and encouragement during the initiation and progress of this study. The suggestions and advice of the other members of the Doctoral Committee are also much appreciated.

Many individuals have made significant contributions to this study. Without their assistance an investigation of this scope could not have been accomplished successfully. In particular, the author is indebted to his colleagues Dr. M. Mirshamsi and Mr. R. Welker for undertaking most of the preliminary experimental work, and to Mr. N. Hardwicke for his active participation and valuable assistance throughout this work. Appreciation is also due to Mr. H. Bradbury of Computer Systems Engineering Inc. for his valuable help in developing the computer program, in performing machine computations as well as in setting up the photographic equipment.

The superb engineering and craftsmanship of the experimental apparatus constructed by Mr. F. McGinnis of Research Instrument Company and Messrs J. C. Hood and J. Edmundson of the Physics Department Instrument Shop are gratefully acknowledged.

Mrs. A. Blancett provided valuable help in preparing this manuscript and the staff of the Oklahoma University Research Institute, especially the draftsman Mr. G. Droescher, the reproduction supervisor Mr. H. Bruemmer and the photographer Mr. J. Williamson, undertook the reproduction.

The author is grateful to Continental Oil Company and Celanese Corporation for providing financial assistance during his course of graduate study. Additional support for this research was provided by the National Science Foundation grant GP-1502 and by the Chemical Research and Development Laboratories, Edgewood Arsenal, through Contract DA-18-035-AMC-116(A).

Finally, I wish to thank my wife for her understanding and inspiration as well as for preparing and editing this manuscript.

TABLE OF CONTENTS

Page

LIST OF TABLES x

LIST OF ILLUSTRATIONS xiii

Chapter

I. INTRODUCTION. 1

Mathematical Presentation of the Problem
Previous Theoretical Work

II. THE ANALOGY BETWEEN DIFFUSION MASS TRANSFER WITH CHANGE OF PHASE AND CONDUCTION HEAT TRANSFER WITH CHANGE OF PHASE 31

The Criteria for the Analogy
Diffusion in Porous Media
The Properties of an Ideal Partially Miscible Binary Liquid System Suitable for the Analog Studies
The Search for a Suitable Binary Mixture

III. A PROPOSED NUMERICAL SOLUTION 47

A Semi-Discrete Approximation
A Fundamental Discrete Solution
Matrix Approximation for $\exp(-r_j Q_j)$
Variants of the Alternating Direction Implicit Methods

IV. THE PROCEDURE AND RESULTS OF SOLVING THE HEAT CONDUCTION PROBLEM ON A HIGH SPEED DIGITAL COMPUTER. 95

The Solution Algorithm
The One-Dimensional Case
The Two-Dimensional Case

V. EXPERIMENTAL APPARATUS AND PROCEDURE. 150

The Apparatus for Testing the One-Dimensional Diffusion Cell

Chapter Page

The Apparatus for the Two-Dimensional Cell

VI. EXPERIMENTAL RESULTS 186

Determination of the Average Diffusion Coefficient from the Experimental Data of the One-Dimensional Cells
The Experimental Results of the One-Dimensional Cells
The Experimental Results of the Two-Dimensional Cells
Final Results
Closing Remarks

VII. CONCLUSIONS AND RECOMMENDATIONS FOR FUTURE WORK. 243

NOMENCLATURE. 252

BIBLIOGRAPHY. 270

APPENDICES

A. GLOSSARY AND A SUMMARY OF SOME KNOWN THEORETICAL RESULTS 277

B. COMPUTER RESULTS FOR THE ONE-DIMENSIONAL CASE. 283

C. THE COMPUTER PROGRAM FOR SOLVING THE TWO-DIMENSIONAL PROBLEMS AND THE TABULATED SOLUTION OF THE TWO-DIMENSIONAL EXAMPLE PROBLEMS. 289

D. EXPERIMENTAL DATA AND ANALYSIS OF THE ONE-DIMENSIONAL CELL. 339

E. EXPERIMENTAL DATA AND ANALYSIS OF THE TWO-DIMENSIONAL CELL. 348

F. PHYSICAL PROPERTIES OF PHENOL-WATER SYSTEM. . . 362

LIST OF TABLES

Table		Page
1.	Variations of ξ with the Latent Heat Parameter $C_s(T_F - T_b)/(L\sqrt{\pi})$	106
2.	Effect of the Pumping Rate on Concentration of Phenol Leaving the Cell	180
3.	Effect of Temperature on the Average Diffusion Coefficient for the Phenol-Water Binary System.	195
4.	Effect of Concentration on the Average diffusivity of the Water Rich Phase at 55°C	195
5.	Average Diffusivity of the Phenol Rich Phase at 55°C.	195
6.	The Conditions and Objectives of the Preliminary Tests with Two-Dimensional Cell	203
7.	The Conditions of Tests 3.2-1 to 3.2-4	218
8.	The Parameters Employed in the Computer Solution of the One-Dimensional Case	284
9.	Computed Values of the Dimensionless Temperature $w(ih,\tau)$	286
10.	The Departure of the Proposed Numerical Solution from the Neumann's Solution	287
11.	The Euclidean Norm of the Departure of the Proposed Numerical Solution from the Neumann's Solution	288
12.	A Listing of the Computer Program as Specialized for Run Number 2.3	294
13.	Input Data Listing for Run Number 2.3.	302
14.	Input Data Listing for Run Number 2.1.	306

Table Page

15. Cumulative Heat Flow, Q, and $Q/\sqrt{\tau}$ for the Four Computed Runs 310

16. Numerical Solution of the Example Problem No. 1 for Various Values of τ. 311

17. Numerical Solution of the Example Problem No. 2 for Various Values of τ. 318

18. Numerical Solution of the Example Problem No. 3 for Various Values of τ. 327

19. Numerical Solution of the Example Problem No. 4 for Various Values of τ. 332

20. Computed Values of $X(x_1,\tau)$ for the Various Values of x_1 and τ 338

21. Experimental Determination of the Average Binary Diffusion Coefficient for Phenol-Water System in Water-Rich Phase at 30°C 340

22. Experimental Determination of the Average Binary Diffusion Coefficient for Phenol-Water System in Water-Rich Phase at 30°C 341

23. Experimental Determination of the Average Binary Diffusion Coefficient for Phenol-Water System in Water-Rich Phase at 40°C 342

24. Experimental Determination of the Average Binary Diffusion Coefficient for Phenol-Water System in Water-Rich Phase at 40°C 343

25. Experimental Determination of the Average Binary Diffusion Coefficient for Phenol-Water System in Water-Rich Phase at 50°C 344

26. Experimental Determination of the Average Binary Diffusion Coefficient for Phenol-Water System in Water-Rich Phase at 50°C 345

27. Experimental Determination of the Effect of Concentration on Average Binary Diffusion of Water-Rich Phase at 55°C. 346

28. Experimental Determination of the Average Binary Diffusion Coefficient for Phenol-Water System in Phenol-Rich Phase. 347

Table Page

29. Evaluation of the Effective Binary Diffusion Coefficient of Phenol-Water System in Whatman Filter Paper Number 52. 350

30. Experimental Results of Test Number 3.2-1. 352

31. Experimental Results of Test Number 3.2-2. 353

32. Experimental Results of Test Number 3.2-3. 355

33. Experimental Results of Test Number 3.2-4. 357

34. The Experimental Values of $\bar{X}(x_1,\tau)$ for x_1=-0.2, 0.0, +0.2 and $x_1 = X(x_1,\tau)$ for all the Tests with a Unit Square Boundary. 358

35. Position of Interface in the Wedge Region External to a Unit Circle. 360

36. Experimental Results of Test Number 3.2-6. 361

37. Solubility Temperature 363

38. Density of Water-Phenol System at Saturation Point. 363

39. Density of Water-Phenol System 364

40. Viscosity of Phenol-Water Solution Relative to Water 365

41. Refractory Indices of Acqueous Solutions of Phenol 366

42. Diffusion of Phenol into Water 367

43. Freezing Points of Phenol-Water Solutions. 367

LIST OF ILLUSTRATIONS

Figure		Page
1.	A Typical Two-Dimensional Closed Region.	15
2.	The Variation of the Dimensionless Parameters φ, φ_1 and φ_2 with the Dimensionless Temperature u .	15
3.	An Arbitrary Region R Divided into Two Sub-Regions by a Continuous Interface Γ_s	35
4.	The Desired Consolute Curve for a Suitable Binary Liquid System	38
5.	The Change of Solubility with Temperatures for Various Substances	45
6.	The Unit Square Region $\mathcal{R}$ Divided into a Union of Rectangular Mesh Regions	54
7.	Variation of $\|\mathbf{e}\|$ with $\chi(\tau)$ for Various Values of δ_x and δ_F.	111
8.	Variation of $\|\tilde{\mathbf{e}}\|$ with $\chi(\tau)$ showing that for all Cases $\|\tilde{\mathbf{e}}\|$ is Uniformly Decreasing for $\chi(\tau)>0.15$	112
9.	Computed Temperature in a Semi-Infinite Slab . . .	115
10.	Variation of $u(x_1,\tau) - w(x_1,\tau)$ with τ at Mesh Points Falling between the Boundary and the Interface.	117
11.	Variation of $u(x_1,\tau) - w(x_1,\tau)$ with τ at Mesh Points Falling between the Boundary and the Interface.	118
12.	Variation of $u(x_1,\tau) - w(x_1,\tau)$ with τ at Mesh Points Falling between the Boundary and the Interface.	119
13.	Computed Values of $w(x',\tau)$ versus $x_1/\sqrt{4\tau}$	121

Figure Page

14. The Semi-Infinite Plane Region, $\bar{R}$", and its Boundary Conditions. 123

15. The Shape of the Semi-Infinite Region $\bar{R}$" of Figure 14 in the x - y Plane and its Corresponding Boundary Conditions. 123

16. The Arrangement of the Mesh Regions in the Corner Region of the Example Problems 125

17. Variations of $\|E\|$ with $\sqrt{\tau}$ for Runs 2.3 and 2.4 . . 132

18. Computed Cumulative Heat Transferred to the Region $\bar{R}$" (Figure 14) versus $\sqrt{\tau}$. 134

19. Departure of Cumulative Heat Transferred to the Region $\bar{R}$" (Figure 14) from that of a Semi-Infinite Slab of Unit Width 136

20. Isotherms and Computer Results for Example No. 1 . 137

21. Isotherms and Computer Results for Example No. 1 . 138

22. Isotherms and Computer Results for Example No. 1 . 139

23. Isotherms and Computer Results for Example No. 1 . 140

24. Isotherms and Computer Results for Example No. 1 . 141

25. Isotherms and Computer Results for Example No. 3 . 142

26. Isotherms and Computer Results for Example No. 3 . 143

27. Isotherms and Computer Results for Example No. 3.. 144

28. Isotherms and Computer Results for Example No. 3 . 145

29. Isotherms and Computer Results for Example No. 3 . 146

30. Growth of the Interface $X(x_1,\tau)$ with $\sqrt{\tau}$ for Various Values of x_1. Position of Interface is taken Arbitrarily at the 0.0159 Isotherm 148

31. The Quartz Capillaries and the Capillary Holder. . 152

32. The Improved One-Dimensional Cell. 152

33. The Final One-Dimensional Diffusion Cell--(a) The Components of the Cell, (b) The Assembled Cell . 156

Figure Page

34. A Cross-Section of the Final One-Dimensional Cell Showing the Improvement in the Inlet and Outlet Tubing Connections. 157

35. The Set-up of the One-Dimensional Cell for Filling with Phenol Saturated Water Solution . . 159

36. A View of the Experimental Apparatus showing the Air Bath, the Micropump, the Cathetometer and the Temperature Controller 161

37. The Plane Region Simulated by the Preliminary Cell 162

38. A Sketch of the Components of the Preliminary Cell 163

39. The Glass Disks Used in the Intermediate Cell. . . 166

40. The Plane Region Simulated by the Intermediate Cell 166

41. (a) An Exploded View of the Intermediate Cell, (b) the Cross-section of the Cell, and (c) the Cross-Section of the Flow Distributor. 168

42. The Arrangement of the Flow Distributor. 172

43. The Components of the Flow Distributor for an Arbitrary Geometry of the Exposed Boundary . . . 172

44. One of the Pair of Glass Disks Used in the Final Cell 175

45. A Photograph of the Final Cell 175

46. A Schematic View of the Air Bath and the Camera. . 177

47. A Front View of the Interior of the Air Bath . . . 178

48. Schematic Diagram of the Air Bath Showing the Relative Positions of the Fans, the Temperature Probe and the Heaters. 178

49. The Micropump. 182

50. A Photograph of the Microprojector 184

51. The Optical Arrangement of the Microprojector. . . 184

52. Micrometer Cross Slide Stage 184

Figure Page

53. The Concentration Profile in a Capillary Initially Containing a Solution of Uniform Concentration, $C_\infty \geq C_S^{II}$ whose Surface x = 0.0 is kept at $C_B < C_S^I$ 189

54. Growth of the Water Rich Phase in a Capillary Tube Initially Containing a Saturated Phenol Rich Phase Whose Surface x = 0.0 is kept at C_B = 0.0 Moles Phenol per Liter. 194

55. Determination of the Average Diffusivity of Phenol Rich Phase at 55°C from the Data on X(t) 195

56. Effect of Concentration Driving Force, $(C_S^I - C_B)$ on the Average Diffusivity of Water. 197

57. (a) Formation of a Meniscus Immediately after Immersion of the Capillary in the Water Bath; (b) Disturbance of the Concentration Field Inside a Capillary caused by the Liquid passing over its Surface.. 199

58. A Plane Region External to a Square Divided into Symmetric Sub-Regions. 201

59. Photographs of the Two-Dimensional Cell showing the Formation and Progress of the Interface between Water and an Emulsion of Phenol in Water 207

60. Photographs of the Two-Dimensional Cell: (a) Immediately after Filling with an Emulsion of Phenol in Water and (b) after 18:00 Hours. . . . 210

61. Photographs of the Two-Dimensional Cell Initially Filled with an Emulsion of Phenol in Water, Using a Nylon Cloth to Stop Aggregation of the Suspended Phase with and without a Filter Paper Belt 212

62. Test 3.1-1. The Progress of the Interface Formed by Passing Pure Water over the Rectangular Boundary of the Filter Paper Sheet Initially Saturated with a Phenol Rich Solution. 214

63. Test 3.1-2. The Interface Formed in Whatman Filter Paper after Passing Water over the Rectangular Boundary for Seven Minutes. The Filter Paper was Initially Saturated with a Phenol Rich Phase. 216

Figure Page

64. Test 3.2-2. Photographs of the Diffusion Cell Showing the Progress of the Interface Developed Around a 1 cm x 1 cm Square Boundary.. . . . 219

65. Test 3.2-3. Photographs of the Diffusion Cell Showing the Progress of the Interface Developed Around a Square Boundary 220

66. Test 3.2-1. Photographs of the Diffusion Cell Showing the Progress of the Interface Developed Around a 1 cm x 1 cm Square Boundary 221

67. Test 3.2-1. Growth of an Interface Around a Corner 223

68. Test 3.2-2. Growth of an Interface Around a Corner 224

69. Test 3.2-3. Growth of an Interface Around a Corner 225

70. Test 3.2-4. Growth of an Interface Around a Corner 226

71. Variation of X(-1,t) with $\sqrt{t/a^2}$ showing the One-Dimensional Nature of the Concentration Field at $x_1 = -1.0$ 228

72. Comparison of the Experimental Position of the Interface at $x_1 = -1.0$ and Neumann's Solution ($X = 2\xi\sqrt{\tau}$).

73. A Comparison of the Computed (Example Problem 1) Values of $X(x_1,\tau)$ and those of the Diffusion Cell Analog. 232

74. A Wedge-Like Region Similar to a Symmetric Section of a Ring of Circles in a large Plane Region 235

75. Test 3.2-5. Progress of the Interface Around a Circular Boundary Situated in a Wedge-Shaped Region and Initially Containing Pure Water. 236

76. Growth of the Interface Around a Circle Situated in a Wedge-Like Region 237

Figure Page

77. Test 3.2-6. Progress of the Interface Around a Circular Boundary Situated in a Wedge-Shaped Region (Top Photo) and Initially Containing Phenol Saturated Water Phase at 55°C . . 239

78. Radial Position of the Interface in a Region External to a Unit Circle for $\mu = 0.0$ and $\xi = 0.551$ (Test 3.2-6) 240

HEAT CONDUCTION WITH CHANGE OF PHASE

CHAPTER I

INTRODUCTION

The problems of transient heat conduction with change of phase have been encountered in studying many physical phenomena, such as ablation cooling, combustion of solids, solidification of large bodies of various melts, formation of permafrost and underground storage of cryogenic liquids.

The one-dimensional melting or solidification problems have been treated extensively in current literature: Boley (7,8), Dewey, Schlesinger and Sashkin (19), Rose (64), Altman (1), Sunderland and Grosh (69), Trench (74), Douglas and Gallie (26), Douglas (20,25), Longwell (56), Hamill and Bankoff (40), Ehrlich (33), Churchill and Teller (14), Churchill and Seider (15). Nevertheless, much work needs to be done to improve the accuracy of the theoretical predictions. In addition, there are many solidification and melting problems which are strongly two-dimensional and can not be approximated by a one-dimensional analysis. Practical solution of this type of melting and solidification problem is the object of this investigation. An immediate application

of the results is in the prediction of heat leak and thickness of the frozen ground around in-ground storage of a cryogenic liquid during the initial cool-down, as well as in the periodic filling and emptying of the storage cavity and several similar problems.

The problem will be treated from two essentially different approaches. Each has its own inherited limitations, but when combined they may produce a complete solution for many two-dimensional heat conduction problems with latent heat. The first approach consists of the development of a suitable implicit numerical procedure which is then used to solve the problem, in a limited number of cases, with the aid of a high speed digital computer. The second approach is the development of an analog by which the two-dimensional temperature field in an object with latent heat is simulated by a geometrically-similar, concentration field produced by chemical diffusion in a partially miscible liquid-liquid binary system.

It will be demonstrated that this analog method is a powerful tool in studying the movement of the solid-liquid interface and heat transfer on the exposed boundary, when the object under consideration is geometrically complex although it suffers mildly from its inherent experimental errors. The numerical solution can be made fairly accurate when dealing with geometrically simple objects with simple boundary conditions. When the boundary is formed of an arbitrary surface, and when the boundary temperature is controlled by conduction,

radiation and convection the numerical treatment of the problem becomes difficult and highly specialized for a particular set of conditions and parameters. However, the proposed numerical solution can be used to obtain the temperature distribution in a composite isotropic medium which changes its state at more than one temperature level, with no restrictions on the shape of the interfaces. These special features of the proposed numerical solution are believed to be unique.

The numerical solution and the analog diffusion will be developed independently because each method can be checked for consistency independent of the other. An identical example is solved by both procedures and a comparison of their results is made. However, this allegory should not be taken as a comparison between the theoretical and experimental results, but rather, as two independent, analytical techniques for solving the problem.

The numerical treatment consists of two parts. First, a relatively general theoretical analysis of the stability and the rate of convergence of the various numerical procedures suitable for solving the problem was investigated. As a result of this analysis, a modified, alternating-direction, implicit (ADI) method was chosen as the basic scheme for solving the problem. A simple, predictor-corrector method was found to be the most suitable way of evaluating the nonlinear coefficients of the parabolic differential equation which describes the temperature field in a medium with latent heat. Second, a trial set of machine computations

was carried out according to the procedure outlined in Chapter III. The results from these trials for the one-dimensional case established the upper bounds for the norm of the error vector when compared to the analytical solution for the one-dimensional case. The latter also provided a basis for judging the errors in the numerical solution of the two-dimensional case.

Many complex two-dimensional, steady state heat conduction (without change of state) problems have been studied by measuring the temperature profile in a scaled model. For transient, two-dimensional heat conduction problems of a large object, especially when a change of state is involved, such as solidification, measurement of temperature in a scaled model has the following drawbacks:

1. To devise a two-dimensional, <u>transient</u>, experimental model, a three-dimensional object must be used. To achieve symmetry along one of the axes, it would be necessary to insulate the corresponding faces perfectly. However, during the transient period, heat will diffuse in all directions so that it would be difficult, if not impossible, to obtain a true, two-dimensional transient field. Another way of stating this point is that the thermal diffusivity of a good conductor is not appreciably different from the thermal diffusivity of a good insulator.

2. For large objects the time-scaling factor involved in a laboratory-sized model is so large that simulation of simple, time dependent, boundary conditions requires an unattainable accuracy. To illustrate this point consider a cylindrical cavity 100 feet in diameter built in the ground and being filled and emptied with a cryogenic liquid every 200 hours. A laboratory sized model could perhaps be a cylinder of water-saturated soil, 2 feet in diameter, with a 2 inch hole bored in its center. For this model the scaling factor for space co-ordinates is 600 and that of time--when the model material and the actual object have identical thermal properties--is 360,000. To simulate the boundary conditions one must be able to fill and empty the cavity in the model within 2 seconds, in addition to making all the measurements.
3. To obtain the temperature profile and location of the interface many thermocouples would have to be immersed into the model. For the above example they should be situated on the two-dimensional plane of the symmetry with a spacing not larger than one twentieth of the diameter of the hole. Their positions must be known (and <u>remain unchanged</u>) to within $\pm$0.001 inch. If the temperature probes are 1/32 inch in diameter and if

they are situated along straight lines, then about one third of the space is occupied by the thermocouples. The presence of the thermocouples produces an appreciable change in the temperature distribution which would have existed in their absence.

Because of these difficulties it is profitable to search for a suitable analog method for simulating the temperature field under consideration. The conduction of heat in an isotropic medium is governed by Fourier's law*,

$$q = - K(T) \frac{\partial T}{\partial n} = - \frac{K(T)}{\rho c(T)} \frac{\partial E}{\partial n} \qquad (a)$$

where q is the heat flux in the direction of n due to the temperature gradient, $\partial T/\partial n$ (or energy gradient $\partial E/\partial n$) and $\rho c(T) = \partial E/\partial T$. The accumulation of energy due to pure conduction is,

$$\nabla \mathbf{q} = \frac{\partial E}{\partial t} = \rho c(T) \frac{\partial T}{\partial t} \qquad (b)$$

where t is time and where bold-faced symbols represent (and hereafter) vector quantities.

Now, if in a continuous and isotropic object a certain flux $\mathbf{j}$ can be developed by a certain potential V such that,

$$\mathbf{j} = - \alpha' (V) \nabla V \qquad (a')$$

$$\nabla \mathbf{j} = \frac{\partial V}{\partial t} \qquad (b')$$

---

*E is the heat content of a unit volume of the system

and

$$\alpha'(V) \Big/ \left(\frac{K(T)}{\rho c(T)}\right) = \text{const.} \qquad (c)$$

then in geometrically similar objects the potential V and the energy E are analogous, provided that the boundary conditions in both cases can be made mathematically identical. For example, the flux of mass by pure diffusion in an incompressible liquid binary system j_A is given by Fick's second law of diffusion: .

$$j_A = - D_{AB}(C_A) \nabla C_A$$

where C_A is concentration of A in moles per unit volume. The accumulation of the species A is then,

$$\nabla j_A = \frac{\partial C_A}{\partial t} \quad .$$

Therefore, the concentration distribution due to the binary diffusion is analogous to the energy distribution (not temperature distribution) due to pure conduction. By a suitable choice of the liquid binary system one can also satisfy the condition (c). For example, at the melting point of a solid $K/\rho c$ is discontinuous, and there is an energy gap ΔE between the solid and liquid which are in contact with each other. The same can be said for a partially miscible, liquid-liquid, binary system.

There are, of course, other fluxes and potentials that satisfy (a') and (b'), but for problems of heat conduction with change of state (c) is a difficult one to fulfil.

For example the flux of electrons through a conducting solid due to a gradient of electrical potential satisfies both (a') and (b'). However, it does not satisfy (c) since $\alpha'(V)$ is essentially independent of the local potential.

The analogy between diffusion and heat conduction is further discussed in Chapter II. At this point it is more appropriate to observe the following apparent advantages of a diffusion analog:

1. Contrary to the heat conduction model, molecular diffusion can be completely stopped on a well defined boundary surface. Thus, for a two-dimensional problem, the analog can consist of a thin liquid film between two flat glass plates, positioned in such a way that the space between them has a two-dimensional similarity with the object under consideration.
2. The location of the interface at any instant can be most accurately obtained by direct photography of the diffusion cell. The concentration profile can be obtained without disturbing the concentration field by a variety of proven techniques, such as interferometry.
3. Contrary to a heat conduction model, where it is very difficult to know how much heat is transferred to the test medium at the boundary and consequently impossible to simulate accurately the desired boundary conditions, concentration

and flow distribution of the liquid passing over the boundary can be very closely controlled. Thus, simulation of a variety of boundary conditions is possible in the diffusion analog.

4. The diffusion coefficient of liquid systems is about one thousand times smaller than its thermal diffusivity. Therefore, for an identical geometrical-scaling factor, the time-scaling factor is one thousand times greater than that of a heat conduction model. Thus, there is considerable latitude in selecting the most convenient size of the model with its corresponding time-scale.

Most of the above observations are true when the diffusion analog is compared to other analogs which the author can visualize. The only serious drawback of a diffusion analog is the difficult task of developing a two-dimensional concentration field which is produced by pure diffusion. Nevertheless, since the potential applications of a diffusion analog are so promising, this experimental investigation was undertaken.

The experimental work on the diffusion cell analog is discussed in Chapters V and VI. It suffices to explain here that the object of these experiments was solely to demonstrate the practicality of producing a pure two-dimensional diffusion field in various geometrical arrangements for application to melting and solidification problems.

Although all the experiments with two-dimensional diffusion in an open field were unsuccessful, it was possible to produce a pure-diffusion, concentration field in a porous medium.

To review the state of art and also to explain the basic concepts developed in the present work, it is necessary to obtain first a general formulation of the problem.

Mathematical Presentation of the Problem

Consider a connected three dimensional region, R', and its boundary surface, Γ'. Let R' contain a uniform and isotropic medium whose state and properties are only temperature dependent. Define the dimensionless temperature, u, by the relation

$$u = \int_{T_1}^{T} K(T')\, dT' \Big/ \int_{T_1}^{T_2} K(T')\, dT', \quad T_2 > T > T_1 \qquad (1.1)$$

where, T = actual temperature,

T_1 and T_2 = two unequal but otherwise arbitrary actual temperatures,

K(T) = thermal conductivity of the medium contained in R'.

Let heat be transferred in R' by pure conduction only, and no heat be generated in R' by a chemical reaction or any other phenomena. Then the dimensionless temperature, $u(\mathbf{x};\tau)$, satisfies:*

---

*See Carslaw and Jaeger (12) for derivation of (1.1). See also Boley and Weiner (9) for an excellent discussion on the coefficients α, β, and γ.

$$\nabla^2 u(\mathbf{x};\tau) = \varphi\big(u(\mathbf{x};\tau)\big)\frac{\partial}{\partial t}u(\mathbf{x};\tau),\ \mathbf{x}\in R';\ \tau > 0 \qquad (1.2a)$$

$$\alpha(\mathbf{x};\tau)\ u(\mathbf{x};\tau) + \beta(\mathbf{x};\tau)\ \frac{\partial}{\partial n}u(\mathbf{x};\tau) = \gamma(\mathbf{x};\tau),\ \mathbf{x}\in\Gamma';\ \tau>0 \qquad (1.2b)$$

$$u(\mathbf{x};0) = G(\mathbf{x}),\ \mathbf{x}\in R' \qquad (1.2c)$$

where, $\mathbf{x} = (x_1, x_2, x_3)$

x_i, $1\le i\le 3$ = a co-ordinate axis in any orthogonal curvilinear co-ordinate system chosen to describe the region, R' (dimensionless),

∇^2 = the Laplacian operator, defined by

$$\left(\prod_{i=1}^{3} g_i\right)^{-1} \sum_{\substack{i=1\\ i\neq j\neq k}}^{3}\left[\tilde{a}_i^{\,2}\frac{\partial}{\partial x_i}\left(\frac{g_i}{g_j g_k}\frac{\partial}{\partial x_i}\right)\right] \qquad (1.2d)$$

$g_i = g_i(\mathbf{x})$

$\tilde{a}_i = a_1/a_i$ for $1\le i\le 3$, a geometrical scaling factor applied to x_i

$$\varphi(u) \equiv \varphi(T) = \Big(\rho c(T_o)\ /\ K(T_o)\Big)^{-1}\Big/\Big(\rho c(T)\ /\ K(T)\Big)^{-1}$$

= dimensionless thermal diffusivity,

$c(T)$ = specific heat = $(\partial E/\partial T)_\rho$

ρ = constant density of the medium in R'

T_o = another arbitrary reference temperature

$\tau = \Big(K(T_o)\ /\ \rho c(T_o)\Big)\ t/a_1^2$ = dimensionless time.

The coefficients α, β and γ are in general dependent on u in addition to $\mathbf{x}$ and t. However, no appreciable loss of the generality is introduced by assuming that they are independent of u. $\partial u/\partial n$ refers to the <u>outward</u> pointing normal on

Γ'. When the boundary condition (1.2b) is of the natural type, which must be the case for heat conduction problems, then in general,

$$\alpha(x;\tau) \geq 0,\ \beta(x;\tau) \geq 0,\ x\epsilon\Gamma',\ \tau > 0$$
$$\alpha(x;\tau) + \beta(x;\tau) > 0,\ x\epsilon\Gamma',\ \tau > 0 \tag{1.3}$$

If the medium in R' undergoes a change of state in some temperature intervals $(T_F - \delta T_F)$ to $(T_F + \delta T_F)$ with absorption or emission of heat, then one can write

$$L + s' = \int_{T_F-\delta T_F}^{T_F+\delta T_F} c(T')\, dT' = \int_{-\delta T_F}^{\delta T_F} c(T' + T_F)\, dT',\ \delta T_F > 0 \tag{1.4}$$

where L is the latent heat of transition, and s' is the sensible heat absorbed in the transition temperature range. Substituting $\varphi(u)$ in (1.4) and setting

$$\frac{L + s'}{1 + s} = \frac{K(T_o)}{c(T_o)} \cdot \int_{T_1}^{T_2} K(T')\, dT'$$

and then

$$1 + s = \int_{-\delta'_F}^{\delta''_F} \varphi(u_F + u')\, du',\ \delta'_F,\ \delta''_F > 0 \tag{1.5}$$

where,

$$\delta'_F = \int_{o}^{\delta T_F} K(T_F - T')\, dT' \Big/ \int_{T_1}^{T_2} K(T')\, dT'$$
$$\delta''_F = \int_{o}^{\delta T_F} K(T_F + T')\, dT' \Big/ \int_{T_1}^{T_2} K(T')\, dT' \tag{1.6}$$

It is known that for pure and homogenous substances δT_F and subsequently δ'_F and δ''_F are negligibly small, but never equal to zero. Therefore, it is more realistic to set $\delta_F \neq 0$ and solve (1.1) with this restriction. For impure substances δT_F is about 3°C or more such that for $T_2 - T_1 = 100°C$. $2\delta_F = \delta'_F + \delta''_F \geq 0.02$, if $K(T_F) / K(T) \geq 2/3$, and $T_1<T<T_2$.

Regardless of how δ_F is defined, the problem is non-linear, even if one divides the region R' into sub-regions, R'_i, each containing only one homogenous phase, and assumes that $\varphi(u)$ is temperature independent in the interior of each sub-region and $\delta_F = 0$. The reason is not so obvious at first glance, because this scheme makes the differential equation (1.2a) linear, which is very desirable. On the other hand, the boundary conditions on the interface of any two adjacent, homogenous phases become nonlinear. More specifically, the temperature in the two adjacent sub-regions R'_i and R'_j are related by the conditions,

$$u^{(i)}(\mathbf{x};\tau) = u^{(j)}(\mathbf{x};\tau) = u^F_{ij}, \quad \mathbf{x}\epsilon\Gamma'_{ij}, \quad \tau > 0$$

$$\left[\frac{\partial u^{(i)}}{\partial n_{ij}}(\mathbf{x};\tau) - \frac{\partial u^{(j)}}{\partial n_{ij}}(\mathbf{x};\tau)\right] = p(\mathbf{x}).l_{ij}\frac{\partial n_{ij}}{\partial \tau}, \quad \mathbf{x}\epsilon\Gamma'_{ij}, \tau>0 \tag{1.7}$$

where the superscripts i,j designate the quantities defined in R'_i and R'_j respectively. Γ'_{ij} is the interface of the two phases i, (or region R'_i) and j, (or region R'_j). l_{ij} is the dimensionless heat of transition from the state "i" to the state "j", and u^F_{ij} is the corresponding transition

temperature. $p(\mathbf{x})$ is a weight function depending on the coordinate system. n_{ij} is a directed normal on Γ'_{ij}.

If one wishes to solve the problem analytically, the above scheme is indeed useful. On the other hand, it brings in a major obstacle in the development of a general numerical solution. To demonstrate these points, consider the alternative formulation of (1.2) obtained by assuming $\delta_F = 0$ and $\varphi \neq \varphi(u)$. Namely:

$$\nabla^2 u^{(i)}(\mathbf{x};\tau) = \varphi \frac{\partial}{\partial t} u^{(i)}(\mathbf{x};\tau), \quad 1 \leq i \leq N_s, \quad \mathbf{x} \in R'_{ij}, \quad \tau > 0 \tag{1.8a}$$

$$\beta_i \frac{\partial u^{(i)}}{\partial n}(\mathbf{x};\tau) + \alpha_i \frac{\partial u^{(i)}}{\partial n}(\mathbf{x};\tau) = \gamma_i, \quad 1 \leq i \leq N_s, \quad \mathbf{x} \in \Gamma'_i, \quad \tau > 0 \tag{1.8b}$$

$$u^{(i)}(\mathbf{x};0) = G_i(\mathbf{x}), \quad 1 \leq i \leq N_s, \quad \mathbf{x} \in R'_i \tag{1.8c}$$

subjected to the interface conditions,

$$u^{(i)}(\mathbf{x};\tau) = u^{(j)}(\mathbf{x};\tau) = u^F_{ij}, \quad i \neq j, \quad 1 \leq i,j \leq N_s, \quad \mathbf{x} \in \Gamma'_{ij}, \quad \tau > 0 \tag{1.8d}$$

$$p(\mathbf{x}) \frac{\partial u^{(i)}}{\partial n_{ij}}(\mathbf{x};\tau) + \frac{\partial u^{(j)}}{\partial n_{ij}}(\mathbf{x};\tau) = l_{ij} \frac{\partial n_{ij}}{dt}, \quad 1 \leq i,j \leq N_s, \quad \mathbf{x} \in \Gamma'_{ij}, \quad \tau > 0 \tag{1.8e}$$

where the notation of (1.7) is adopted, and N_s designates the number of isolated phases in R'. Γ'_i is the portion of Γ' belonging to R'_i. Note that N_s does not necessarily indicate the number of the thermodynamic states of the medium in R'. Figure 1 shows a typical two-dimensional region with four sub-regions.

To solve the problem analytically one first obtains a formal solution which satisfies (1.8a, b, and c) but not

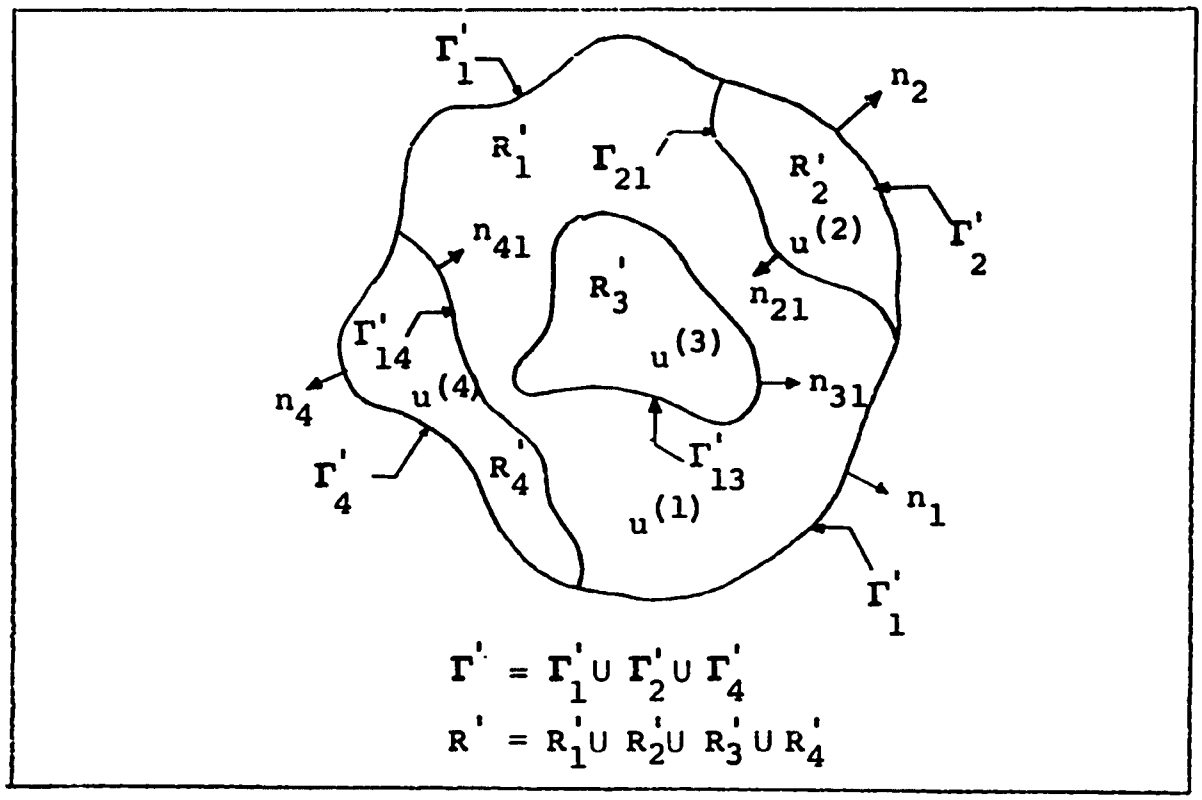


Figure 1. A Typical Two-Dimensional Closed Region.

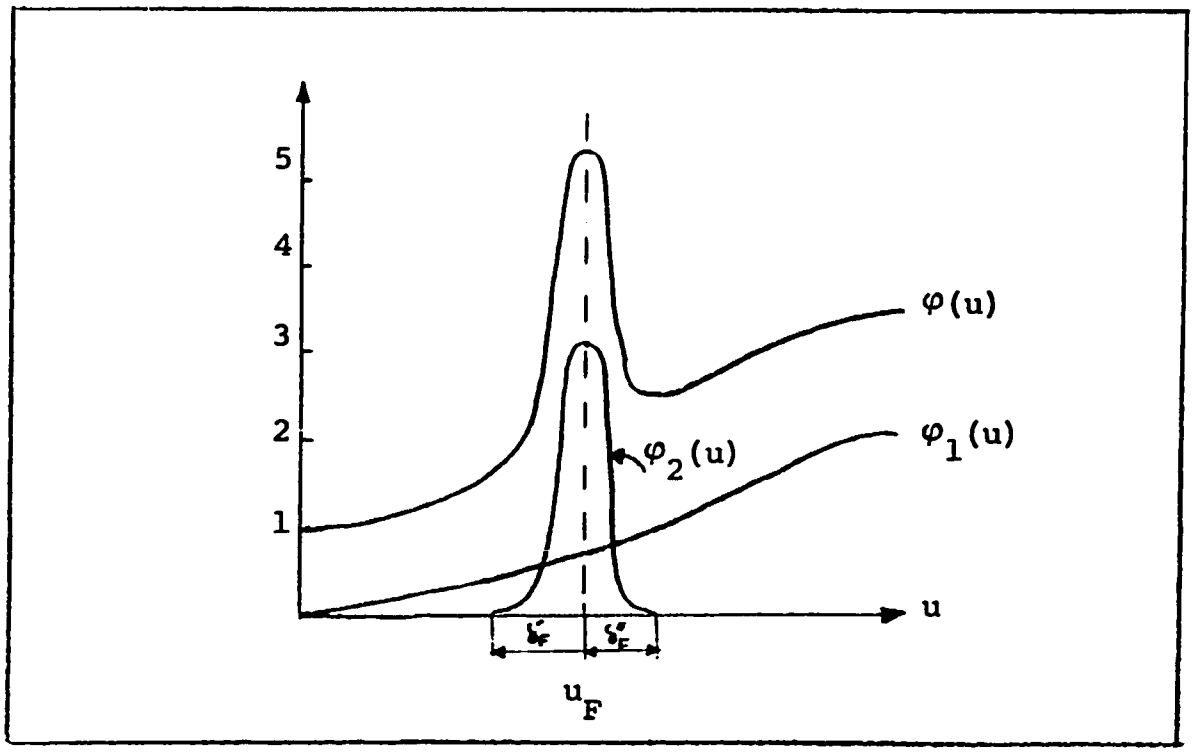


Figure 2. The Variation of the Dimensionless Parameters φ, φ_1 and φ_2 with Dimensionless Temperature u.

necessarily (1.8d and e) for each i, $1 \leq i \leq N_s$. Many special cases can be solved without undue difficulty. The next step is to force these solutions to satisfy the interface conditions (1.8d and e). The solution obtained is of course in an integral form. Once these steps are completed, an ambitious investigator may then venture into correcting the solution to take into account the temperature dependency of φ. At first glance, all these steps appear very feasible and practical. The situation looks even brighter when one tries the above ideas by first solving a simple problem, which traditionally has been that of linear flow of heat in a semi-infinite bar initially at $u(x_1;\tau) = 1$, with its surface $x_1 = 0$ kept at zero temperature or at which a constant amount of heat is removed for $\tau > 0$. The analytical solution for this case has a very convenient functional form, and can be readily computed (7, 8, 9, 12, 35).

In reality, however, there is a wide and dangerous gap between being able to derive an analytical solution for a simple one-dimensional problem and being able to do the same for even the simplest two-dimensional problem. The difficulty is essentially in reducing the formal integral solutions of the problem to a form suitable for computation. The integral equations are in such a form that even an attempt to approximate them by numerical methods presents some insurmountable obstructions.

The numerical solution of (1.8) also presents some unnecessary complications which revolve essentially around

the interfacial conditions (1.8d and e). These complications arise in locating one or many interface surfaces, the direction of the normal at several points on these surfaces, and finally in calculating their displacements as one moves from one time level to another. Here again the situation is not very bad if one is dealing with a one-dimensional problem where the interface is presented by a single moving point. In fact many clever schemes have been developed for this special case (25, 26, 74). But, unfortunately none of these schemes are applicable to the problem in higher dimensions. A co-ordinate transformation was originally proposed by the author (41) which maps the interface onto the circle $r = \frac{1}{2}$, provided that the region R' is divided only into two regions each containing only one homogenous phase. This transformation solved many, but not all, of the difficulties in developing an efficient numerical solution.

Once a suitable functional form for $\varphi(u)$ is assumed, the job of solving (1.2) numerically becomes a relatively easy matter. In this case one need not undertake the impossible task of writing a numerical procedure for locating the internal interfaces, nor does one need to develop a method for computing $\partial u^{(i)}/\partial n_{ij}$ and $\partial u^{(j)}/\partial n_{ij}$ immediately to the left and to the right of the interface R'_{ij}, for all $1 \leq i,j \leq N_s$. Instead, one solves the problem for $u(\mathbf{x};\tau)$, $\mathbf{x} \in R'$, and then plots the isotherms for $u = u^F_{ij}$, $1 \leq i,j \leq N_s$.

In view of the above observations, it seems natural to take Equation (1.2) as the starting equation for developing

a numerical solution of the problem rather than Equation (1.8), such as is demonstrated in Chapter III.

In the case of one transition temperature, if one lets

$$\frac{K(T_o)}{\rho c(T_o)} = \max_{T_1 \le T \le T_2} \left\{ \frac{K(T)}{\rho c(T)} \right\},$$

then $\varphi(u)$ may be expressed by

$$\varphi(u) = 1.0 + \varphi_1(u) + \varphi_2(u) \tag{1.9a}$$

where

$$1 = \int_{-\delta'_F}^{+\delta''_F} \varphi_2(u_F + u')\, du' \tag{1.9b}$$

$$s = \int_{-\delta'_F}^{+\delta''_F} \left(1.0 + \varphi_1(u_F + u')\right) du'. \tag{1.9c}$$

The general behavior of $\varphi(u)$, $\varphi_1(u)$ and $\varphi_2(u)$ is shown in Figure 2. The function $\varphi_1(u)$ is a positive smooth function and is usually defined for a medium under consideration. $\varphi_2(u)$ in some instances is either undefined or given as a pulse function. In both cases one must define a functional form for $\varphi_2(u)$ such that $u(\mathbf{x};\tau)$ is best approximated. One logical choice is:

$$\varphi_2(u) = \lambda \exp\left[-\beta^2 (u - u_F)^2\right] \tag{1.10}$$

where β is so chosen that,

$$\int_{-\infty}^{\infty} \varphi_2(u)\, du = \sqrt{\pi}\,\frac{\lambda}{\beta}\ \mathrm{erf}(\infty) = \frac{\sqrt{\pi}\lambda}{\beta} =$$

$$\int_{-\delta_F'}^{+\delta_F'} \varphi_2(u_F + u')\, du' + |\epsilon| = 1.0 + |\epsilon|$$

with $|\epsilon|$ sufficiently small. For example, if $\beta\delta_F' \geq 3$, then $|\epsilon| < 4 \times 10^{-4}$. Obviously, when $N_s > 2$, similar ideas can be applied to every individual phase. In solving the problem numerically one is primarily concerned with two important properties of $\varphi(u)$, namely,

$$\begin{aligned} &1.\ \ \varphi(u) \geq 1.0 \quad \text{for} \quad -\infty < u < \infty \\ &2.\ \ \max_{-\infty<u<\infty} \left\{\varphi(u)\right\} \leq M + 1.0 \end{aligned} \tag{1.10a}$$

where M is a positive number independent of u. The size of M plays an important role in the accuracy of any numerical solution of the problem. In general, it is desirable to choose M such that the combined discretization error and error due to assuming a value of δ_F' larger than the actual one is minimized.

Previous Theoretical Work

In the following, a brief account of some heuristic thoughts and ideas developed by previous investigators in solving the free boundary problems are given. Further discussion on the published literature is given throughout Chapters II, III and IV.

Analytical Solutions of the Stefan Problem

The first published discussion on the problems of heat conduction in a medium undergoing a change of state was given by Stefan (67) in his study of the polar ice thickness. For this reason such problems are referred to as the Stefan problem.

So far, many special cases of the Stefan problem have been solved analytically. These solutions are, in general, for the one-dimensional flow of heat in a finite or semi-infinite region. In this section only those solutions will be discussed which invite further investigation or are amendable to more complicated cases. For an excellent review of the existing solution see Carslaw and Jaeger (12) and Grosh and Sunderland (39). For a comprehensive theoretical treatment, as well as bibliography, reference should be made to Friedman (35). On this basis, the author recognizes three fundamental approaches to the problem, namely, Neumann (cf. 63), Boley (7) and Lightfoot (54). These solutions are reviewed below.

Neumann's solution. Consider a semi-infinite slab, $x \equiv x_1 > 0$, initially containing a liquid at T_∞ with the surface $x = 0$ maintained at zero temperature for $t > 0$. Let the freezing temperature of this liquid be $T_F > 0$. Then the temperature $T(x,t)$ in the semi-infinite slab is given (12) by

$$T_s(x,t) = \frac{T_F}{\operatorname{erf}\xi} \operatorname{erf}\frac{x}{2\sqrt{\alpha_s t}}, \quad t > 0, \; x > 0 \qquad (1.11a)$$

$$T_L(x,t) = T_\infty - \frac{(T_\infty - T_F)}{\operatorname{erfc}(\xi\sqrt{\frac{\alpha_s}{\alpha_L}})} \operatorname{erfc} \frac{x}{2\sqrt{\alpha_L t}} \tag{1.11b}$$

$$X(t) = 2\xi\sqrt{\alpha_s t} \tag{1.11c}$$

where,

X(t) = position of the interface

Subscripts s and L designate the solid phase and the liquid phase, respectively, and ξ is the root of the transcendental equation

$$(e^{-\xi^2}/\operatorname{erf}\xi) - \left[\sqrt{\frac{\alpha_L}{\alpha_s}} \cdot c_L \frac{(T_\infty - T_F)}{c_s T_F}\right] \cdot \left[e^{-\xi^2\alpha_s/\alpha_L} \Big/ \operatorname{erfc}\left(\xi\sqrt{\frac{\alpha_s}{\alpha_L}}\right)\right] = \frac{\xi L \pi^{\frac{1}{2}}}{c_s T_F} \tag{1.11d}$$

where,

L = latent heat of fusion

α = thermal diffusivity

c = specific heat.

Subscripts s and L designate the solid phase and the liquid phase, respectively. Note that for each phase α and c are assumed to be constants but are not necessarily the same for both phases. The solution (1.10) was given by Franz Neumann in his lectures in the 1860's (cf. 63). Neumann's solution is indeed the most useful and important solution of the Stefan problem. It provides a good order of magnitude check for the more complex problems, as well as giving the functional form of the functions describing the progress of the interface.

Let T(x,t) be the temperature in the region x > 0 and H(Z) be the Heaviside unit function.** Then, one can write the Neumann solution in a more elegant form:

$$T(x,t) = H\big(x - X(t)\big)\frac{T_F}{\operatorname{erf}\xi} \cdot \operatorname{erf}\frac{x}{\sqrt{4\alpha_s t}} + H\big(X(t) - x\big) \cdot \left[T_\infty - \frac{T_\infty - T_F}{\operatorname{erfc}\ \xi\sqrt{\frac{\alpha_s}{\alpha_L}}} \operatorname{erfc}\frac{x}{\sqrt{4\alpha_L t}} \right] \tag{1.12}$$

Now, if the boundary temperature is given by

$$T(o,t) = f(t)$$

then onecan apply Duhamel's theorem to get

$$T(x,t) = \frac{T_F}{\operatorname{erf}\xi} \int_o^t f(t-t_1) \frac{\partial}{\partial t_1} \left[H(x - X(t_1)) \operatorname{erf}\frac{x}{2\sqrt{\alpha_L t_1}} \right] dt_1$$

$$+ \left[T_\infty - \frac{T_\infty}{\operatorname{erfc}\ \xi\sqrt{\frac{\alpha_s}{\alpha_L}}} \right]$$

$$\left\{ \int_o^t f(t-t_1) \frac{\partial}{\partial t_1} \left[H\big(X(t_1) - x\big) \operatorname{erfc}\frac{x}{2\sqrt{\alpha_L t_1}} \right] dt_1 \right\}$$

Recently some attempts have been made to solve the above integro-differential equation.

Boley's method (7). Compared with the logical procedure described earlier, the essential feature of this

---

**H(Z) = 1 for Z > 0, H(Z) = 0 for Z < 0

method is that it deals mathematically with a fictitious body, whose shape is unchanged and is identical with that of the body before any phase transformation occurs. The fictitious body is considered to be exposed to an imaginary heat input and initial temperature distribution whose magnitude is adjusted so as to satisfy the appropriate solid--liquid interface conditions. In this way the original boundary value problem is replaced by an ordinary integro-differential equation. The latter can be solved numerically or in series form without any difficulty, thus providing an exact solution. This method is not in general limited to the one-dimensional case.* However, the integro-differential equations involved usually become algebraically unmanagable.

To illustrate the method, consider again the flow of heat in a semi-infinite slab containing a liquid initially at zero temperature. Let the melting temperature be T_F, and let heat be removed at $x = 0$ at a constant rate Q. Let $T_L(x,t)$ and $T_S(x,t)$ be the temperatures in the liquid phase and the solid phase, respectively. Assume the entire region $x > 0$ contains a fictitious liquid subjected to the boundary condition,

$$K\frac{\partial T_1}{\partial x} = Q + f_1(t)$$

such that $T_L(x,t) = T_1(x,t)$ for $x \geq X(t)$. Next, let the solution $T_2(x,t)$ be the temperature of a fictitious solid

---

*See Hashemi (41) for further discussion.

phase in the entire region $x > 0$, having an unknown initial temperature $g(x)$ such that

$$T_2(x,t) = T_s(x,t) \text{ for } 0 \leq x \leq X(t)$$

Then one may write:

$$\frac{\partial^2 T_1(x,t)}{\partial x^2} = \frac{1}{\alpha_I} \frac{\partial}{\partial t} T_1(x,t),\ x > 0,\ t > 0$$

$$K_I \frac{\partial T_1}{\partial x}(0,t) = Q + f_1(t),\ x = 0, t > 0 \qquad (1.13)$$

$$T_1(x,0) = 0,\ x > 0$$

$$\frac{\partial^2 T_2}{\partial x^2}(x,t) = \frac{1}{\alpha_{II}} \frac{\partial}{\partial t} T_2(x,t)$$

$$K_{II} \frac{\partial T_2}{\partial x}(x,t) = Q \qquad (1.14)$$

$$T_2(x,0) = g(x)$$

where T_1 and T_2 are subjected to the additional conditions,

$$T_1\big(X(t),t\big) = T_F,\ t > 0$$
$$T_2\big(X(t),t\big) = T_F,\ t > 0$$

$$K_{II} \frac{\partial T_2}{\partial x} = f_2(t),\ x = X(t) \qquad (1.15)$$

$$K_I \frac{\partial T_1}{\partial x} = f_2(t) - \rho L \frac{dX(t)}{dt},\ t > 0,\ x = X(t)$$

The boundary value problems (1.13) and (1.14) can be solved in terms of the unknown functions $g(x)$ and $f_1(t)$.* The system of equations, (1.13), (1.14) and (1.15), contains six unknowns. Applying the four conditions (1.15) to the

*See Carslaw and Jaeger (12), or any other text book on heat conduction, for solution of (1.13) and (1.14).

solutions of (1.13) and (1.12) one obtains six equations to be solved for the unknown functions T_1, T_2, f_1, f_2, $X(t)$, and g. The details of this procedure are given by Boley (7). The most important result is the expression,

$$X(t) = \frac{\sqrt{\pi\alpha_I}T_F}{Q}\left\{\frac{2m}{3\pi}\left(\frac{t}{t_m}-1\right)^{3/2} - \frac{m^2}{4\sqrt{\pi}}\left(\frac{t}{t_m}-1\right)^2 - \frac{4m}{15\pi}\left(\tfrac{1}{2} - m^2 - \frac{16m}{3\pi^{3/2}}\right)\left(\frac{t}{t_m}-1\right)^{5/2} + \left[\frac{4Dm^2}{9\pi^2} + \frac{m^2}{12\sqrt{\pi}}\left(\frac{35m}{8\sqrt{\pi}} - m^2 + \tfrac{1}{2}\right)\right]\left(\frac{t'}{t_m}-1\right)^3 + \cdots\right\} \tag{1.16}$$

where,

$$m = \frac{\sqrt{\pi}}{2}\cdot\frac{c_I}{L}\,T_F$$

$$D = \alpha_I/\alpha_{II}$$

t_m = the time at which $T_1(o,t)$ is equal to T_F.

Lightfoot's method (54). Let the thermal properties of the two phases be the same and consider the region $x > 0$ initially in the liquid state at a temperature $T_\infty > T_F$. Let the position of the interface at time t be $X(t)$ and let $X(t)$ move at a velocity $\dot{X}(t)$. Then the heat of solidification is released at a rate $L\rho\dot{X}(t)$. One may consider this solidification boundary as a moving source of heat of strength $L\rho\dot{X}(t)$. If the surface $x = 0$ is kept at zero temperature, then the solution of the problem becomes:*

---

*See Carslaw and Jaeger (12) section (11.4) and (10.3) for derivation of this solution.

$$T(x,t) = T_\infty \operatorname{erf} \frac{x}{2(\alpha t)^{\frac{1}{2}}} + \frac{L}{2c\sqrt{\pi\alpha}} \int_0^t \frac{\dot{X}(t_1)dt_1}{(t-t_1)^{\frac{1}{2}}}$$

$$\left\{ \exp\left[-\left(x - X(t_1)\right)^2 / 4\alpha(t - t_1)\right] - \exp\left[-\left(x + X(t_1)\right)^2 / 4\alpha(t - t_1)\right] \right\} \qquad (1.17)$$

Lightfoot (54) has solved the above integral equation by assuming,

$$X(t) = 2\xi(\alpha t)^{\frac{1}{2}}$$

and making use of the condition,

$$T\left(X(t),t\right) = T_F \qquad (1.18)$$

The results are identical to (1.10) when $\alpha_s = \alpha_L = \alpha$, and $K_s = K_L = K$. What makes the Lightfoot method interesting is the fact that the solution is the sum of two terms, each of which is in turn a solution of a simple heat conduction problem.

All that is required to be done is to use condition (1.18) to obtain the functional form of X(t), thus making it possible to write at least an integral solution for the more complex problems. Such a solution can yield the numerical values of the temperature and position of the interface by a variety of techniques. The simplest one is the graphical integration method.

It must be noted that both Lightfoot's method and Boley's method follow almost the same principles. However,

Boley's method does not impose any restriction on the physical properties of the two phases. Besides, it is not necessary to guess a particular functional form for X(t).

The existance theorem for Stefan problems was given by Douglas (25) and was further developed by Kyner (48, 49). For other methods see Kolodner (47), Sestini (65, 66). Oleinik (59) considered the nonlinear problem as well as several phase transitions. His solutions, however, satisfy the boundary conditions only in some generalized sense.

Numerical Solutions of the Stefan Problem

Practically all of the numerical methods suggested by the various authors are restricted to one-dimensional problems. The melting and solidification problem in higher dimensions is left almost entirely untouched. Most authors have preferred to study the numerical solution of the boundary value problem,

$$u_t(x,t) = u_{xx}(x,t),\ 0 < x < X(t),\ t > 0 \qquad (1.19a)$$

$$u_x(0,t) = -1 \quad ,\ t > 0 \qquad (1.19b)$$

$$u(x,t) = 0 \quad ,\ x \geq X(t),\ t > 0 \qquad (1.19c)$$

$$\frac{dX(t)}{dt} = -u_x\big(X(t),t\big) \quad ,\ t > 0 \qquad (1.19d)$$

$$X(0) = 0 \qquad (1.19e)$$

However, the numerical methods developed for solving (1.19) can be adapted to the case for which the conditions (1.19c) and (1.19d) are replaced by,

$$u\left(X(t),t\right) = 0$$

$$u(x,0) = a \ , \ a > 0, \ x > 0 \qquad (1.20)$$

$$u_x\left(X^+(t),t\right) - u_x\left(X^-(t),t\right) = \frac{dX(t)}{dt}$$

where the superscripts + and - indicate that the derivatives are taken immediately on the left and on the right of the interface, respectively.

The last two conditions in (1.19) may be replaced by the equivalent condition,

$$t = X(t) + \int_0^{X(t)} u(x,t)\, dx \qquad (1.21)$$

which amounts to the heat balance over the whole system.

Douglas and Gallie (26) and Douglas (25) suggested the following numerical procedure:*

Let,

$$t_n = \sum_{k=0}^{n-1} \Delta t_k \qquad (1.22)$$

Then choose Δt_n, such that

$$X(t_n) = X_n = n.\Delta x \qquad (1.23)$$

where Δx is the uniform mesh spacing. Next, let $W_{i,n}$ be the approximate solution of the problem at $t = t_n$ and let,

$$t_{n+1} = X_{n+1} + \sum_{i=0}^{n} W_{i,n}\, \Delta x \qquad (1.24)$$

$$\Delta t_n = t_{n+1} - t_n$$

---

*This procedure is slightly different from the original one.

Then solve the difference system,

$$\Delta^2_x W_{i,n+1} = (W_{i,n+1} - W_{i,n}) / \Delta t_n \ , \ i = 1,\ldots,n \qquad (1.25a)$$

$$W_{1,n+1} - W_{o,n+1} = -\Delta x \qquad (1.25b)$$

$$W_{n+1,n+1} = 0$$

Douglas (25) has proved the uniqueness theorem for the above solution as well as evaluating its rate of convergence. Note that the backward difference scheme in (1.25a) is in general unconditionally stable for all $\Delta t > 0$. Douglas (25) demonstrated that after some simple modifications, the uniqueness theorem also applies when the differential equation is generalized to a nonlinear one.

Trench (74) studied the solution of the problem by an explicit method, taking fixed time steps. He proved that for $\Delta t/\Delta x^2 < \delta$, ($\delta = \frac{1}{2}$ when the differential equation is linear; otherwise it is some known positive number) the discrete, forward difference solution is unique and converges to the solution of the continuous problem. Ehrlich (33) has discussed the uses of the Crank-Nicholson equation for generalization of (1.19).

Rose (64) has proposed a method for solving (1.19) that is analogous to a procedure introduced by Lax (52) to compute shock wave propagation in first order, hyperbolic equations. He has not yet succeeded in demonstrating the convergence for the method, but his numerical evidence is

encouraging. Rose notes that his method is essentially independent of dimensionality, but he has yet to try such a problem.

CHAPTER II

THE ANALOGY BETWEEN DIFFUSION MASS TRANSFER WITH CHANGE OF PHASE AND CONDUCTION HEAT TRANSFER WITH CHANGE OF PHASE

The analogy between diffusion mass transfer and heat conduction is well known, and the subject is discussed by many authors, for example Crank (17), Jost (44), and Carslaw and Jaeger (12). For this reason the reference here will be brief and oriented toward the application of this known principle in solving heat conduction problems with a free boundary (or change of state). Included also in this chapter is a comprehensive discussion on the desired properties of the binary liquid systems suitable for simulating heat conduction problems with change of phase.

Consider again the rate laws and the accumulation laws for diffusion in a partially miscible, liquid-liquid system and for heat conduction with change of phase in an isotropic medium, namely:

	Diffusion	Heat Conduction	
Rate law	$\mathbf{j}_A = D_{AB}(C_A)\nabla C_A$	$\mathbf{q} = \alpha(E)\nabla E$	(2.1)
Accumulation law	$\frac{\partial C_A}{\partial t} = \nabla \mathbf{j}_A$	$\frac{\partial E}{\partial t} = \nabla \mathbf{q}$	(2.2)

where,

$\mathbf{j}_A$ = mass flux of component A,

D_{AB} = diffusion coefficient of component A in B,

α = thermal diffusivity = $K/\rho c$, where $\rho c = \left(\frac{\partial E}{\partial T}\right)_V$ covers the entire temperature range including the phase transition as noted in Figure 2,

$\mathbf{q}$ = conduction heat flux,

E = internal energy (heat content) of a unit volume of the system

$$E(T) = \int_{T_R}^{T} \rho c(T')\, dT'$$

Combining the above two laws and assuming that ρ is constant, one gets:

Diffusion
$$\frac{\partial C_A}{\partial t} = \nabla D_{AB}(C_A) \nabla C_A \qquad (2.3a)$$

Heat Conduction
$$\frac{\partial E}{\partial t} = \nabla \alpha(E) \nabla E \qquad (2.3b)$$

Clearly the parabolic differential equations (2.3a) and (2.3b) are mathematically similar. To demonstrate the complete analogy between the two phenomena it is also necessary to show the boundary conditions and the interface conditions are also similar. These two conditions take the following form:

Boundary Condition:

1) Diffusion
$$D_{AB}\frac{\partial C_A}{\partial n} + K(C_A, \mathbf{x})(C_A - C_A^B) = 0 \qquad (2.4a)$$

2) Heat Conduction
$$\alpha(E)\frac{\partial E}{\partial n} + h(E, \mathbf{x})(E - E^B) = 0 \qquad (2.4B)$$

Interface Condition:

1) Diffusion $$D_{AB}^{+}\nabla C_A^{+} - D_{AB}^{-}\nabla C_A^{-} = p(\mathbf{x})\Delta C_A \frac{\partial n}{\partial t},\ \mathbf{x}\in\Gamma_s' \quad (2.5a)$$

2) Heat Conduction $$\alpha^{+}(E)\nabla E^{+} - \alpha^{-}(E)\nabla E^{-} = p(\mathbf{x})\Delta E \frac{\partial n}{\partial t},\ \mathbf{x}\in\Gamma_s' \quad (2.5b)$$

where,

$K(C_A,\mathbf{x})$ = film coefficient of mass transfer at the boundary,

$h(E,\mathbf{x})$ = film coefficient of heat transfer at the boundary,

$\mathbf{n}$ = an outward directed normal on the interface,

Γ_s' = the interface between the two co-existing phases,

$p(\mathbf{x})$ = a weight function depending on the co-ordinate system such that $p(\mathbf{x})\,dn$ gives the local change of the phase volume,

Superscripts + and - indicate immediately on the left and immediately on the right of the interface,

ΔC_A = equilibrium concentration change across the interface,

ΔE = latent heat of the change of state (melting or solidification),

C_A^{B} = the external boundary concentration of A,

E_B = environmental heat content defined by

$$\int_{T_R}^{T_B} \rho c \cdot dT$$

where T_B is the external boundary temperature and ρ and $c(T)$ are the internal properties of the conducting region at the boundary.

Here again the mathematical similarity of Equations (2.4a) and (2.4b) as well as (2.5a) and (2.5b) is obvious. To establish the criteria for direct analogy between the binary diffusion and the heat conduction, the above system of equations should be written in a suitable dimensionless form with the minimal number of parameters.

The Criteria for the Analogy

Consider a connected region R', and its boundary surface Γ', as shown in Figure 3. Let there be at time t a continuous interface Γ'_s separating the two coexisting phases contained by R'. Imagine that R' had originally contained a liquid (or liquid phase I) at a uniform temperature T_o (or concentration C_{oA}) and, due to imposing some temperature conditions (or concentration conditions) on Γ', a solid phase (or liquid phase II) forms and expands in region R'. Then in the absence of chemical reaction and heat transfer (or mass transfer) by convection or any process other than conduction (or diffusion), the energy content $E(\mathbf{x},t)$ (or concentration $C_A(\mathbf{x},t)$) satisfies the following boundary value problems:

Differential Equation:

$$\nabla \alpha^*(u(\mathbf{x},\tau))\nabla u(\mathbf{x},\tau) = \frac{\partial}{\partial \tau} u(\mathbf{x},\tau),\ \mathbf{x}\in R',\ \tau > 0 \qquad (2.7a)$$

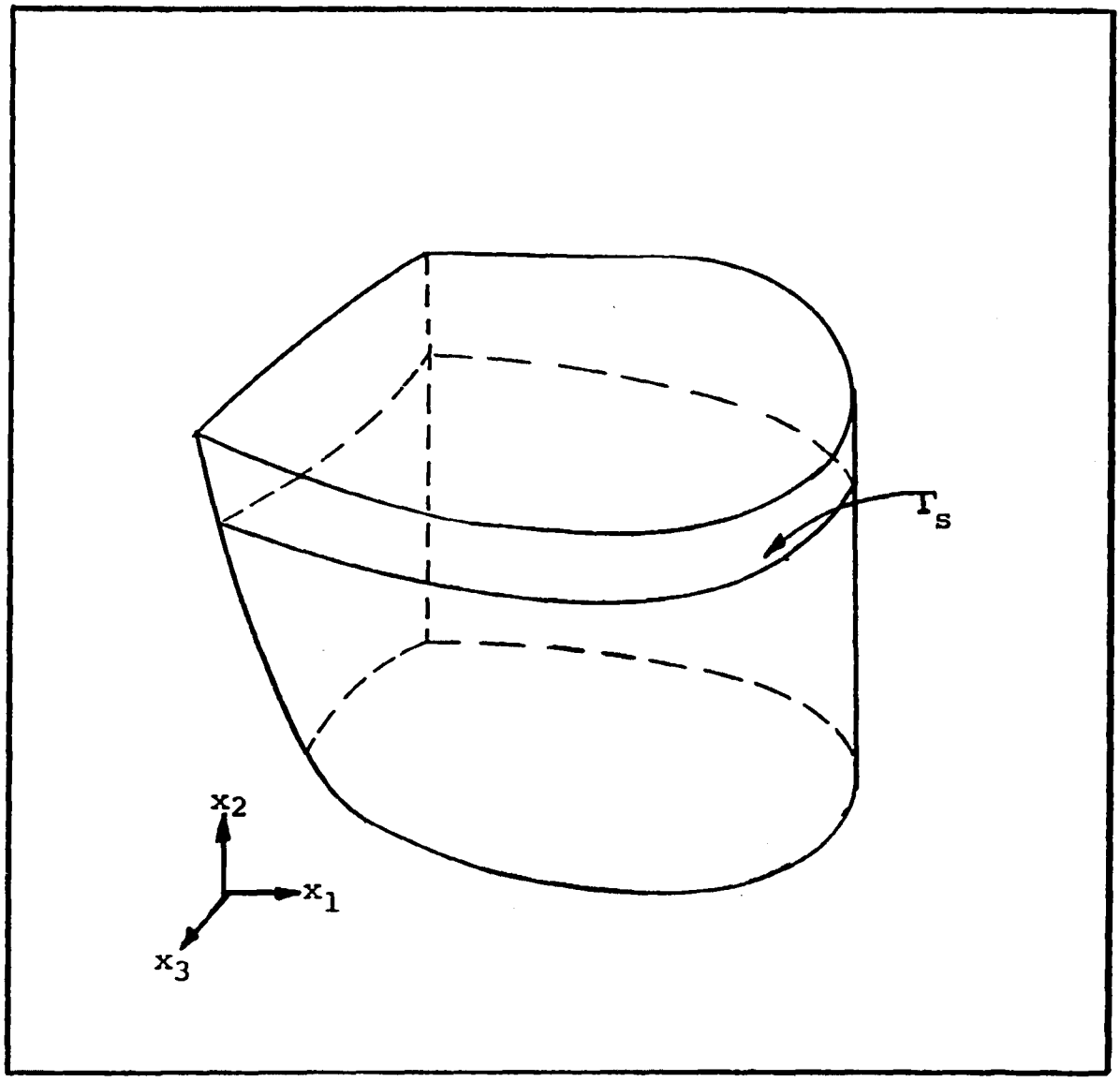


Figure 3. An Arbitrary Region R Divided into Two Sub-Regions by a Continuous Interface Γ_s. (Each of the Two Sub-Regions Contains one of the Two Co-Existing Phases).

Boundary Condition:

$$u(\mathbf{x},\tau) + \tilde{h}(x,\tau)\Big(u(\mathbf{x},\tau) - f(\mathbf{x},\tau)\Big) = 0,\ \mathbf{x}\in\Gamma',\ \tau>0 \qquad (2.7b)$$

Initial Condition:

$$u(\mathbf{x},0) = u_o,\ \mathbf{x}\in R' \qquad (2.7c)$$

Interface Condition:

$$\nabla u^{+}(\mathbf{x},\tau) - \varkappa\nabla u^{-}(\mathbf{x},\tau) = p(\mathbf{x})\frac{\partial n}{\partial \tau}(\mathbf{x},\tau),\ \mathbf{x}\in\Gamma_s',\ \tau > 0 \qquad (2.7d)$$

$$u^{+}(\mathbf{x},\tau) = 0,\ \mathbf{x}\in\Gamma_s',\ \tau > 0 \qquad (2.7e)$$

$$u^{-}(\mathbf{x},\tau) = 1,\ \mathbf{x}\in\Gamma_s',\ \tau > 0 \qquad (2.7f)$$

where,

Heat Conduction	Diffusion
$u = \dfrac{E - E_F^I}{E_F^{II} - E_F^I},\ E_F^{II} \neq E_F^I$	$u = \dfrac{C_A - C_s^I}{C_s^{II} - C_s^I},\ C_s^{II} \neq C_s^I$
$\alpha^*(u) = \dfrac{\alpha'(u)}{\alpha'(0)}$	$\alpha^*(u) = \dfrac{D'_{AB}(u)}{D'_{AB}(0)}$
$\alpha'(u) = \alpha(T) \equiv \alpha(E)$	$D'_{AB}(u) = D_{AB}(C_A)$
$\varkappa = \alpha'(1)/\alpha'(0)$	$\varkappa = D'_{AB}(1)/D'_{AB}(0)$
$\tau = \alpha'(0)t/a_1^2$	$\tau = D'_{AB}(0)t/a_2^2$
$u_o = \dfrac{E_o - E_F^I}{E_F^{II} - E_F^I}$	$u_o = \dfrac{C_o - C_s^I}{C_s^{II} - C_s^I}$
$f(\mathbf{x},\tau) = \dfrac{E_B - E_F^I}{E_F^{II} - E_F^I}$	$f(\mathbf{x},\tau) = \dfrac{C_A^B - C_s^I}{C_s^{II} - C_s^I}$
$\tilde{h}(\mathbf{x},\tau) = \dfrac{h(\mathbf{x},\tau)}{\alpha\big(u(\mathbf{x},\tau)\big)};\ \mathbf{x}\in\Gamma$	$\tilde{h}(\mathbf{x},\tau) = K(\mathbf{x},\tau)/D_{AB}\big(u(\mathbf{x},\tau)\big);\ \mathbf{x}\in\Gamma$

(2.8)

a_1 and a_2 are geometrical scaling factors in the heat conduction problem and the diffusion problem, respectively. Therefore, in geometrically similar regions, the dimensionless energy content, u, or the dimensionless concentration, u, at the same dimensionless time, τ, and for the geometrically similar points are identical, provided that the dimensionless parameters $\varkappa$, u_o and the functions $\alpha^*(u)$, $f(\varkappa,\tau)$ and $\tilde{h}(\varkappa,\tau)$ are the same for both cases. The coefficients $\varkappa$ and α^* depend solely on the physical properties of the heat conducting media (or binary liquid systems). The functions $f(\varkappa,\tau)$ and $\tilde{h}(\varkappa,\tau)$ can be adjusted by a proper choice of the boundary conditions, while u_o depends on the initial temperature (or concentration).

The choice of a suitable, partially miscible binary liquid system therefore depends solely on $\varkappa$ and α^*, provided that it is practically possible to match u_o and $f(\varkappa,\tau)$ by a suitable choice of the initial concentration and boundary concentration, respectively. The matching of the function $\tilde{h}(\varkappa,\tau)$ usually requires some ingenuity and a thorough knowledge of the film coefficient of mass transfer. However, it is essentially independent of the choice of a particular binary liquid system. The theoretical possibility of being able to match u_o and $f(\varkappa,\tau)$with practically all partially miscible binary liquid systems is, of course, unquestionable. Because the quantity $(C_s^{II} - C_s^I)$ approaches zero as the temperature of the system approaches the critical solution temperature (Figure 4), it is possible, by a proper choice of the temperature, to adjust the ratio $(C_o-C_s^I)/(C_s^{II}-C_s^I) = u_o$

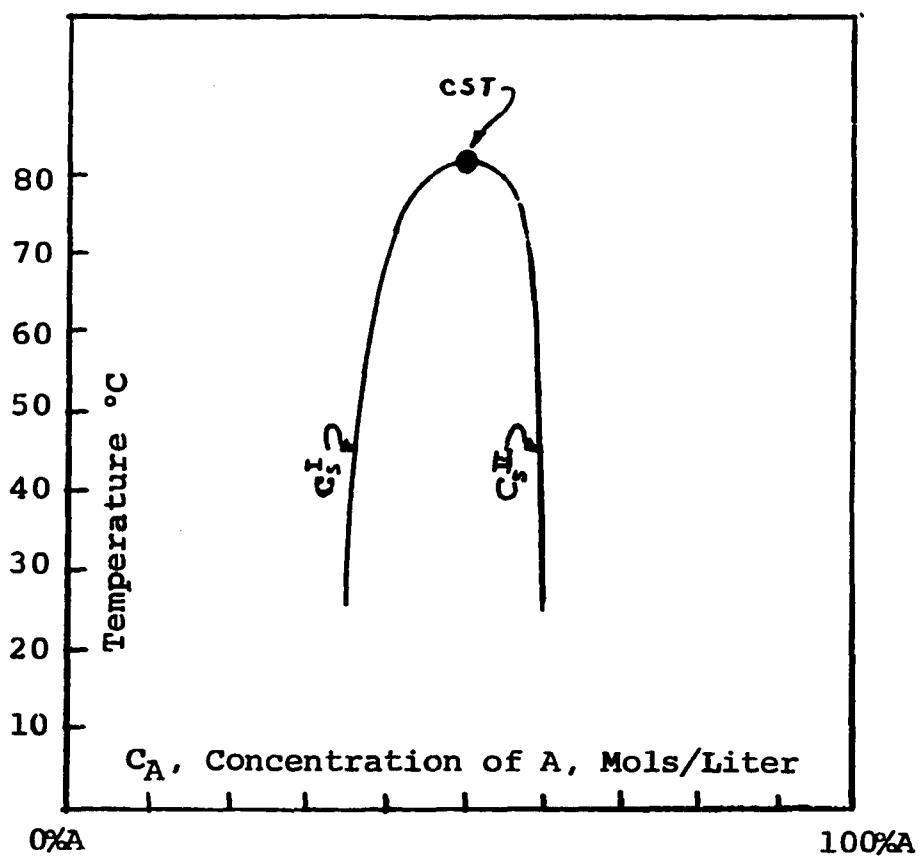


Figure 4. The Desired Consolute Curve for a Suitable Binary Liquid System. (Note that there is very small change in C_s^I and C_s^{II} around room temperature. Note also that at room temperature $(C_A - C_s^I) / (C_s^{II} - C_s^I)$ can vary between zero to about 1.5 thus permitting simulation of a wide range of boundary and initial conditions at ambient temperature.)

to any desired value. The same holds for the desired range of the ratio $(C^B - C_s^I)/(C_s^{II} - C_s^I) = f$.

Diffusion in Porous Media

In chapters V and VI it will be seen that it is most difficult, if not impossible, to produce a true two-dimensional diffusion field in a non-porous region. On the other hand, reasonably good results may be obtained in porous media. When the size of the pores are macroscopically small, the diffusion equation (2.7a), the boundary conditions (2.7b), the initial conditions (2.7c) and the interfacial conditions (2.7d, e and f) all remain unchanged, provided that the porous medium is macroscopically isotropic. However, the value of the ordinary diffusion coefficient appearing in the dimensionless time $\tau = D'_{AB}(0)t/a_2^2$ must be replaced by an effective diffusion coefficient, $\mathfrak{D}_{AB}(0)$ for the porous medium under consideration. The effective diffusivity for porous media is related to the ordinary diffusivity by the relation

$$\mathfrak{D}_{AB} = \frac{\omega_1}{\eta\omega_2} D_{AB} = \omega D_{AB} \tag{2.9}$$

where,

$$\omega = \frac{\omega_1}{\eta\omega_2}$$

ω_2 = effective porosity = (volume of the pores available for diffusion)/(total volume),

ω_1 = (mean cross-sectional area open for diffusion)/(total cross-sectional area),

η = "tortuosity", "lithologic factor" or "labyrinth factor" = (actual diffusion path)/(linear path).

For a macroscopically uniform and isotropic medium ω_1, ω_2, η, and consequently, ω are constant and independent of the position or concentration. The majority of authors working on porous media have assumed that $\omega_1/\omega_2 \cong 1.0$. There are many instances in which this assumption is a very poor one. However, it holds very closely for the porous medium used in the present investigation (Whatman filter paper Number 52). The tortuosity, η, is then the only factor that plays an important role in fibrous material such as filter paper. Carman (11) observed that in unconsolidated beds of spherical particles the actual distance traveled by a fluid in the direction of the flow is about $\sqrt{2}$ times the linear path, i.e., $\eta = 1.415$ and $\omega \cong .71$. Van der Poel (75) found that for unconsolidated glass powder and sand packs, η varies between 1.4 and 1.7. For fibrous material one would expect that η is slightly less than 1.4, so that $\omega \cong .75$.

It is usually very difficult to arrive theoretically at a reliable value for η. However, the experimental measurement of the quantity ω_1/η can readily be made by making use of the analogy between steady state diffusion and electrical conduction in porous media. The analogy is simply based on the fact that the electrical conductivity of a conducting fluid in non-conducting porous media is equal to ω_1/η times the electrical conductivity of the fluid alone. Knowing the electrical conductivity of the fluid, one can calculate ω_1/η.

This method was suggested by Klinkenberg (46). He also reported some crude experimental data to substantiate his theoretical argument. More recently Dullien and Scott (32) and Fatt (34) successfully used the electrical conductivity method to make the measurements. An excellent discussion and review of the state of art on the experimental techniques for evaluating ω_1 / η and ω_2 is given by Welker (82).

The Properties of an Ideal, Partially Miscible Binary Liquid System Suitable for the Analog Studies

Before selecting a binary liquid system suitable for the present investigation, it is advisable to specify first of all the desired properties of such a system and then to search for the pair of liquids which best fulfills these requirements. The desired properties are:

1. Availability in a very pure state.
2. Easy to analyze accurately (to about 10^{-5} moles per liter) the concentration of one component in the other.
3. Availability of reliable data on:
   a. equilibrium concentrations (C_s^I and C_s^{II}) at various temperature levels,
   b. density of the solution at all compositions,
   c. refractive index at all concentrations,
   d. viscosity at all concentrations and the temperature levels of interest,
   e. integral and differential binary diffusion coefficient,

f. surface tension and interfacial tension,

g. freezing point and boiling point at various compositions.

4. Non-corrosive and weak solvent for resins and other polymers.

5. Low viscosity.

6. No density change greater than 5 percent between the two equilibrium phases.

7. Very low interfacial tension ($\approx$0.1 dyne per cm.).

8. Non-flammable, non-toxic, and non-caustic.

9. Sufficient change of refractive index between the phases to allow observation of the interface.

10. Strong change of refractive index or color with concentration to allow use of a simple technique for measuring the concentration profile developed by diffusion.

11. A consolute curve similar to that shown in Figure 4 to allow simulation of a variety of initial and boundary conditions at room temperature.

Admitting that it is impossible to find a particular binary system which satisfies all the above requirements, one is forced to concentrate on the most critical requirements. The requirements 3, 7 and 11 are perhaps the most important ones for the first evaluation of the diffusion cell analog. Nevertheless, when one wishes to solve a particular heat transfer problem, χ is the only parameter that dictates the choice of a particular binary mixture.

The Search for a Suitable Binary Mixture

If two common liquids are partially miscible, then most probably one of them is weakly polar and the other one is either non-polar or strongly polar. The degree of their mutual solubility depends on how closely they are polar or non-polar. This explanation of the phenomena is very crude, but it serves the purpose here. Therefore, water, as a strongly polar liquid, is the first choice for one of the components of the binary mixture desired. The reasons are:

1. It is abundantly available in very pure state.
2. It is the most extensively studied single fluid.
3. The properties of aqueous solution are more thoroughly studied, so that one would expect to find a wealth of experimental data on any partially miscible binary system having water as one of the components.
4. The methods for the analysis of water for most common liquids are well developed.
5. It is the safest liquid to handle.

Having chosen one of the components the choice of the second one becomes relatively easy. There are several excellent references covering all the experimental data on the properties of aqueous solutions (55, 68, 72). The critical solution temperatures and the general shape of the consulate curves of an almost complete spectrum of the binary liquid mixtures are tabulated by Gould (38).

In the course of conducting a search for the best binary liquid system, it was observed that the requirement of density very sharply limits the choice. When one wishes to simulate a heat transfer problem, one is essentially concerned with the matching of the densities, rather than the requirement that the two phases have almost the same density. However, when it is desired to compare the results of the diffusion analog with the known theoretical results, the density of the two phases should be essentially uniform in order to avoid the possibility of bulk flow occuring in addition to pure diffusion. Unfortunately, a solution to the transport equation involving both bulk flow and diffusion is not available.

As a result of the search, the binary systems phenol-water, aniline-water, isobutric acid-water, acetylacetone-water, and bezaldehyde-water appeared to be more suitable for the present investigation. The consulate curves for these systems are shown in Figure 5. Further examination revealed that the system of phenol and water is the best choice. The advantages of this system over the other are:

1. A more suitable critical solution temperature (66°C).
2. Low interfacial tension (about 0.1 dyne per cm. at 55°F).
3. A more complete published data on the properties of this system.
4. Availability in a very pure state.

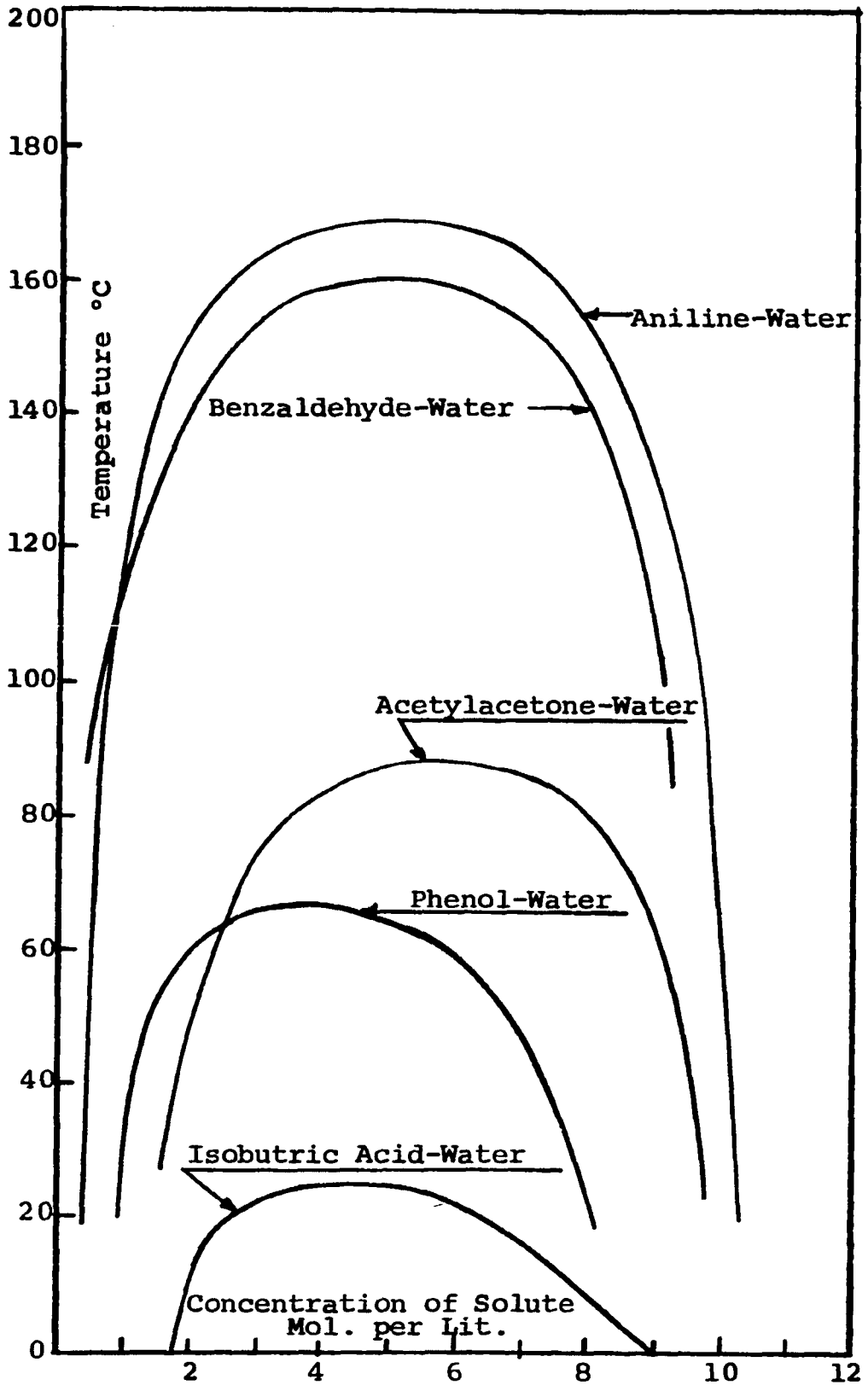


Figure 5. The Change of Solubility with Temperatures for Various Substances.

5. The techniques for analyzing water for phenol content are well advanced and reliable.

The short-comings of this system are:

1. Phenol is a strong solvent, attacking materials of construction.
2. Phenol has a high freezing point (41.6°C).
3. It irritates the skin upon contact, which gives rise to some handling problems.
4. It is transparent in the visible light spectrum thus negating visual observation of the concentration profile developed in a diffusion cell.

Nevertheless, this system was taken as the best choice for the present feasibility studies, even though other systems may prove to be more desirable in future work.

CHAPTER III

A PROPOSED NUMERICAL SOLUTION

The difficulties in developing a practical analytical solution for the problems of two-dimensional heat conduction with change of state leave two alternative approaches open for further investigation: 1) simulation of the temperature field in a scaled model, and 2) approximation by a suitable numerical procedure. The former was considered in the previous chapters. The theoretical aspects of the latter are covered in the present chapter, and the practicality of solving the problem on a high speed digital computer is discussed in the following chapter.

For any numerical method it is first necessary to establish the criteria for stability prior to carrying on the machine computations. Second, in the absence of any rigorous analytical upper and lower bounds on the solution of the continuous problem, it is equally necessary to obtain the correct order of accuracy of a discrete numerical method used to solve the general problem. However, the order of accuracy specifies only the rate of convergence of a numerical solution, but it does not give the absolute error. Last, but not least, one needs to have a sound basis for adopting a

particular numerical method from the numerous possible choices. The fruitless and costly effort of many investigators in verifying these problems by actual machine computations have demonstrated the wastefulness of a trial and error approach.

The various numerical solutions are treated here essentially from the point of view of stability. The equivalence of stability and convergence of a consistent numerical procedure for solving a system of first order homogenous differential equations was shown by Lax and Richtmyer (53) in their most original treatment of the stability of linear, finite difference equations. Recently, Thompson (70) has extended the analysis of Lax and Richtmyer to the systems of first order, quasi-linear differential equations. Thompson's analysis is for stationary finite-difference approximations. For non-stationary finite-difference methods, it is doubtful that his treatment can be generally extended. Unfortunately the analysis of Lax and Richtmyer (53) and also Thompson (70) have little to offer about the magnitude of the discretization error.

To facilitate the choice of a suitable numerical method for solving the problems of heat conduction with change of state, a method of analysis is developed which treats most of the numerical techniques on a common basis. This method was originally devised by Varga (76, 77) for studying the numerical solution of a linear, parabolic, partial differential equation with constant coefficients. The following is an extension of this method to the study of the numerical

solutions of the quasi-linear parabolic partial differential equations which arose from the proposed formulation of the latent heat problems, Equation (1.2). The analysis is carried out step by step in the following manner. First, the Laplacian operator, ∇^2, in (1.2a) is formally replaced by a difference operator obtained by employing the common, five-point difference approximation. This procedure reduces the problem to a system of first order, quasi-linear differential equations, which is then approximated to obtain a fundamental, discrete implicit solution. Although this solution is not amenable to any practical computation, it serves as a foundation for generating systematically many practical numerical solutions. In fact, almost all the common numerical methods for solving parabolic, partial differential equations become the special cases of a more general approximation technique. Such a technique can be developed by applying the ideas in the Padé, classical, rational approximation of analytic functions to the approximation of matrix equations.

These techniques (semi-descrete approximation, fundamental discrete and the approximation of matrix equations) are presented below. A glossary of the less familiar terms used in this chapter is covered in Appendix A, as well as a collection of the known theoretical results which are frequently referred to in the following development.

A Semi-Discrete Approximation

Let the temperature field in the continuous region R' be symmetric with respect to one of the co-ordinate axes,

say x_3. Let R" be a connected, open and bounded set in the plane $x_3 = a_3$, where a_3 is a constant. Let Γ" be the boundary of R". Let R"$\subset \mathcal{R}$" where $\mathcal{R}$" is the region $x_1, x_2 \geq 0$. Apply the transformation:

$$x = \frac{x_1}{1 + x_1} , \qquad y = \frac{x_2}{1 + x_2} \tag{3.1}$$

to map the plane region $\mathcal{R}$" into the unit square $\mathcal{R}$ in the x-y plane, R" and Γ" into R and Γ, respectively. Then, the initial-boundary value problem (1.2) for the transformed region R$\subset\mathcal{R}$ becomes:

$$\frac{\partial}{\partial x}\left[P(x,y)\frac{\partial}{\partial x} u(x,y;\tau)\right] + \frac{\partial}{\partial y}\left[Q(x,y)\frac{\partial}{\partial y} u(x,y;\tau)\right]$$
$$= \psi(x,y)\ \varphi\left(u(x,y;\tau)\right)\frac{\partial}{\partial \tau} u(x,y;\tau),\ (x,y)\in R,\ \tau > 0 \tag{3.2a}$$

$$\frac{\partial}{\partial n} u(x,y;\tau) + \bar{\alpha}(x,y)\ u(x,y;\tau) = \bar{\gamma}(x,y;\tau),\ (x,y)\in\Gamma,\ \tau>0 \tag{3.2b}$$

$$u(x,y;0) = G(x,y),\ (x,y)\in R \tag{3.2c}$$

where,

$$\psi(x,y) = g_1 g_2 g_3 \Big/ \left[(1-x)^2(1-y)^2\right] > 0,\ (x,y)\in R$$

$$P(x,y) = \frac{g_1}{g_2 g_3}\left(\frac{1-x}{1-y}\right)^2 > 0,\ (x,y)\in R$$

$$Q(x,y) = \frac{g_2}{g_1 g_3}\left(\frac{1-y}{1-x}\right)^2\left(\frac{a_1}{a_2}\right)^2 > 0,\ (x,y)\in R \tag{3.3}$$

$$g_i,\ 1 \leq i \leq 3 = g_i(x_1,x_2,a_3) \equiv g_i(x,y,\frac{a_1}{a_3}),\ (x,y)\in R$$

$$\bar{\alpha}(x,y) = \frac{\alpha(x,y)}{\beta(x,y)}$$

$$\bar{\gamma}(x,y,\tau) = \gamma(x,y,\tau) \;/\; \beta(x,y)$$

$$\frac{\partial}{\partial n} = (1 - x)^2 \frac{\partial}{\partial x} + (1 - y)^2 \frac{\partial}{\partial y}, \quad (x,y) \in \Gamma$$

The coefficients $\bar{\alpha}$ and $\bar{\gamma}$ arise from the boundary condition

$$K(T)\frac{\partial T}{\partial n} + h(x_1,x_2,T,T_e)(T - T_e) = 0, \quad (x,y) \in \Gamma \tag{3.4}$$

where,

T_e = environmental temperature

$h(x_1,x_2,T,T_e)$ = film coefficient of heat transfer at the surface.

In terms of the dependent variable u and the independent variables x and y, the boundary condition (3.4) becomes

$$(1 - x)^2\frac{\partial u}{\partial x} + (1 - y)^2\frac{\partial u}{\partial y} + \left[\frac{h(x,y,T,T_e)}{\frac{1}{T-T_1}\int_{T_1}^{T} K(T')dT'}\right] u(x,y,t) \tag{3.5}$$

$$= h(x,y,T,T_e)T_e$$

Therefore,

$$\beta(x,y,T) = \frac{1}{T - T_1} \int_{T_1}^{T} K(T')dT' > 0$$

$$\alpha(x,y,T,T_e) = h(x,y,T,T_e) > 0 \tag{3.6}$$

$$\gamma(x,y,T,T_e) = \left[\frac{h(x,y,T,T_e)}{(T - T_1)} \int_{T_1}^{T} K(T')dT'\right] T_e$$

Now, from the physical considerations it can be concluded that:

1. If $h \to 0$, $\partial T/\partial n \to 0$ and consequently $\partial u/\partial n \to 0$.
2. If $h \to \infty$, $T \to T_e$ and therefore $u \to u_e$.
3. If $0 < h < \infty$, $0 < \alpha, \beta, \gamma < \infty$.

The above conditions are obviously equivalent to Equation (1.3). Clearly, β is the average thermal conductivity in the interval T_1 to T, which in general is a weak function of T.

To simplify the treatment of the boundary conditions, throughout this work it is assumed that,

$$\bar{\alpha} = \frac{\alpha}{\beta} = \bar{\alpha}(x,y)$$
$$\bar{\gamma} = \frac{\gamma}{\beta} = \bar{\gamma}(x,y;\tau) \text{ only.} \tag{3.7}$$

The assumption (3.7) is usually justified. However, there are boundary conditions for which (3.7) is a very poor approximation.

Before proceeding with the development of a discrete analog for (3.2), it is instructive to observe the following points:

1. The initial-boundary value problem (3.2) is written for the general, orthogonal, curvilinear, co-ordinate systems, and likewise for its numerical solution.
2. The unit square region $\mathcal{R}$ is a mathematical plane region. It is invariant under any co-ordinate

transformation in (x_1, x_2, x_3) space. Its choice is purely for the convenience it offers in developing a general numerical solution for (3.2).

3. $P(x,y)$, $Q(x,y)$ and $\psi(x,y)$ are all positive functions for $0 \leq x,y \leq 1$. Their exact functional forms depend on the choice of the spatial coordinates in (x_1, x_2, x_3) space. Their functional form, however, is of little concern in the following development.

To develop a semi-discrete solution for (3.2) replace the unit square region $\mathcal{R}$ by a set $\mathcal{R}_h = \mathcal{R}_h(L_1, L_2)$ of a family L_1 of lines parallel to the x axis, and a family of L_2 lines parallel to the y axis. Call the intersection (x_i, y_j), of the ith horizontal line and the jth vertical line the mesh point (i,j). Designate the distance from a mesh point (i,j) to its adjacent mesh points in the direction of increasing x, increasing y, decreasing x, and decreasing y by $h_{i+1} = h_{i+1}(x)$, $k_{j+1} = k_{j+1}(y)$, $h_i = h_i(x)$, and $k_j = k_j(y)$, respectively. The four points adjacent to (x_i, y_j) are, therefore, $(x_i + h_{i+1}, y_j)$, $(x_i - h_i, y_j)$, $(x_i, y_j + k_{j+1})$, and $(x_i, y_j - k_j)$ as shown in Figure 6. Associate with every mesh point (i,j) a rectangular mesh region r_{ij} defined by, $\frac{1}{2}h_i \leq x - x_i \leq \frac{1}{2}h_{i+1}$, $-\frac{1}{2}k_j \leq y - y_j \leq \frac{1}{2}k_{j+1}$, also shown in Figure 6. Let the boundary of the mesh region r_{ij} be c_{ij}. For simplicity assume that R is the union of such rectangles. Designate the set of all points (i,j) which fall in the region R by R_h. As can be

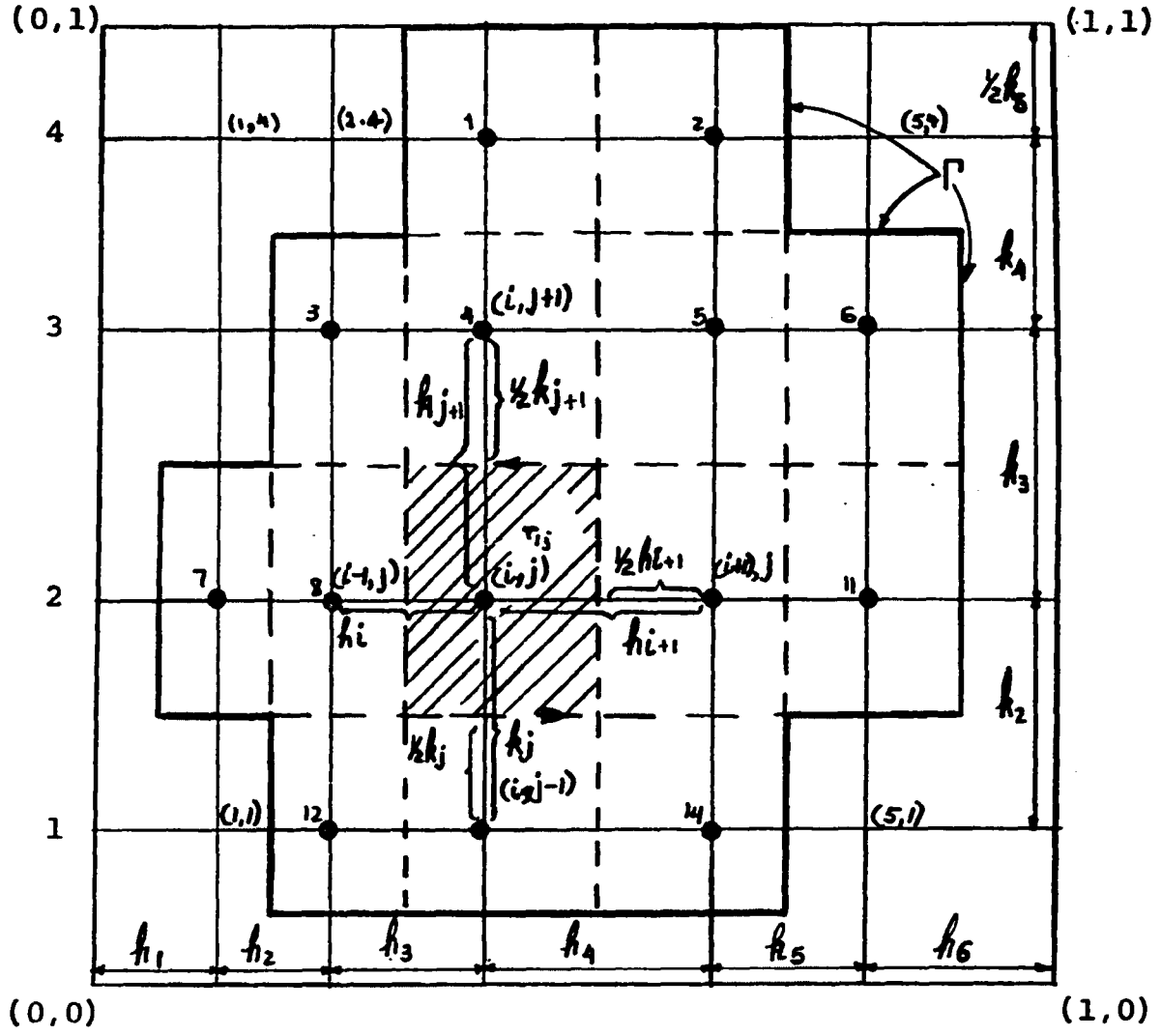


Figure 6. The Unit Square Region $\mathcal{R}$ divided into a Union of Rectangular Mesh Regions. (The Boundary Γ of the Region of Interest is shown by the Heavy Solid Lines.)

seen in Figure 6, all the mesh points (i,j) are interior to R and so do not coincide with Γ. However, Γ may coincide with as many as three sides of the mesh region r_{ij}. Clearly $u(x_i,y_j;\tau) \equiv u_{ij}(\tau)$ is unknown for every mesh point $(i,j)\epsilon R_h$.

Now, by integrating Equation (3.2a) over a mesh region $(i,j)\epsilon R_h$,

$$-\iint_{r_{ij}} \left[\frac{\partial}{\partial x}\left(P(x,y)\frac{\partial}{\partial x}u(x,y;\tau)\right) + \frac{\partial}{\partial y}\left(Q(x,y)\frac{\partial}{\partial y}u(x,y;\tau)\right)\right] dxdy \tag{3.8}$$
$$= -\iint_{r_{ij}} \left[\psi(x,y)\ \varphi\left(u(x,y;\tau)\right)\frac{\partial}{\partial \tau}u(x,y;\tau)\right] dxdy;\ (i,j)\epsilon R_h$$

The surface integral on the left hand side of the above equation can be reduced to a line integral over c_{ij}--the boundary line of r_{ij}--by making use of Green's theorem. Namely:

$$-\oint_{c_{ij}} \left[P(x,y)\frac{\partial}{\partial x}u(x,y;\tau)\right]dy + \oint_{c_{ij}} \left[Q(x,y)\frac{\partial}{\partial y}u(x,y;\tau)\right]dx \tag{3.9}$$
$$= -\iint_{r_{ij}} \left[\psi(x,y)\ \varphi(u)\frac{\partial u}{\partial \tau}\right] dxdy$$

Approximating the above line integral by central differences, rearranging and replacing the surface integral

$$\iint_{r_{ij}} \psi\varphi\ dxdy \qquad \text{with} \qquad \tilde{\psi}_{i,j}\ \varphi_{i,j}\ \frac{du_{ij}}{dt},$$

$$-c_{i,j}\,u_{i-1,j} + a_{i,j}\,u_{i,j} - b_{i,j}\,u_{i+1,j} +$$

$$-f_{i,j}\,u_{i,j-1} + d_{i,j}\,u_{i,j} - e_{i,j}\,u_{i,j+1} = \tilde{\psi}_{i,j}\,\varphi\big(u_{i,j}(t)\big)\frac{du_{i,j}}{dt} + s_{i,j} + \theta_{i,j}, (i,j)\in R_h \tag{3.10}$$

where,

$$c_{i,j} = \frac{2kh}{h_i(h_{i+1}+h_i)}\,P(x_i - \frac{h_i}{2}, y_j)\,\sigma_{i-1,j} = c'_{i,j}\,\sigma_{i-1,j}$$

$$b_{i,j} = \frac{2kh}{h_{i+1}(h_{i+1}+h_i)}\,P(x_i + \frac{h_{i+1}}{2}, y_j)\,\sigma_{i+1,j} = b'_{i,j}\,\sigma_{i+1,j}$$

$$a_{i,j} = \delta_{i-1,j}\,c'_{i,j} + \delta_{i+1,j}\,b'_{i,j}$$

$$f_{i,j} = \frac{2kh}{k_j(k_j+k_{j+1})}\,Q(x_i, y_j - \frac{k_j}{2})\,\sigma_{i,j-1} = f'_{i,j}\,\sigma_{i,j-1}$$

$$e_{i,j} = \frac{2kh}{k_{j+1}(k_j+k_{j+1})}\,Q(x_i, y_j + \frac{k_{j+1}}{2})\,\sigma_{i,j+1} = e'_{i,j}\,\sigma_{i,j+1} \tag{3.11}$$

$$d_{i,j} = \delta_{i,j-1}\,f'_{i,j} + \delta_{i,j+1}\,e'_{i,j}$$

$$\tilde{\psi}_{i,j} = \tfrac{1}{4}\Big[(h_i + h_{i+1})(k_j + k_{j+1})\Big]^{-1} \iint_{r_{ij}} \psi(x,y)\,dxdy \cong \psi(x_i, y_j)$$

$$s_{i,j} = \sigma'_{i-1,j}\,c'_{i,j} + \sigma'_{i+1,j}\,b'_{i,j} + \sigma'_{i,j-1}\,f'_{i,j} + \sigma'_{i,j+1}\,e'_{i,j}$$

$\theta_{i,j}$ = discretization error

$$t = \tau/(kh)$$

$$\sigma_{i,j} = 1 \quad \text{if } (i,j)\in R_h$$
$$= 0 \quad \text{if } (i,j)\notin R_h$$

$$\sigma'_{i,j} = 2\,\bar{\gamma}_{i,j} \Big/ \left[\bar{\alpha}_{i,j} + 2(1-z_{i,j})^2 / \underline{h}_{i,j}\right], \text{ if } (i,j)\in \Gamma'_h$$
$$= 0 \quad \text{otherwise}$$

$$\delta_{i,j} = 1 \quad \text{if } (i,j)\in R_h$$

$$= 2 \Big/ \left[1 + 2(1-z_{i,j})^2 / \underline{h}_{i,j}\right] \quad \text{if } (i,j)\in \Gamma'_h$$
$$= 0 \quad \text{otherwise}$$

$$z_{i,j} = x_{i\pm\frac{1}{2}} \quad \text{if } (i\pm1,j)\in R_h$$
$$= y_{j\pm\frac{1}{2}} \quad \text{if } (i,j\pm1)\in R_h$$

$$\underline{h}_{i,j} = h_{i+1} \quad \text{if } (i-1,j)\in R_h$$
$$= h_i \quad \text{if } (i+1,j)\in R_h$$
$$= k_{j+1} \quad \text{if } (i-1,j)\in R_h$$
$$= k_j \quad \text{if } (i+1,j)\in R_h$$

$$h = \max_i \{h_i\}, \qquad k = \max_j \{k_j\}$$

and Γ'_h is the union of all mesh points $(i,j)\notin R_h$ such that either $(i\pm1,j)\in R_h$ or $(i,j\pm1)\in R_h$.

Clearly, the coefficients $a_{i,j}$, $b_{i,j}$, $c_{i,j}$, $d_{i,j}$, $f_{i,j}$, and $\psi_{i,j}$, have no time dependent entries when $\bar{\alpha} = \bar{\alpha}(x,y)$. On the other hand $s_{i,j}$, and $\theta_{i,j}$, may or may not be time dependent. It may be verified by inspection that,

$$c_{i+1,j} = b_{i,j} \quad \text{for } (i+1,j),\ (i,j)\in R_h$$
$$f_{i,j+1} = e_{i,j} \quad \text{for } (i,j+1),\ (i,j)\in R_h \qquad (3.12)$$

Let R_h be the union of n mesh regions, r_{ij}. Then one can write n equations of the type (3.10) to be solved for

n unknown values of $u_{i,j}(t)$, $(i,j)\epsilon R_h$. This system of equations can be written as

$$C\Phi \frac{du_l(t)}{dt} + (H^{(s)} + V^{(s)})\, u_l(t) = s_l(t) + \theta_l(t)$$
$$u_l(0) = g_l \qquad (3.13)$$

where $u_l(t)$, $s_l(t)$ and $\theta_l(t)$ are n-dimensional vectors whose entries are respectively $u_{i,j}(t)$, $s_{i,j}(t)$ and $\theta_{i,j}(t)$, $(i,j)\epsilon R_h$. C and Φ are both n x n positive diagonal matrices with the diagonal entries $\psi_{i,j}$ and $\varphi_{i,j}$, respectively. $H^{(s)}$ and $V^{(s)}$ are real n x n matrices with positive diagonal entries and non-positive off-diagonal entries. Both $H^{(s)}$ and $V^{(s)}$ have at most three non-zero entries per row. If one orders the mesh points by rows, i.e., from left to right, top to bottom, then $H^{(s)}$ is in addition the direct sum of tri-diagonal symmetric matrices, i.e.,

$$H^{(s)} = \text{diag}\,(H_1^{(s)}, H_2^{(s)}, \ldots H_j^{(s)}, \ldots H_J^{(s)}) \qquad (3.14)$$

where,

$$H_j^{(s)} = \begin{bmatrix} a_{i',j} & -b_{i',j} & & & \\ -b_{i',j} & a_{i'+1,j} & -b_{i'+1,j} & & \\ & \ddots & \ddots & \ddots & \\ & & \ddots & \ddots & -b_{i''-1,j} \\ & & & -b_{i''-1,j} & a_{i'',j} \end{bmatrix} \qquad (3.15)$$

J = number of vertical grid lines in R_h,

$(i'-1,j) \notin R_h$ but $(i',j)\epsilon R_h$

$(i''+1,j) \notin R_h$ but $(i'',j)\epsilon R_h$

If, on the other hand, the mesh points are ordered by columns, i.e., from top to bottom and from left to right, then V is the direct sum of tri-diagonal symmetric matrices. Namely:

$$V^{(s)} = \text{diag}\,(V_1^{(s)}, V_2^{(s)}, \ldots V_i^{(s)} \ldots V_I^{(s)}) \qquad (3.16)$$

where,

$$V_i^{(s)} = \begin{bmatrix} d_{i,j'} & -e_{i,j'} & & & \\ -e_{i,j'} & d_{i,j'+1} & -e_{i,j'+1} & & \\ & \ddots & \ddots & \ddots & \\ & & & -e_{i,j''-1} & \\ & & & -e_{i,j''-1} & d_{i,j''} \end{bmatrix} \quad \begin{matrix} ,(i,j'),(i,j'') \in R_h \\ ,(i,j'-1),(i,j''+1) \notin R_h \end{matrix}$$

and I is the number of columns in R_h. However, one cannot in general make both $H^{(s)}$ and $V^{(s)}$ tri-diagonal. Nevertheless, it is clear that both $H^{(s)}$ and $V^{(s)}$ are similar to tri-diagonal stieltjes matrices.

Let

$$\begin{aligned} V^{(c)} &= C^{-1} V^{(s)} \\ H^{(c)} &= C^{-1} V^{(s)} \\ A^{(c)} &= V^{(c)} + H^{(c)} \end{aligned} \qquad (3.17)$$

Then it is easy to verify that when x_1 and x_2 belong to one of the common co-ordinate systems the entries of $H^{(c)}$ and $V^{(c)}$ satisfy the following relations:

$$\begin{aligned} c'_{i,j} &= \eta_j c'_i & f'_{i,j} &= \eta'_i f'_j \\ b'_{i,j} &= \eta_j b'_i & e'_{i,j} &= \eta'_i f'_j \end{aligned} \qquad (3.18)$$

where the subscripts i and j designate that the corresponding functions depend only on x_i and y_j, respectively. As a result a significant reduction is realized in the number of

coefficients which should be computed and stored when one attempts to solve the problem numerically on a computer. However, the matrices $H^{(c)}$ and $V^{(c)}$ will no longer be symmetric. Instead, it will be shown that each is similar to a non-negative diagonal matrix. For example, if x_1 and x_2 belong to Cartesian co-ordinates, one obtains:

$$\eta_i = 1 \qquad i = 1,2....$$

$$\eta'_j = 1 \qquad j = 1,2....$$

$$c'_i = \frac{2kh}{h_i(h_{i+1} + h_i)} \left(\frac{1 - x_i + \frac{1}{2}h_i}{1 - x_i}\right)^2$$

$$b'_i = \frac{2kh}{h_{i+1}(h_{i+1} + h_i)} \left(\frac{1 - x_i - \frac{1}{2}h_{i+1}}{1 - x_i}\right)^2 \qquad (3.19)$$

$$f'_j = \frac{2kh}{k_j(k_{j+1} + k_j)} \left(\frac{1 - y_j + \frac{1}{2}k_j}{1 - y_j}\right)^2$$

$$e'_j = \frac{2kh}{k_{j+1}(k_{j+1} + k_j)} \left(\frac{1 - y_j - \frac{1}{2}k_{j+1}}{1 - y_j}\right)^2$$

Substituting $A^{(c)}$ in Equation (3.13),

$$\Phi(\mathbf{u}_1(t)) \frac{d\mathbf{u}_1(t)}{dt} + A^{(c)}\mathbf{u}_1(t) = \mathbf{s}_2(t) + \boldsymbol{\theta}_2(t)$$
$$\mathbf{u}_1(0) = \mathbf{g}_1 \qquad (3.20)$$

where,

$$\mathbf{s}_2(t) = C^{-1}\mathbf{s}_1(t)$$
$$\boldsymbol{\theta}_2(t) = C^{-1}\boldsymbol{\theta}_1(t)$$

Before proceeding to study the solutions of Equation (3.20), some additional points concerning the developments leading to it are well worth considering.

Further Remarks and Observations

So far, it was assumed that the thermal properties of the heat conducting medium under consideration were functions of temperature only. In other words $\varphi(u)$ is a unique function of u only. When the physical properties are not uniform throughout the region R, one may assume

$$\varphi_m = \Lambda_m\left(1 + \varphi_{1,m}(u_m) + \varphi_{2,m}(u_m)\right), \quad 1 \le m \le n \tag{3.21}$$

where Λ_m is a positive constant so chosen that the functions $\varphi_{1,m}$, and $\varphi_{2,m}$, $1 \le m \le n$, each has essentially the same functional form for all mesh points in R_h. One then defines the diagonal matrices C and Φ as follows:

$$\begin{aligned} C &= \text{diag } (\psi_1\Lambda_1, \ldots, \psi_m\Lambda_m, \ldots \psi_n\Lambda_n) \\ \Phi &= \text{diag } (\varphi_{1,1} + \varphi_{2,1}, \ldots \varphi_{1,n} + \varphi_{2,n}) + I \end{aligned} \tag{3.22}$$

where I is the identity matrix. As before, one would require that,

$$0 \le \varphi_{1,m} + \varphi_{2,m} \le M \tag{3.23}$$

where M is a positive constant independent of $u_m(t)$. Further reduction in the number of the computed coefficients of the matrix $A^{(C)}$ can be realized if, instead of Equation (3.17), one lets,

$$A = C^{-\frac{1}{2}}(H^{(s)} + V^{(s)})\, C^{-\frac{1}{2}} = H + V$$

$$\mathbf{u}(t) = C^{\frac{1}{2}}u_1(t),\ \mathbf{s}(t) = C^{-\frac{1}{2}}s_1(t),\ \boldsymbol{\theta}(t) = C^{-\frac{1}{2}}\theta_1(t) \tag{3.24}$$

where A is now a symmetric matrix and the matrix C is defined by Equation (3.22).

It can be shown (24, 36) that the n-dimensional vector, $\boldsymbol{\theta}$, arising from the discretization of the space co-ordinates satisfies,

$$\|\boldsymbol{\theta}(t)\| = O(h^2 + k^2),\ \text{as } h,k \to 0 \tag{3.25}$$

where h and k are defined by Equation (3.11). Substituting (3.24) in (3.20)

$$\Phi(\mathbf{u})\frac{d\mathbf{u}(t)}{dt} + A\mathbf{u}(t) = \mathbf{s}(t) + \boldsymbol{\theta}(t)$$
$$\mathbf{u}(0) = \mathbf{g} \tag{3.20'}$$

It should be noted that by the above procedure the complex nonlinear problem, Equation (1.8), is reduced to a system of first order differential equations without appreciable loss of the generality. Any general method for solving (3.20) is the general solution of the two-dimensional problems in any composite medium with more than one transition temperature. It is readily seen that in arriving at (3.20') no assumptions were made on the possible shape and the direction of movements of the interface (s). However, (3.20) cannot be solved directly for the position of the interface (s). This information should be obtained from the knowledge of the temperature distribution in the medium under consideration.

When the region R is a union of rectangles and half rectangles, and the mesh spacing is sufficiently fine, a slight modification in the coefficients of the matrix A can take care of the half rectangle mesh regions which, of course, are adjacent to the boundary of R. Such modifications are well explained by Forsythe and Wasow (36) and Varga (77). The simplest, and perhaps equally accurate method to deal with these mesh regions is, however, to multiply the corresponding $\varphi_{i,j}$ by the ratio of the area of the triangular mesh region and the area of the rectangular mesh region in which the mesh point (i,j) is situated.

It can be seen by inspection of Equation (3.11) that all the off-diagonal entries of the n x n matrix A are time independent. For the mesh points adjacent to the boundary the diagonal entries of A = A(t) are dependent on t when $\tilde{\alpha}_{i,j}$ is a function of time. In such cases one may write

$$A(t) = A + D(t)$$

where A is a constant matrix and D(t) is a time dependent diagonal matrix. Clearly D(t) has just a few non-zero diagonal entries. In the subsequent developments it is assumed that D(t) = 0, i.e., $\bar{\alpha}_{i,j} \neq \bar{\alpha}_{i,j}(t)$ for $(i,j) \in \Gamma_h'$. However, most of the results are applicable to the case of time dependent $\tilde{\alpha}_{i,j}$.

If one numbers the mesh point $(i,j) \in R_h$, by a natural ordering, i.e., from left to right and top to bottom, Figure 6, then the directed graph, G(A), of the n x n matrix A is strongly connected (77) so that the matrix $A^{(s)}$ is

irreducible. It can be verified by inspection of Equation (3.11) that for $A^{(s)} = (a^{(s)}_{i,j})$,

$$\left| a^{(s)}_{i,i}\ (t) \right| \leq \sum_{\substack{j=1 \\ j \neq i}}^{n} \left| a^{(s)}_{i,j} \right|, \quad 1 \leq i \leq n$$

with the strict inequality being true for at least one $a^{(s)}_{i,i}$, $1 \leq i \leq n$. It follows that $A^{(s)}$ is an irreducibly diagonally dominant, real n x n matrix with positive diagonal entries, so that by Lemma A-2, the matrix $A^{(s)}$ is non-singular, and the eigenvalues, λ_i, $1 \leq i \leq n$ of $A^{(s)}$ satisfy,

$$\mathcal{R}\, \lambda_i > 0 \quad \text{for all} \quad 1 \leq i \leq n \tag{3.26}$$

In addition, since $A^{(s)}$ is symmetric, then its eigenvalues are real and, by Equation (3.26), positive, so that $A^{(s)}$ is positive definite. To show that $A^{(c)}$ and A are also positive definite, let $\mathbf{y}$ be any non-zero real vector. Then,

$$(A\mathbf{y},\mathbf{y}) = (C^{-\frac{1}{2}}A^{(s)}C^{-\frac{1}{2}}\mathbf{y},\mathbf{y}) = (A^{(s)}C^{-\frac{1}{2}}\mathbf{y},C^{-\frac{1}{2}}\mathbf{y}) = (A^{(s)}\mathbf{y}_1,\mathbf{y}_1) > 0$$

where $\mathbf{y}_1 = C^{-\frac{1}{2}}\mathbf{y}$, and $(A^{(s)}\mathbf{y}_1,\mathbf{y}_1) > 0$ because $A^{(s)}$ is positive definite, and so is A. Now, since the matrix $C^{\frac{1}{2}}\, A^{(c)}C^{-\frac{1}{2}} = C^{-\frac{1}{2}}A^{(s)}C^{-\frac{1}{2}} = A$ has the same eigenvalues as those of $A^{(c)}$, then $A^{(c)}$ is also positive definite.

A Fundamental Discrete Solution

The system of differential equations, Equation (3.20'), can be directly solved on an analog computer when n, the number of equations involved, is less than twenty (84). For $n > 20$, the required capacity of the analog computer exceeds

the capacity of the commercially available analog computers. Although it is possible to solve Equation (3.20') by a digital analog computer for n >> 20, the common method is to reduce Equation (3.20') to a system of algebraic equations by discretizing the time co-ordinates and then solving this system on a suitable digital computer (73).

In the following, the continuous solution of Equation (3.20') is studied first, because of its important role in the understanding of the accuracy of the various numerical procedures suitable for solving such problems. Then, a fundamental discrete approximation of (3.20') is developed, which serves as a basis for generating several possible numerical methods. A unified treatment is then given to all these methods.

To proceed with the analysis, let us assume first that $\mathbf{s}$ and $\boldsymbol{\theta}$ are time independent, and let

$$\mathbf{v}(t) = \mathbf{u}(t) - A^{-1}(\mathbf{s} + \boldsymbol{\theta}) \tag{3.27}$$

Then (3.20') becomes

$$\begin{aligned} &\frac{d\mathbf{v}(t)}{dt} + \Phi^{-1}\big(\mathbf{u}(t)\big)\, A\mathbf{v}(t) = \mathbf{o} \\ &\mathbf{v}(0) = \mathbf{v}_o = \mathbf{u}_o - A^{-1}(\mathbf{s} + \boldsymbol{\theta}) \end{aligned} \tag{3.28}$$

or alternatively,

$$\begin{aligned} &\frac{d\mathbf{v}(t)}{dt} + A\mathbf{v}(t) = \mathbf{f}\big(t,\mathbf{v}(t)\big)\ ,\ t \geq t_o \geq 0 \\ &\mathbf{v}(t_o) = \mathbf{v}_o \end{aligned} \tag{3.29}$$

where,

$$\mathbf{f}(t,\mathbf{v}(t)) = \left[I - \Phi^{-1}(\mathbf{u}(t))\right] A\mathbf{v}(t)$$

Multiplying both sides of (3.29) by $\exp(tA) = \sum_{i=0}^{\infty} (tA)^i/i!$, integrating and rearranging,

$$\mathbf{v}(t) = e^{-tA}\mathbf{v}(t_o) + \int_{t_o}^{t} e^{-(t-t')A}\mathbf{f}(t',\mathbf{v}(t'))\, dt', \quad t > t_o \qquad (3.30)$$

Clearly, (3.30) is a solution of (3.29). Before proceeding any further, it is necessary to demonstrate that (3.30) exists, and furthermore, if the system (3.29) has any other solution $\mathbf{W}(t;\mathbf{v}_o,t_o)$ such that $\mathbf{W}(t_o;\mathbf{v}_o,t_o) = \mathbf{v}_o$ then it must be equal to $\mathbf{v}(t)$ given by (3.30). The criteria for existence and uniqueness of a bounded solution for the systems of the type (3.29) are extensively discussed by several authors, e.g., La Salle and Lefschetz (51), Bellman (3), Cesari (13), Coddington and Levinson (16) and Wintner (83). For the case of (3.29) the fact that A has only non-negative eigenvalues and $(I - \Phi^{-1})$ is a positive diagonal matrix, which is bounded in norm, ensures the existence of a solution $\mathbf{v}(t;\mathbf{v}_o,t_o)$ for $t\epsilon[t_o,\infty]$ when $\|\mathbf{v}_o\|$ is sufficiently small. A Lipschitz condition of the type

$$\left\|\Phi^{-1}(\mathbf{u}_1)\, A\mathbf{v}_1 - \Phi^{-1}(\mathbf{u}_2)\, \mathbf{v}_2\right\| \leq K\left\|\mathbf{v}_1 - \mathbf{v}_2\right\| \text{ for all } t \geq t_o$$

where K is a positive constant, guarantees uniqueness of the solution $\mathbf{v}(t;\mathbf{v}_o,t_o)$ and also the continuity with respect to the initial vector $\mathbf{v}_o$ (13).

Clearly, the solution (3.30) is valid if A has no time dependent entries. When A = A(t), then (3.30) is the solution of (3.29) if, and only if, A(t) and dA(t)/dt commute. This last condition can hardly be satisfied.

Most recently Thompson (70) has studied the difference approximation of the quasi-linear equation,

$$\frac{d\mathbf{v}(t)}{dt} + A(t)\ \mathbf{v}(t) = \mathbf{f}(t,\mathbf{v}) \qquad \mathbf{v}(0) = \mathbf{v}_o \tag{3.31}$$

His analysis is an extension of the fundamental work of Lax and Richtmyer (53) on the equivalence of stability (in the sense of Lax and Richtmyer) and convergence of a consistent numerical procedure for solving systems of homogenous first order differential equations. Thompson first develops a generalized solution for (3.31) and then studies the difference approximations of such generalized solutions. The following Lemma 3.1 summarizes his results concerning this generalized solution. First, however, a definition will be given.

Let $\mathfrak{B}$ denote a Banach space and $\mathfrak{I}$ a finite interval [0,T]. Let $\mathfrak{C}$ denote the class of strongly continuous mapping from $\mathfrak{I}$ into $\mathfrak{B}$. Then:

Definition 3.1. A mapping $\mathbf{u}(.)$ from $\mathfrak{I}$ into $\mathfrak{B}$ will be called a generalized solution to (3.31) provided $\mathbf{u}(.) \in \mathfrak{C}$ and

$$\mathbf{u}(t) = \mathbf{E}(t)\ \mathbf{u}_o + \int_o^t \mathbf{E}(t-\eta)\ \mathbf{f}\big(t,\mathbf{u}(\eta)\big)\ d\eta$$

Lemma 3.1. Let $\{E(t)\}$, $t \geq 0$ be strongly continuous one-parameter semi-group of bounded linear operators from $\mathfrak{B}$ into $\mathfrak{B}$ such that $E(0) = I$. Let $f(t,v)$ be strongly continuous, and let there exist a positive number M such that $\|f(t,v_1) - f(t,v_2)\|_m \leq M\|v_1 - v_2\|_m$. Then, there is one, and only one, generalized solution to (3.31). Furthermore, if a solution to (3.31) exists*, it must be the generalized solution. [(70), Theorem 3.1 and 3.2].

Clearly, $\{\exp(-tA)\}$ is a semi-group of the above Lemma. If the n x n matrix $X(t)$ is the solution of (2),

$$\frac{dX(t)}{dt} = A(t)\ X(t)$$

$$X(o) = I$$

Then the unique solution of (3.31) may be expressed by

$$v(t) = X(t)\ v_o + \int_o^t X(t - \eta)\ f(\eta,v)\,d\eta,\quad t > 0 \qquad (3.32)$$

Here again $\{X(t)\}$ is a semi-group of Lemma 3.1. The importance of Lemma 3.1 is in justifying a generalized solution for all problems of the type (3.31). It is then possible to study the various difference approximations of (3.31), regardless of the functional form of the operator $E(t)$.

Returning to the system (3.29), it is evident from the physical nature of the problem that one would require

---

*See Hille and Phillips (42), Theorem 3.3.2 for the existence theorems concerning (3.29).

$$\mathbf{v}(t) \to \mathbf{o} \qquad \text{uniformly as } t \to \infty,$$

i.e., the solution $\mathbf{v}(t) = \mathbf{o}$ as $t \to \infty$. Let, for an interval $0 < t_{j-1} \le t \le t_j$,

$$\tilde{\Phi}_j = \Phi(u(\xi)) \quad , \; t_{j-1} \le \xi \le t_j$$

$$Q_j = \tilde{\Phi}_j^{-1} A \tag{3.33}$$

$$\Sigma = \tilde{\Phi}_j^{-1}\, \Phi - I$$

$$\beta(t,\mathbf{v}) = (\tilde{\Phi}_j^{-1}\, \Phi - I)\Phi^{-1} A\mathbf{v}(t) = -\Sigma \frac{d\mathbf{v}(t)}{dt}$$

$$= (\beta_1(t,\mathbf{v}),\ \beta_2(t,\mathbf{v}),\ \ldots,\ \beta_n(t,\mathbf{v})) \quad , \; t_{j-1} \le t \le t_j$$

Substituting the above quantities in (3.29), multiplying both sides of the resulting equation by $Z(-t) = \exp[-(t_{j-1} - t)Q_j]$ integrating and rearranging,

$$\mathbf{v}(t_j) = Z(t_j)\ \mathbf{v}(t_{j-1}) + \int_{t_{j-1}}^{t_j} Z(-\eta)\ \beta(\eta,\mathbf{v})d\eta \tag{3.34}$$

$$= Z_j\ \mathbf{v}(_{j-1}) + \alpha_j$$

where,

$$Z_j = \exp(-r_j Q_j)$$

$$r_j = t_j - t_{j-1} > 0$$

$$\alpha_j = \int_{t_{j-1}}^{t_j} \exp\left[(\eta - t_{j-1})Q_j\right]\ \beta(\eta,\mathbf{v})d\eta$$

Clearly for a set of positive parameters,

$$\mathcal{S} = (r_j \,|\, r_j > 0,\ j = 1,2.....)$$

(3.34) may also be expressed by

$$\mathbf{v}(t_m) = \sum_{i=1}^{m} \prod_{j=i}^{m} Z_j \quad \boldsymbol{\alpha}_i + \prod_{j=1}^{m} Z_j \mathbf{v}_o \tag{3.35}$$

Some general properties of the operator Z_j, $j = 1,2....$ deserve further attention. First, because $-Q_j$ is an essentially positive matrix in the sense described in the glossary (Appendix A), then by Lemma A-4,

$$Z_j > 0 \qquad \text{for all } r_j > 0,$$

i.e., all entries of Z_j are strictly positive real numbers. Consequently, the product

$$\prod_{j=i}^{m} Z_j$$

is also a positive matrix for all $r_j > 0$, $1 \leq j \leq m$ and all $m \geq 1$, so that every entry of the vector solution $\mathbf{v}(t_m)$ is connected through positive coefficients to all entries of $\mathbf{v}_o$, and all entries of the vectors $\boldsymbol{\alpha}_j$, for $1 \leq j \leq m$. This behavior is, of course, the well known characteristic of the solution of the heat equations (35).

Theorem 3.1. Let A be a positive definite matrix and $\tilde{\Phi}$ a positive diagonal matrix. Then all the eigenvalues $\sigma_i(Z)$, $1 \leq i \leq n$ of the matrix $Z(r) = \exp(-r\tilde{\Phi}^{-1}A)$ are positive and satisfy, $0 < \sigma_i(Z) < 1$ for all $1 \leq i \leq n$, and all $r > 0$. Furthermore, let $\|Z(r)\|$ be the spectral norm of the n x n matrix $Z(r)$, then,

1) $\|Z(r)\| < 1$ for $r > 0$

2) $\|Z(r + \Delta r)\| / \|Z(r)\| < 1$ for $\Delta r, r > 0$.

Proof: let $Q = \tilde{\Phi}^{-1}A$ and $Q^{(s)} = \tilde{\Phi}^{-\frac{1}{2}}A\tilde{\Phi}^{-\frac{1}{2}}$. Because A is positive definite, then for any non-zero and real vector $\mathbf{y}$ one can write,

$$(Q^{(s)}\mathbf{y},\mathbf{y}) = (\tilde{\Phi}^{-\frac{1}{2}}A\tilde{\Phi}^{-\frac{1}{2}}\mathbf{y},\mathbf{y}) = (A\tilde{\Phi}^{-\frac{1}{2}}\mathbf{y},\tilde{\Phi}^{-\frac{1}{2}}\mathbf{y}) > 0$$

It follows that $Q^{(s)}$ is positive definite and consequently $Q = \tilde{\Phi}^{-\frac{1}{2}}Q^{(s)}\tilde{\Phi}^{+\frac{1}{2}}$ is also positive definite. Now, the necessary and sufficient condition for Z(r) to be convergent is that $\rho(Z)$, the spectral radius of Z(r), be less than unity. To prove that $\rho\big(Z(r)\big) < 1$ for $r > 0$, let $\mathbf{x}_i$ be an eigenvector of Q and σ_i its corresponding eigenvalue. Then Z(r) has an eigenvector $\mathbf{x}_i$ and an eigenvalue $e^{-r\sigma_i}$ (6). Let the n positive eigenvalues of the n x n matrix Q be

$$0 < a = \sigma_1 \leq \sigma_2 \ldots . \leq \sigma_n = b$$

then

$$\rho\big(Z(r)\big) = \max_{1\leq i\leq n} \{e^{-r\sigma_i}\} = e^{-ra} < 1$$

To prove the last part of the above theorem, one notes that (77)

$$\|Z(r)\|^2 = \rho\big(Z^*(r)Z(r)\big)$$
$$= \rho\big(\exp(-rQ^*)\ \exp(-rQ)\big)$$

where $\rho(B)$ is the spectral norm of the n x n matrix B, and B^* is the transposed conjugate of B. On the other hand, since

$Z(r)$ is non-singular, then $Z^{-1}(r) = Z(-r)$. Let $\sigma_i(Z^*Z)$, $1 \le i \le n$ be the eigenvalues of the symmetric and positive definite matrix $Z^*(r)\ Z(r)$. Then,

$$\sigma_i\left(Z^*(r)\ Z(r)\right) = \frac{1}{\sigma_i\left(Z^*(-r)\ Z(-r)\right)}\ ,\quad 1 \le i \le n$$

where, $Z(-r) = \exp(rQ)$. Let $\mathbf{y}$ be any non-zero real vector such that $(\mathbf{y},\mathbf{y}) = 1.0$. Then

$$\left(Z^*(-r)\ Z(-r)\mathbf{y},\mathbf{y}\right) = 1 + \left(\sum_{i=1}^{\infty} \frac{(rQ^*)^i}{i!} \cdot \sum_{j=1}^{\infty} \frac{(rQ)^j}{j!}\mathbf{y},\mathbf{y}\right)$$

$$= 1 + (S\mathbf{y},\mathbf{y})$$

where

$$S \equiv \sum_{i=1}^{\infty} \frac{(rQ^*)^i}{i!} \sum_{j=1}^{\infty} \frac{(rQ)^j}{j!}$$

Now if S is positive definite, then $(S\mathbf{y},\mathbf{y}) = |\delta| > 0$ and consequently

$$\left\|Z(r)\right\| = \{\rho\left(Z^*(r)\ Z(r)\right)\}^{\frac{1}{2}} = \{\max_{1\le i\le n} \left|\sigma_i\left(Z^*(r)\ Z(r)\right)\right|\}^{\frac{1}{2}}$$

$$= \{\max_{1\le i\le n} \left|\frac{1}{\sigma_i\left(Z^*(-r)\ Z(-r)\right)}\right|\}^{\frac{1}{2}} < 1$$

To prove that the above relation holds, one observes that S is a matrix polynomial of the type

$$\sum_{m,n=1}^{\infty} a_{m,n}(Q^*)^m\ Q^n$$

where $a_{m,n} > 0$ for all $r > 0$. Therefore, if $m \le n$, and $\mathbf{y}$ is

any non-zero vector, for any positive definite real matrix Q one can write:

$$\left((Q^*)^m\, Q^n\, \mathbf{y},\mathbf{y}\right) = (Q^{n-m}.\ Q^m\mathbf{y},\ Q^m\mathbf{y})$$

$$= (Q^{n-m}\ \mathbf{z},\mathbf{z}) > 0$$

where $\mathbf{z} = Q^m\mathbf{y}$. The same is true if $m > n$. Thus S is positive definite for all $r > 0$.

The above theorem also implies that for a set of m positive parameters $r_j > 0$, $1 \le j \le m$, and a positive and finite interval [a,b] such that

$$t_i = \sum_{j=1}^{i} r_j \qquad 0 < i \le m, \quad t_i \in [a,b]$$

$$\mathbf{v}(t_m) = \lim_{m \to \infty} \prod_{j=1}^{m} Z_j\ \mathbf{v}(t_o)$$

for sufficiently small $\|\mathbf{v}_o\|$. Therefore,

$$\bar{\mathbf{v}}(t_m) = \prod_{j=1}^{m} Z_j\ \mathbf{v}_o$$

formally approximates $\mathbf{v}(t_m)$. It is evident that $\bar{\mathbf{v}}(t_m)$ is the unique solution of the system,

$$\frac{d\bar{\mathbf{v}}(t)}{dt} + Q\bar{\mathbf{v}}(t) = \mathbf{o} \qquad t_{m-1} \le t \le t_m \qquad (3.36)$$

for the initial vector $\bar{\mathbf{v}}(t_{m-1})$.

Corollary 1. The solution $\bar{\mathbf{v}}(t_m) = \prod_{j=1}^{m} Z(r_j)\mathbf{v}_o$ is uniformly

bounded in norm (i.e., spectral norm) for all values of $r_j > 0$, $1 \geq j \geq m$, and for all $\|v_o\|$ sufficiently small. Furthermore, $\bar{v}(t_m)$ approximates $v(t_m)$, the solution of (3.29), such that,

1) $\bar{v}(t_m) \to v(t_m) \to 0$ as $t_m \to \infty$, $m \to \infty$.

2) Let $\bar{\epsilon}(t_m) = v(t_m) - \bar{v}(t_m)$, and $\alpha_j = \left(Z^{-1}(r_j) - I\right)\delta_j$, then,

$$\|\bar{\epsilon}(t_m)\| < \max_{1\leq j\leq m} \{\|\delta_j\|\} = \|\delta_K\| = O((\Delta\tau_K)^2),$$

where $\Delta\tau_K = khr_K$ [See (3.11)].

Proof: From Theorem 3.1, one concludes that $\|Z(r_j)\| < 1$ for all $r_j > 0$, $1 \leq j \leq m$. Therefore, $\|\bar{v}(t_j)\| = \|Z(r_j)\,\bar{v}(t_{j-1})\| \leq \|Z(r_j)\|\,\|\bar{v}(t_{j-1})\| < \|\bar{v}(t_{j-1})\|$, and $\bar{v}(t_j)$ is uniformly bounded in the spectral norm. From (3.35) one obtains,

$$\bar{\epsilon}(t_m) = v(t_m) - \bar{v}(t_m) = \sum_{i=1}^{m} \prod_{j=1}^{m} Z(r_j)\alpha_i$$

$$= \sum_{i=1}^{m} \prod_{j=i+1}^{m} Z(r_j)\left(I - Z(r_i)\right)\delta_i$$

and consequently,

$$\|\bar{\epsilon}(t_m)\| \leq \left\|\sum_{i=1}^{m} \prod_{j=i+1}^{m} Z(r_j)\left(I - Z(r_i)\right)\right\| \max_{1\leq i\leq n} \{\|\delta_i\|\}$$

$$= \left\|I - \prod_{j=1}^{m} Z(r_j)\right\| \cdot \|\delta_K\| < \|\delta_K\|$$

where,

$$\|\delta_K\| = \max_{1\leq i\leq n} \{\|\delta_i\|\}$$

It was observed before that $\rho\left(Z(r)\right) < 1$ for all $r > 0$. Thus the series $\left[I - Z(r_j)\right]^{-1} = I + Z(r_j) + Z^2(r_j) + \ldots$ is convergent for all $r_j > 0$ [(77), Theorem 3.7], so that δ_j exists for all $r_j > 0$, when α_j exists. Now, let

$$e^{-r_j a_j} = \left\| Z(r_j) \right\|, \text{ then } 0 \leq a_j \leq \sigma_1(Q_j)$$

and

$$\left\| \left[I - Z(r_j)\right]^{-1} \right\| \leq 1/\left(1 - e^{-r_j a_j}\right) = \frac{e^{r_j a_j}}{e^{r_j a_{j-1}}} \qquad (3.37)$$

Assume that $\Sigma dv/d\tau \leq M_1 \Delta\tau$ where M_1 is a positive number independent of $\Delta\tau$, and $\Delta\tau = (t - t_{j-1})kh$. Then,

$$\left\| \delta_j \right\| = \left\| \left[I - Z(r_j)\right]^{-1} \int_0^{r_j} Z(r_j - \eta)\ \Sigma \frac{dv}{d\eta}\, d\eta \right\|$$

$$\leq \frac{M_1}{1 - e^{r_j a_j}} \int_0^{\Delta\tau_j} \left\| Z(r_j - \eta) \right\| \Delta\tau\, d(\Delta\tau),\ \Delta\tau_j > 0$$

$$\leq \tfrac{1}{2} \frac{M_1}{1 - e^{-r_j a_j}} (\Delta\tau_j)^2 \ , \quad 1 \geq j \geq m \qquad (3.38)$$

$$= M(\Delta\tau_j)^2$$

where $M = \tfrac{1}{2}M_1/(1 - e^{-r_j a_j})$. Consequently, for a fixed $\infty > r_j > 0$,

$$\left\| \delta_j \right\| = o\left((\Delta\tau_j)^2\right) \text{ as } \Delta\tau_j \to 0,\ 1 \leq j \leq m$$

and also

$$\left\| \delta_K \right\| = o\left((\Delta\tau_K)^2\right) \text{ as } \Delta\tau_K \to 0,\ \infty > r_K > 0 \qquad (3.39)$$

It was assumed throughout the above development that dv/dt exists and is bounded. Because $v(t)$ is the exact

representation of a heat conduction phenomena, $d\mathbf{v}/dt$ exists for all physically possible boundary conditions. One may doubt, however, that when the temperature at the exposed boundary surface is changed abruptly, M_1 may become extremely large. However, none of the entries of $\mathbf{v}(t)$ fall on such a boundary, but rather, some distance away from it so that any sudden temperature change at the boundary surface is sufficiently dampened before it reaches the mesh points adjacent to the exposed boundary.

Recall that $\mathbf{v}(t_m) = \mathbf{u}(t_m) - A^{-1}(\mathbf{s} + \boldsymbol{\theta})$, and therefore,

$$\bar{\mathbf{v}}(t_m) = \mathbf{u}(t_m) - A^{-1}(\mathbf{s} + \boldsymbol{\theta}) - \tilde{\boldsymbol{\epsilon}}_m \tag{3.40}$$

Let

$$\bar{\mathbf{u}}(t_m) = \bar{\mathbf{v}}(t_m) + A^{-1}(\mathbf{s} + \boldsymbol{\theta}) \tag{3.41}$$

and

$$\tilde{\mathbf{u}}(t_m) = Z(r_m)\left[\tilde{\mathbf{u}}(t_{m-1}) - A^{-1}\mathbf{s}\right] + A^{-1}\mathbf{s}$$

Then it is clear that

$$\tilde{\mathbf{u}}(t_m) = \prod_{j=1}^{m} Z(r_j)\, \mathbf{u}_o + \left[I - \prod_{j=1}^{m} Z(r_j)\right] A^{-1}\mathbf{s} \tag{3.42}$$

and therefore,

$$\tilde{\boldsymbol{\epsilon}}(t_m) = \bar{\mathbf{u}}(t_m) - \tilde{\mathbf{u}}(t_m) = \left[I - \prod_{j=1}^{m} Z(r_j)\right] A^{-1}\boldsymbol{\theta} \tag{3.42'}$$

Thus, from (3.25) and (3.39) one immediately concludes that

$$\left\| \tilde{\boldsymbol{\epsilon}}(t_m) \right\| = O(h^2 + k^2)$$

and

$$\left\| \mathbf{u}(t_m) - \tilde{\mathbf{u}}(t_m) \right\| \le \left\| \tilde{\boldsymbol{\epsilon}}(t_m) \right\| + \left\| \bar{\boldsymbol{\epsilon}}(t_m) \right\| = O\left((\Delta r_K)^2\right) + O(h^2 + k^2)$$

When $\mathbf{s}$ is time dependent, let the approximate solution $\tilde{\mathbf{u}}(t_m)$ be defined by

$$\tilde{\mathbf{u}}(t_m) = Z(r_m)\left[\tilde{\mathbf{u}}(t_{m-1}) - A^{-1}\mathbf{s}(t_m - \frac{r_m}{2})\right] + A^{-1}\mathbf{s}(t_m - \frac{r_m}{2}) \quad (3.43)$$

or

$$\tilde{\mathbf{v}}(t_m) = \tilde{\mathbf{u}}(t_m) - A^{-1}\mathbf{s}(t_m - \tfrac{1}{2}r_m) = Z(r_m)\,\bar{\mathbf{v}}(t_{m-1}) \quad (3.43')$$

Then one can state the following:

Corollary 2. Let $\mathbf{s}$ be time dependent and $d\mathbf{s}(t)/dt$ exist. Then, under the hypotheses of corollary 1, the approximate solution (3.43') is uniformly bounded in norm for all sufficiently small $\mathbf{u}_o$ and $\mathbf{s}$. Furthermore, $\tilde{\mathbf{u}}(t_m)$ is a second order correct approximation of $\mathbf{u}(t_m)$, the solution of (3.20'), i.e.,

$$\|\tilde{\epsilon}_m\| = \|\mathbf{u}(t_m) - \tilde{\mathbf{u}}(t_m)\| = O\left((\Delta\tau_K)^2\right) + O(h^2 + k^2)$$

The proof of the first part of the above corollary immediately follows from Theorem 3.1 and Corollary 1. Defining $\mathbf{v}(t)$ and $\boldsymbol{\beta}(t,\mathbf{v}(t)$ by the following relation:

$$\mathbf{v}(t) = \mathbf{u}(t) - A^{-1}\mathbf{s}(\xi)$$

$$\boldsymbol{\beta}(t,\mathbf{v}) = -(\tilde{\Phi}^{-1}\,\Phi - I)\,\frac{d\mathbf{v}(t)}{dt} + \tilde{\Phi}^{-1}\,\mathbf{s}(t) - \tilde{\Phi}^{-1}\,\mathbf{s}(\xi) \quad (3.44)$$

where $t_{j-1} \le \xi \le t_j$ for all $j = 1,2,\ldots,$ it is easy to show that here again $\boldsymbol{\beta} \le M_1\,(\tau - \tau_{j-1})$. Thus, all the results of Theorem 3.1 and Corollary 1 follow.

We shall refer to $\tilde{\mathbf{u}}(t)$ as the <u>fundamental discrete solution</u> of the system (3.20'). It is evident that any stable

numerical procedure for solving (3.43) which agrees up to m^{th} terms in t with $\tilde{\mathbf{u}}(t)$ is an mth order approximation of $\tilde{\mathbf{u}}(t)$, but at most it is only second order approximation of $\mathbf{u}(t)$. Therefore, for $m > 2$, the overall order of approximation is not further improved.

As far as mathematical analysis is concerned, the fundamental discrete solution (3.43) has many attractive properties. But unfortunately when n is large this solution is not amendable to any practical computation. The reason is that computation of a power series of large matrices requires a storage capacity far beyond that of the largest, commercially available, automatic computers. For the problem in hand the situation is much worse because of an additional iterative procedure which arises from the nonlinearity of the problem. One might ask why, if the solution (3.43) is not a practical numerical method for solving the problem, it was necessary to study its properties at all. The answer is that (3.43) serves as the foundation of many practical solutions. In other words, it is easy to derive most of the commonly recommended numerical methods by applying a simple approximation technique to approximate the exponential operator $Z(r_j)$. In this manner it is possible to apply a unified treatment for studying the stability and the rate of convergence of these derived approximation methods. All these points were observed by Varga (76) in solving the homogenous matrix differential equation

$$\frac{d\mathbf{v}(t)}{dt} + A\mathbf{v}(t) = \mathbf{o}$$

The attempt here is to demonstrate that a similar analysis is adaptable to the solution of (3.20').

As a consequence of Corollary 2, one observes that if $\tilde{\Phi}_j = \Phi\left(\tilde{u}(t_{j-1})\right)$, then $\beta(t,v)$ is at least first order correct in τ, so that the solution (3.43) is second order correct in τ. Thus, for a second order correct approximation a predictor corrector scheme is not necessary. However, the absolute value of the error is substantially reduced if

$$\tilde{\Phi}_j = \Phi\left(\tilde{u}(t_j - \tfrac{1}{2}r_j)\right)$$

is used in (3.43). To obtain $\tilde{\Phi}_j$ one would, of course, require a predictor-corrector scheme of the type:

1. Predictor

$$\begin{aligned}\tilde{v}(t_m - \tfrac{1}{2}r_m) &= Z(\tfrac{1}{2}r_m)\ \tilde{v}(t_{m-1}) \\ &= \exp\left[-\tfrac{1}{2}r_m\ \Phi\left(\tilde{u}(t_{m-1})\right)\right]\ \tilde{v}(t_{m-1})\end{aligned} \tag{3.44a}$$

2. Corrector

$$\begin{aligned}\tilde{v}(t_m) &= Z(r_m)\ \tilde{v}(t_{m-1}) \\ &= \exp\left[-r_m\ \Phi\left(\tilde{u}(t_m - \tfrac{1}{2}r_m)\right)\right]\ \tilde{v}(t_{m-1})\end{aligned} \tag{3.44b}$$

where,

$$\tilde{v}(t_j) = \tilde{u}(t_j) - A^{-1}s(t_j - \tfrac{1}{2}r_j) \tag{3.45}$$

Matrix Approximation for $\exp(-r_j Q_j)$

Consider an analytical scaler function f(z). One may expand f(z) in the neighborhood of the origin to get,

$$f(z) = a_o + a_1 z + a_2 z^2 + \ldots. \tag{3.46}$$

f(z) can be approximated by the Padé rational approximation,

$$f(z) \cong \frac{n_{p,q}(z)}{d_{p,q}(z)} \tag{3.47}$$

where $n_{p,q}(z)$ and $d_{p,q}(z)$ are respectively polynomials of degree q and p in z. In addition it is assumed that $d_{p,q}(0) \neq 0$. For any pair of the non-negative integers p and q, $n_{p,q}(z)$ and $d_{p,q}(z)$ are so chosen to agree with as many leading terms of the Taylor's series expansion of f(z) as possible. It can be shown* that

$$d_{p,q}(z)\ f(z) - n_{p,q}(z) = 0\left(|z|^{p+q+1}\right), \text{ as } z \to 0 \tag{3.48}$$

It has been shown by Hummel and Seebeck (43) that if

$$f(z) = \exp(-z)$$

then**

$$\begin{aligned} n_{p,q}(z) &= \sum_{k=0}^{q} \frac{(p+q-k)!q!}{(p+q)!k!(p-k)!} \cdot (-z)^k \\ d_{p,q}(z) &= \sum_{k=0}^{p} \frac{(p+q-k)!p!}{(p+q)!k!(p-k)!} \cdot z^k \end{aligned} \tag{3.49}$$

To apply the above results to $Z(r_j)$, formally replace z by $r_j Q_j$ to get

$$\begin{aligned} Z(r_j) = \exp(-r_j Q_j) &\cong \left[d_{p,q}\ r_j Q\ \right]^{-1} n_{p,q}(r_j Q_j) \\ &\equiv E_{p,q}(r_j Q_j) \end{aligned} \tag{3.50}$$

---

*See Wall (80), Chapter XX for an up to date discussion on Padé approximation of analytical functions.

**See also Varga (77), Chapter VIII.

$E_{p,q}(r_jQ_j)$ is called the Padé approximation (p,q) of $Z(r_j)$. In analogy to (3.47) it is clear that $E_{p,q}(r_jQ_j)$ agrees through the $(p+q)^{th}$ term in r_j with the series expansion of $Z(r_j)$. Therefore, for $(p+q) \geq 1$, $E_{p,q}(r_jQ_j)$ is, in the sense of Lax and Richtmyer, a consistent approximation of $Z(r_j)$.

From the definition of $E_{p,q}(r_jQ_j)$ and (3.49), it is clear that the Padé approximation $E_{0,1}$, $E_{1,0}$ and $E_{1,1}$ are exactly forward difference, backward difference and Crank-Nicholson approximation methods, respectively. Many high order accuracy approximation methods can also be generated by taking $p,q > 1$.

To establish the convergence criteria for the general Padé approximation, we state the following theorem:

Theorem 3.2. Let the eigenvalues of Q be positive real numbers. Then $\| E_{p,q}(rQ) \| < 1$ for all $r > 0$, if and only if, $p \geq q$.

Before giving the proof of the above theorem, it is instructive to study its consequences. The statement that $\|E_{p,q}(rQ)\| < 1$ implies that, if in (3.43) the operator $Z(r_j)$ is replaced by $E_{p,q}(r_jQ_j)$, $1 \leq j \leq m$, then the numerical procedure

$$w(t_m) = E_{p,q}(r_mQ_m)\left[w(t_{m-1}) - A^{-1}s(t_m - \tfrac{1}{2}r_m)\right] + A^{-1}s(t_m - \tfrac{1}{2}r_m) \tag{3.51}$$

is uniformly bounded in norm for all $r_j > 0$, $1 \geq j \geq m$ and

all $p \geq q$. Thus, Theorem 3.2 establishes the necessary and sufficient conditions for uniform stability of such a numerical procedure.

Proof: Let us first assume that $E_{p,q}$ is Hermitian. For this special case,

$$\left\| E_{p,q}(rQ) \right\| \equiv \rho\left(E_{p,q}(rQ)\right) = \max_{1\leq i\leq n} \left| n_{p,q}(r\sigma_i) \,/\, d_{p,q}(r\sigma_i) \right|$$

$$= \max_{1\leq i\leq n} \left| n_{p,q}(r\sigma_i) \right| / \left| d_{p,q}(r\sigma_i) \right|, \quad \sigma_i, r > 0$$

From (3.49) it is quite clear that

$$0 < \left| n_{p,q}(z) \right| < \left| d_{p,q}(z) \right|, \text{ for } p \geq q \text{ and } z > 0$$

so that

$$\rho\left(E_{p,q}(rQ)\right) \equiv \max_{1\leq i\leq n} \left| n_{p,q}(r\sigma_i) \,/\, d_{p,q}(r\sigma_i) \right| < 1 \qquad (3.52)$$

which provides the proof for the theorem for the special case for which $E_{p,q}$ is Hermitian. Nevertheless, the spectral radius of $E_{p,q}(rQ)$ for $r > 0$, is always less than unity as long as Q has positive eigenvalues and $p \geq q$. If $E_{p,q}$ is not Hermitian, then in general

$$\left\| E_{p,q}(rQ) \right\| = \left\{\rho(E^*_{p,q}\, E_{p,q})\right\}^{\frac{1}{2}} \geq \rho(E_{p,q}) < 1$$

where E^* is the conjugate transpose of E.

Clearly $E^*_{p,q}\, E_{p,q}$ is Hermitian and non-negative definite, i.e., all its eigenvalues are real and satisfy

$$\lambda_i(E^*_{p,q}\, E_{p,q}) \geq 0, \quad 1 \leq i \leq n$$

where $\lambda_i(A)$ is the ith eigenvalue of A. Now

$$E^*_{p,q}\, E_{p,q} \equiv I - d^{*-1}_{p,q}(d^*_{p,q}\, d_{p,q} - n^*_{p,q}\, n_{p,q})d^{-1}_{p,q}$$

$$\equiv I - D^*SD$$

where

$$D = d^{-1}_{p,q}(rQ)$$

$$S = d^*_{p,q}(rQ)\; d_{p,q}(rQ) - n^*_{p,q}(rQ)\; n_{p,q}(rQ)$$

Clearly both $d^*_{p,q}\, d_{p,q}$ and $n^*_{p,q}\, n_{p,q}$, are in general Hermitian and non-negative definite. Therefore, S is in general Hermitian and has real eigenvalues, λ_i, $1 \le i \le n$, with corresponding eigenvectors $\mathbf{x}_i$, $1 \le i \le n$. Consider,

$$\mathbf{y}_i = D^{*-1}\mathbf{x}_i;\ (\mathbf{y}_i, \mathbf{y}_i) = 1$$

then,

$$(\mathbf{y}_i,\ E^*_{p,q}\, E_{p,q}\, \mathbf{y}_i) = 1 - (\mathbf{y}_i,\ D^*SD\, \mathbf{y}_i)$$

$$= 1 - (\mathbf{x}_i,\ S\mathbf{x}_i) \qquad (3.53)$$

$$= 1 - \lambda_i(\mathbf{x}_i,\ \mathbf{x}_i)$$

$$\max_{1\le i\le n} \left|(\mathbf{y}_i,\ E_{p,q}\, E^*_{p,q}\, \mathbf{y}_i)\right| = \left\|E_{p,q}\right\|^2 = \max_{1\le i\le n} \{1 - \lambda_i\}$$

If S is positive definite, then $\lambda_i(S)$ must satisfy

$$1 > \lambda_i > 0$$

and

$$\left\|E_{p,q}\right\| = (1 - |\delta|)^{\frac{1}{2}} < 1 \text{ where } |\delta| > 0 \qquad (3.54)$$

Thus, the problem is now to demonstrate that S is positive definite and not negative definite. Consider first the

important case of $p = q = 1$, for which

$$S = \frac{4}{r} (Q + Q^*)$$

Clearly, if Q has positive real eigenvalues, then S is positive definite. Now, for $p \geq q \geq 0$, inspection shows that S is a polynomial in Q and Q^* with positive constant coefficients.

Let this series be

$$\sum_{m,n} a_{n,m} (Q^*)^m Q^n \text{ where } a_{n,m} \geq 0$$

Let $\mathbf{y}$ be any non-zero vector, and $\mathbf{y}^*$ its conjugate transposed. Let $n > m$, then

$$\mathbf{y}^* (Q^*)^m Q^n \mathbf{y} = [Q^m \mathbf{y}]^* Q^{n-m} [Q^m \mathbf{y}]$$

$$= \mathbf{z}^* Q^{n-m} \mathbf{z} > 0$$

where $\mathbf{z} = Q^m \mathbf{y}$. The same is, of course, true if $m > n$. Consequently,

$$\mathbf{y}^* S \mathbf{y} = \mathbf{y}^* \Big[\sum_{m,n} a_{n,m} (Q^*)^m Q^n \Big] \mathbf{y} > 0$$

Thus S is positive definite for all $p \geq q$. For $p < q$, it is evident that there exists an $r > 0$ such that S is no longer positive definite, and consequently $\| E_{p,q} \| > 1$. This last statement completes the proof of the above theorem.

Since only unconditionally stable numerical solutions are of interest, the stability analysis of $E_{p,q}(rQ)$ when $p < q$ is omitted. The treatment of the approximation methods for $\exp(-rQ)$ is completed by stating:

Corollary . Let $Q = \underline{Q}_1 + \underline{Q}_2 + \ldots + \underline{Q}_N$ where the eigenvalues of $\underline{Q}_i$, $1 \leq i \leq N$, are non-negative real numbers and at least one $\underline{Q}_i$, $1 \leq i \leq N$, has positive eigenvalues. Let in addition,

$$M(rQ) \equiv \prod_{j=1}^{N} \exp(r\underline{Q}_j)$$

formally approximate $\exp(rQ)$. Then the spectral norm of

$$\mathcal{E}_{p,q}(rQ) \equiv \prod_{j=1}^{N} E_{p,q}(r\underline{Q}_j)$$

is less than unity for all $r > 0$, if and only if, $p \geq q$.

Proof: by Theorem 3.2,

$$\left\| E_{p,q}(rQ_j) \right\| \leq 1, \quad 1 \leq j \leq N, \text{ if } p \geq q,$$

with strict inequality for at least one j, $1 \leq j \leq N$. Thus,

$$\left\| \mathcal{E}_{p,q} \right\| \leq \prod_{j=1}^{N} \left\| E_{p,q}(rQ_j) \right\| < 1$$

From Theorem 3.2, it is clear that the forward difference and Crank-Nicholson methods both suggest unconditionally stable procedures for solving the quasi-linear problem in hand.

From the Corollary of Theorem 3.2 it is easy to conclude that alternating direction implicit methods are also unconditionally stable. In fact, the treatment of the problem in this chapter has been primarily to prove the unconditional stability of this technique and its variants, which

will be described in detail in the following section. However, the treatment opens the door for many other numerical methods not yet commonly used.

Variants of the Alternating Direction Implicit Methods

Since the pioneer work of Peaceman and Rachford (60) and Douglas and Rachford (30), many investigators have studied this rather interesting technique extensively for solving linear parabolic and elliptic partial differential equations (4, 5, 10, 18, 22, 23, 29, 45, 58, 61, 77, 78, 79). Although a general theory for the non-stationary ADI method has not yet been developed, the experimental computations reported in the literature have been encouraging enough to make this method commonly used.

To describe the basic ideas in the ADI method, consider partitioning (3.24) of the n x n matrix A, and let

$$Z(r_j) \equiv \exp[-r_j \tilde{\Phi}_j^{-1} (H + V)]$$

Then, if $\tilde{\Phi}_j^{-1} H$ and $\tilde{\Phi}_j^{-1} V_j$ commute,

$$\begin{aligned} Z(r_j) &\equiv \exp(-r_j \tilde{\Phi}_j^{-1} H) \exp(-r_j \tilde{\Phi}_j^{-1} V) \\ &\cong E_{1,1}(-r_j \tilde{\Phi}_j^{-1} H) E_{1,1}(-r_j \tilde{\Phi}_j^{-1} V) \qquad (3.55) \\ &\equiv T_1(r_j) \end{aligned}$$

Thus,

$$\begin{aligned} T_1(r_j) &= (I+2r_j\tilde{\Phi}_j^{-1}H)^{-1}(I-2r_j\tilde{\Phi}_j^{-1}H)(I+2r_j\tilde{\Phi}_j^{-1}V)^{-1}(I-2r_j\tilde{\Phi}_j^{-1}V) \qquad (3.56) \\ &= (\rho_j\tilde{\Phi}_j+H)^{-1}(\rho_j\tilde{\Phi}_j-H)(\rho_j\tilde{\Phi}_j+V)^{-1}(\rho_j\tilde{\Phi}_j-V) \end{aligned}$$

where $\rho_j = 2/r_j$. Permuting the factors, which is of course valid when $\tilde{\Phi}_j^{-1} H$ and $\tilde{\Phi}_j^{-1} V$ commute, results in

$$T(r_j) = (\rho_j\tilde{\Phi}_j + V)^{-1}(\rho_j\tilde{\Phi}_j - H)(\rho_j\tilde{\Phi}_j + H)^{-1}(\rho_j\tilde{\Phi}_j - V) \qquad (3.57)$$

If the commutative property does not hold, then $\exp(-rQ)$ agrees with $\exp(-r\tilde{\Phi}^{-1}H) \cdot \exp(-r\tilde{\Phi}^{-1}V)$ through linear terms. However, by direct computation one can verify that $T(r)$ agrees with $\exp(-rQ)$ through quadratic terms.

From Theorem 3.2 and its corollary, it is clear that

$$\| T(r) \| < 1 \text{ for } r > 0$$

if $\tilde{\Phi}^{-1} H$ and $\tilde{\Phi}^{-1} V$ have non-negative eigenvalues with at least one of them positive definite. Therefore, for these conditions the numerical solution

$$\begin{aligned} \mathbf{v}_1(t_m) &= T(r_m)\ \mathbf{v}_1(t_{m-1}) \\ &= \prod_{j=1}^{m} T(r_j)\ \mathbf{v}_o \end{aligned} \qquad (3.58)$$

is unconditionally stable for all $r_j > 0$, $1 \le j \le m$. Furthermore $\lim_{m\to\infty} \mathbf{v}_1^{(m)} \to o$ for $r_j > 0$, $1 \le j \le m$. To carry out the actual computations, one has to introduce an intermediate step

$$(\rho_m\tilde{\Phi}_m + H)\ \mathbf{v}_1^{(m+\frac{1}{2})} = (\rho_m\tilde{\Phi}_m - V)\ \mathbf{v}_1^{(m)} \qquad (3.59a)$$

followed by

$$(\rho_m\tilde{\Phi}_m + V)\ \mathbf{v}_1^{(m+1)} = (\rho_m\tilde{\Phi}_m - H)\ \mathbf{v}_1^{(m+\frac{1}{2})} \qquad (3.59b)$$

where

$$\mathbf{v}_1^{(m)} = \mathbf{v}_1(t_m)$$

Note that $v_1^{(m+\frac{1}{2})}$ should not be confused with the value of $v_1(t_m - \frac{1}{2}r_m)$. One can apply the same procedure for the predictor formula of (3.45) to approximate $\tilde{\Phi}^{(m+\frac{1}{2})}$ prior to any computation step of (3.59). It must be kept in mind that the predictor equation should only approximate $w(t)$ at time level $(t_m - \frac{1}{2}r_m)$ with an error $O(\Delta r_m + h^2)$. The stability of the predictor formula should not, therefore, be of primary concern (27, 28). There is a variety of choice for the predictor formula. To avoid using two separate logics, and consequently simplifying the computer program, the predictor-corrector scheme proposed here employs the same logic for both steps (i.e., (3.59a) and (3.59b). For the purpose of analysis, it is convenient to work with the vector solution $v_1^{(m)}$, $m = 1,2,....$ However, eventually one wishes to solve the problem for

$$w^{(m)} = v_1^{(m)} + A^{-1}s(t_m - \tfrac{1}{2}r_m)$$

In terms of $w^{(m)}$, $m = 1,2....$, (3.59a) and (3.59b) become

$$(\rho_m\tilde{\Phi}_m + H)w^{(m+\frac{1}{2})} = (\rho_m\tilde{\Phi}_m - V)w^{(m)} + s^{(m+\frac{1}{2})} \qquad (3.60a)$$

$$(\rho_m\tilde{\Phi}_m + V)w^{(m+1)} = (\rho_m\tilde{\Phi}_m - H)w^{(m+\frac{1}{2})} + s^{(m+\frac{1}{2})} \qquad (3.60b)$$

where

$$s^{(m+\frac{1}{2})} = s(t_m - \tfrac{1}{2}r_m)$$

The procedure (3.60) is the Peaceman and Rachford method. It is interesting to study also the other variants of the ADI method. The Douglas and Rachford iterative method is defined by (3.60a) and

$$(\rho_m \tilde{\Phi}_m + V)w^{(m+1)} = 2\rho_m \tilde{\Phi}_m w^{(m+\frac{1}{2})} - (\rho_m \tilde{\Phi}_m - V)w^{(m)} \qquad (3.60c)$$

It can be shown that the Douglas-Rachford method is also unconditionally stable for all $r > 0$, if H is positive definite and V non-negative definite or visa versa. Another important variant of these alternative, direction implicit methods is given by Wachspress and Habetler (79). Clearly, the diagonal matrix $\tilde{\Phi}$ can be multiplied by a constant, real, diagonal matrix F, without either affecting the alogarithm for the direct solution of the problem, or essentially increasing the arithmetic work required in carrying out the computation. Let

$$w_1^{(m)} = F^{\frac{1}{2}} w^{(m)}$$

$$H = F^{-\frac{1}{2}} H F^{-\frac{1}{2}} \qquad (3.61)$$

and $$V = F^{-\frac{1}{2}} H F^{-\frac{1}{2}}$$

Then the Peaceman-Rachford method, (3.60), in terms of the new variable becomes

$$\begin{aligned}(\rho_m \tilde{\Phi}_m + \tilde{H})w_1^{(m+\frac{1}{2})} &= (\rho_m \tilde{\Phi}_m - \tilde{V})w_1^{(m)} + F^{-\frac{1}{2}} g^{(m+\frac{1}{2})} \\ (\rho_m \tilde{\Phi}_m + \tilde{V})w_1^{(m+1)} &= (\rho_m \tilde{\Phi}_m - \tilde{H})w_1^{(m+\frac{1}{2})} + F^{-\frac{1}{2}} g^{(m+\frac{1}{2})}\end{aligned} \qquad (3.62)$$

Wachspress and Habetler (79) recommend the use of the diagonal matrix, F, for conditioning the matrices H and V. They demonstrated that in a rectangular region with non-uniform mesh spacing, where usually H and V do not commute, one can find a matrix F such that:

$$\tilde{H}\,\tilde{V} = \tilde{V}\,\tilde{H}$$

However, it was demonstrated by Birkhoff, Varga and Young (5) that $\tilde{H}$ and $\tilde{V}$ commute, if and only if, the region, R, is a rectangle. Nevertheless, Wachspress and Habetler (79) recommend the use of the conditioning matrix F for non-rectangular regions. Recently, however, Wachspress (78) has given a more satisfactory explanation on how a suitable conditioning matrix accelerates the convergence, as well as suggesting possible ways of constructing such matrices. Actually, a natural choice of F is the positive diagonal matrix C, which has already been employed, by letting

$$H = C^{-\frac{1}{2}} H(s) C^{-\frac{1}{2}}$$

Much of the work in current literature is devoted to the computation of the best acceleration parameter ρ in the solution of the Dirichlet boundary value problem by a succession of ADI iterations. The difficulty in finding the best acceleration parameter (or parameters) in the case of parabolic equations lies in the fact that here one is interested in obtaining accurate values of the unknowns at each time level as well as those of steady state conditions. In the solution of the Dirichlet problem, one wishes to reach the steady state solution as fast as possible without much concern for the value of the unknowns at each intermediate iteration step. This point can be best visualized by noting that for the Dirichlet problem the error at any iteration step is given by (5)

$$\epsilon^{(m)} = \prod_{j=1}^{m} T(r_j)\ \epsilon(0) \tag{3.63}$$

while that of our solution to the parabolic differential equation (3.2) is from two sources:

$$\text{a)}\quad \epsilon_1(t_m) = v(t_m) - \tilde{v}(t_m) = \sum_{j=1}^{m} \prod_{j=i}^{m} Z(r_j)\ \alpha_i + \left[I - \prod_{i=1}^{m} Z(r_j)\right] A^{-1}\theta \tag{3.64a}$$

$$\text{b)}\quad \epsilon_2(t_m) = \left[\prod_{j=1}^{m} Z(r_j) - \prod_{j=1}^{m} T(r_j)\right] v_o \tag{3.64b}$$

For the Dirichlet problem, one usually continues the iteration until $\|\epsilon^{(m)}\|$ is sufficiently small. To minimize the number of iterations, one only needs to minimize $\|\prod_{j=1}^{m} T(r_j)\|$. All the recent works on finding better acceleration parameters (i.e., r_j's or ρ_j's) are essentially for minimizing the norm $\|\prod_{j=1}^{m} T(r_j)\|$. Although much has been said on the applicability of these acceleration parameters to the case of the parabolic differential equation, it is evident from (3.64a) and (3.64b) that the minimization of $\|\prod_{j=1}^{m} T(r_j)\|$ is not a critereon for improving the accuracy of the numerical solution of a parabolic differential equation. Regretably, most authors have overlooked not only the dominant error vector $\epsilon_1(t_m)$ which arises from the nonlinearity of the problem and discretization of the space co-ordinates, but also the way $\epsilon_2^{(m)}$ propagates and expands. In solving the system (3.20') one should search for a set of parameters $\delta = (r_j \mid r_j > 0,\ j = 1,2....m)$ such

that $\bar{r}_j$, $1 \leq j \leq m$ is maximum of $r_j > 0$, $1 \leq j \leq m$ for which $\| \epsilon_1(t_m) + \epsilon_2(t_m) \| < \delta$ where δ is a given positive number indicating the desired accuracy of the solution.

With the present state of art in solving the quasi-linear problems of the type (3.20'), not much can be said on the best set of parameters . However, for a fixed source vector, ■, a logical requisite is

$$0 < a \leq r_1 < r_2 < r_3 \ldots . < r_m = b$$

where a and b are determined from the accuracy requirement (36, 73). In the following chapter it will be shown that reasonably good results may be obtained by defining r_j by a relation of the type

$$\left(\sum_{i=1}^{j+1} r_i \right)^{1/2} - \left(\sum_{i=1}^{j} r_i \right)^{1/2} = a, \quad 1 \leq j \leq m$$

where a is a prescribed positive constant.

Finally, it must be observed that for $r_j \neq 0$, $1 \leq j \leq m$ both $\prod_{j=1}^{m} Z(r_j)$ and $\prod_{j=1}^{m} T(r_j)$ approach the null matrix as $m \to \infty$, so that

$$\epsilon_1(t\ ) + \epsilon_2(t\ ) \to A^{-1}\theta \text{ as } m \to \infty$$

Therefore,

$$\max_{1 \leq m} \left\| \{ \prod_{j=1}^{m} Z(r_j) - \prod_{j=1}^{m} T(r_j) \} \right\|$$

should occur after a few iterations. The spectral norm of the n x n matrix

$$\prod_{j=1}^{m} Z(r_j) - \prod_{j=1}^{m} T(r_j)$$

can behave erratically when r_j is large. This phenomenon is responsible for what some investigators have called instability of the ADI method for large values of r_j (50, 62, 79). In reality, the numerical procedure (3.58) is uniformly bounded in norm, so that by all definitions of stability it is stable. To elucidate these points by way of a primitive example, let $V\mathbf{w}(t) = \mathbf{0}$ (i.e., one-dimensional flow of heat), and assume that $\tilde{\Phi} = I$, then there exists a unitary matrix U such that $UHU' = D$, where $D = (d_{ij})$ is a positive diagonal matrix and U' is the transpose of U. Furthermore, $\|UHU'\| = \|H\| = \|D\| = \max_{1\le i\le n} \{d_{ii}\}$. Then

$$\left\| \prod_{j=1}^{m} Z(r_j) - \prod_{j=1}^{m} T(r_j) \right\| = \left\| \exp(-t_m D) - \prod_{j=1}^{m} \left(\frac{2}{r_j} + D\right)^{-1} \left(\frac{2}{r_j} - D\right) \right\|$$

$$= \max_{1\le i\le n} \left\{ e^{-t_m d_{ii}} - \prod_{j=1}^{m} \left[\frac{2 - r_j d_{ii}}{2 + r_j d_{ii}}\right] \right\}$$

Now, when r_j is very large and m is odd, the product

$$\prod_{j=1}^{m} \left[\frac{2 - r_j d_{ii}}{2 + r_j d_{ii}}\right]$$

may well become negative for all d_{ii}, $1 \le i \le n$. Consequently, the departure of the numerical solution (3.58) from the exact solution may be much larger than the magnitude of the exact solution. At the same time, the solution (3.58) is convergent, stable and second order correct.

Summarizing, the above development leads to an unconditionally stable and second order correct numerical procedure for solving two-dimensional latent heat problems.

The detailed study of the growth of the error vector produces a clearer understanding of criteria for minimizing the departure of the numerical solution from the exact solution of the problem. It was demonstrated that, contrary to the case of the Dirichlet problem, the error of the numerical solution of a parabolic differential equation is not necessarily minimized when

$$\left\| \prod_{j=1}^{m} T(r_j) \right\| , \quad m \geq 1$$

is minimized.

The acceleration parameter r_j plays an important role in minimizing the computer time requirement for solving such problems numerically. To arrive at the best set of parameters r_j, $j = 1,2....$, one has to first solve the following problem:

> Given $t > 0$ and $|\delta| > 0$, find a minimum positive integer M and a set of acceleration parameters $r_j > 0$, $1 \leq j \leq M$, such that:
>
> 1) $\sum_{j=1}^{M} r_j = t$ 2) $\left\| \prod_{j=1}^{M} Z(r_j) - \prod_{j=1}^{M} T(r_j) \right\| \leq |\delta|$

Such a minimization problem is indeed very difficult to solve. The author has not been able to find in the published literature any solution to such problems, inspite of its importance in solving parabolic differential equations of physics and engineering. It is evident that further work needs to be done before one can predict theoretically the most efficient set of acceleration parameters for solving the problem in hand.

CHAPTER IV

THE PROCEDURE AND RESULTS OF SOLVING THE HEAT CONDUCTION PROBLEM ON A HIGH SPEED DIGITAL COMPUTER

In the previous chapter, the theoretical aspects of solving the heat conduction problem numerically were discussed. A predictor-corrector, ADI (alternating direction, implicit) method was proposed for solving the temperature field in an object with latent heat. The purpose of the present chapter is to prescribe a procedure for computing the temperature field on a high speed digital computer, utilizing the proposed method. In addition, the numerical solution of a few example problems are described. The objectives for solving these example problems were two-fold: 1) to gain experience in translating the theoretical results into the computer language as well as determining, by trial calculation, the accuracy, limitations and computer-time requirements of the proposed solution; 2) to provide, by way of numerical evidence, a partial answer to some of the problems which were not amenable to satisfactory theoretical treatment. It must be kept in mind, however, that these trial results are not used as further evidence for the validity of the theoretical predictions of the previous chapter.

To explain more specifically the benefits of a few trial computations, consider again the proposed predictor-corrector formula, namely:

$$w^{(o)} = C^{\frac{1}{2}} u(o) \tag{4.1a}$$

$$\tilde{w}^{(m+\frac{1}{2})} = \tilde{T}(\tfrac{1}{2}r_{m+1}) \left[w^{(m)} - A^{-1}s\right] + A^{-1}s, \quad m=0,1,2.... \tag{4.1b}$$

$$\tilde{\Phi}^{(m+\frac{1}{2})} = \tilde{\Phi}(C^{-\frac{1}{2}}w^{(m+\frac{1}{2})}) \tag{4.1c}$$

$$w^{(m+1)} = T(r_{m+1}) \left[w^{(m)} - A^{-1}s\right] + A^{-1}s, \quad m=0,1,2... \tag{4.1d}$$

In the previous chapter, it was established that the spectral norm of both T and $\tilde{T}$ is less than one for all $r_m > 0$, m=0,1,2.. Thus, the proposed solution is unconditionally stable. Furthermore, it was established that the solution is second order correct. That is to say*,

$$\left\|\epsilon^{(m)}\right\| = O\left((\Delta\tau_K)^2 + h^2 + k^2\right), \text{ for all } \Delta\tau/kh \neq 0.$$

There was very little to be said on how to prescribe the most efficient set of parameters:

$$\mathcal{S} = \{r_m \mid r_m > r_o > 0, \ m=1,2,...\}$$

On the other hand, the statement that the solution is second order correct ensures the convergence of the numerical solution as well as specifying how the discrete solution approaches the continuous solution. But, it does not say much on the order of magnitude of the error. In other words, by

$$\left\|\epsilon\right\| = O\left((\Delta\tau)^2\right)$$

we merely mean that there exists a positive number, M, whose

---

*The symbol O here reads order of $(\Delta\tau)^2$.

magnitude is not usually specified, such that $\|\epsilon\| \leq M(\Delta\tau)^2$. Thus, the order relation for itself does not specify $\Delta\tau$ for a given value of $\|\epsilon\|$. The size of M depends on the steepness of the temperature field and the boundary conditions [see (3.38) and (3.64a and b)]. It has a specific value for a particular problem, especially for the nonlinear heat conduction problem in hand. A realistic, theoretical appraisal of M for nonlinear problems is usually very difficult. Many of the suggested short cut methods, such as a simple Fourier analysis can easily be misleading.

The significance of the proposed solution is in assuming a finite transition temperature range instead of zero. By making this rather realistic assumption, a great difficulty in locating the interface and obtaining the spatial derivatives of the temperature on the left and right of this interface has been resolved (see discussion in Chapter I). It was emphasized earlier that the dimensionless transition temperature range, δ_F, must be sufficiently large. The questions that were left somewhat unanswered are: Should one wish to approximate by the proposed method the solution of a latent heat problem for which $\delta_F = 0$, then what is the best value of δ_F? Next, for any sufficiently large δ_F what mesh spacing and set of parameters S would give a minimum required accuracy?

The above questions can be answered by trial calculations for any particular problem. On the other hand, the purpose of this investigation has been to develop the

foundation of a practical solution for obtaining the transient temperature field due to pure conduction in a medium with latent heat. It is beyond the scope of this work to obtain validated answers for all the above mentioned problems and for all the important cases of practical interest. Nevertheless, conducting a limited number of wisely chosen trial computations is well justified. A few numerical evidences may hopefully serve to show how the theoretical results of Chapter III can be extended. It would also serve to illustrate just how useful the proposed solution is and how one may improve its accuracy by inspecting the first set of computed results.

Before trying to specify the example problems, it is necessary to decide on a suitable solution algorithm in order to obtain further insight into the nature of the proposed solution as well as indicating what example problems will produce the most useful information with the minimum use of computer time.

The Solution Algorithm

To solve (4.1) in the manner suggested in the preceeding chapter, one divides the steps (4.1b) and (4.1d) into two sub-steps. Thus, for (4.1b) one can write

$$w^{(m+\frac{1}{2})} = \left[\frac{2}{r_{m+1}}\,\tilde{\Phi}^{(m+\frac{1}{2})} + H\right]^{-1} \cdot \left[\left(\frac{2}{r_{m+1}}\,\tilde{\Phi}^{(m+\frac{1}{2})} - V\right) w^{(m)} + s\right] \quad (4.2a)$$

$$w^{(m+1)} = \left[\frac{2}{r_{m+1}}\,\tilde{\Phi}^{(m+\frac{1}{2})} + V\right]^{-1} \cdot \left[\left(\frac{2}{r_{m+1}}\,\tilde{\Phi}^{(m+\frac{1}{2})} - H\right) w^{(m+\frac{1}{2})} + s\right] \quad (4.2b)$$

It was mentioned earlier that, if one orders the mesh points by rows, H becomes tri-diagonal. If, on the other hand, one orders the mesh points by columns, then V is tri-diagonal. But, in general, one can not make both H and V tri-diagonal. However, in actual computation one has the choice of reordering the mesh points after each step of computation such that one is always dealing with the problem of reducing tri-diagonal matrices. In this way the solution algorithm is exactly the same for (4.2a) and(4.2b). Let $\mathbf{n} = (n_1, n_2, \ldots, n_n)$ be defined by

$$\mathbf{n} = \left[\frac{2}{r_{m+1}} \tilde{\Phi}^{(m+\frac{1}{2})} - V\right] w^{(m)} + s \tag{4.3a}$$

and let

$$B = \left[\frac{2}{r_{m+1}} \tilde{\Phi}^{(m+\frac{1}{2})} + H\right] \tag{4.3b}$$

then, (4.2a) becomes,

$$w^{(m+\frac{1}{2})} = B^{-1} \mathbf{n} \tag{4.4}$$

Because B is tri-diagonal, one can solve (4.4) directly by the Gaussian elimination method. To solve (4.4), let

$$\begin{aligned} w_j &= (w_{i',j}, w_{i'+1,j}, \cdots w_{i'',j}) \\ w_i &= (w_{i,j'}, w_{i,j'+1}, \cdots w_{i,r} \cdots w_{i,j''}) \end{aligned} \tag{4.5}$$

where i is used as a row index and j as column index. $i' = i'(j)$ and $i'' = i''(j)$ indicate that the jth row begins at the mesh point (i',j) and ends at the mesh point (i'',j). $j' = j'(i)$ and $j'' = j''(i)$ indicate that the ith column begins at the mesh point $(i,j'(i))$ and ends at the mesh point $(i,j''(i))$.

The matrix H may be written as:

$$H = \begin{bmatrix} H_1 & & & \\ & H_2 & & \\ & & \ddots & \\ & & & H_J \end{bmatrix} \qquad (4.6a)$$

where

$$H_j = \eta_j \cdot \begin{bmatrix} a_{i'} & -b_{i'} & & & \\ -b_{i'} & a_{i'+1} & -b_{i'+1} & & \\ & \ddots & \ddots & \ddots & \\ & & & a_{i''-1} & -b_{i''-1} \\ & & & -b_{i''-1} & a_{i''} \end{bmatrix} \qquad (4.6b)$$

Next, one writes (4.4) alternatively:

$$w_j^{(m+\frac{1}{2})} = B_j^{-1} n_j \qquad 1 \le j \le J \qquad (4.7)$$

where

$$B_j = \frac{2}{r_{m+1}} \tilde{\Phi}_j^{(m+\frac{1}{2})} + H_j$$

and n_j is defined similarly to w_j. The matrix problem (4.7) can be directly solved by the following algorithm. Defining

$$a_i^* = \frac{2}{r_{m+1}} \varphi_{i,j} \cdot \eta_j^{-1} + a_i \qquad (4.8)$$

$$c_{i'}^* = b_{i'}/a_{i'}^*; \quad c_i^* = b_i/(a_i^* - b_{i-1} c_{i-1}^*), \quad i' \le i \le i''-1$$

$$g_{i'}^* = \eta_j^{-1} n_{i',j}/a_{i'}^*; \quad g_i^* = \frac{(\eta_j^{-1} n_{i,j} + b_{i-1} g_{i-1}^*)}{(a_i^* - b_{i-1} c_{i-1}^*)}, \quad i' \le i \le i''$$

the components $w_{i,j}$, $i' \le i \le i''$ are given recursively by

$$w_{i'',j} = g^*_{i''}$$
$$w_{i,j} = g^*_i + C^*_i \cdot w_{i+1,j};\ i' \le i \le i''-1 \tag{4.9}$$

One repeats the above step for all rows to obtain all entries of $w^{(m+\frac{1}{2})}$. In a similar fashion, one can solve (4.2b) column by column. Namely, one first writes

$$w_i^{(m+1)} = \bar{B}_i^{-1} \cdot \bar{n}_i \quad 1 \le i \le I \tag{4.10}$$

where

$$\bar{n} = [\frac{2}{r_{m+1}} \tilde{\Phi}^{(m+\frac{1}{2})} - H]\ w^{(m+\frac{1}{2})} + s$$

$$\bar{n}_i = (\bar{n}_{i,j'}, \ldots \bar{n}_{i,j+r} \ldots \bar{n}_{i,j''})$$

$$\bar{B}_i = [\frac{2}{r_{m+1}} \tilde{\Phi}_i^{(m+\frac{1}{2})} + V_i]$$

and

$$V_i = \eta_i' \begin{bmatrix} d_{j'} & -e_{j'} & & & \\ -e_{j'} & d_{j'+1} & -e_{j'+1} & & \\ & \ddots & \ddots & \ddots & \\ & & & -e_{j''-1} & \\ & & -e_{j''-1} & d_{j''} & \end{bmatrix} \tag{4.10'}$$

Then one solves (4.10) by an algorithm similar to (4.8) and (4.9).

The above developments specify how the numerical calculations should be carried out. What is left to be studied is the problem of minimizing the computer storage requirement

for solving the problem with a relatively fine mesh. For brevity, the discussions on the methods of optimizing the storage requirement of the proposed solution are omitted. However, the procedure outlined below is believed to require the minimum amount of storage and manipulation of data. Note that in the following outline the equal sign (=) is used to designate the machine command for replacing the quantity on the left of the equal sign by the quantity on its right.

A Proposed Procedure for Solving the Problem on a Digital Computer

I $\mathbf{w}^{(0)} = C^{\frac{1}{2}}\,\mathbf{u}(0)$

$\tilde{\Phi}^{(0)} = \Phi(\mathbf{u}(0))$ Note: $\varphi_{i,j} = 1+\lambda \exp[-\beta^2(u_{i,j}- u_F)^2]$

$m = 0$

II $m = m + 1;$

If m even, $\rho = \frac{2}{r_{m+1}}$; if m odd, $\rho = \frac{4}{r_{m+1}}$

III $\mathbf{n}_i = (\rho\, \tilde{\Phi}_i - V_i)\mathbf{w}_i^{(m)} + \mathbf{s}_i \qquad 1 \le i \le I$

$\bar{\mathbf{n}} = (\rho\, \tilde{\Phi}_j + H_j)^{-1} \cdot \mathbf{n}_j \qquad 1 \le j \le J$

solve by Gaussian elimination method

$\mathbf{n}_j = \bar{\mathbf{n}} \qquad 1 \le j \le J$

IV $\bar{\mathbf{n}} = (\rho\, \tilde{\tilde{\Phi}}_j - H_j) \cdot \mathbf{n}_j + \mathbf{s}_j \qquad 1 \le j \le J$

$\mathbf{n}_j = \bar{\mathbf{n}} \qquad 1 \le j \le J$

$\bar{\mathbf{n}} = (\rho\, \tilde{\tilde{\Phi}}_i + V_i)^{-1} \cdot \mathbf{n}_i \qquad 1 \le i \le I$

solve by Gaussian elimination

$\mathbf{n}_i = \bar{\mathbf{n}} \qquad 1 \le i \le I$

V $\tilde{\Phi}^{(m)} = \Phi(C^{-1}n)$

If m even, $w^{(m+1)} = n$

If m odd, go to II

To obtain an idea of the storage requirement of the above solution, consider an N x N square mesh region. It is clear from (4.10') and (4.6) that only 6N coefficients specify V and H completely, and at most s contains 4N non-zero entries. On the other hand, w, n, and $\tilde{\Phi}$ each have N^2 entries while $\bar{n}$ has only N entries. Therefore, all together the subscripted variables require storage space for $(3N^2 + 11N)$ words. Not all the $(3N^2 + 11N)$ words need to be stored on the fast memory. In fact, one can store the component of w on a tape and read into the fast memory only the components which correspond to one row at a time. The same applies to n and $\tilde{\Phi}$. Usually it is preferable to store only w and $\tilde{\Phi}$ on the tape and to choose a computer with enough capacity to store n on the fast memory. Therefore, the minimum space in the fast memory would be (14N) words, the maximum $(3N^2 + 11N)$ words, and the recommended capacity should be $(N^2 + 13N)$ words.

The One-Dimensional Case

When the temperature field is symmetric with respect to one of the two spatial co-ordinates, say y, the problem becomes one-dimensional. The proposed predictor-corrector method in this case reduces to

$$\tilde{w}^{(m+\frac{1}{2})} = [\frac{4}{r_{m+1}} \tilde{\Phi}^{(m)} + H]^{-1}[(\frac{4}{r_{m+1}} \tilde{\Phi}^{(m)} - H)w^{(m)} + 2s] \qquad (4.11a)$$

$$\tilde{\Phi}^{(m+\frac{1}{2})} = \Phi(\tilde{w}^{(m+\frac{1}{2})}) \qquad (4.11b)$$

$$w^{(m+1)} = [\frac{2}{r_{m+1}} \tilde{\Phi}^{(m+\frac{1}{2})} + H]^{-1}[(\frac{2}{r_{m+1}} \tilde{\Phi}^{(m+\frac{1}{2})} - H)w^{(m)} + 2\blacksquare] \qquad (4.11c)$$

The similarity between the basic solution algorithm for the one-dimensional case and that of the two-dimensional problem is obvious. For this reason it seems advisable to study the one-dimensional problem first. Also, in solving the one-dimensional problem useful information on the behavior and the accuracy of the proposed solution might be obtained.

It was mentioned earlier that only a limited number of heat conduction problems with latent heat have been solved analytically, and all of these solutions are for the one-dimensional problem. Comparison with these exact solutions is the only way to obtain an accurate estimate of the error of any numerical solution of the problem. In fact, in solving a two-dimensional problem one first assumes boundary conditions such that for parts of the two-dimensional region under consideration the temperature field is theoretically one-dimensional (e.g., along an axis sufficiently distant from a corner). One then compares the numerical solution for this region with the corresponding exact solution.

The influence of the prescribed transition range, δ_F, and other parameters, arising from the physical properties of the system, on the accuracy of the solution is essentially independent of the dimensionality of the problem. Thus, the one-dimensional solution can be used to study the

effects of these parameters and consequently to obtain the values of δ_F which give the best results. The one-dimensional solution can also establish an approximate procedure to evaluate the parameters r_m, m=1,2,...., recursively.

Consider now the Neumann solution for a semi-infinite bar $x_1 > 0$ described in Chapter I. If the bar contains initially a liquid at its freezing point, T_∞, and at time $t \geq 0$ the boundary temperature is reduced to T_b, then the temperature in the solid phase is given by:

$$u(x_1,t) = \frac{T - T_\infty}{T_b - T_\infty} = 1 - \frac{1}{\text{erf } \xi} \cdot \text{erf } \frac{x_1}{2\sqrt{\alpha_s t}} \qquad (4.12)$$

$$u\big(X(t),t\big) = 0$$

where

$$X(t) = 2\xi\sqrt{\alpha_s t}$$

$$\xi e^{\xi^2} \text{ erf}\xi = \frac{C_s(T_\infty - T_b)}{\sqrt{\pi}\ L} = \beta/\pi\lambda$$

$$\beta = 3/\delta_F$$

$$\delta_F = \frac{\Delta T_F}{(T_\infty - T_b)}$$

$$T_b = T(0,t); \quad t > 0$$

The principal value in solving this particular problem, both numerically and analytically, lies in gaining insight into the behavior of numerical solutions. Although the numerical solution is difficult (due to a very steep temperature distribution when t is small), its analytical solution has a very simple and useful form since it depends on only one

parameter which can be either ξ, or $c_s(T_\infty - T_b) / L\sqrt{\pi}$. Let $x = x_1/(a + x_1)$ and $\tau = \alpha_s t/a^2$. Then,

$$u(x,t) = 1 - \frac{1}{\text{erf}\xi} \cdot \text{erf} \frac{x/(1-x)}{2\sqrt{\tau}} \tag{4.13}$$

$$\chi(t) = \frac{2\xi\sqrt{\tau}}{1 + 2\xi\sqrt{\tau}}$$

For a uniform mesh spacing h (1/h = N is an integer), the numerical solution depends on h, δ_F, and the recursive formula for $r_m = \Delta\tau_m/h^2$, m=1,2,.... A tabulation of ξ versus the latent heat parameter $c_s(T_\infty - T_b) / (L\sqrt{\pi})$ and the corresponding values of λ/β is given in Table 1. The table shows that, as ξ changes from 0 to 4, the latent heat parameter changes from 0 to 10^8. It seems, then, that ξ is a better parameter with which to work.

TABLE 1

VARIATIONS OF ξ WITH THE LATENT HEAT PARAMETER $c_s(T_F - T_b) / (L\sqrt{\pi})$

ξ	$\frac{c_s(T_F - T_b)}{L\sqrt{\pi}}$	$\frac{\lambda}{\beta}$	erf ξ
0.000	0.000000	∞	0.000000
0.050	0.002825	112.601	0.056372
0.100	0.011359	28.023	0.112463
0.500	0.334160	0.95256	0.520500
1.000	2.290710	0.13895	0.842701
2.000	108.684960	0.0293	0.995322
3.000	≈24000.000000	0.000013	0.999975
4.000	$\approx 10^8$	$\approx 3\times10^{-9}$	1.000000

Because the interface moves at a velocity equal to $2\xi\sqrt{\tau}$, and because the temperature field is essential linear

in the solid phase, it seems logical to prescribe $\Delta \tau_m$, m=1,2, 3,.... such that the interface moves a fixed fraction of the mesh spacing as one goes from one time level to another. Namely, one defines r_m by the relations

$$\chi(\tau_{m-1}+ r_m) = \chi(\tau_m) = \chi(\tau_{m-1}) + \delta_x h$$

$$r_m = \frac{\Delta \tau_m}{h^2} = \{\chi(\tau_m) / [2\xi(1 - \chi(\tau_m)]\}^2 - \frac{1}{h^2} \sum_{r=1}^{m-1} \Delta \tau_r \qquad (4.14)$$

where δ_x = movement of the interface in fractions of h for the period $\sum_{r=1}^{m-1} \Delta \tau_r$ to $\sum_{r=1}^{m} \Delta \tau_r$.

The above choice ensures that the time levels are so chosen that the error due to discretization of time is not increasing as $\Delta \tau_m$ is increased with m. It has the additional advantage of permitting $\Delta \tau_m$ to be increased as one proceeds with the computation, thus resulting in appreciable saving in computation time requirement.

The formula (4.14) suggests that r_m should be decreased as ξ is increased. When the latent heat effect is identically zero, then ξ approaches infinity so that r_m should be zero or infinitely small. In reality one can assume that $L\sqrt{\pi} / [c_s(T_F - T_b)] = 10^{-8}$ without introducing an error more than the round-off error. For this value of the latent heat parameter, the corresponding value of ξ is 4.0, which can be used successfully in (4.14) to obtain the values of r_m, m=1,2,....

In general one does not have an expression for X(t), and the above procedure for calculating r_m may look fruitless at the first glance. However, one can usually obtain an approximate upper bound for the rate of movement of the interface and then use this approximate relation to calculate r_m (8, 35). It is not necessary at all that the interface in any actual problem moves by a fixed amount δ_x at every time step. The thing that one should make sure of is that it does not exceed δ_x. In fact, when the boundary temperature is time dependent, and perhaps periodic, one can take T_b as the minimum value of temperature on the boundary within each interval and use (4.14) to calculate the values of r_m for that interval. The only revision in (4.14), to make it suit the case of periodic boundary conditions, is in letting m = 0 at the beginning of any period.

Allowing $w_i^{(m)}$ to be the computed value of the unknown at the mesh point i at time level m, and $u_i^{(m)}$ the corresponding value of Neumann's solution for $\delta_F = 0$, one defines the Euclidean norm of the departure of the numerical solution by:

$$\left\| e^{(m)} \right\| = \{ \sum_{i=1}^{N_1} [w_i^{(m)} - u_i^{(m)}]^2 \}^{\frac{1}{2}} \qquad (4.15)$$

and the average departure by

$$\left\| \tilde{e}^{(m)} \right\| = \frac{1}{N_1} \left\| e^{(m)} \right\|$$

where N_1 is the number of mesh points falling in the interval $0 \le x \le X(t)$. Once the value of δ_F for which $\|e\|$ is

minimum is found, then one uses this value to study the effect of ξ and h on the accuracy of the solution. For most of the practical problems of melting and solidification ξ varies between 0.1 and 2.0. One does not expect much change in the accuracy of the solution when ξ is varied between 0.1 and 2.0. Thus, it is not very profitable to solve the problem for various values of ξ. On the other hand, h might be a significant factor in determining the accuracy of the solution. It will not be very useful to show the effect of h on the accuracy of the solution when all the other parameters are kept constant because it has already been established that the solution is second order correct in h. What would be interesting to investigate is the problem of obtaining a numerical solution for the time interval 0 to τmax. Then, keeping δ_xh constant, what would be the best value of h? In other words, if one changes h, but keeps the computer time constant by way of increasing $\Delta\tau_m$, m=1,2,..., which value of h gives the best results?

The Computer Results for the One-Dimensional Case

Based on several previous experiments with the one-dimensional problem (41) it was assumed that the uniform mesh spacing h = 0.01 will result in a spatial discretization error which would be satisfactory for the present investigation. Fixing the mesh spacing at h = 0.01, the one-dimensional problem was solved first for the following values of ξ, δ_F, δ_x and λ.

Run Number	ξ	δ_F	δ_x	λ
1.1	0.50	0.001	0.25	2857.650
1.2	0.50	0.01	0.25	285.765
1.3	0.50	0.1	0.25	28.577
1.4	0.50	0.001	0.50	2857.650
1.5	0.50	0.001	1.00	2857.650

An additional run (Run 1.6) was completed for h = 0.005, δ_x = 0.5 and δ_F = 0.1. Figure 7 is a plot of $\|e^{(m)}\|$ (see (4.15) for definition of $\|e^{(m)}\|$) versus $\chi(\tau) = X(\tau) / (1 + X(\tau))$ for Runs 1.1,2,3,4 and 6. $\chi(\tau)$ is the dimensionless position of the interface predicted by Neumann's solution (4.13). The computation time for these runs varied between 10 to 15 minutes on the University of Oklahoma IBM 1410 computer, depending on δ_x and the time interval.

It is evident from Figure 7 that the dominant factor in determining the accuracy of the solution at large values of $\chi(t)$ is the dimensionless transition range δ_F. Observe that the accuracy of solutions for all the cases plotted in this figure is within the normal acceptable range. However, the sudden jumps of $\|e^{(m)}\|$ at certain steps, followed by a long period in which $\|e^{(m)}\|$ decreases despite the increase in the number of mesh points falling in the region 0 to $\chi(t)$, are both heuristic and alarming. No satisfactory explanation can be given for this behavior of $\|e^{(m)}\|$. However, a partial answer may be found in the remarks made at the end of Chapter III. Note that for δ_F = 0.1 and δ_x = 0.25, $\|e^{(m)}\|$ does not increase suddenly; rather it follows a wavy pattern at the beginning and then slowly decreases. In Figure 8

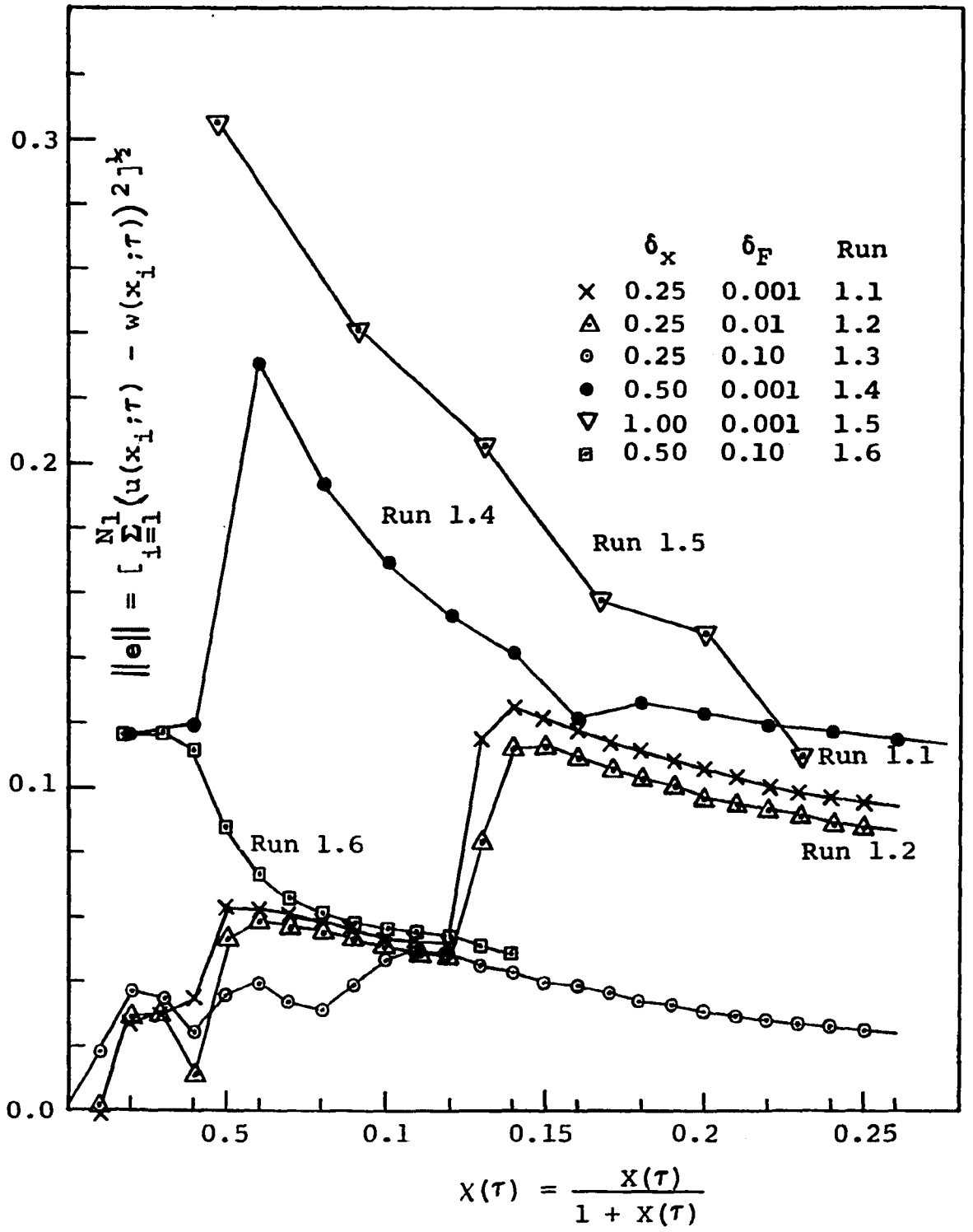


Figure 7. Variation of $\|e\|$ with $X(\tau)$ for various values of δ_x and δ_F, (ξ=0.5)

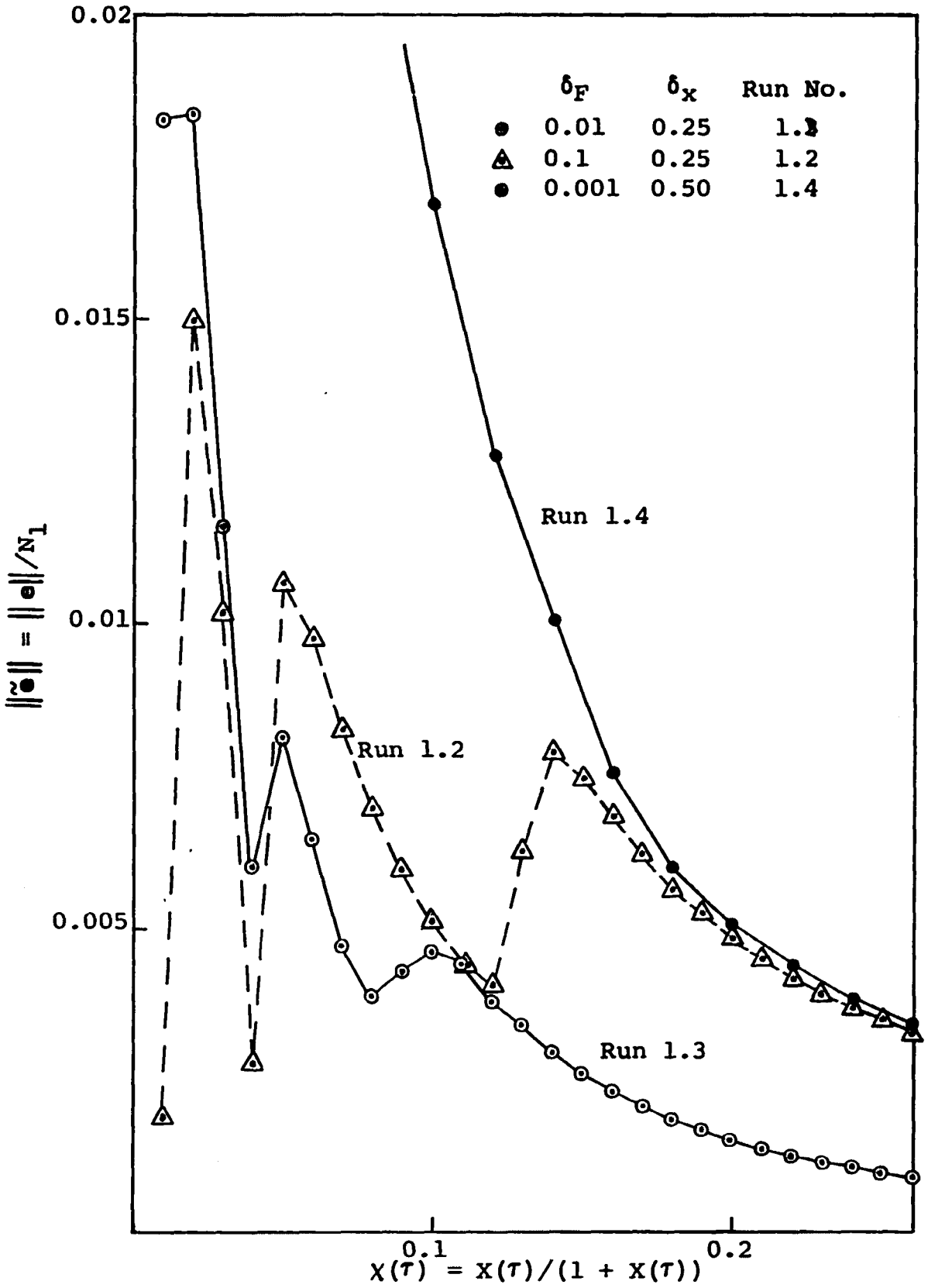


Figure 8. Variation of $\|\tilde{e}\|$ with $\chi(\tau)$ showing that for all Cases $\|\tilde{e}\|$ is uniformly decreasing for $\chi(\tau) > 0.15$.

the average error for mesh points in the region $0 \leq ih \leq \chi(t)$ is plotted versus $\chi(\tau)$. Note that for $\delta_x = 0.25$, the average error gradually decreases to less than 0.001. This general trend will carry on for $\chi(\tau) > 0.20$. For this reason there was no point in carrying the computations any further.

One of the reasons for choosing the boundary condition $u(o,t) = 1.0$, instead of a flux-type boundary condition, was the fact that initially $\partial u(x,\tau) / \partial t$ and $\partial u(x,\tau) / \partial x$, at $x = 0.01$ are very large. Consequently, the maximum error occurs at small values of τ, and the error-reduction effect of the operator $T(r_j)$, defined by (3.56), can be more readily studied. The flux-type boundary condition, on the other hand, imposes a strong uniformity on the derivatives $\partial u/\partial \tau$ and $\partial u/\partial x$ so that the initial error would be negligibly small.

It is clear that the objective of these trial computations was to exaggerate the erratic behavior of the Euclidean norm of $\epsilon_2^{(m)}$ defined by (3.64b). Observe that $\| e^{(m)} \| = \| \epsilon_1^{(m)} + \epsilon_2^{(m)} + \delta \|$ where $\delta = \delta(\delta_F)$ arises from the departure of the Neumann solution from that of linear flow of heat in a medium with a transition range $\delta_F \neq 0$. Clearly, $\|\delta\|$ is larger for $\delta_F = 0.1$ than that for $\delta_F < 0.1$. Inspection of Figure 7 reveals the fact that $\|\delta(\delta_F)\| \approx 0.02$ for $\delta_F = 0.1$ and $0.01 \leq \chi(\tau) \leq 0.25$.

Run 1.6, for which $h = 0.005$ and $\delta_x = 0.5$, was carried out to show if the accuracy of computations can be improved by decreasing h and increasing δ_x such that the computation time remains the same. It is seen in Figure 7 that the result was negative.

The computed dimensionless temperature $w(x,\tau)$ for Run 1.3 is plotted in Figure 9 versus χ for values of τ ranging between 0.00277 to 0.111. Note the smoothness of the computed results. Note also the change of scale from linear to logarithmic on the $w(x,\tau)$ axis which was done to demonstrate how fast $w(x,\tau)$ approaches zero for $x > \chi(\tau)$. Observe that the process of melting (or solidification) begins at $w(x,\tau) = 0.1$. It is completed when $w(x,\tau) = 0.0$. In this respect, the interface can be taken to be either at the point where melting is initiated (i.e., where $w(x,\tau) = 0.1$) or at the point where it is completed (i.e., where $w(x,\tau) = 0.0$). However, none of these choices are desirable because in the numerical results $w(x,\tau)$ can never be equal to absolute zero. Its value at $x_1 = X(\tau)$ is around 0.01 and decreases rather sharply to 10^{-5} at a few mesh points beyond $X(\tau)$. The upper limit $w = 0.1$ is unsuitable, because at $w = 0.05$, 3.5 per cent of the melting (or solidification) process is completed, i.e., 3.5 per cent of the latent heat is added (or removed) at $w = 0.05$. At $w = 0.003$ this figure is 90 per cent, and that of $w = 0.0159$ is about 50 per cent. Consequently, it seems more suitable to take the position of the isotherm $w = 0.0159$ as the position of the interface, especially when one wishes to compare it with that predicted by Neumann's solution.

Equally important as the Euclidean norm of the error vector is the sign of $(u - w)$. The accuracy of the computed values of $w(x,\tau)$ plotted in Figure 9 is such that it is

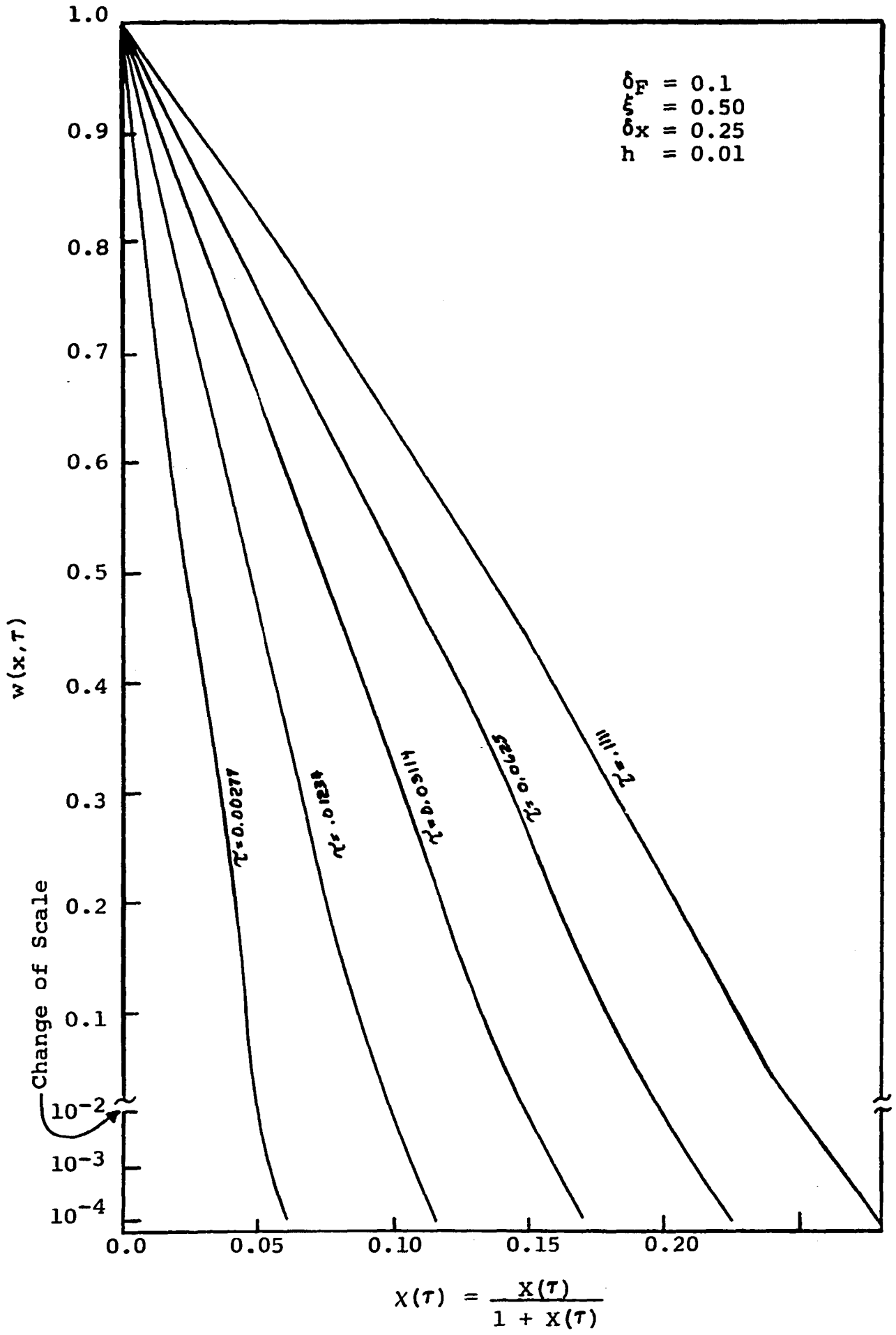


Figure 9. Computed Temperature in a Semi-Infinite Slab.

difficult to observe this change of sign. Figure 10 is a plot of $u(x_1,t) - w(x_1,t)$ versus $x_1 / \sqrt{4\tau}$ for $\delta_x = 1.0$, $\delta_F = 0.001$ and $\xi = 0.5$, at several time levels. Figures 11 and 12 are similar plots for $\delta_F = 0.05$ and 0.1 respectively. The transformation $x = x_1 / (1 + x_1)$ was not used in computing the values of $w(x_1,\tau)$ from which the data reported in these figures were derived. Observe the oscillation in the values of (u-w) with the mesh points as well as with the time levels. It is evident that the values of r_j corresponding to $\delta_x = 1.0$ are appreciably large. Nevertheless, the solution $w(x_1,\tau)$ is stable and uniformly convergent as $\tau \rightarrow \infty$ in addition to being second order correct in $\Delta\tau$. Observe also that the magnitude of the center of oscillation of $u(x_1,\tau) - w(x_1,\tau)$ progressively decreases with time.

It is interesting to observe that for $\delta_x = 0.25$ and $\xi = 0.5$, the value of $\Delta\tau/h^2$ increases from the initial value of 0.0625 to 29.95 at $\chi(t) = 0.25$. The corresponding values for $\delta_x = 1.0$ are 1.13636 and 123.47. If an explicit numerical solution were used, then $\Delta\tau/h^2$ should have been kept below one-half by stability limitations (24).

The computer results presented here graphically are covered in tabulated form in Appendix B. These results were selected from twenty five runs which were carried out using the University of Oklahoma IBM 1410 computer.

Finally, it is worth mentioning that for most one-dimensional problems, one can obtain a fairly accurate solution for small values of τ. Using such values as the initial

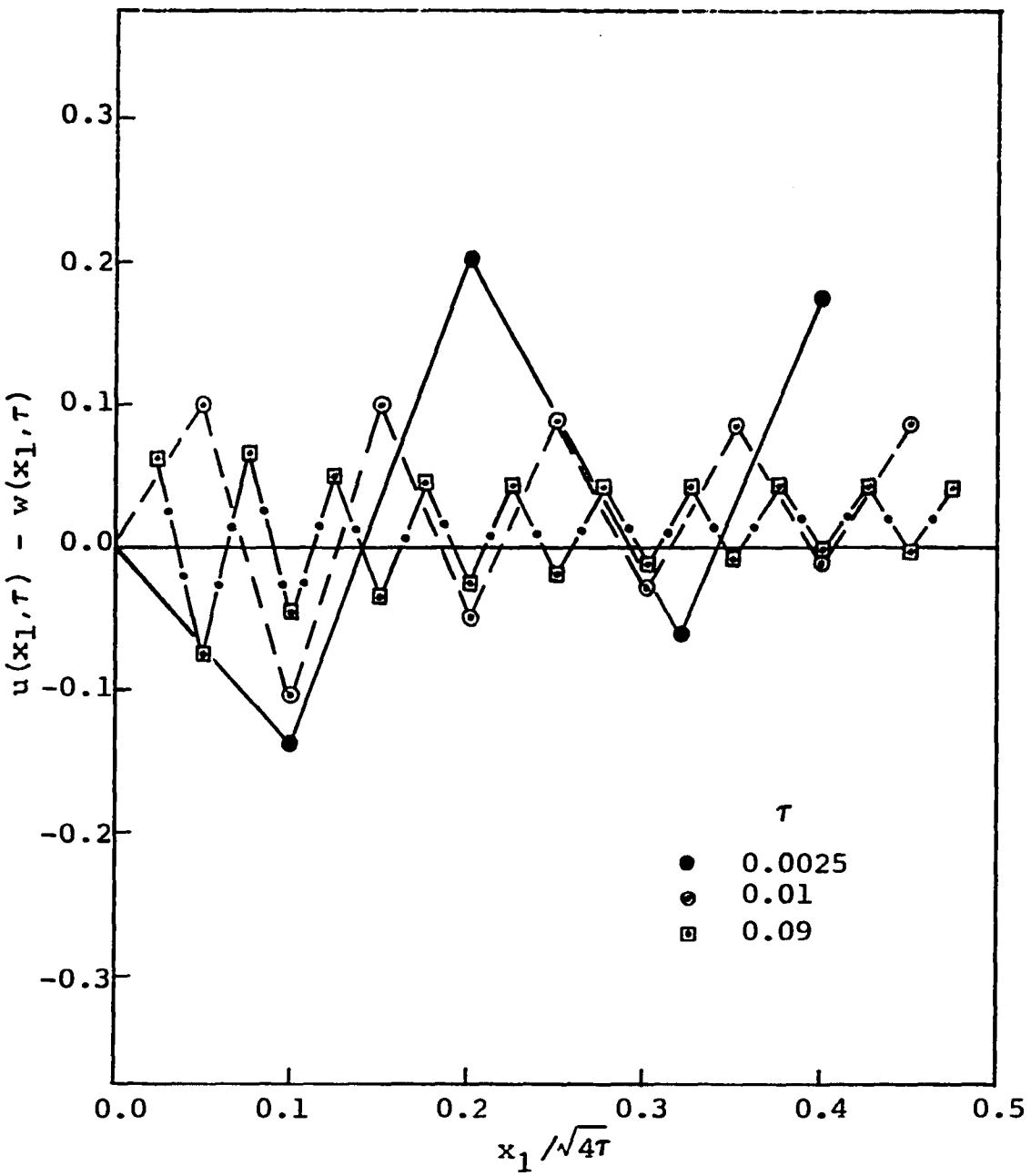


Figure 10. Variation of $u(x_1,\tau) - w(x_1,\tau)$ with τ at Mesh Points Falling Between the Boundary and the Interface, (for δ_x=1.0, δ_F=0.001 and ξ=0.50).

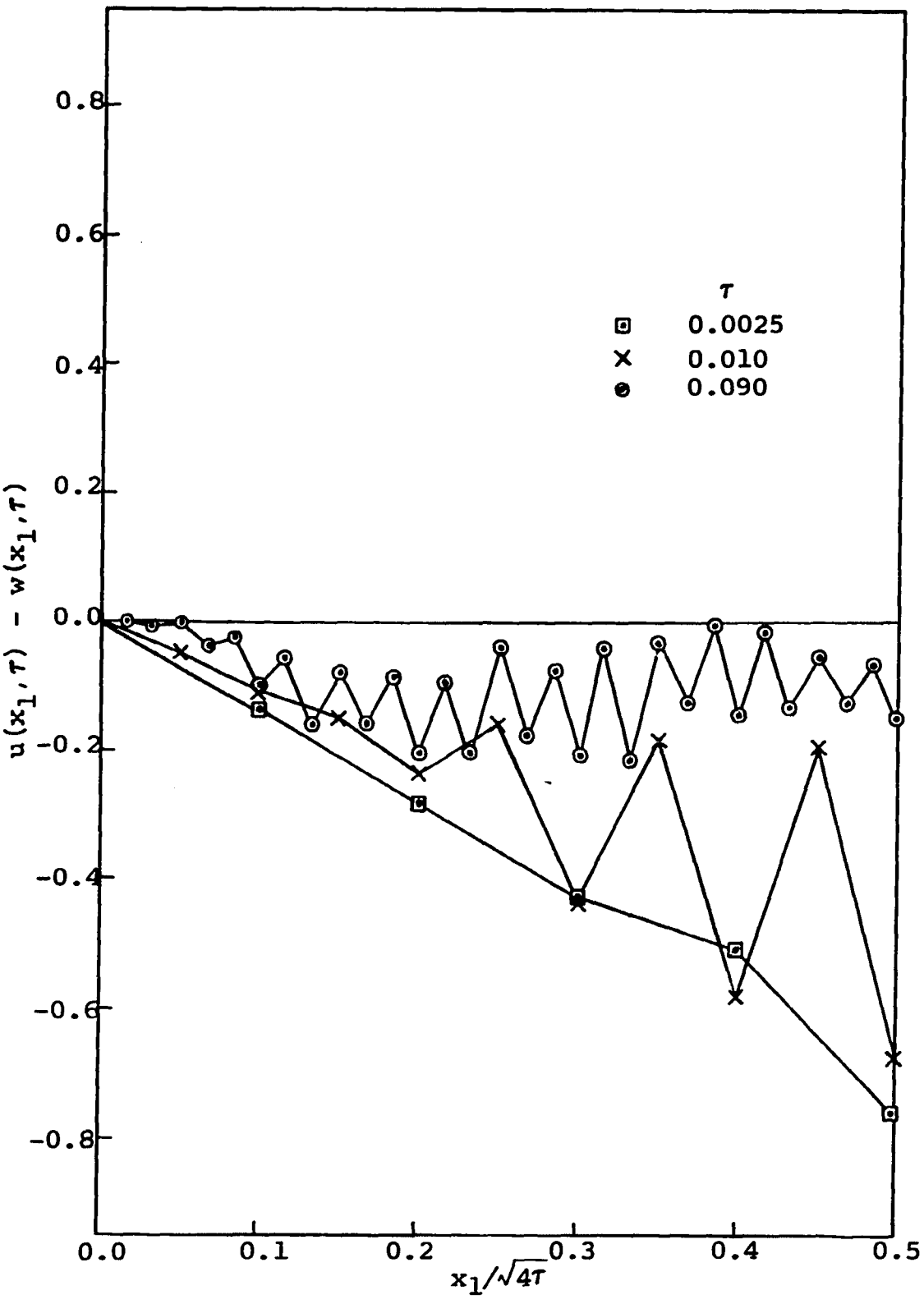


Figure 11. Variation of $u(x_1,\tau) - w(x_1,\tau)$ with τ at Mesh Points Falling between the Boundary and the Interface, (for δ_x=1.0, δ_F=0.05 and ξ=0.50).

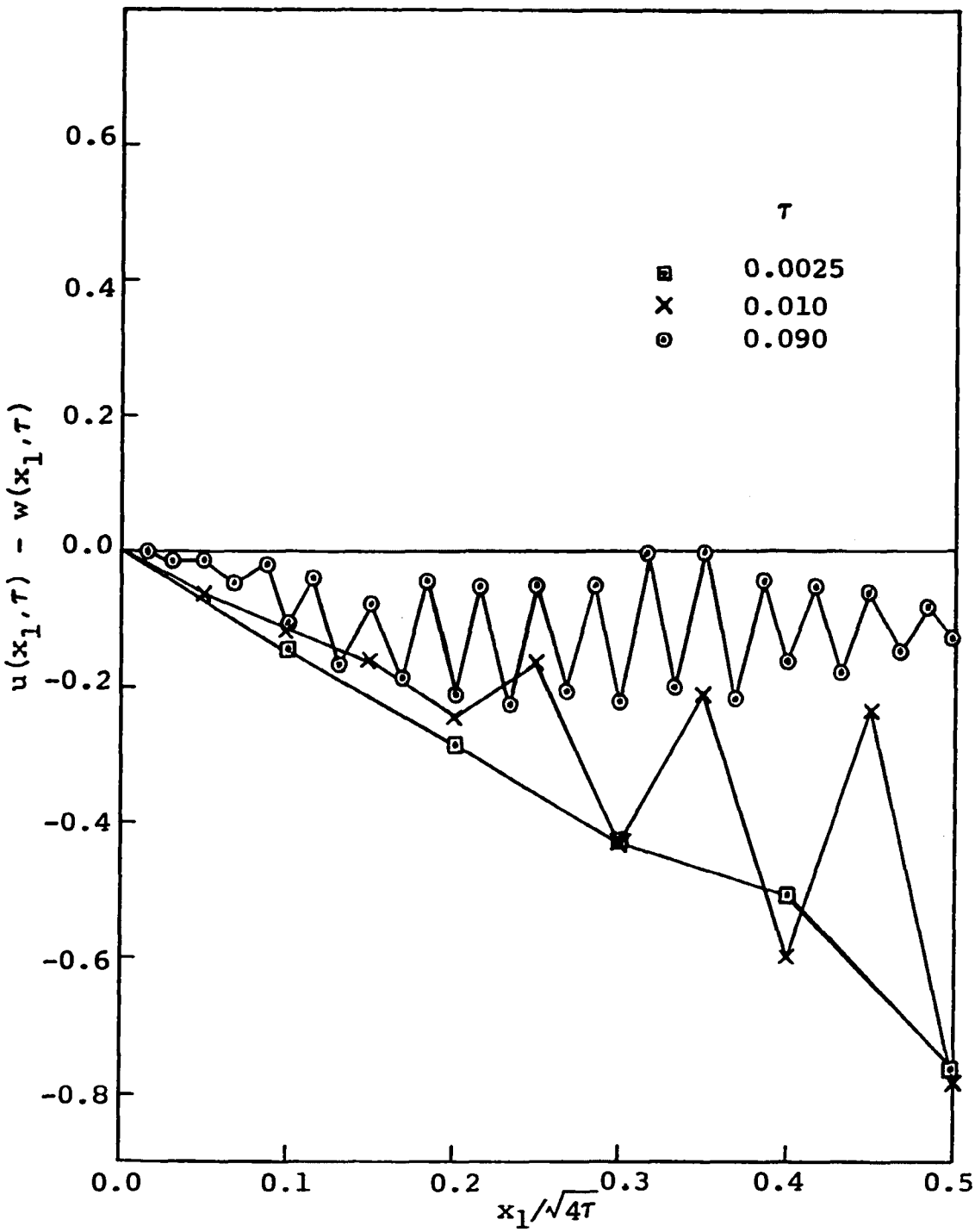


Figure 12. Variation of $u(x_1,\tau) - w(x_1,\tau)$ with τ at Mesh Points Falling between the Boundary and the Interface, (for δ_x=1.0, δ_F=0.10 and ξ=0.5)

condition in the computer solution substantially reduces the large initial error which in turn improves the accuracy of the solution in the subsequent time levels. Indeed, for $\delta_x = 1.0$ and an initial condition $w(ih,\tau_o) = 1\text{-erf}(ih/\sqrt{4\tau_o})/\text{erf}\ \xi$, $1 \leq i \leq 5$, where $\tau_o = 0.0025$, the accuracy of the solution was several times improved. Figure 13 is a plot of $w(ih,\tau)$ versus $ih/\sqrt{4\tau}$ for $\tau > \tau_o$, $\delta_x = 1.0$, $\delta_F = 0.05$ and $\xi = 0.5$. The solid line in this figure is the exact solution. The dotted line is the best curve passing through all the computed points. Note that the departure of the dotted line from the analytical solution is essentially due to prescribing a finite transition range δ_F instead of zero. Compare the departure of the data points from this average curve with those of Figures 10, 11 and 12. In all the above mentioned runs the same recursion formula was used to evaluate r_j at each time level.

The Two-Dimensional Case

The analysis of the one-dimensional case served as a preliminary step towards solving the two-dimensional problems. It was concluded that the recursion formula (4.14) can be successfully used to evaluate the acceleration parameter r_j, $j=1,2,\ldots$ by choosing δ_x sufficiently small. It was further observed that if the temperature distribution for a small, elapsed time is computed separately and fed into the computer as the initial temperature distribution, the accuracy of the numerical solution can be significantly improved.

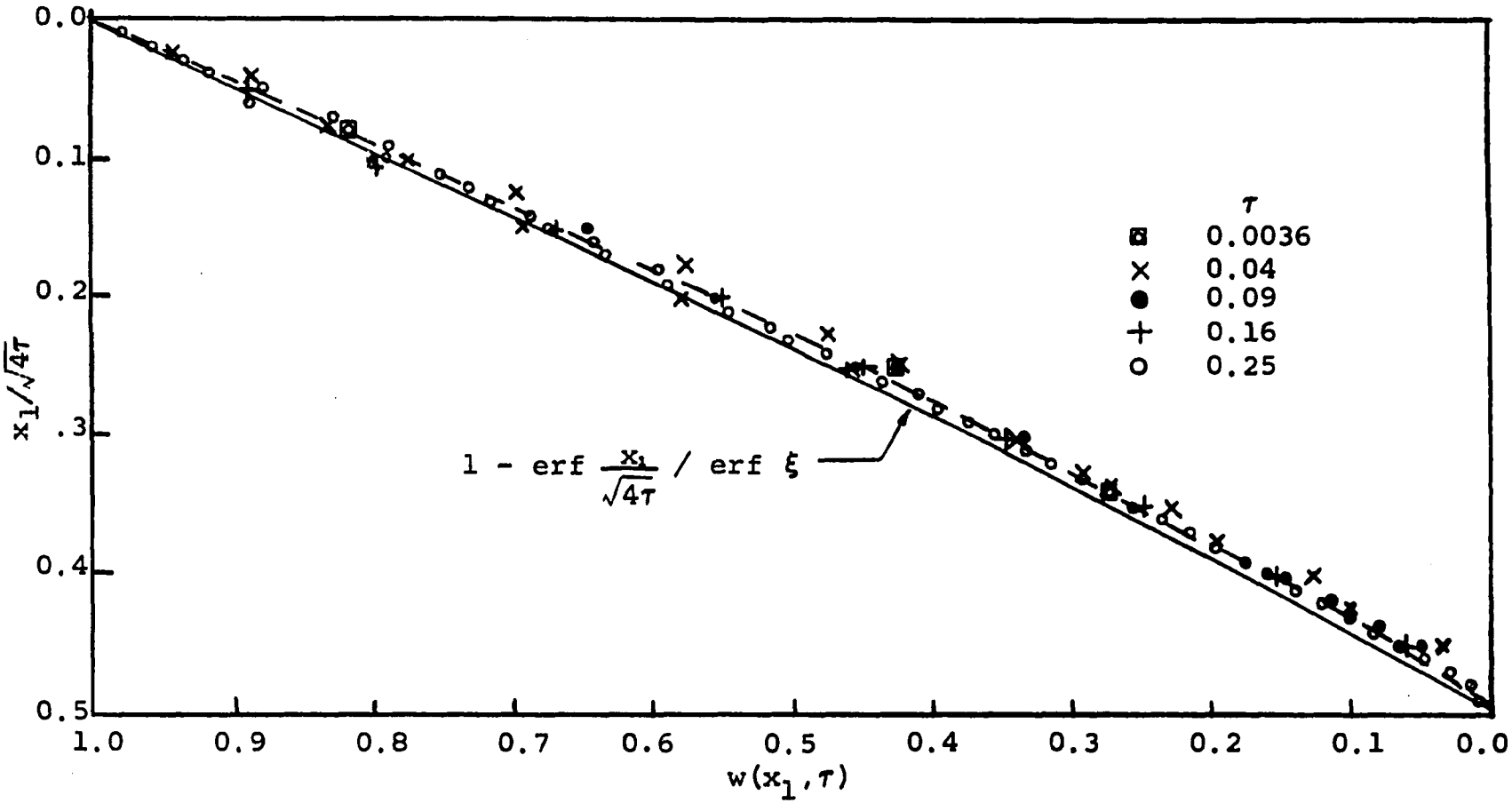


Figure 13. Computed Values of $w(x_1,\tau)$ versus $x_1/\sqrt{4\tau}$ (for δ_x=1.0, δ_F=0.05, ξ= 0.5 and $w(x_1,\tau_o) = 1 - (\text{erf}\ x'/\sqrt{4\tau_o})/\text{erf}\ \xi$; τ_o=0.0025).

There are three main objectives for solving a few two-dimensional example problems. First, to discover how successfully one can use the one-dimensional results in setting up the parameters for solving the two-dimensional problems. This information is indeed very significant and practical when one is engaged in performing actual machine computations. The reason is that the computer time requirement for solving a two-dimensional problem may be over 100 times more than that required to solve a one-dimensional problem for the same elapsed times. Thus, it is important to eliminate as many preliminary two-dimensional runs as possible. Secondly, it is desired to study the problems of accuracy of the proposed numerical solution; the problems being characteristics of the two-dimensional problems. Finally, it is intended to provide a comparison between the numerical results and those of the diffusion cell analog.

The two-dimensional region, R", considered for this study was a semi-infinite, plane region (in Cartesian coordinate system) bounded internally by a square of side 2 (dimensionless and arbitrary). It was assumed that the region was originally at its initial transition temperature (i.e., $u(x_1, x_2, 0) = 0.0$, $x_1, x_2 \epsilon R"$) and for time $\tau > 0$ the temperature along the exposed boundary (i.e., $u(x_1, x_2, \tau) = 1.0$; $x_1, x_2 \epsilon \tilde{\Gamma}"$, where $\tilde{\Gamma}"$ is the exposed boundary). For these conditions, the region R" can be divided into eight symmetric sub-regions $\bar{R}"$. Figure 14 shows one of such symmetric regions and the associated boundary conditions.

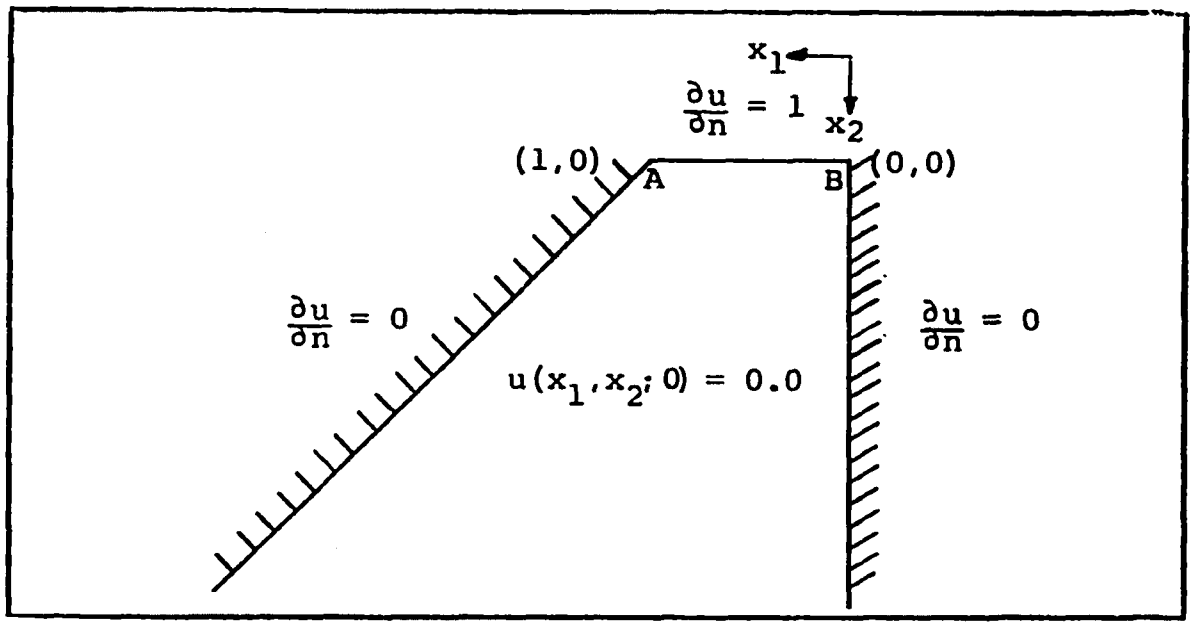


Figure 14. The Semi-Infinite Plane Region, $\overline{R}$", and its Boundary Conditions.

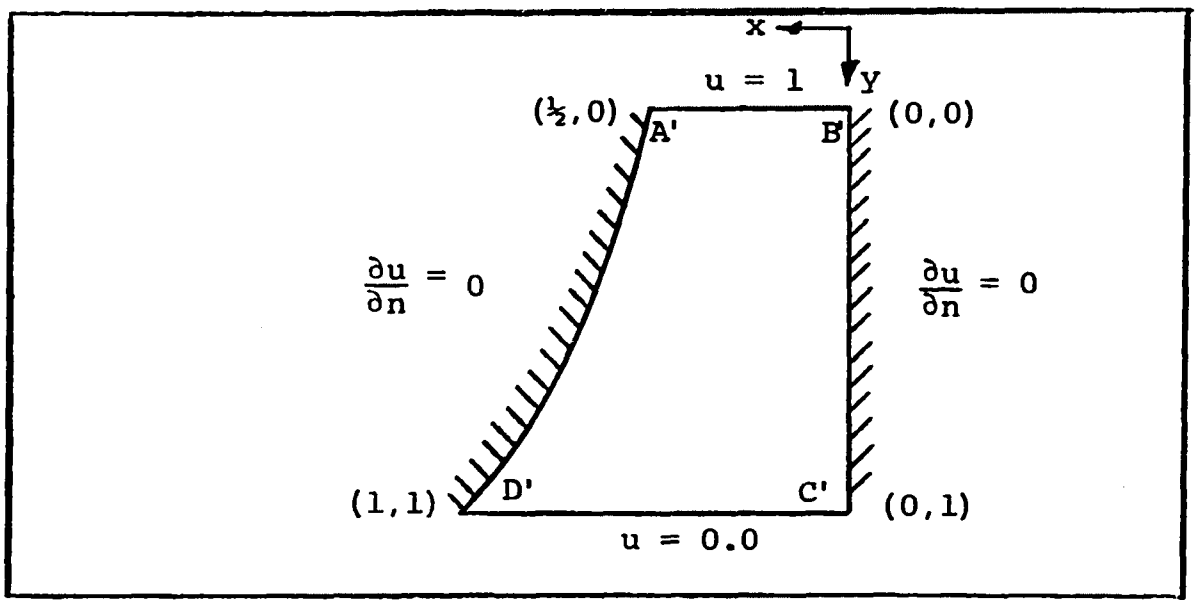


Figure 15. The Shape of the Semi-Infinite Region, $\overline{R}$", of Figure 14 in the x - y Plane and its Corresponding Boundary Conditions.

Figure 15 shows the shape and size of this region in x - y plane (see (3.1) for the definition of x and y). The reasons for choosing a constant temperature boundary condition at the exposed boundary are those cited in the one-dimensional case. Here again, when τ is not very large, one may assume that the temperature field is essentially linear along a vertical line away from the corner.

When the medium under consideration is initially at its transition temperature, there will be no temperature change beyond the interface. For this reason, the region of interest at any time step is between the interface and the exposed (input) boundary (i.e., the line $x_2 = 0.0$ in Figure 14, or y = 0.0 in Figure 15). Therefore, for the time interval* of interest in the present work, the co-ordinate transformation of (3.1) may not be required, due to the fact that it is not necessary to compute the entries of u for points far beyond the interface. Arranging the mesh region $r_{i,j}$ like those of Figure 16 one can limit the row index at each time level to just a few lines beyond the interface, thus avoiding a substantial amount of unnecessary computation.

Two arrangements of the mesh spacing were considered. First, a uniform mesh spacing, i.e., k = h = 1/20. Thus, the region R" was divided into square and right triangles of side h = 1/20 by a set of equally spaced horizontal and vertical parallel lines. Figure 16 shows this arrangement as well as

---

*In most cases $0<\tau<2$. Beyond this point, the error becomes a well-behaved function which approaches $A^{-1}\theta$ asymptotically as the number of successive iterations approaches infinity. See Chapter III.

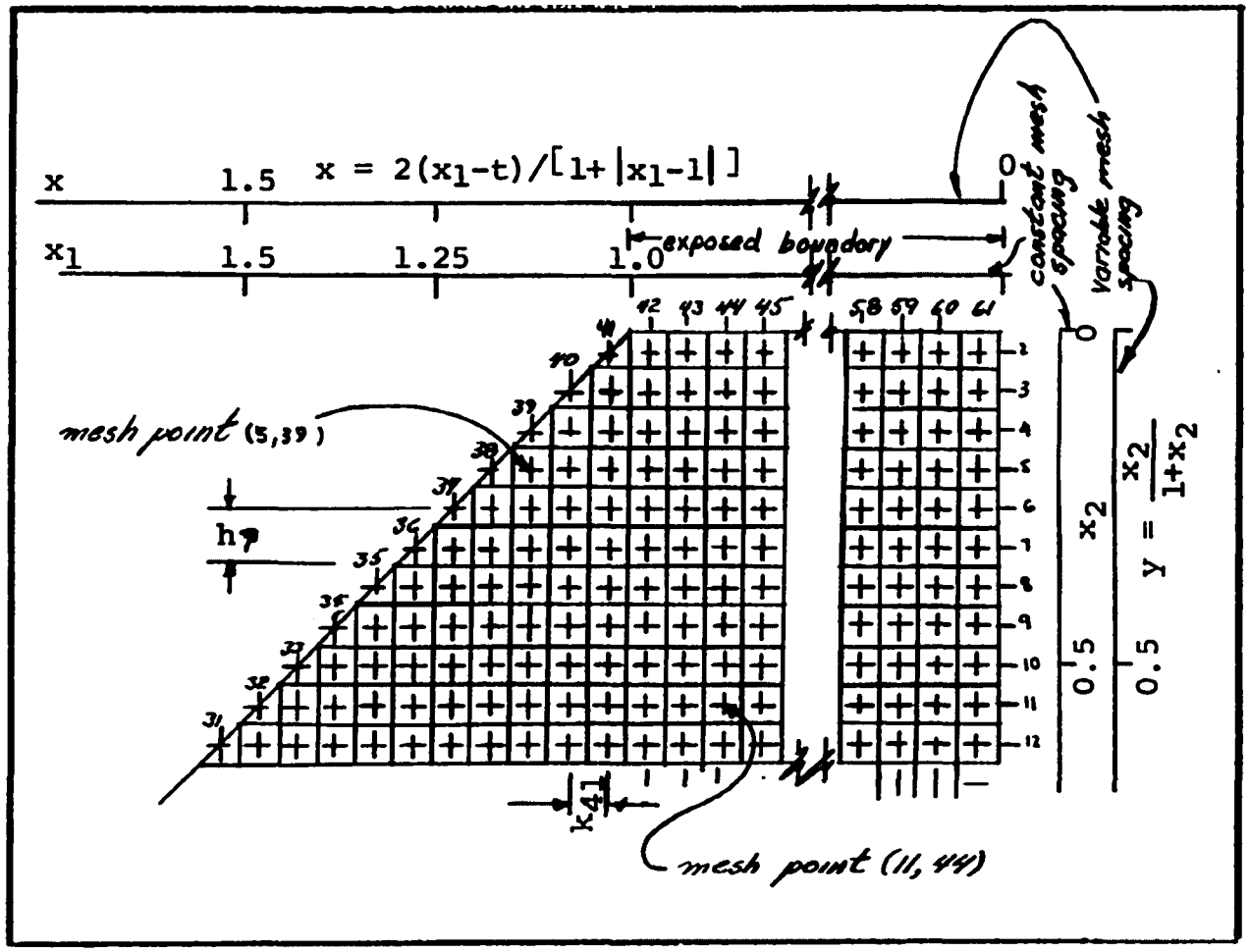


Figure 16. The Arrangement of the Mesh Regions in the Corner Region of the Example Problems. (The Spatial Position of the Mesh Points are given by the Co-ordinates x_1 and x_2 for the Case of Constant Mesh Spacing and x and y for the Case of Variable Mesh Spacing.)

the numbering of the mesh points which was used for machine computations. It is clear that the part of the region $\bar{R}''$ shown in Figure 16 is enclosed in a rectangular region $3 \leq x_1 \leq 0$, $2 \leq x_2 \leq 0$. Beyond this enclosed region negative indices can be used. Thus, it is assumed that for the time interval of interest there is no detectable change in the temperature at the boundary $x_2 = 2$. To divide the entire semi-infinite region $\bar{R}''$ into uniform mesh regions one needs an infinite number of equally spaced horizontal and vertical lines, which of course is not practical. To improve this situation one either uses the co-ordinate transformation, Equation (3.1), with a uniform mesh spacing, or one uses a variable mesh spacing which divides the entire region into a finite number of mesh regions. The latter was adopted for the second arrangement considered here. Figure 16 shows both arrangements. The mesh spacing increases as the row index, i, increases and as the column index, j, gets larger than 42 or smaller than 41. This arrangement was used because the temperature field was expected to depart more from that of the linear case around the corner DAB' in Figure 15.

The computer program was written such that the mesh spacing can be specified by entering the values of $x_{2,i}$ and $x_{1,j}$, $(i,j) \epsilon R_h$ instead of the mesh spacings h_i and k_j, $(i,j) \epsilon R_h$. For the case of variable mesh spacing the following formula was used to compute $x_{2,i}$ and $x_{1,j}$ which in turn gives the position $(x_{2,i}, x_{1,j})$ of any mesh point $(i,j) \epsilon R_h$ (see Figure 16).

$$x_{2,i} = \frac{(i - 1.5)h}{1 - (i - 1.5)h} \qquad 40 \geq i \geq 2$$

$$x_{1,j} = 1.0 - \frac{(j - 41.5)h}{1 - (j - 41.5)h}, \quad 61 \geq j \geq 42 \tag{4.16}$$

$$x_{1,j} = 1.0 + \frac{(41.5 - j)h}{1 - (41.5 - j)h}, \quad 41 \geq j \geq 2$$

$$h = 1/20$$

The acceleration parameter r_m, $m \geq 1$ for the above two arrangements was computed by the following procedure. Let $\chi(\tau_m) = \chi(\tau_o)+m\delta_x h$. Then for the uniform mesh spacing,

$$r_m = \left[\left(\frac{1}{2\xi}\chi(\tau_m)\right)^2 - \tau_{m-1}\right] \Big/ h^2, \quad m \geq 1 \tag{4.17}$$

and for the non-uniform mesh spacing

$$r_m = h^{\frac{1}{2}} \left\{\left[\frac{\chi(\tau_m)}{2\xi(1 - \chi(\tau_m))}\right]^2 - \tau_{m-1}\right\}, \quad m \geq 1 \tag{4.18}$$

The dimensionless total heat transferred, δQ_m, at the exposed boundary in the interval τ_{m-1} to τ_m can be approximated by

$$\delta Q_m = \frac{\delta q_m/a}{\rho c_o(T_b - T_F)} = \int_{\tau_{m-1}}^{\tau_m} \left[\iint \varphi\left(u(x_1, x_2;\tau')\right) \frac{\partial u(x_1, x_2;\tau')}{\partial \tau'} dx_1 dx_2\right] d\tau'$$

$$\approx \sum_{i,j} \tfrac{1}{4} \varphi_{i,j}^{(m-\frac{1}{2})} [w_{i,j}(\tau_m) - w_{i,j}(\tau_{m-1})](x_{2,i+1} - x_{2,i-1})$$
$$(x_{1,j-1} - x_{1,j+1}), \qquad x_1, x_2 \epsilon \bar{R}'', (i,j) \epsilon R_h \tag{4.19}$$

where

δq_m = total heat transferred at the exposed boundary in the interval τ_{m-1} to τ_m, BTU.

a = the actual length of the exposed boundary, and

ρ, c_o, T_b, T_F and φ are as defined previously in Chapter I. $x_{1,j}$ and $x_{2,i}$ are the spatial positions of the mesh point (i,j), $(i,j) \epsilon R_h$ (see Figures 15 and 16). The cumulative heat transfer at the exposed boundary, $Q(\tau_m)$ was then obtained as the sum of all δQ_j, $1 \leq j \leq m$, i.e.,

$$Q(\tau_m) = \sum_{j=1}^{m} \delta Q_j$$

The Computer Program for the Two-Dimensional Problems

The above mentioned, two example problems were used for final de-bugging and study of the accuracy of a devised computer program capable of solving problems of two-dimensional heat conduction in a locally isotropic medium with one or more transition temperatures. The program was written in Fortran language. Nearly 600 man hours, plus 20 hours of IBM 1410 and 1.5 hours of CDC 1604, were consumed before this computer program was completely de-bugged and ready to solve the example problems. Of course, the development of such a program would have required half as much effort if the program was written for the specific case of the example problems.

The program is based on the procedure outlined on page 102.

Except when very high accuracies are desired, the number of mesh regions in the rectangular closure of a region of practical interest is not expected to exceed 4000. The high speed digital computer, CDC 1604, has a core storage capacity of 32,000 ten digit words, so that it has sufficient capacity for storing in its fast memory all the subscripted variables involved in the proposed solution. For this reason the computer program assumes that all the subscripted variables are stored in the core storage. However, a slight modification in the program will allow the use of the tape units for storing the entries of the diagonal matrix $\tilde{\Phi}$ and the vector $\mathbf{w}$.

To solve a desired two-dimensional problem using the devised computer program, one first replaces the plane region R by a network of mesh points R_h with the procedure described in Chapter III. One then lets $\mathfrak{R}_h$ be a rectangular network of mesh points which contains R_h such that at least the second horizontal and vertical grid lines in $\mathfrak{R}_h$ coincides partly with the first horizontal and vertical grid lines in R_h, respectively (Figure 15). One also lets the number of horizontal and vertical grid lines in $\mathfrak{R}_h$ be at least two lines more than those in R_h. Next one numbers the grid lines in $\mathfrak{R}_h$ from top to bottom and from left to right, (Figure 16). To define the arbitrary network R_h for the computer program, one first defines the dimensionless temperature such that its value will always be positive in the region R. Then one lets $w_{i,j} = -1.0$ for $(i,j) \epsilon \tilde{R}_h$ where $\tilde{R}_h$ is the complement of R_h with respect to $\mathfrak{R}_h$.

Aside from specifying the network R_h, one should provide the computer with the following input data:

1. Initial values of $w_{i,j}(\tau_o)$, $(i,j)\epsilon R_h$. If for any mesh point (i,j) the initial value of $w_{i,j}$ is not specified, the program sets it equal to zero or any other desired positive number.
2. The entries of the matrices H and V.
3. The entries of the source vector **s** if **s** is fixed. If some entries $s_{i,j}$ of **s** are time dependent, then a function $s_{i,j} = s_{i,j}(\tau)$ should be defined to modify the values of $s_{i,j}$ as τ is increased.
4. The functional form of $\varphi(u_{i,j})$ and associated coefficients.
5. A recursion formula for r_j, $j \geq 1$ and associated coefficients.

A listing of this program as revised to solve the example problems is covered in Appendix C.

The Computed Temperature Field Around a Corner

The temperature field around the corner shown in Figure 14 was solved for the case of constant mesh spacing and that of the variable mesh spacing. The high speed digital computer CDC 1604 of the Southern Methodist University was employed to carry out the computations. Two sets of computations were completed for each case. One with $\delta_x = 0.25$ and the other with $\delta_x = 0.50$. The latent heat parameters ξ and the dimensionless transition range δ_F for all cases were

0.5 and 0.1 respectively. To obtain an idea of the accuracy of the computer results, it was assumed that for small values of τ, the temperature distribution along the 55th vertical grid line is essentially one-dimensional. Then the Euclidean norm of the departure of the vector $w_{55}(\tau) = (w_{2,55}, w_{3,55} \cdots w_{N1,55})$ from that of the Neumann solution was computed in a similar way to that of the one-dimensional case.

The four computation runs were numbered as follows:

Problem Number	Run Number	Mesh Spacing	δ_x	ξ
1	2-1	constant	0.25	0.5
2	2-2	constant	0.5	0.5
3	2-3	variable	0.25	0.5
4	2-4	variable	0.5	0.5

Figure 17 is a plot of

$$\left\| E(\tau) \right\| = \left[\sum_{i=2}^{N_1} \left(u(x_{2,i};\tau) - w_{i,55}(\tau) \right)^2 \right]^{\frac{1}{2}} \quad \text{versus } \sqrt{\tau}$$

for Runs 2.3 and 2.4, where N_1 is a positive integer such that $x_{2,N_1} \leq 2\xi\sqrt{\tau}$, and $u(x_{2,i};\tau)$ is the Neumann solution of the one-dimensional temperature field in a region $x_2 \geq 0$. Note that the values of $\left\| E(\tau) \right\|$ for $\sqrt{\tau} \leq 0.5$ are almost the same as those of the numerical solution of the one-dimensional case for $\delta_x = 0.25$ and $\delta_F = 0.1$ (see Figure 7). For $\sqrt{\tau} > 0.5$, $\left\| E(\tau) \right\|$ uniformly increases with τ, which indicates the increasing corner effect on the 55th vertical grid line rather than an increase in the error of the numerical solution. However,

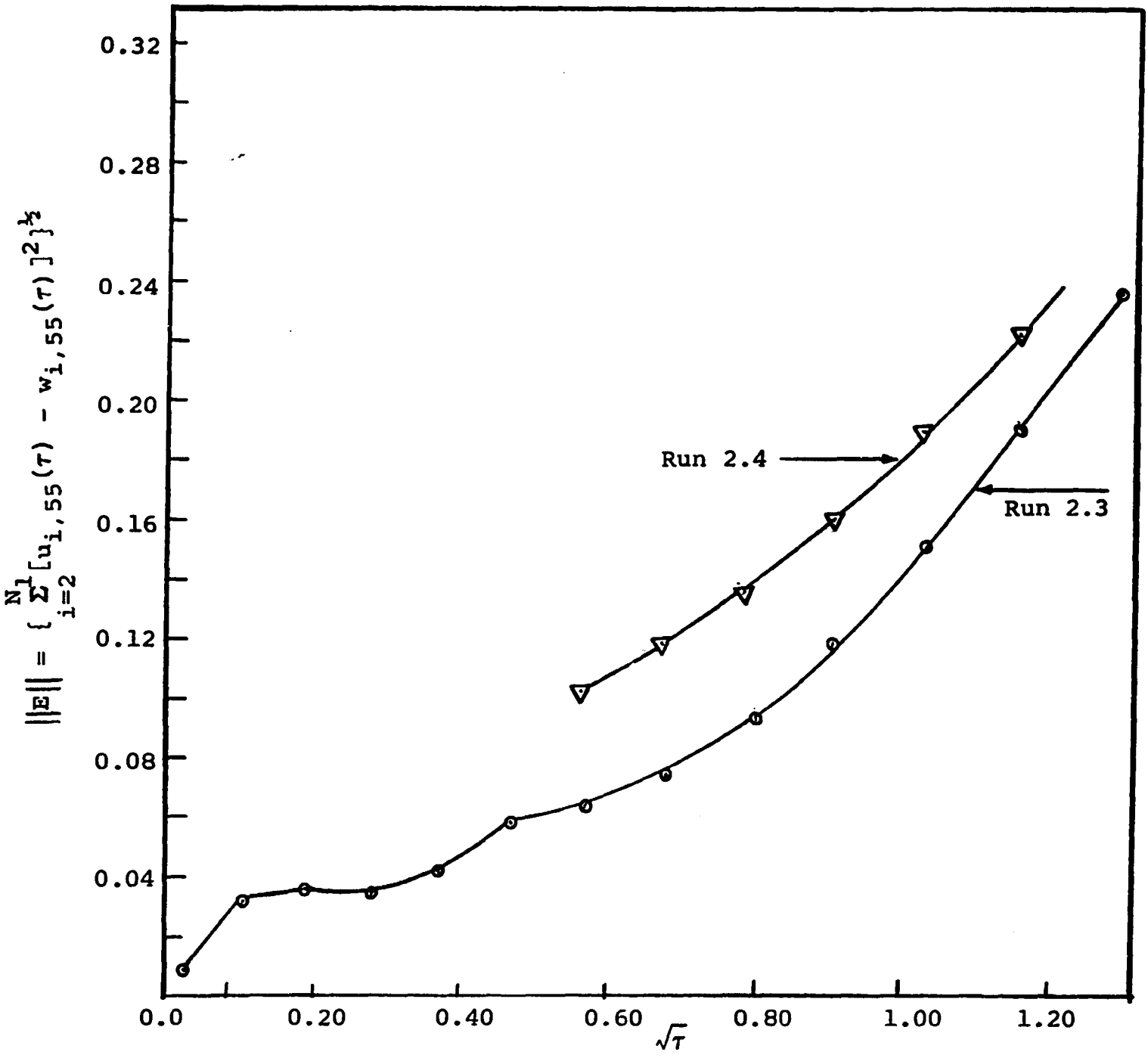


Figure 17. Variations of $\|E\|$ with $\sqrt{\tau}$ for Runs 2.3 and 2.4.

the difference between the values of $\| E(\tau) \|$ for Runs 2.3 and 2.4 is an indication of an increased discretization error when δ_x is increased from 0.25 to 0.5.

One of the most useful quantities in judging the correctness of the solution is the cumulative heat transfer at the exposed boundary calculated by equation (4.19). This quantity is especially useful when the heat flux at the exposed boundary is prescribed instead of the temperature. The reason being the fact that in this case the cumulative flux at the boundary is known so that the computed values of $Q(\tau)$ provide an excellent check on the correctness of the numerical solution. In Figure 18 the computed values of $Q(\tau)$ for all the four runs is plotted versus $\sqrt{\tau}$. Note how closely the results of Runs 1 and 3 agree with each other. Note also that for Runs 2 and 4, which required almost half as much computer time as Runs 1 and 3, the error in $Q(\tau)$ is not really very significant. The dotted line in Figure 18 gives the values of $Q(\tau)$ if the semi-infinite region under consideration were bounded by the lines $x_1 = 0$, $x_1 = 1.0$ and $x_2 = 0$.

The case of variable mesh spacing is indeed important in solving the problem of semi-infinite heat conduction in plane regions, because of the reduced number of computation steps when τ is large. It can easily be concluded from Figure 18 that a proper choice of variable mesh spacing can be made without any sacrifice in the accuracy of the solution, inspite of the fact that here the ratios of the maximum and minimum eigenvalues of the matrices H and V are much larger.

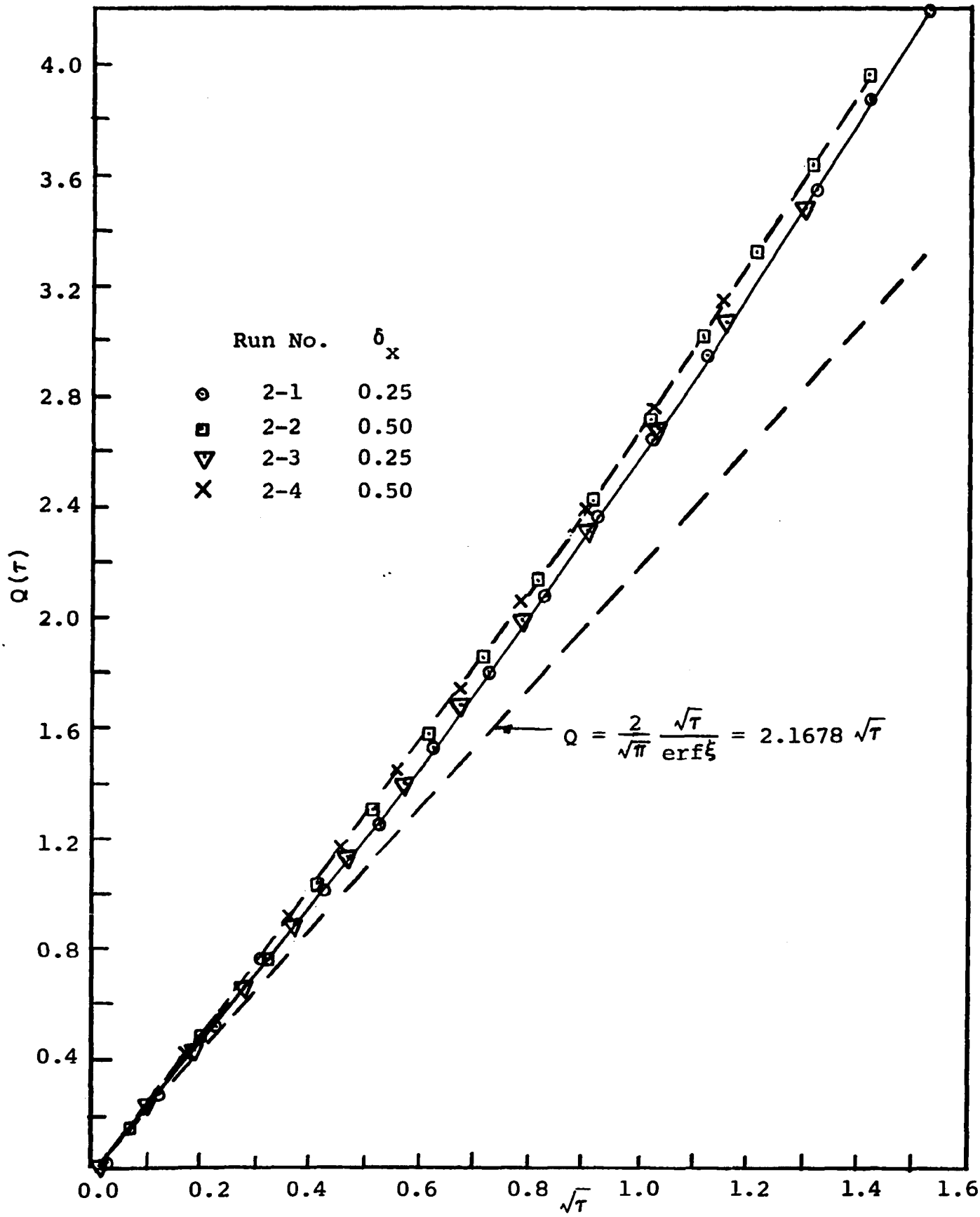


Figure 18. Computed Cumulative Heat Transferred to the Region R" (Figure 14) versus $\sqrt{\tau}$

Figure 19 shows the departure of $Q(\tau)$ for the corner from that of a semi-infinite slab of a unit width. The ratio $Q/\sqrt{\tau}$ increases uniformly with $\sqrt{\tau}$ for the corner while that of the semi-infinite slab is constant for all $\tau > 0$.

Figures 20 through 24 show the movement of the isotherms $u(x_1, x_2, \tau) = 0.75, 0.5, 0.25, 0.05, 0.0159$ and 0.003 for Example Problem 1. The last three isotherms correspond to 3.5 per cent, 50 per cent and 90 per cent transition, respectively. These figures are the reduced photographs of the computer output at various time levels. The isotherms were drawn by interpolating between the values of $u_{i,j}(\tau)$, $(i,j) \epsilon R_h$ of the adjacent mesh points. The decimal points in the printed values of $u_{i,j}$ locate the actual position of the mesh points with respect to the co-ordinate axes shown on the top and right of the figures. The presentation of data in this form not only saved a substantial amount of effort, which would have been consumed in converting the computer outputs to a graphical form, but it also preserved all the information in a very neat manner and thus allowed accurate sketches of any other isotherms.

Figures 25 through 29 are similar plots for Example Problem 3. The co-ordinates y and x in these figures are defined by $y = x_2/(1 + x_2)$ and $x = x_1/(1 + |x_1|)$. The position of the interface may be taken to be that of the isotherm $u_{i,j}(\tau) = 0.0159$ which corresponds to 50 per cent removal of the latent heat of transition. For large values of τ, the isotherms $u_{i,j}(\tau) = 0.003$ and $u_{i,j}(\tau) = 0.05$ are also drawn.

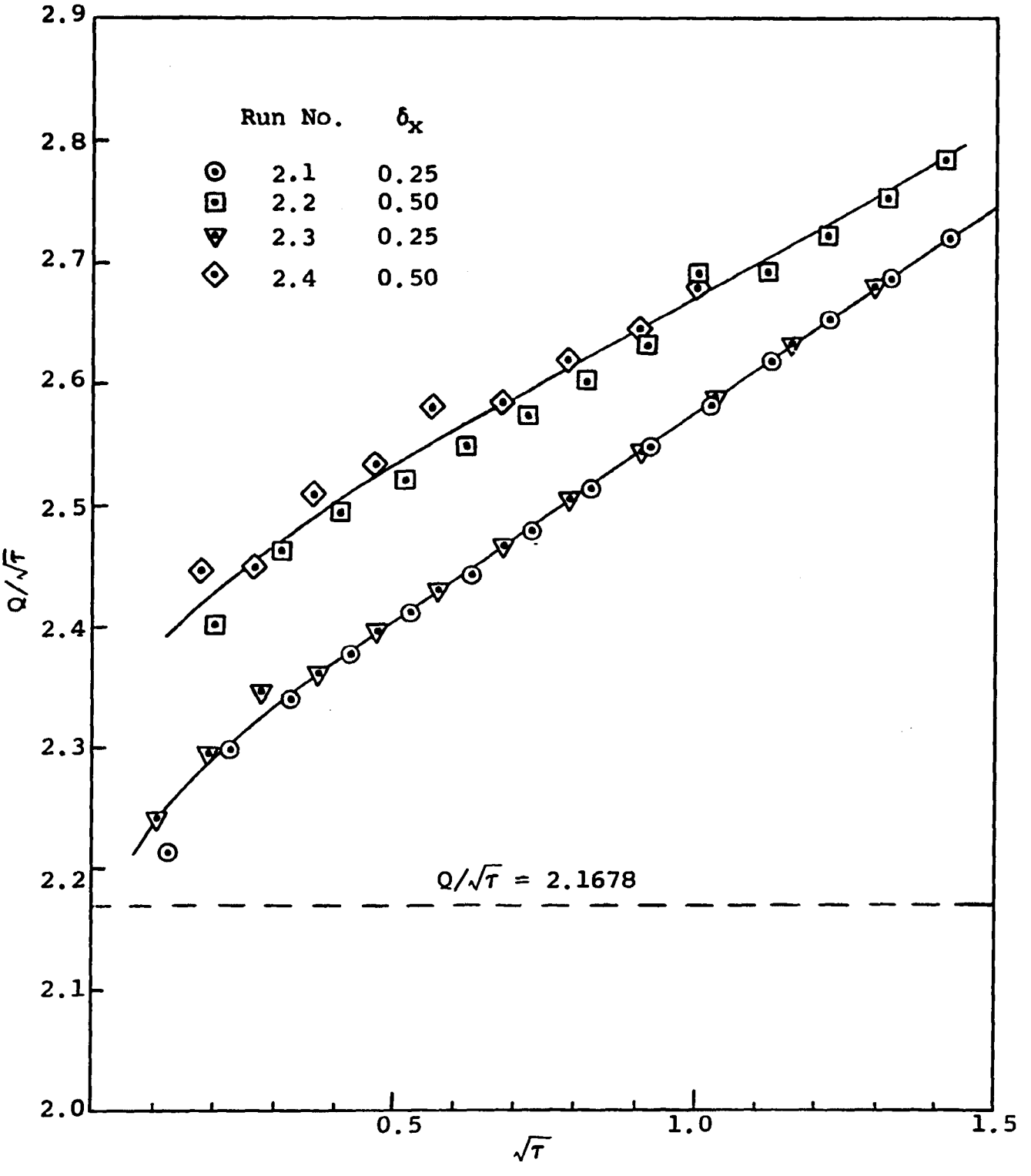


Figure 19. Departure of Cumulative Heat Transferred to the Region R" (Figure 14) from that of a Semi-Infinite Slab of Unit Width.

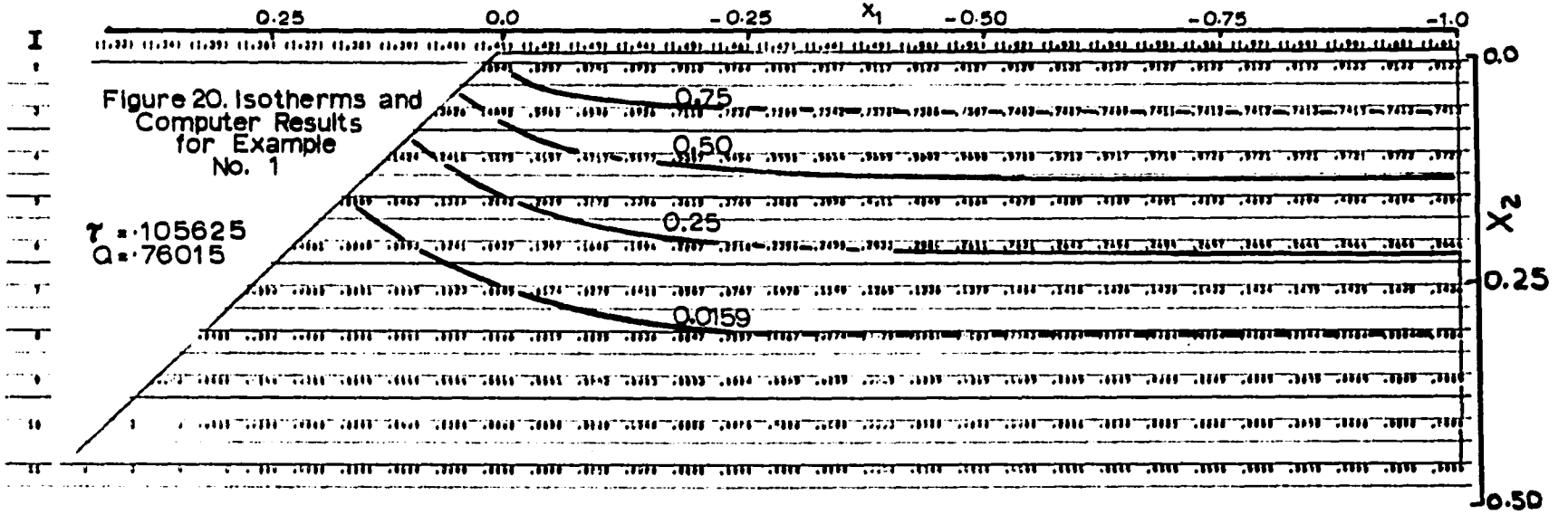


Figure 20. Isotherms and Computer Results for Example No. 1

τ = .105625
Q = .76015

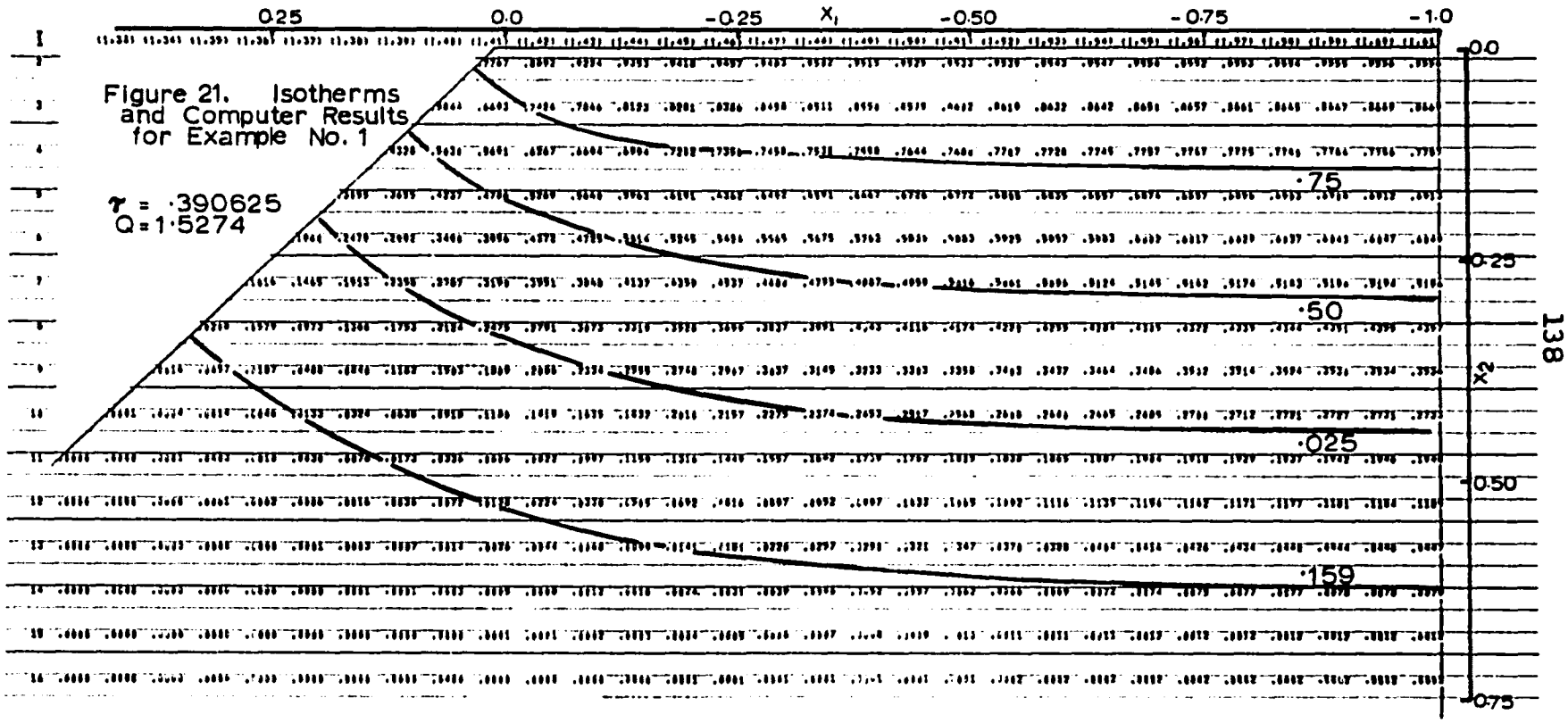


Figure 21. Isotherms and Computer Results for Example No. 1

γ = ·390625
Q = 1·5274

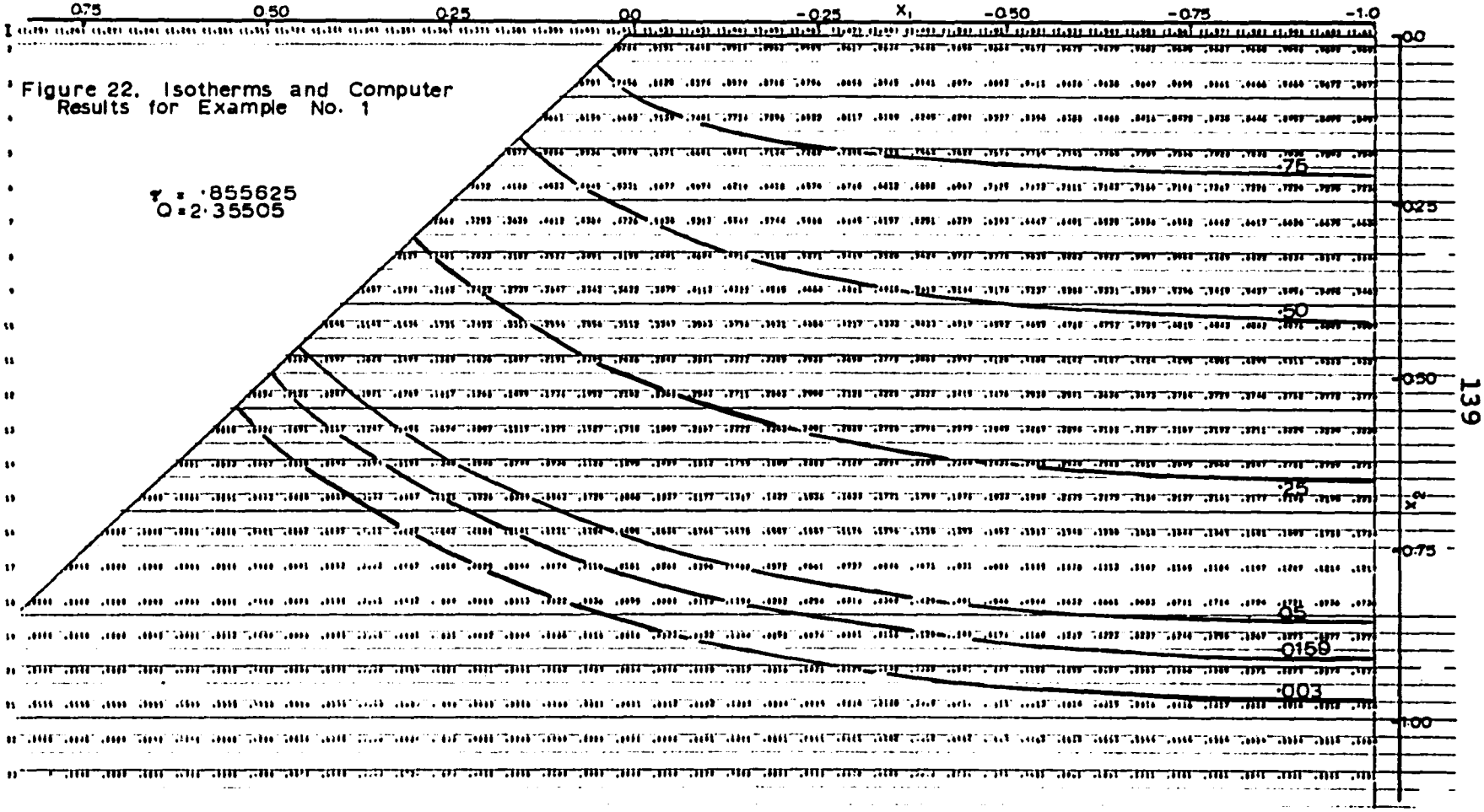


Figure 22. Isotherms and Computer Results for Example No. 1

$\gamma = .855625$
$Q = 2.35505$

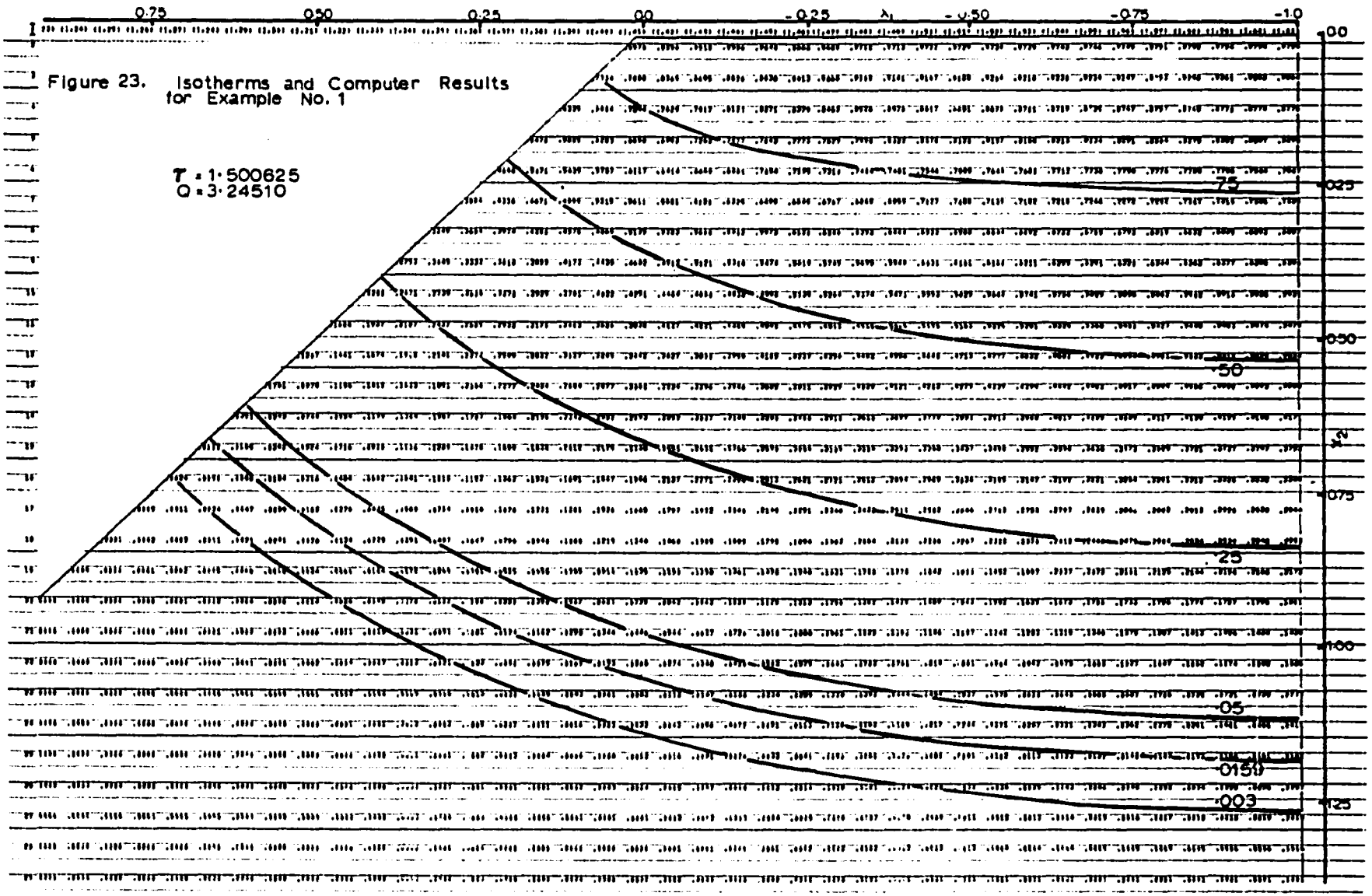


Figure 23. Isotherms and Computer Results for Example No. 1

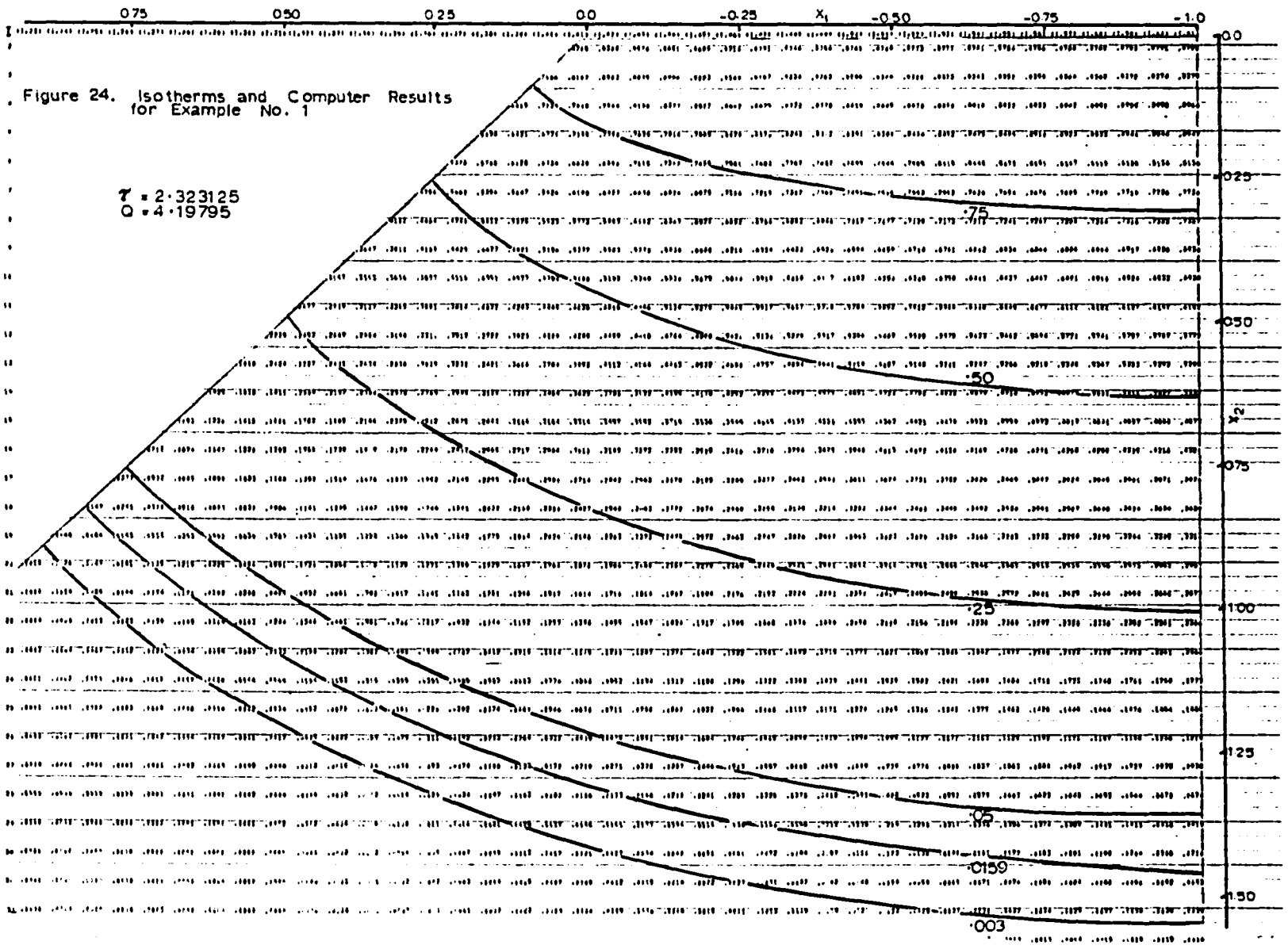


Figure 24. Isotherms and Computer Results for Example No. 1

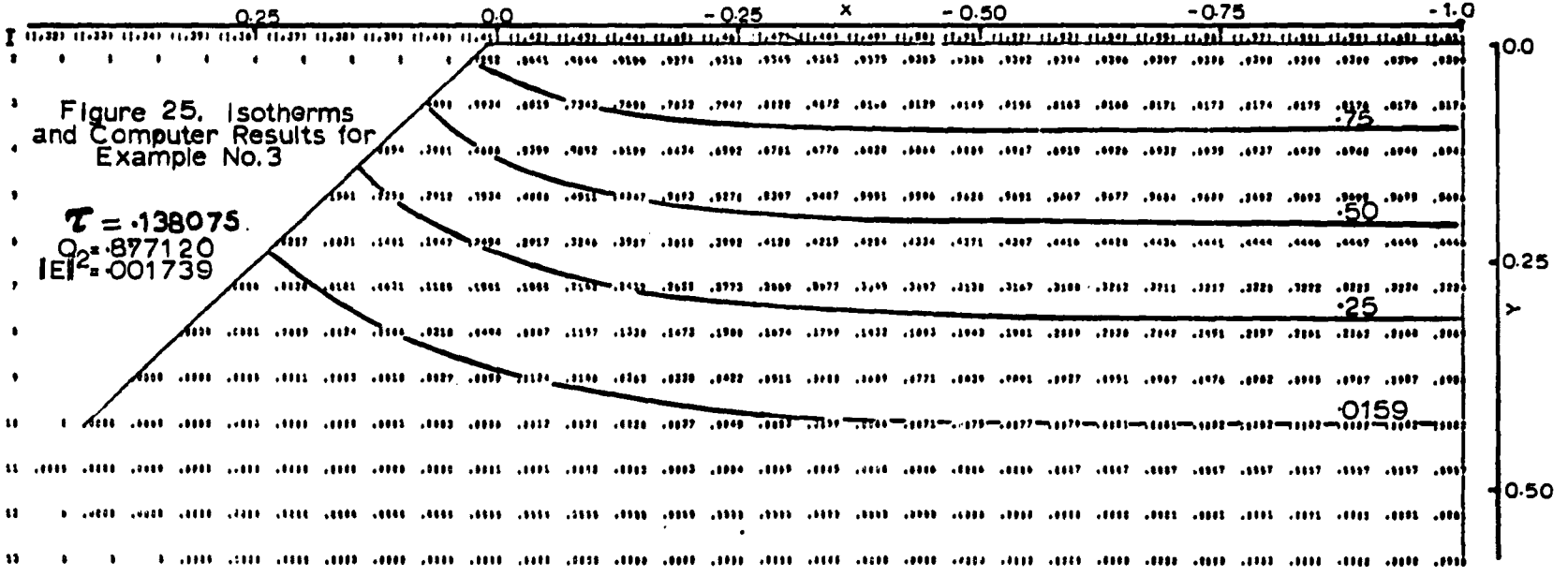


Figure 25. Isotherms and Computer Results for Example No. 3

$\tau = .138075$

$Q_2 = .877120$

$|E|^2 = .001739$

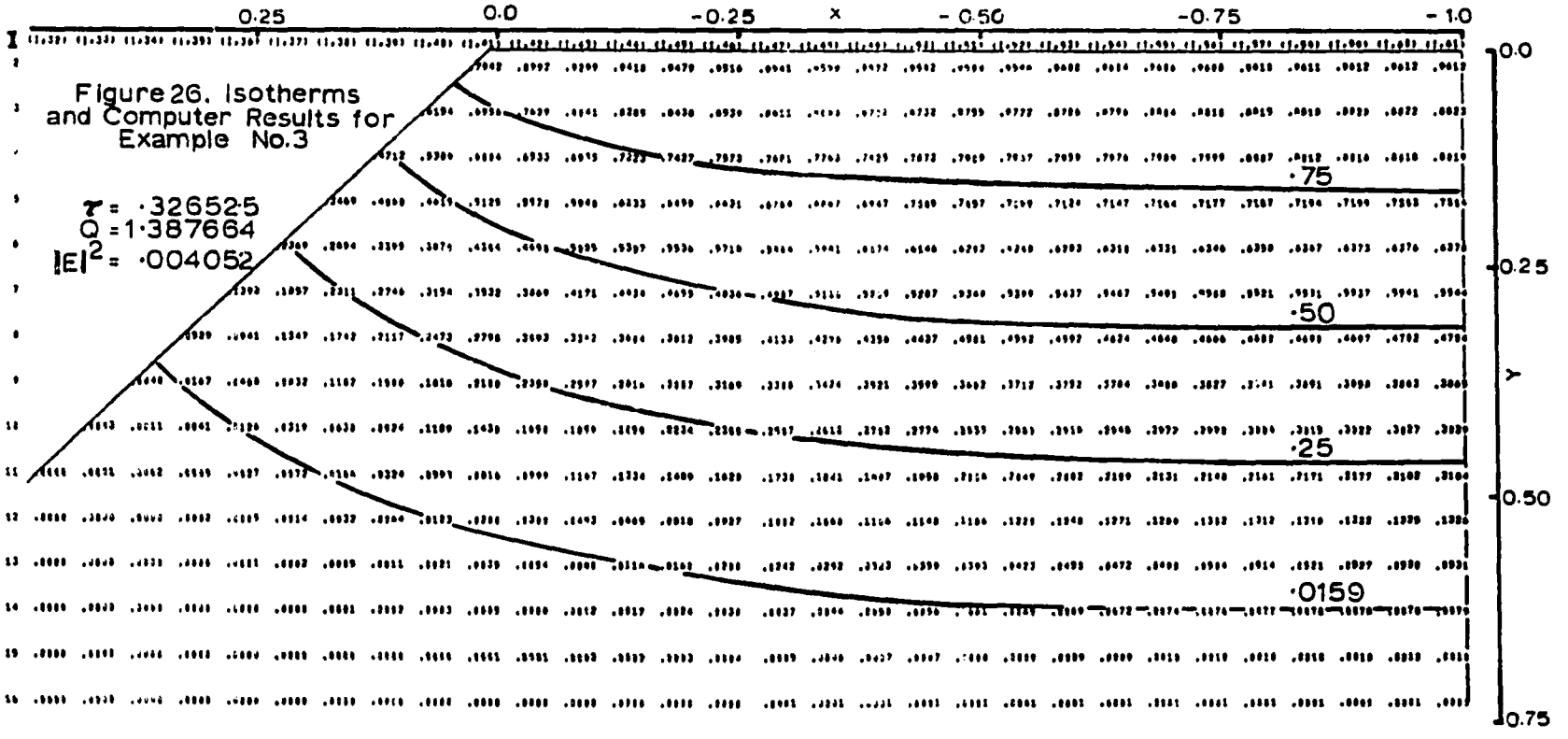


Figure 26. Isotherms and Computer Results for Example No.3

τ = ·326525
Q = 1·387664
$|E|^2$ = ·004052

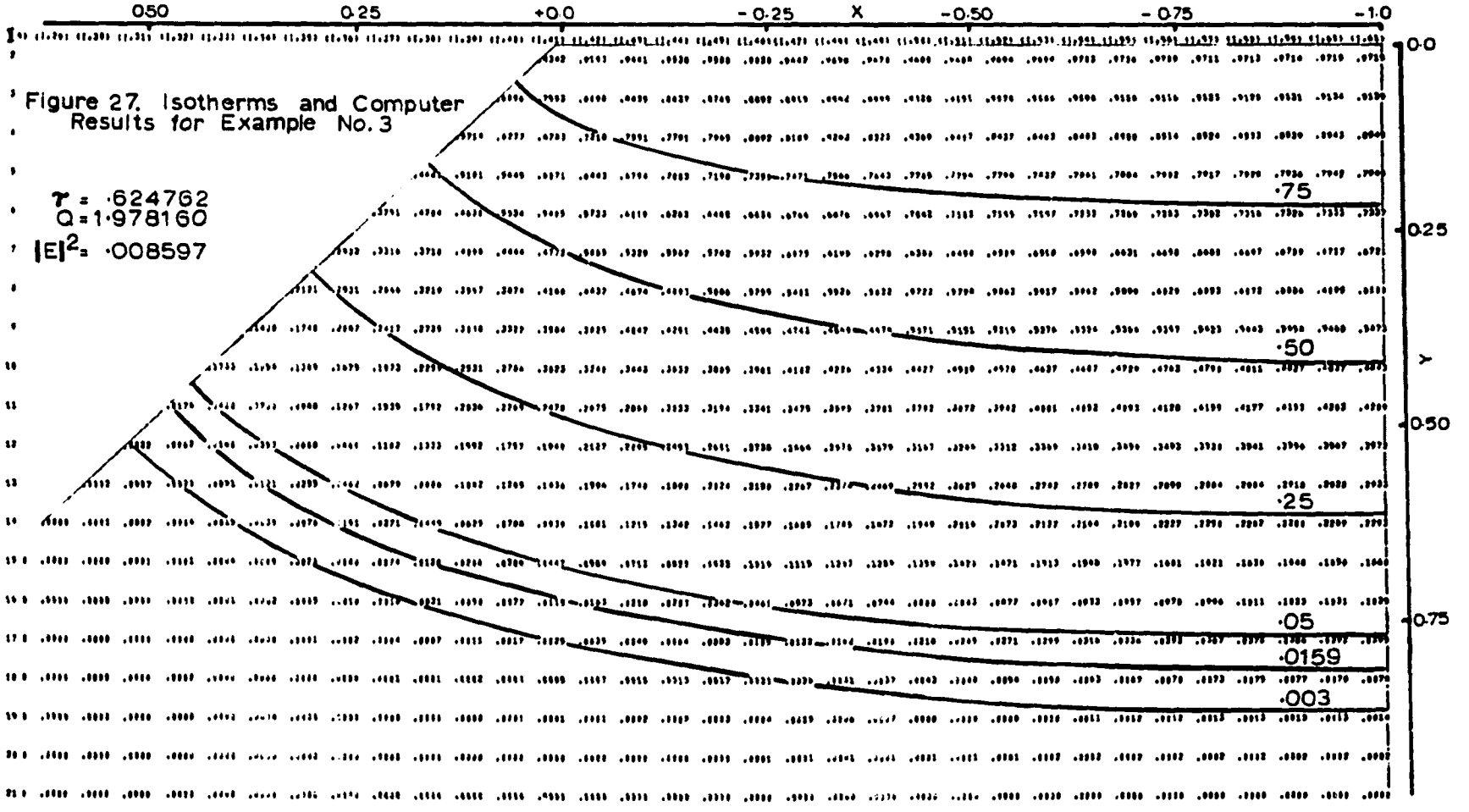


Figure 27. Isotherms and Computer Results for Example No. 3

τ = ·624762
Q = 1·978160
$|E|^2$ = ·008597

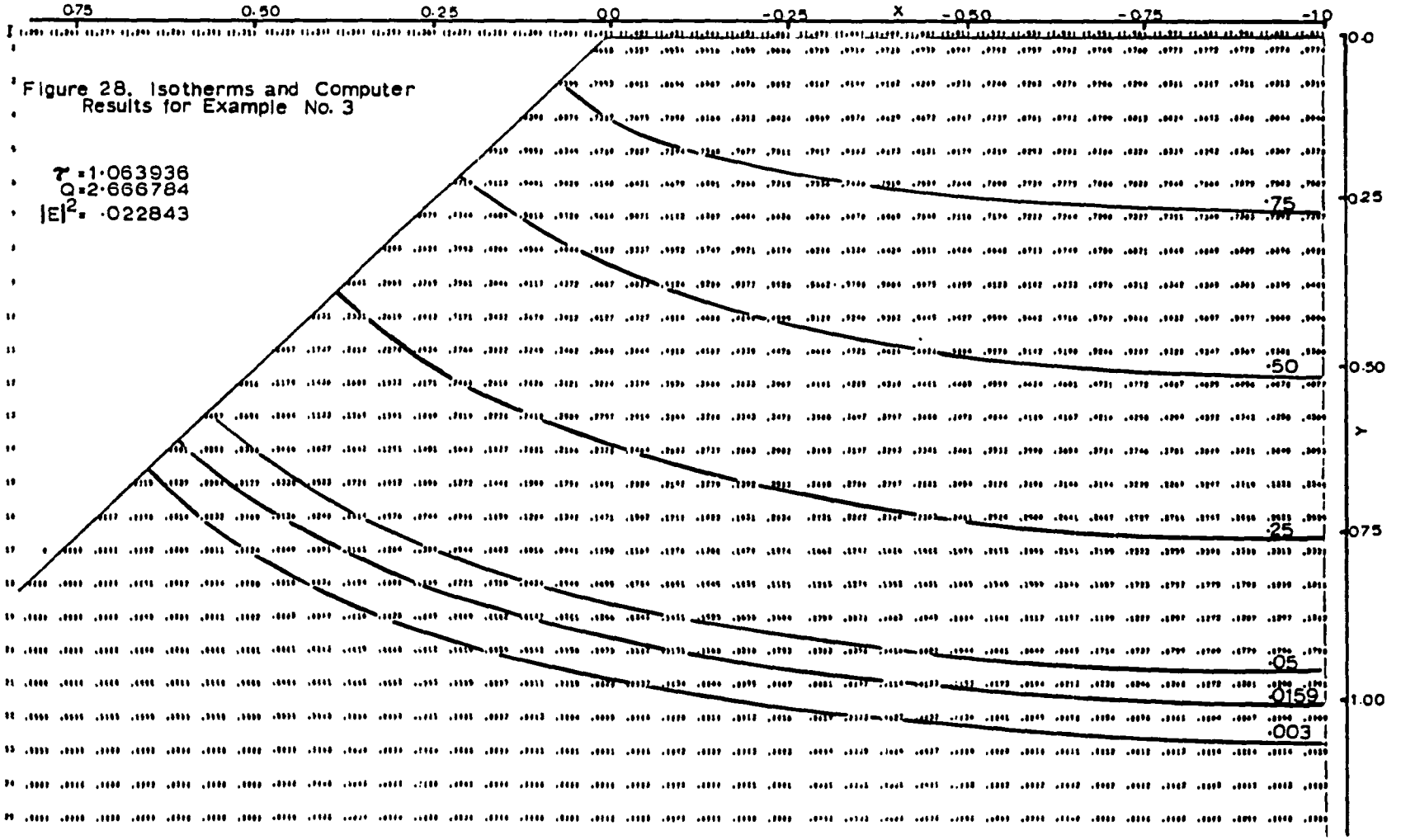


Figure 28. Isotherms and Computer Results for Example No. 3

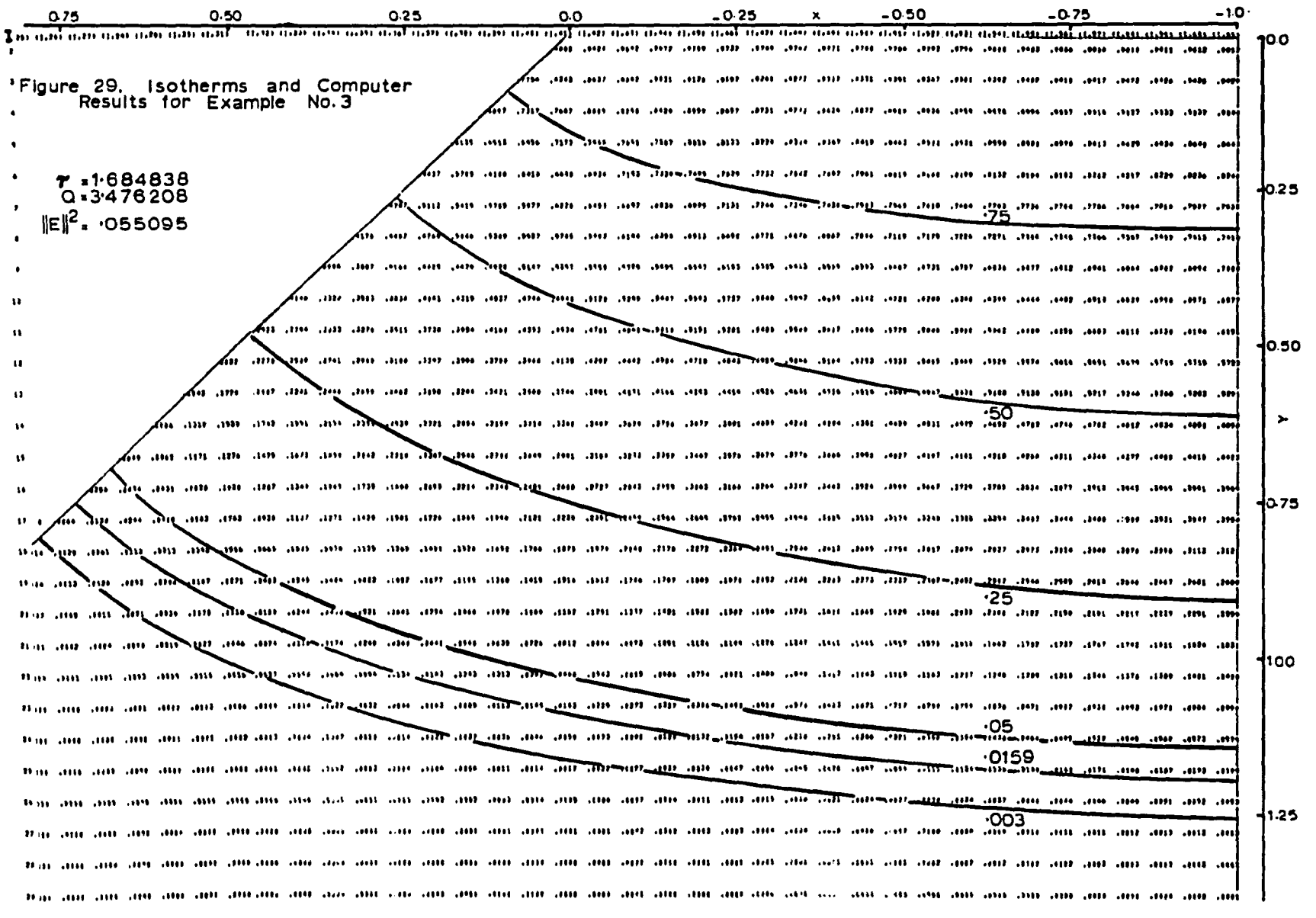


Figure 29. Isotherms and Computer Results for Example No. 3

These two isotherms correspond respectively to 90 per cent and 3.50 per cent phase change.

The results of Runs 2.2 and 2.4, as well as those of Runs 2.1 and 2.3 which are not covered in Figures 20 through 29 are given in Appendix C. Included also in this appendix is the complete listing of the input data for all the runs. These data are included to provide a detailed standard for testing future computer programs. Figure 30 gives the location of the 0.0159 isotherm which has been taken arbitrarily as the position of the interface, where 50 per cent of the phase transition has been completed. The curves in Figure 30 were obtained by cross-plotting Figures 20 through 24.

A detailed study of Figures 20 through 29 indicates the smoothness and uniformity of the computed results. It also shows that the erroneous behavior of the numerical solution for the one-dimensional case shown by Figures 10, 11 and 12 is unlikely to occur for the two-dimensional problems. The reason lies in the fact that the operator:

$$T(r) = (\frac{2}{r}\tilde{\Phi} + V)^{-1}(\frac{2}{r}\tilde{\Phi} - H)(\frac{2}{r}\tilde{\Phi} + H)^{-1}(\frac{2}{r}\tilde{\Phi} - V)$$

is very unlikely to have negative entries for even large values of r, while some of the entries of

$$(\frac{2}{r}\tilde{\Phi} + H)^{-1}(\frac{2}{r}\tilde{\Phi} - H)$$

can very well become negative when r is sufficiently large.

The above experiments definitely demonstrated the usefulness of the recursion formulae (4.14), (4.17) and

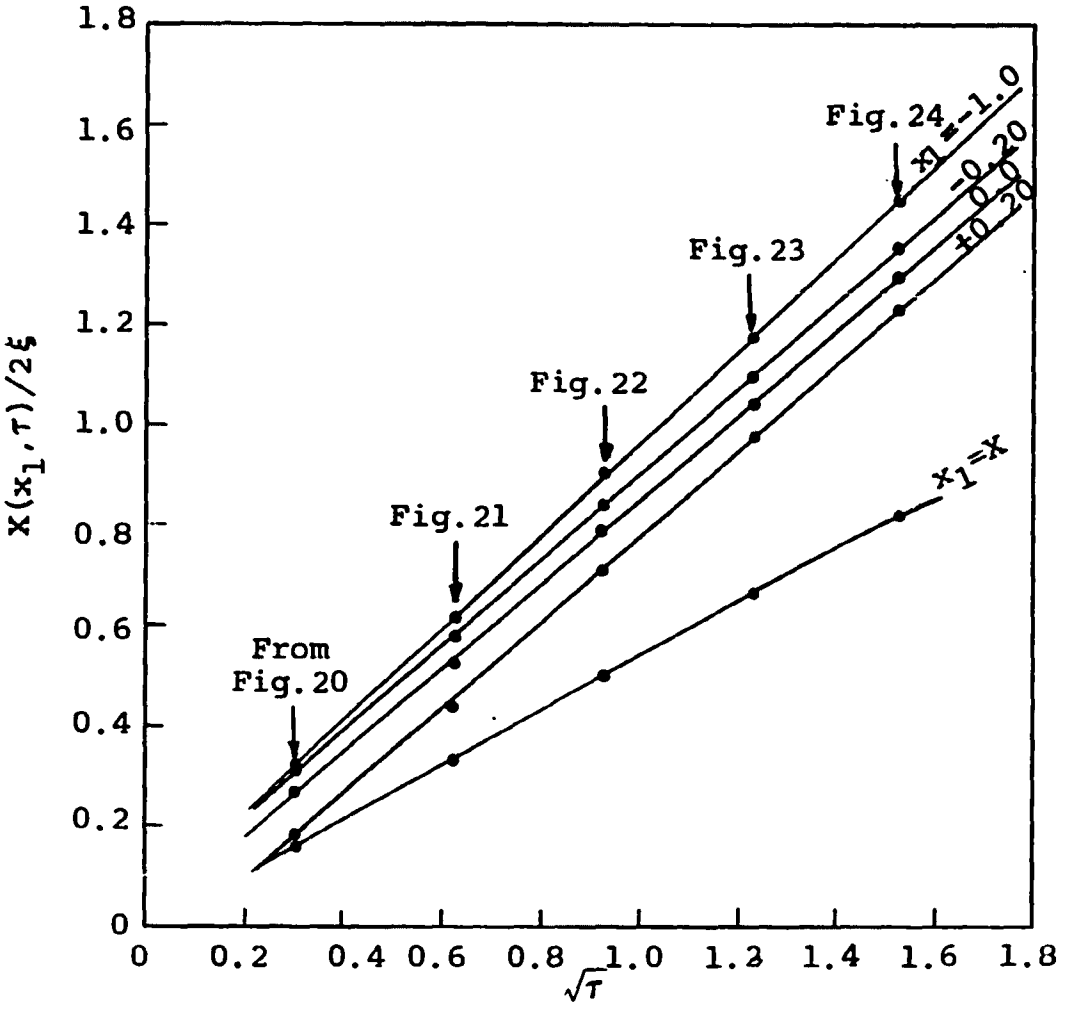


Figure 30. Growth of the Interface $X(x_1,\tau)$, with $\sqrt{\tau}$ for Various Values of x_1. Position of Interface is taken Arbitrarily at the 0.0159 Isotherm.

(4.18) for r, when the source vector ∎ is fixed. The general use of such formulae when ∎ is strongly time dependent remains to be investigated.

It deserves to be mentioned that r should be so chosen that the increment in $u_{i,j}(\tau)$ for two consecutive time levels does not exceed a small fraction of the transition temperature range δ_F for all points (i,j) close to the interface. Otherwise

$$\sum_{k=1}^{m} \tilde{\varphi}_{i,j}\left(w_{i,j}(t_k - \tfrac{1}{2}r_k)\right)\left[w_{i,j}(t_k) - w_{i,j}(t_{k-1})\right]$$

deviates very appreciably from

$$\int_{u_{i,j}(0)}^{u_{i,j}(t_m)} \varphi_{i,j}(u)\, du$$

which results in a strong departure of the numerical solution from the exact solution. This limitation must be seriously examined when ∎ is strongly time dependent, or when $u_F \neq u_{i,j}(0)$, $(i,j) \epsilon R_h$.

CHAPTER V

EXPERIMENTAL APPARATUS AND PROCEDURE

Two separate experimental set-ups were built: one for testing one-dimensional diffusion cells and the other for testing two-dimensional diffusion cells. The one-dimensional diffusion cell was developed as a preliminary to the development of a two-dimensional diffusion cell. For both cases, several designs and arrangements of the diffusion cells were tested, until the data obtained from the one-dimensional and the two-dimensional diffusion cell analogs were adequate for the purpose of the present investigation. The apparatus for testing the diffusion cells also included conventional equipment such as temperature bath, micropump, cathetometer, and associated measuring equipment, which will be discussed only briefly. On the other hand, since the designs of the diffusion cells are critical, they deserve more detailed treatment. The successive improvements in the one-dimensional cells were directed toward increasing the accuracy of the measurements, while those of the two-dimensional cell were for the purpose of producing a pure two-dimensional diffusion field.

The Apparatus for Testing the One-Dimensional Diffusion Cell

The apparatus for the first series of the one-dimensional tests was essentially that previously developed by Walls (81) and Mirshamsi (57) for the measurement of the diffusion coefficient in liquid metals. It consisted of four quartz capillary tubings mounted on a capillary holder and immersed in a water bath in which the temperature was controlled to $\pm 0.5°C$ (Figure 31). The capillary holder was connected by a shaft to a 1-RPM synchronous motor. A screw mechanism on the motor was used to move the capillary holder vertically and to rotate it at a speed of 1-RPM. The vertical movement was to allow automatic immersion or withdrawal of the capillaries in and out of the water bath. The rotation of the capillary holder was maintained throughout the experiment to maintain a constant boundary concentration without excessive turbulence. The portion of the water bath in which the capillaries were immersed was isolated from the rest of the water reservoir by a beaker containing distilled water. 2-mm ID and 1-mm ID capillaries were used at one time or another. The length of the capillaries were varied from 3.8 cm in the tests with saturated phenol solution to 15 cm in the tests with pure phenol.

The cells were lowered in the bath such that their top was barely above water level and were kept in this position until temperature equilibrium was reached. A phenol solution containing both co-existing phases was kept in a

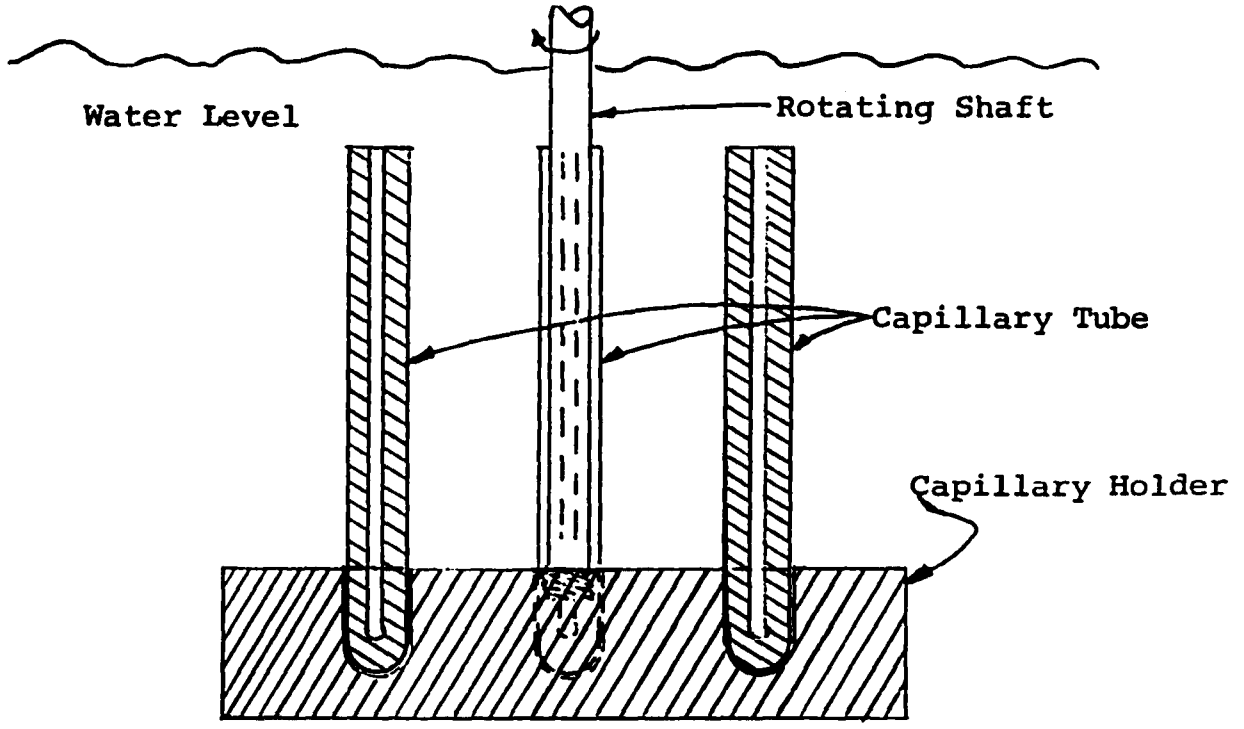


Figure 31. The Quartz Capillaries and the Capillary Holder.

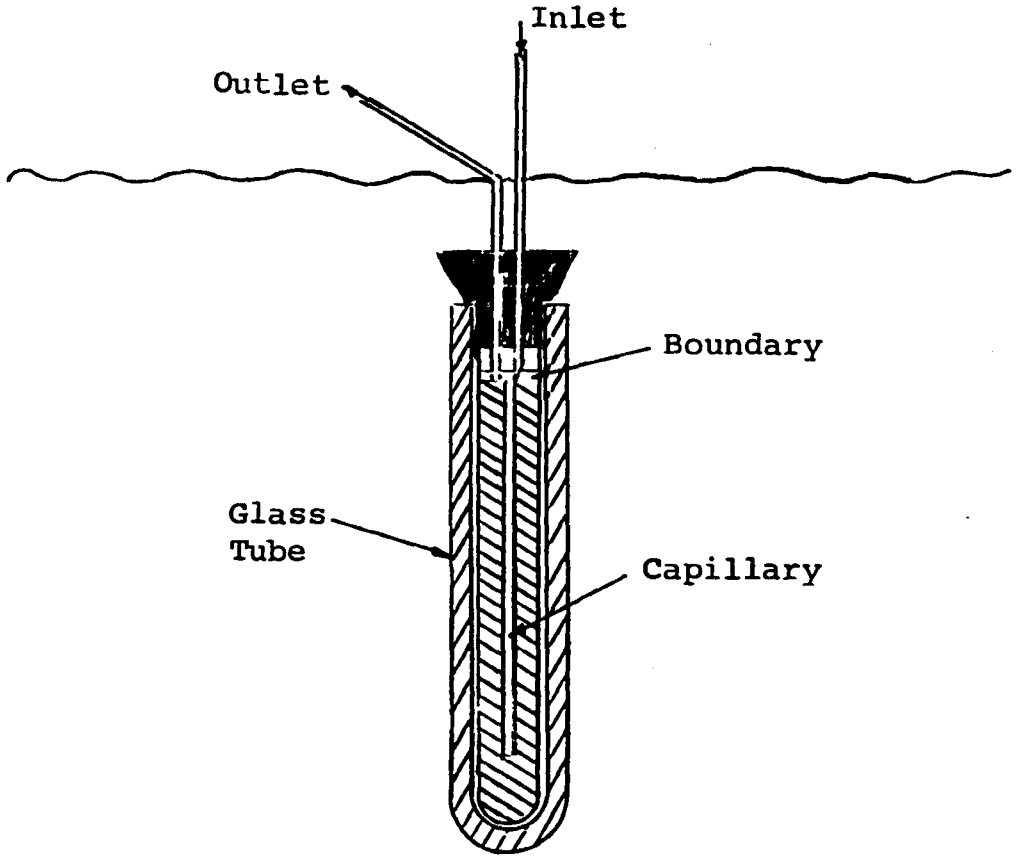


Figure 32. The Improved One-Dimensional Cell. (The Capillary Tubing is Enclosed in a Glass Tube Immersed in a Water Bath to allow better Temperature Control and also better Control of the Concentration at the Boundary of the Capillary).

container immersed in the water bath. The lower phase (phenol-rich phase) was partly withdrawn by a preheated hypodermic syringe which was immediately used to fill the capillaries. Upon submerging the capillaries, an interface was formed on the top, open end of the capillaries. This interface gradually moved inward due to the diffusion of phenol in water and water in phenol. The capillaries were graduated on their external surface to allow accurate measurement of the position of the interface by means of a telescope. Several runs were completed at 30°, 40°, 50° and 60°C.

The above method, however useful, left much to be desired. The difficulties and the causes of error in the measurement of the position of the interface were:

1. The beaker in which the capillaries were submerged was not stirred, thus making the control of temperature very unstable. The excessive evaporation of water at 50° and 60°C, and the unstable temperature control caused some appreciable temperature fluctuation.
2. At 50°C and higher, the continuous deaeration of water gave rise to the formation of air bubbles over the surface of the capillaries which not only made measurement of the interface very faulty but also made it difficult to maintain a constant concentration at the open end of the capillaries. In fact, it is likely that the passage of the diffusing molecules was blocked by these bubbles.

3. The measurement of the position of the interface was very inaccurate because the capillaries were graduated on the outside. When viewing them through the telescope, the capillaries and the interface were not at the same focal distance.

To resolve these experimental difficulties the following changes were made:

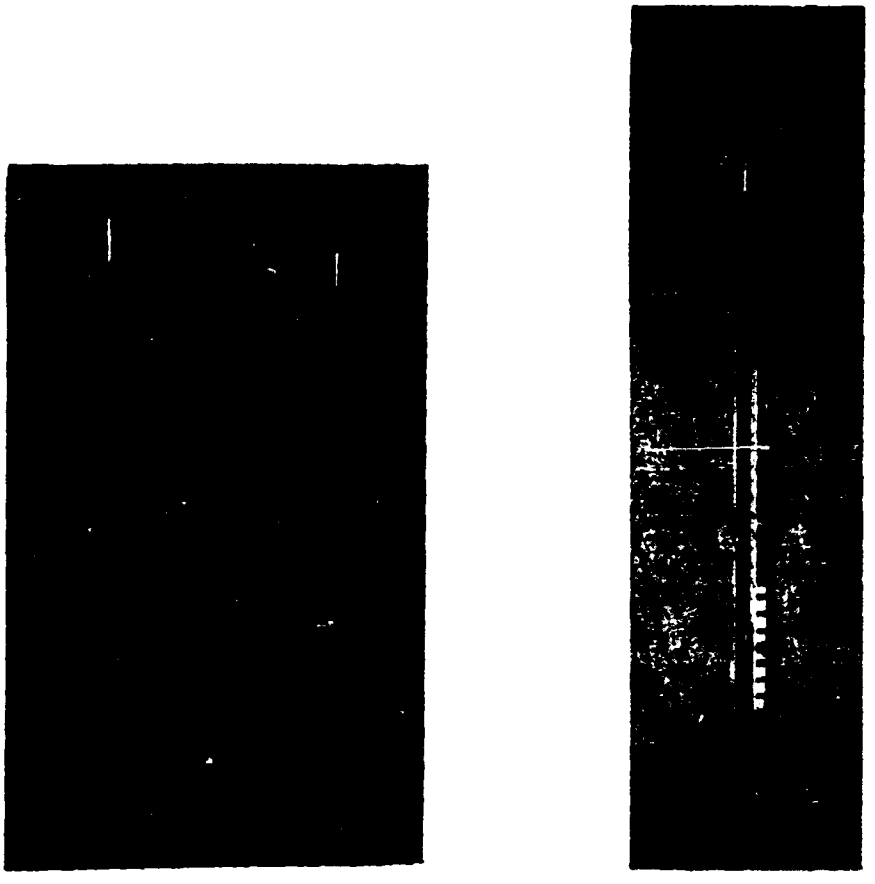
1. The capillaries were enclosed in fitted glass tubes, which were longer than the cells. The tubes were closed at the top with rubber stoppers. Inlet and outlet lines were provided through the stoppers for the water flow to pass the boundary (Figure 32). This assembly was then kept in the agitated water bath.
2. A cathetometer which could read to ±0.005 cm was used to read the position of the interface.

With this modified arrangement, a series of tests were conducted at 55°C with a saturated phenol-rich phase in the cell, and a water phase containing various amounts of phenol (between 0.0 to 0.956 moles per liter) being passed over the boundary. The flow of water solution was maintained by gravity at about 1 cc per hour. Although these tests were more conclusive than the previous ones, they introduced some difficulties and shortcomings of their own. These difficulties can be summarized as follows:

1. The formation of air bubbles inside the capillary and on the top destroyed many tests.

2. Vibration of the cells due to excessive agitation of the water bath was believed to disturb the diffusion field in the capillaries.
3. The stopper arrangement for introducing the inlet and outlet tubings proved to be awkward, especially in filling the capillaries.
4. The sudden formation of a meniscus, as before, introduced appreciable initial error, as was the case with the previous tests.
5. The gravity flow of the water solution was not uniform and needed constant inspection for the possible stoppage.

In view of the above difficulties, it was found advisable to construct a new one-dimensional cell which could be operated with the minimal experimental error. A photograph of this cell is shown in Figure 33. A detailed drawing is given in Figure 34. The glass tubing in which the capillary was inserted was joined to a brass cap by a transparent epoxy resin. To avoid phenol attacking the epoxy, the interior part of the joint was filled with silicone rubber. The cap was screwed to the brass head and completely sealed with a teflon packing, Figure 34. The inlet and outlet tubings were sealed with O-rings such that the entire assembly was vacuum tight. The bottom of the capillary was seated on a stiff spring which forced it upward against the extended stem of the cell's head. The solution entered the top of the capillary through one side of the extended head and left from



(a) (b)

Figure 33. The Final One-Dimensional Diffusion Cell--(a) The Components of the Cell, (b) The Assembled Cell.

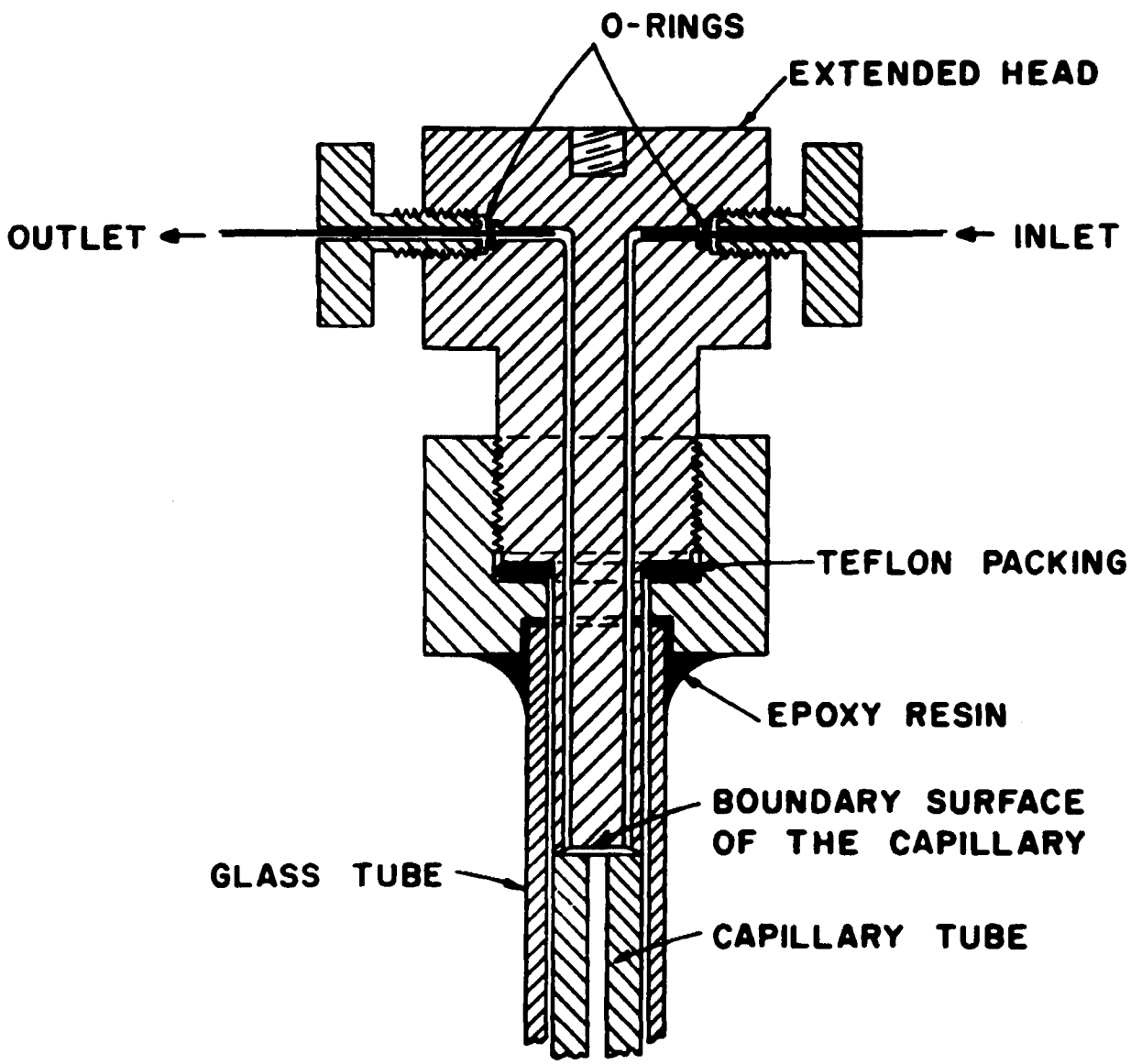


Figure 34. A Cross-Section of the Final One-Dimensional Cell Showing the Improvement in the Inlet and Outlet Tubings Connection.

the opposite side as shown in Figures 33 and 34. The flow channel on the top of the capillary was about 0.02 cm thick and about 0.3 cm wide. The micropump (which is described below) was employed to pump the solution into the cell. The speed of pumping was maintained constant at about 3 cc per hour. The cell was mounted vertically in the air bath, designed for the two-dimensional cell, in order to overcome many of the difficulties that were experienced with the water bath in addition to maintaining a much better temperature control and being able to conduct the one-dimensional tests along with the two-dimensional ones. To fill the cell, the outlet tubing was closed at the end and the cell was evacuated by connecting container "A" (where the solution to be fed into the cell was kept) to a vacuum pump, Figure 35. By suddenly opening container "A" to the atmosphere, the back pressure pushed the solution into the cell and filled the capillary. By this arrangement the solution was completely deaerated prior to being fed into the capillary. This technique completely solved the problem of air bubble formation in the cell.

Two tests were completed with this cell. Both were carried out at 55°C with pure water in the capillary and a phenol solution containing about 8 per cent water being pumped over the boundary surface of the cell. Since phenol solution is slightly heavier than water, the cell was mounted upside down to avoid convection inside the cell. The capillary tube was 1 mm ID and about 15 cm long. The results from the one-dimensional cells are discussed in the next chapter.

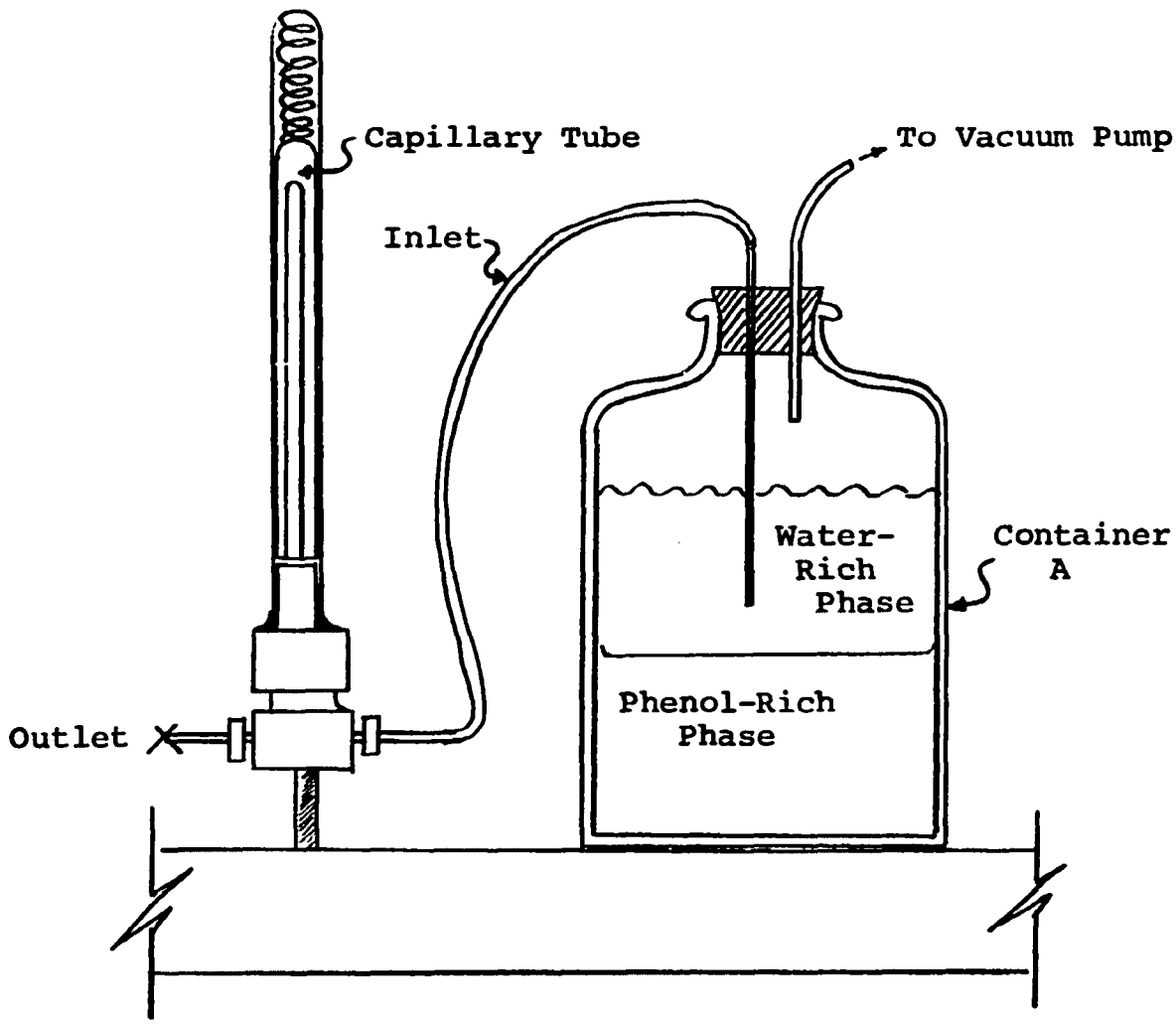


Figure 35. The Set-up of the One-Dimensional Cell for Filling with Phenol Saturated Water Solution. (The Entire Assembly was kept in the Air Bath).

The Apparatus for the Two-Dimensional Cells

The apparatus consisted of:

1. The two-dimensional diffusion cells.
2. An air bath.
3. A micropump.
4. A Graflex f/4.7 camera and associated arrangement.
5. A Sherr micro-projector.

The general layout of the apparatus is shown in Figure 36. The specific items are described below.

Most of the experimental effort in this work was centered in the development of the two-dimensional diffusion cell. Three different cells were constructed and tested. The first one was a complete failure in most respects. It, however, pointed out several important factors which should be taken into account in the design of future cells. Based on the knowledge gained from this cell, a second cell was constructed. With this cell it was possible to isolate several phenomena responsible for strong disturbance of the diffusion field and to study them separately. These experiments also demonstrated that several costly complications in the design of the cell were unnecessary. The third cell was then built and tested. The final results of the third cell definitely established the practicality of a two-dimensional diffusion cell analog, but it left much to be desired for accuracy and ability to measure all the important variables.

The design of these cells are discussed below. The experimental procedure is omitted from the discussions because

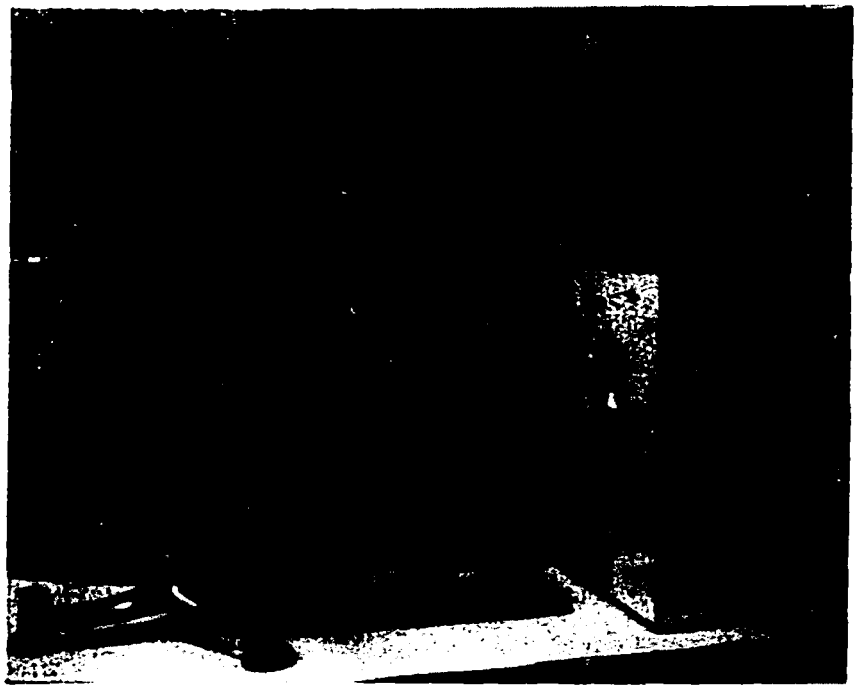


Figure 36. A View of the Experimental Apparatus showing the Air Bath, the Micropump, the Cathetometer and the Temperature Controller.

it was essentially trivial on one hand and different for each of several tests conducted, on the other hand. Only a brief account of the experimental procedure for the final test with the third cell is given.

The Preliminary Two-Dimensional Cell

This cell was designed to simulate the L-shaped region shown in Figure 37; it consisted of a liquid film contained between two parallel plates which were separated by a distance which could be varied between 0.1 mm to 1 mm. To simulate the boundary conditions a solution of desired concentration was passed over the boundary in a direction perpendicular to the plane of the liquid film in the cell.

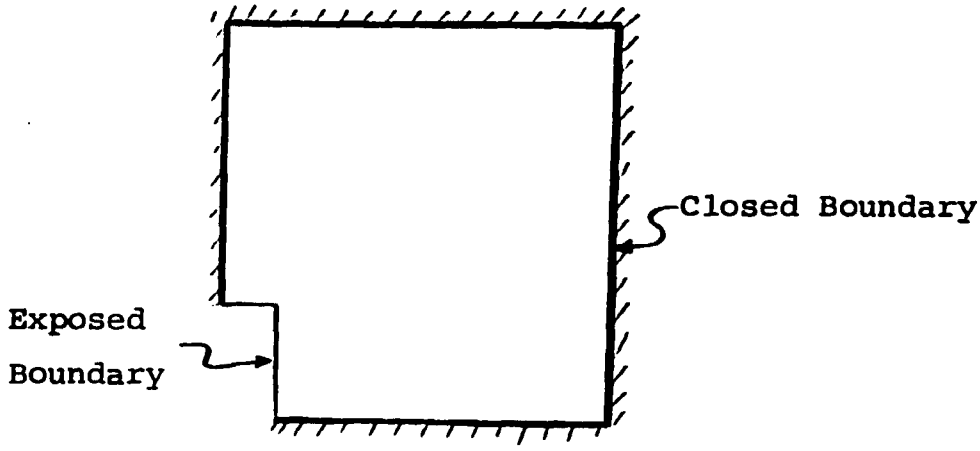
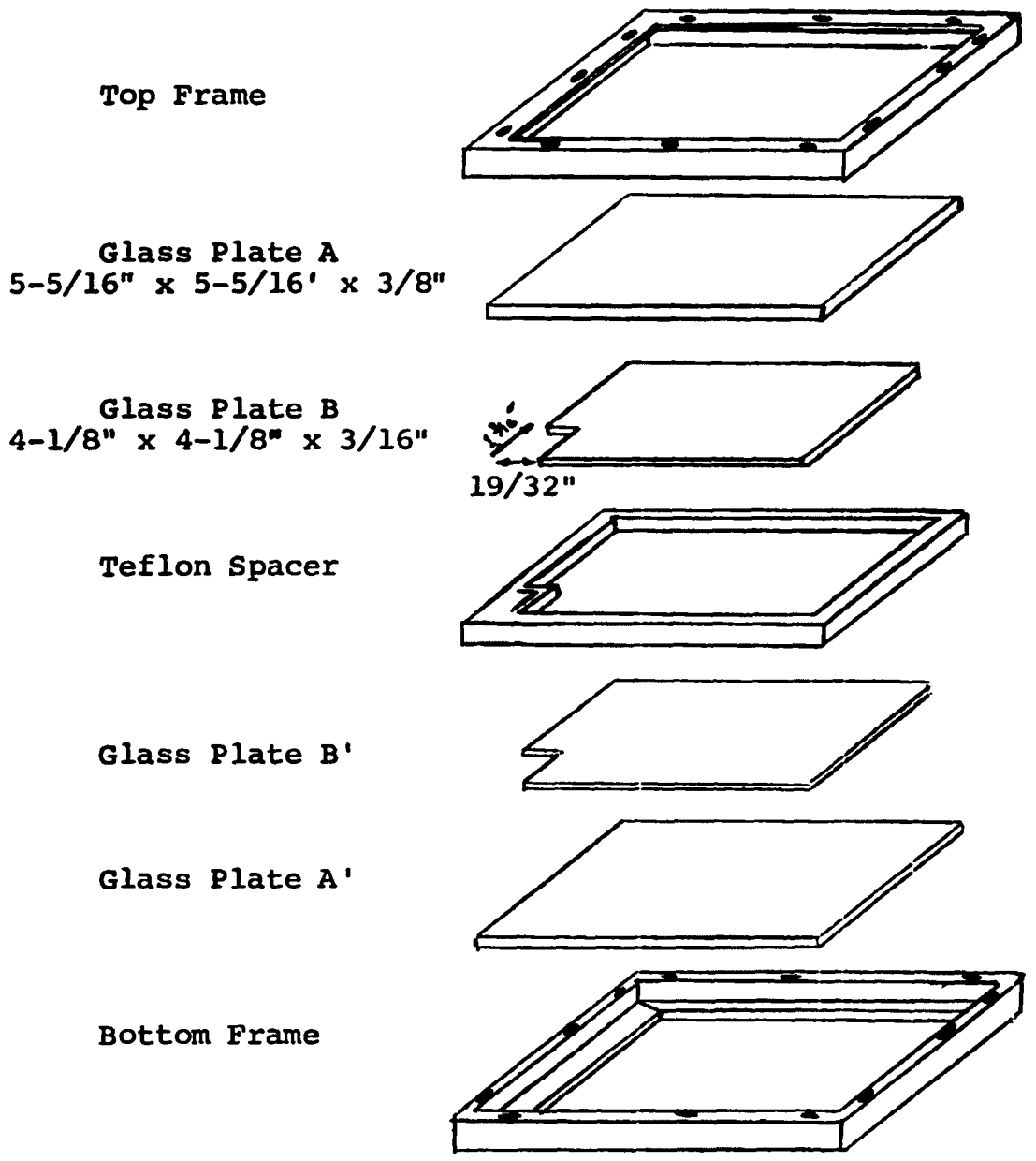
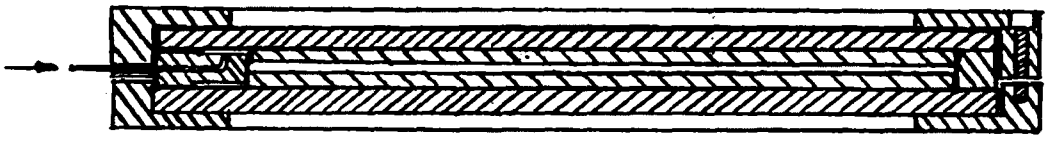


Figure 37. The Plane Region Simulated by the Preliminary Cell.

Figure 38 shows the various components of the cell. It consists of two L-shaped, 3/16 inch thick by 4 1/8 inch x 4 1/8 inch flat pyrex glass plates, two 3/8 inch thick by 5/16 inch x 5 5/16 inch square pyrex glass plates, a spacer and two frames. Each square glass plate was glued by a transparent



Exploded View of the Preliminary Cell



Cross-Section of the Preliminary Cell

Figure 38. A Sketch of the Components of the Preliminary Cell.

epoxy resin to an L-shaped plate. When the glass plates were mounted on the spacer (see Figure 38) the clearance between the L-shaped plates was 0.004 inch. To increase the clearance between the L-shaped plates, a thin gasket of a desired thickness was placed on one face of the spacer. Thus, the volume in the cell represented an L-shaped film of the desired thickness.

The metal frames were used to keep the glass plates compressed against the spacer. To completely seal the spacer against the glass plates, a film of silicone rubber (Dow-Corning silastic 881 RTV rubber) was spread over the two faces of the spacer. The glass plates were then mounted on the spacer and the frames were used to compress the plates against the spacer so that the fluid silicone rubber would spread evenly over the contact surfaces. The entire assembly was then kept at 50°C for about three hours to let the silicone rubber harden.

An inlet and an outlet channel were provided on the spacer to allow filling and emptying of the cell as well as passing any desired solution over the exposed boundary. The first spacer was made out of stainless steel. It was later replaced by a teflon spacer to avoid breaking the glass plates due to uneven compression against the hard steel spacer.

The results of the tests carried out with this cell are discussed in the following chapter. These tests indicated the following defects:

1. The dimensional stability of the cell was very poor. A slight pressure change in the inlet pipe made the glass plates bulge out, thus sucking in the solution on the boundary, and pushing it back when the pressure returned to normal.
2. Uneven distribution of flow over the boundary.
3. The L-shaped glass plates were not exactly of the same dimension which made it very difficult to match them properly at the open boundary.
4. Phenol gradually attacked the epoxy used to join the glass plates together.
5. The hold-up volume of the flow distributor's channel was very large compared to the flow rate.
6. The operation of the cell was very awkward. Several pieces of glass plates broke while the cell was being assembled or dismantled.

These difficulties pointed out that a more careful design with much more stringent specifications was desired.

The Intermediate Cell

In the second cell, instead of using four glass plates, two, 3/4 inch thick by 5 inch diameter pyrex glass disks were used. At the center of each disk a 2 cm x 1 cm rectangular cavity of 0.3 cm depth was cut out by sand blasting. At the center of each cavity a 1/16 inch hole was bored through the disks. Figure 39 shows a photograph of these glass disks.



Figure 39. The Glass Disks Used in the Intermediate Cell.

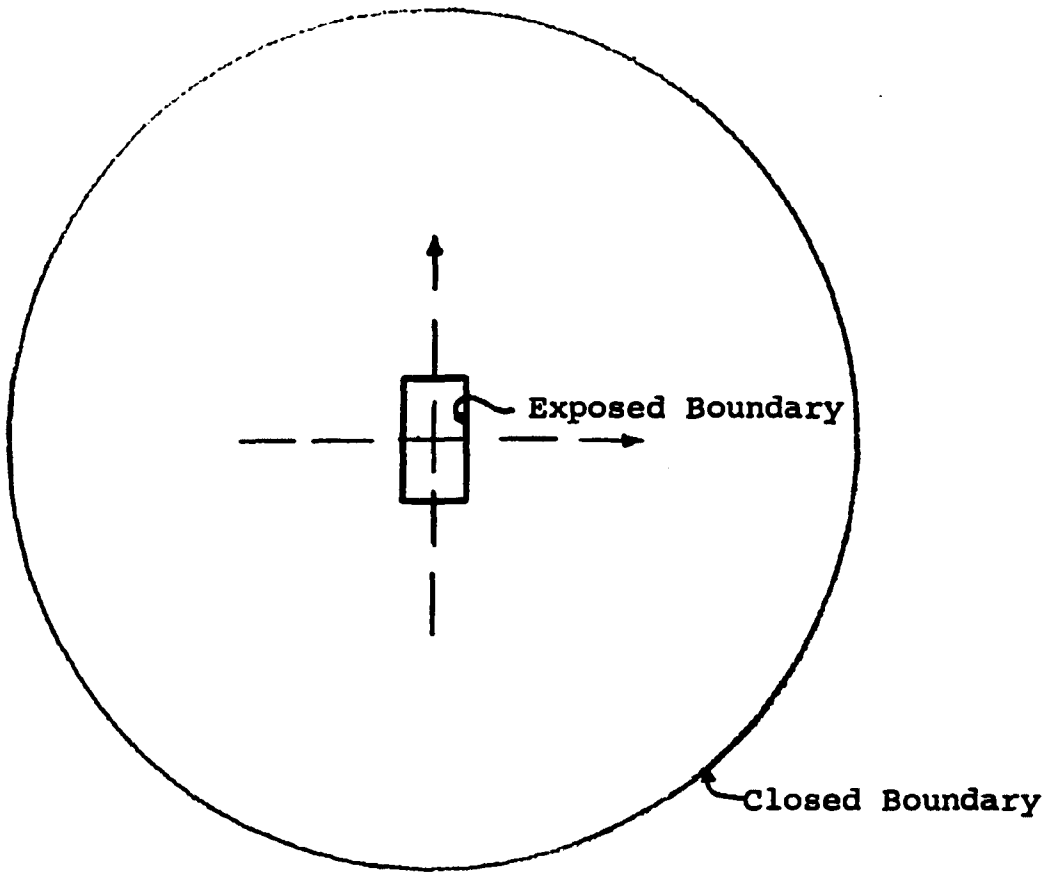


Figure 40. The Plane Region Simulated by the Intermediate Cell.

The hole was enlarged on the opposite faces of both glass disks to allow installation of an O-ring port for connecting the inlet or outlet tubings. When the flat faces of the two disks are brought together to form the internal cavity in the center, the arrangement represents a region shown in Figure 40. The exposed boundary here consists of four corners while that of the previous cell consisted of one corner. As in the previous cell, the closed boundary is so far away from the corners, that for all practical purposes, it can be taken as at infinity: that is, the region between the flat side of the glass disks represents a semi-infinite plane region exterior to a rectangular slice taken from an infinitely long rectangular parallelopiped.

A metal ring was used to keep the disks a precise distance apart, Figure 41. A flow distributor was mounted in the central cavity such that the flow of liquid passed over the open boundary in a direction normal to the plane of the disks. An aluminum cylindrical frame was used for holding the disks in place. The two O-rings mounted on the frame effectively sealed the space between the disks. Figure 41a shows this arrangement with dimensions of the various components of the cell in Figure 41b.

The advantages of this cell over the previous one were several. The most important ones were:

1. A much better dimensional stability was attained. Under normal operating conditions, no detectable bending of the glass was observed, even when the

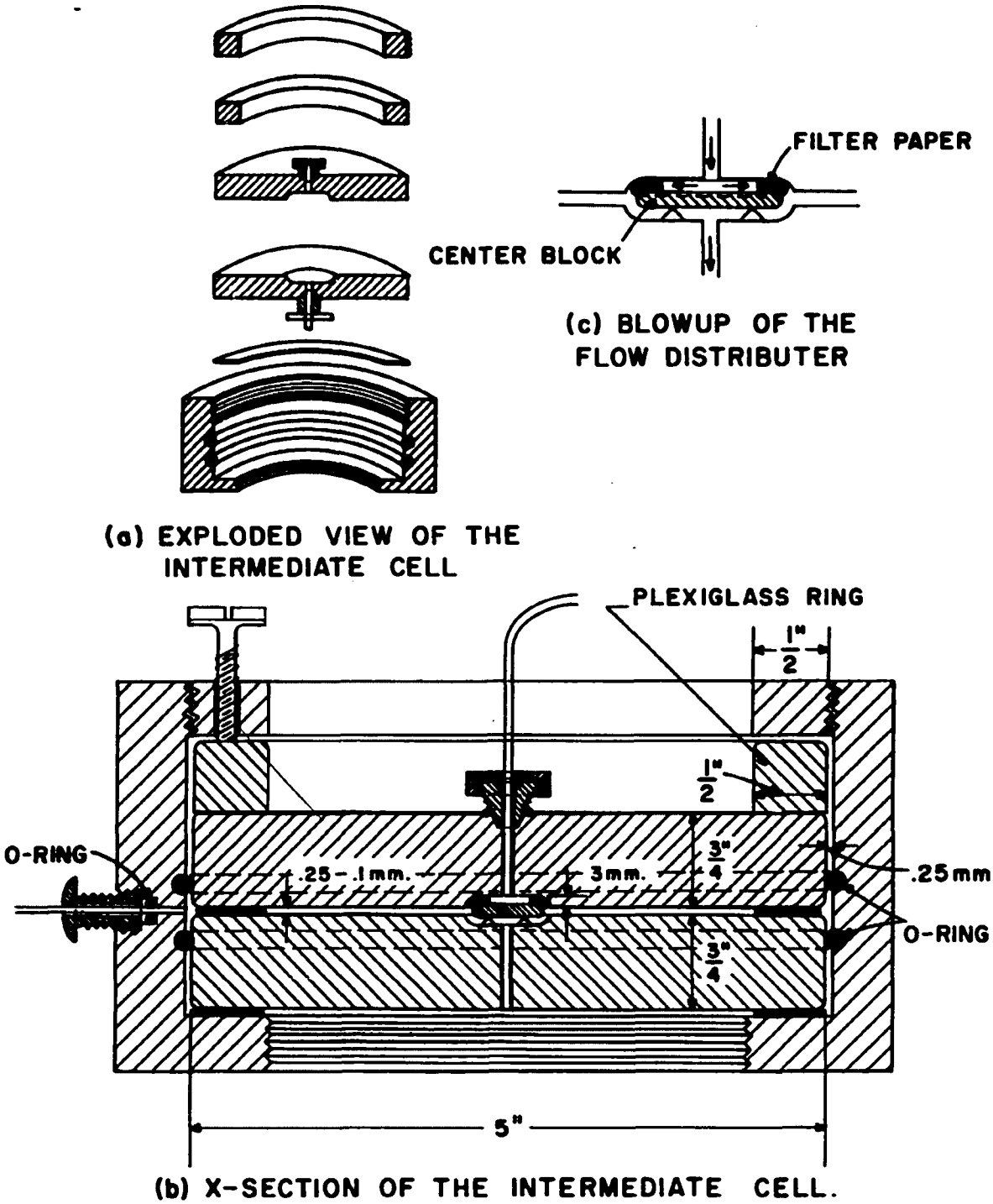


Figure 41. (a) An Exploded View of The Intermediate Cell, (b) the Cross-Section of the Cell, and (c) the Cross-Section of the Flow Distributor.

spacing between the disks was as small as 0.05 mm. The thickness of the plexiglass ring shown in Figure 41b was so chosen to compensate thermal expansion of the aluminum frame, so that the thickness of the film between the glass disks remained essentially constant with temperature change.

2. The direct connection of the inlet and outlet tubings to the glass proved to be very effective in improving the filling of the cell as well as allowing an easy connection.
3. Several flow distributors were tried, the one shown in Figure 41c proved most effective. As can be seen, the solution entering the cell passes through a uniform thickness of filter paper which provides sufficient pressure drop to allow uniform distribution of the flow. The filter paper acted also as a dampener for possible pressure surges in the upstream tubing. By connecting the exit pipe to an atmospheric reservoir, the static pressure in the cell was maintained constant to avoid elastic deformation of the disks. This arrangement also made it possible to reduce the residence volume of the flow channel in the cell from 1 cc to less than 0.1 cc.
4. The circular frame arrangement with the O-rings made the assembling or opening of the cell a

very easy matter so that several preliminary tests could be carried out every day.

The construction of the cell parts did not introduce any undue difficulty, except for the cutting of the cavities and the holes in the glass disks. After experimenting with a number of techniques over a period of months, it was found that a sand-blasting technique was the best. To cut the cavities by this method, an aluminum template was first made. This template was then fastened to the surface of the glass disks and sand blasted until the cavity's depth was about 3 mm. The bottom of the cavities were then flattened and polished with special diamond drill bits, using dental drilling techniques. The holes were also drilled with special diamond drilling bits. Although the rectangular cut in the template was perfect, the surface corners of the cavity did not turn out knife-edge sharp. There was some microscopic chipping of the glass on the edges.

The first pair of disks, after being completely built, disintegrated into small pieces while resting on a desk, due to residual stresses. Although the purchase order called for annealed glass, the disks were apparently not annealed. The next pair of disks were annealed in a glass annealing furnace before cutting the cavities and holes. No evidence of stress concentration was found.

After conducting a number of experiments to determine the feasibility of obtaining a pure diffusion field, the following conclusions were reached on this design of the cell:

1. Even at a rate of 1 cc per hour the flow passing the boundary disturbed the liquid in the cell which suggested that the boundary should be separated from the passing solution by a suitable membrane. To avoid interference of the interfacial tensions with these observations, the cell was charged with a finely divided emulsion of phenol in water and pure water was passed over the boundary. The movement of the dispersed phenol phase was then viewed through a 20X telescope.
2. The need for a membrane suggested a very important simplification in the cell design. With the membrane separating the forced flow at the boundary from the stationary liquid in the cell, there was no longer any need for the elaborate cutting of the cavities. A flow distributor such as the one shown in Figure 42 would be more effective and much easier to place in the cell. This arrangement also simplified the problem of introducing various shapes in the exposed boundary for simulating desired flow fields. Figure 43 shows the components of the flow distributor for an arbitrary shape of the exposed boundary.
3. The metal O-ring ports for the inlet and outlet tubings and the metal ports for the flow distributor in the bottom disk's cavity were joined to

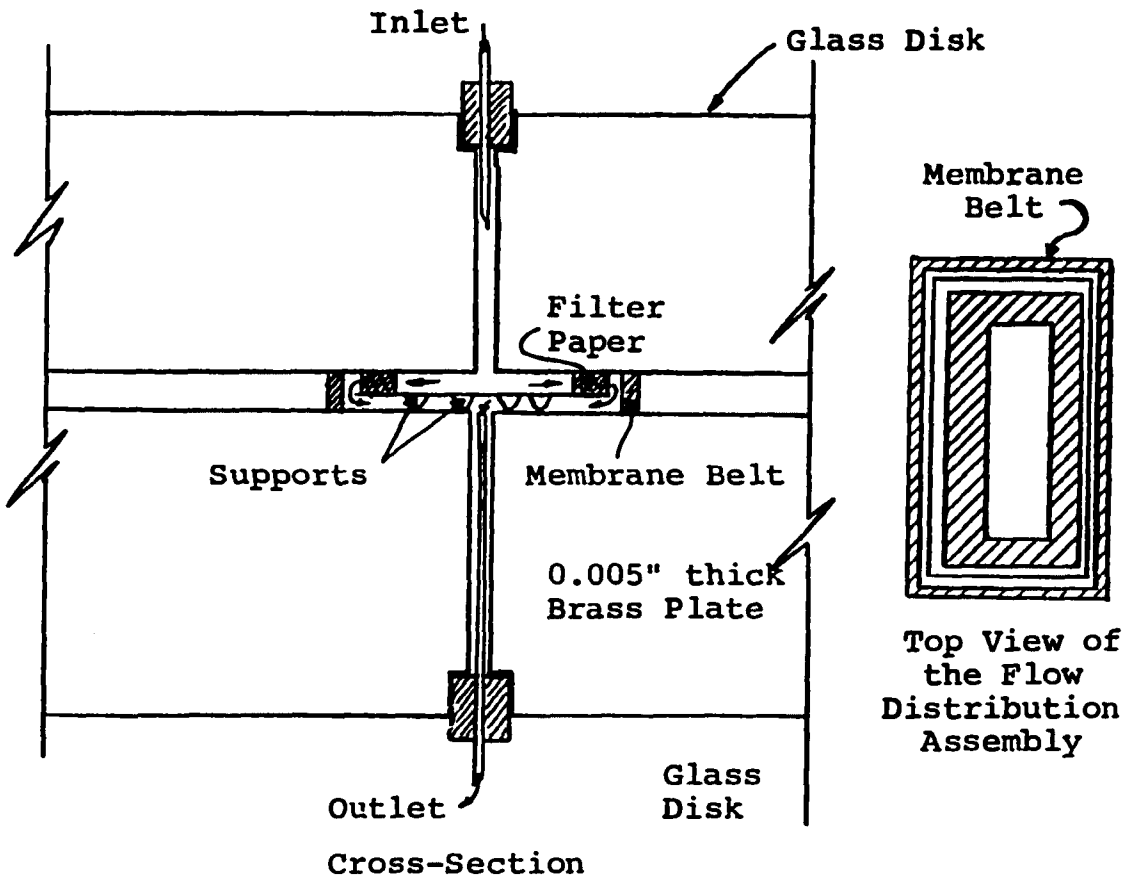


Figure 42. The Arrangement of the Flow Distributor.

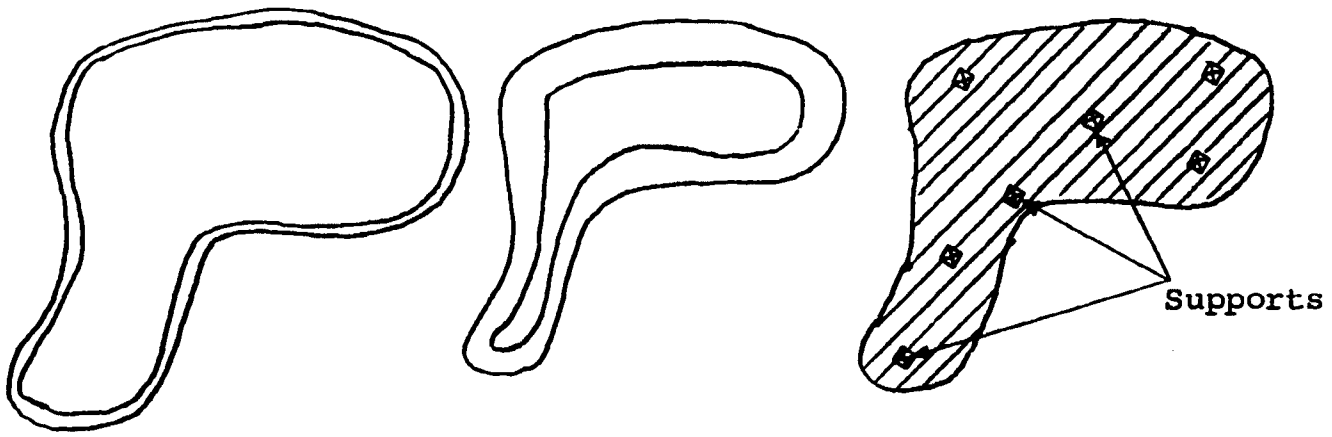


Figure 43. The Components of the Flow Distributor for an Arbitrary Geometry of the Exposed Boundary.

the glass surfaces by a suitable epoxy resin. After several days, the thermal expansion of the metal peices and the epoxy due to thermal cyclings of the cell developed surface cracks in the glass disks, which propagated with time (see Figure 39, the left glass disk).

4. In all tests the cell was filled by evacuating a container, connected to the outlet tubing and containing the solution to be charged into the cell. The tubing was immersed in the solution in the container so that when the vacuum was lifted the cell was charged automatically. To reduce the amount of residual air, the cell was purged with water vapor prior to filling. The large O-rings on the frame presented a serious difficulty in getting rid of all air because of the dead volume around them. The air bubbles left in the grooves in which the O-rings were situated gradually dissolved partially in the deaerated solution in the cell, causing bulk movements at the boundary as well as acting as a cushion for any pressure surge in the cell. Note that a pressure change of the order of 1/10 inch of water can create a volume change in the bubbles, which compared to the volume of the film between the glass disks with a spacing of, say, 0.1 mm, is indeed very large. The above difficulty was, however,

overcome by using a smaller ring for the spacer and filling the space beyond it with silicone rubber. The O-rings on the aluminum frame were then only used to avoid direct contact between the glass disks and the metal frame.

Despite the above mentioned defects, the tests completed with this cell were very conclusive. They identified the various phenomena which were responsible for the bulk flow in the cell.

The Final Cell

The last two-dimensional cell was identical to the intermediate cell except for the glass disks and the boundary flow distribution parts. A 1/16 inch hole was bored in the center of each disk. On one side the hole was widened to ¼-inch to allow plugging of a silicone rubber stopper, Figure 44. The inlet or outlet tubings were connected to the disks through the silicone rubber stoppers. The preliminary tests with this cell demonstrated that there is little hope for producing a two-dimensional diffusion field in a non-porous media. Most of the tests were then carried out with porous media. The porous medium used for the present investigation was ordinary Whatman filter paper Number 52. Four layers of the filter paper were pressed together and cut into a shape representing the closed boundary. They were then covered on both faces with two, 4-mil. thick polyethylene sheets, compressed between two thick glass plates and heated for 20 minutes in an oven kept at 120°C. The polyethylene sheets



Figure 44. One of the Pair of Glass Disks Used in the Final Cell.

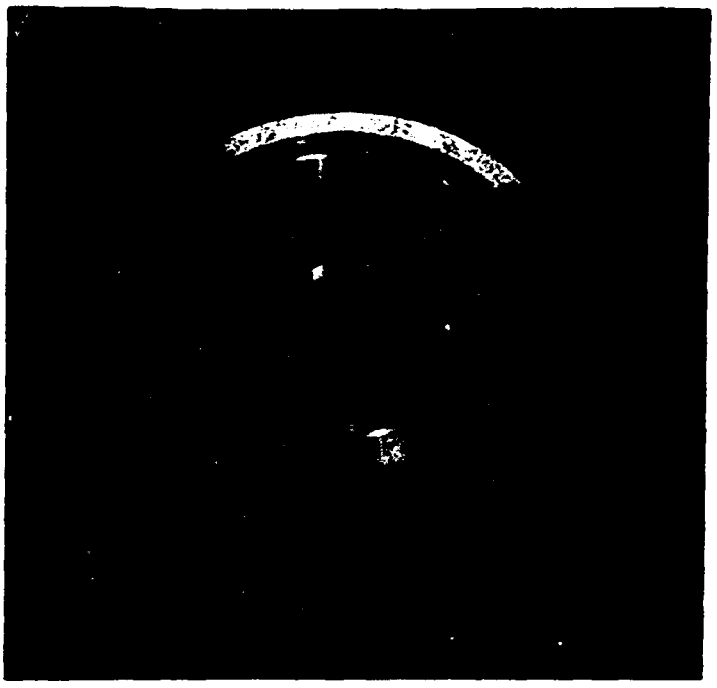


Figure 45. A Photograph of the Final Cell.

melted over the faces of the filter papers, thus sealing them completely and most effectively. After cooling to room temperature, the desired shape of the boundary was cut out. Figure 45 shows a photograph of the cell with a 25° wedge shaped filter paper sealed between the glass disks. The exposed boundary here is a circle of 1 cm in diameter. The white ring in the middle is made of 0.5 mm filter paper compressed to 0.30 mm and is used to distribute the flow evenly over the boundary. Underneath this ring there is a 0.125 mm thick circular bronze sheet. The spacing between this circle and the bottom glass disk was about 0.45 mm. Surrounding the wedge is a rubber spacer which covers most of the remaining surface of the disk. Silicone rubber was used for sealing the wedge around the periphery in order to avoid possible leakage of air when filling the cell and expansion of the polyethylene sheets around the sides.

The Air Bath

The air bath was designed to provide a constant temperature environment for the cell. Figure 46 shows the various components of the bath and the relative position of the camera. A photograph of the air bath is shown in Figure 47. The positions of the fans, the heaters and the temperature controller probe were determined by trial and error to get the best temperature control. Several chromel-alumel thermocouples were installed in the bath for measuring the temperature distribution. An accurate potentiometer was used

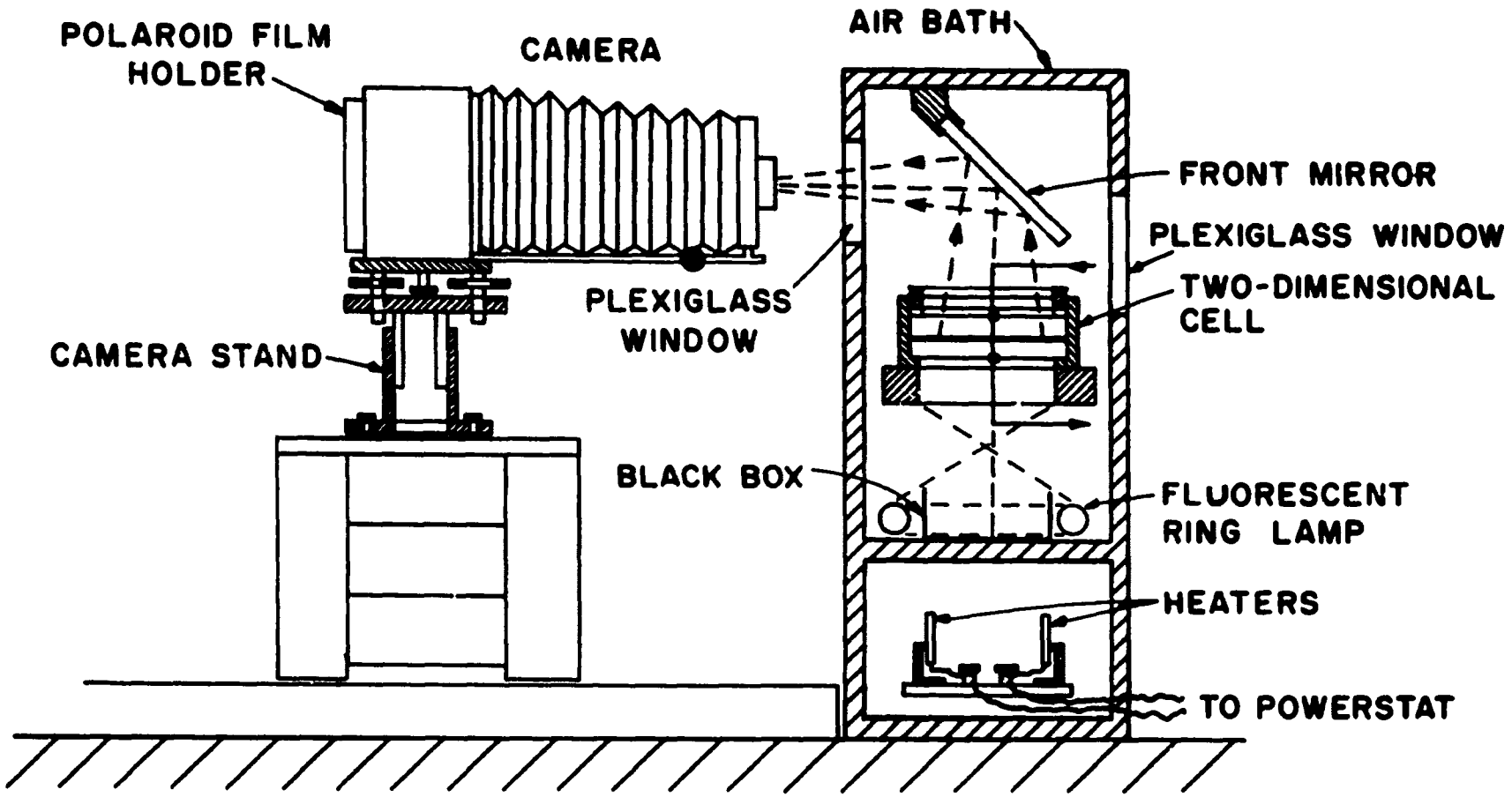


Figure 46. A Schematic View of the Air Bath and the Camera.

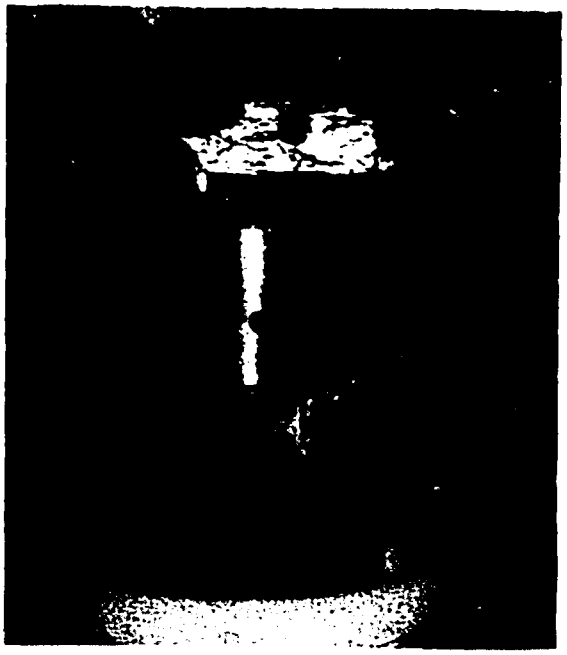


Figure 47. A Front View of the Interior of the Air Bath

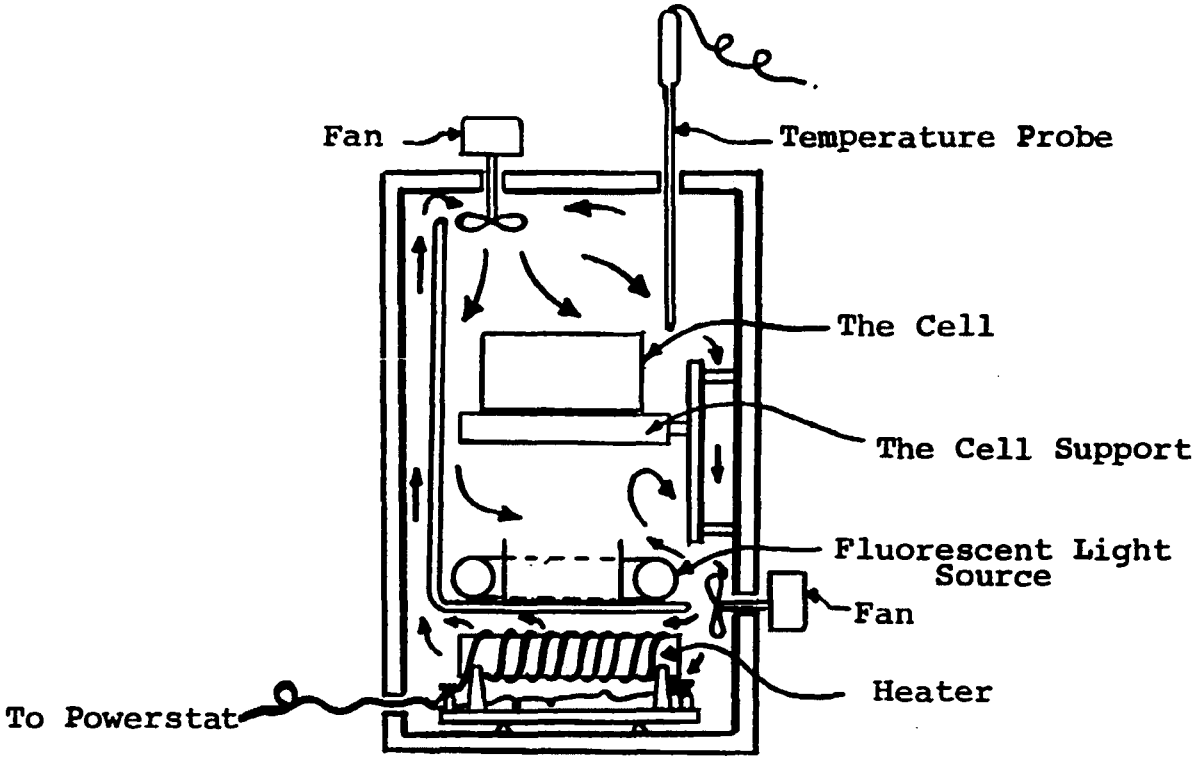


Figure 48. Schematic Diagram of the Air Bath Showing the Relative Positions of the Fans, the Temperature Probe and the Heaters.

to read the temperature. It was observed that, with the arrangement shown in Figure 48, the maximum temperature difference at the various points in the bath was less than ±0.25°C. The controller was supposed to control the temperature with an accuracy of ±0.01°C. However, since the readings of the potentiometer were not better than ±0.1°C, the higher accuracy cannot be claimed for the present set-up.

The walls of the bath were made of a layer of transite and a layer of plexiglass with a few sheets of corrugated paper between them to reduce heat loss. The heater had a capacity of 33 Watts at 120 Volts. The maximum power output of the temperature controller (Bailey Precision Temperature Controller Model 104) was rated at 300 Watts. A powerstat was connected between the temperature controller and the heater to allow more flexible control. Normally, the powerstat was set at 60 Volts.

The cell was supported in the bath by a metal stand. The stand was so designed to allow movement in all directions. The stand was originally designed to hold the cell in a precise position on the existing interferometer at the University of Oklahoma Chemical Engineering Laboratory. However, the use of the interferometer for measuring the concentration profile in the cell never materialized, due to unsuccessful attempts to produce a pure two-dimensional diffusion field in a nonporous region.

To avoid gravitational flow in the cell, the stand was adjusted such that the liquid film in the cell was in a

perfect horizontal position. Large windows were provided at the front and back of the cell to allow observation and also photographing of the cell.

The Micropump

To maintain a fixed boundary condition in the two-dimensional cell it was necessary to pass a solution of known composition over the boundary at a precise rate. The desired range for the rate of pumping was found to be between 1.0 - 5.0 cc per hour. These figures were reached from the consideration that the concentration change of the solution having passed over the boundary should be between 10^{-2} - 10^{-3} moles per liter. If the cell contains saturated phenol solution and if pure water is passed over the boundary, then, assuming the diffusion flux at the boundary is essentially that of a one-dimensional model, the concentration of the water solution leaving the cell for the temperatures ranging from 30°C to 60°C is given in Table 2.

TABLE 2

THE EFFECT OF THE PUMPING RATE ON THE CONCENTRATION OF PHENOL LEAVING THE CELL

Temperature	30°C	40°C	50°C	60°C
Pumping Rate cc per hr per cm^2 of the boundary surface	Concentration times $\sqrt{time}$ moles $hr^{\frac{1}{2}}$ per liter			
10	0.0274	0.03235	0.0341	0.0327
100	0.00274	0.003235	0.00341	0.00327
500	0.000548	0.000647	0.000682	0.00065
1000	0.000274	0.000323	0.00034	0.000327

To arrive at the values of concentration times $\sqrt{time}$, the values of diffusivity obtained from the preliminary test with the one-dimensional cell were used. For the concentration to be in the range 10^{-2} to 10^{-3} moles per liter between t = 1.0 hour and t = 100 hours a pumping rate of about 20 cc per hour per cm^2 of the boundary is required. Now, if the boundary is 1 cm x 1 cm square and the thickness of the liquid film in the cell is 0.025 cm, then the desired pumping rate will be 20 x 4 x 0.025 = 2.0 cc per hour.

Several possible micropumps were investigated. Finally, the pump described below was found to fulfill the desired accuracy, dependability and flexibility. The pump, Figure 49, consisted of a 1 RPM synchronous geared motor, a reduction gear box, a horizontally moving rack and a hypodermic syringe. The gear box reduced the speed to 1/360 RPM. The output of the gear box is transmitted to horizontal movement of the racks through spur gears A and B, Figure 49. The rack then pushes the plunger of the hypodermic syringe, thus pumping the solution out at a uniform rate. By either changing the size of the hypodermic syringe or changing the spur gears A and B, a wide range of pumping rates can be obtained. Substantial changes in the pumping rate can also be achieved by replacing the motor with one of a different speed.

The additional syringe and the threeway cock shown in Figure 49 were used to facilitate recharging the pump. For most of the tests a 20 cc syringe was used. The pumping rate for this syringe was 3.02 cc per hour. With this rate, the

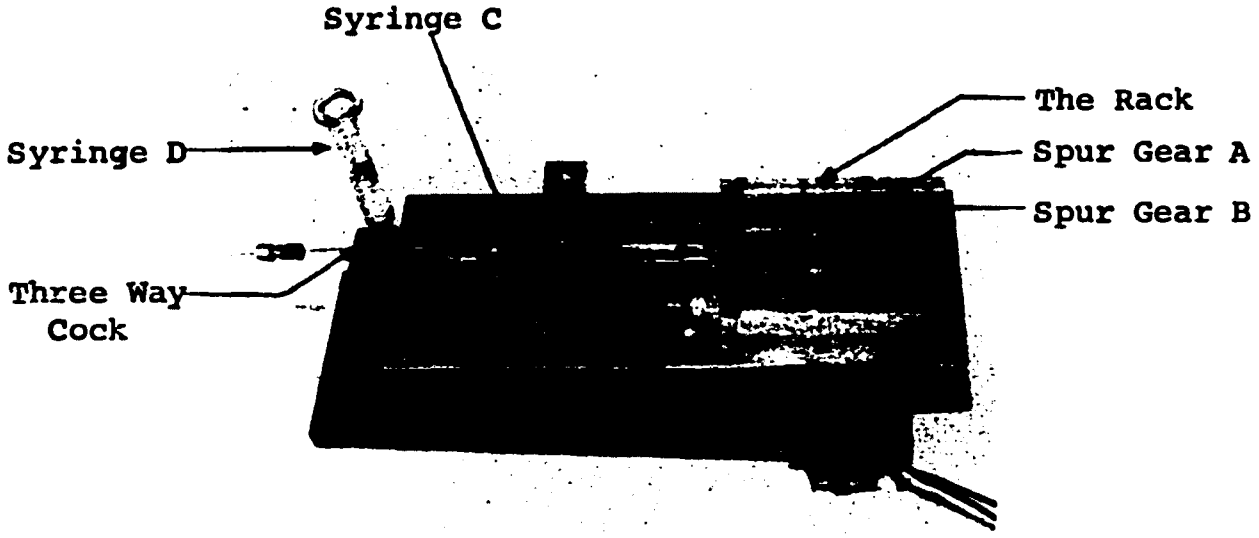


Figure 49. The Micropump

pump was recharged every eight hours. The procedure for recharging involved the following steps:

1. Pour the solution into the syringe D, Figure 49.
2. Disengage the rack.
3. Turn the cock so that syringes C and D are connected.
4. Fill C by pulling its plunger outward.
5. Engage the rack.
6. Turn the cock back.

It usually took less than a minute to recharge the pump. The interruption in the flow for this period had no detectable effect on the diffusion process in the cell.

Camera and Associated Optical Arrangement

The optical set-up for taking the photographs of the interface developed in the cell is shown in Figure 46. A

ring shaped fluorescent lamp was used to provide a diffused source of light. A black box, located in the center opening of the ring lamp, provided a black background for the camera. This arrangement was found very effective in sharpening the contrast between the two phases. The camera used was a Graflex f/4.7 model. It was mounted on a tripod stand to allow adjustment of the camera to the horizontal position. Polaroid films were used for taking the photographs so that they could be examined immediately. As seen in Figure 46, a flat front mirror was mounted on the air bath ceiling at a 45° angle to the horizontal plane so that the cell could be viewed with the horizontally mounted camera.

The Microprojector

A Scherr microprojector, Figure 50, was used to read the position of the interface from the photographs of the two-dimensional cell. The optical arrangement of the projector is shown in Figure 51. A micrometer cross slide stage with readings in 0.0001 inch, Figure 52, was placed on the work table of the microprojector. The photographs were placed between two glass disks and positioned on the micrometer cross slide stage. By turning the micrometer's knobs, the interface was brought to fall on the center of the cross lines of the projector screen and the micrometer readings were recorded. This procedure was repeated for the points of interest on the interface and the boundary. These x - y readings were then converted to a desired dimensionless form in a suitable

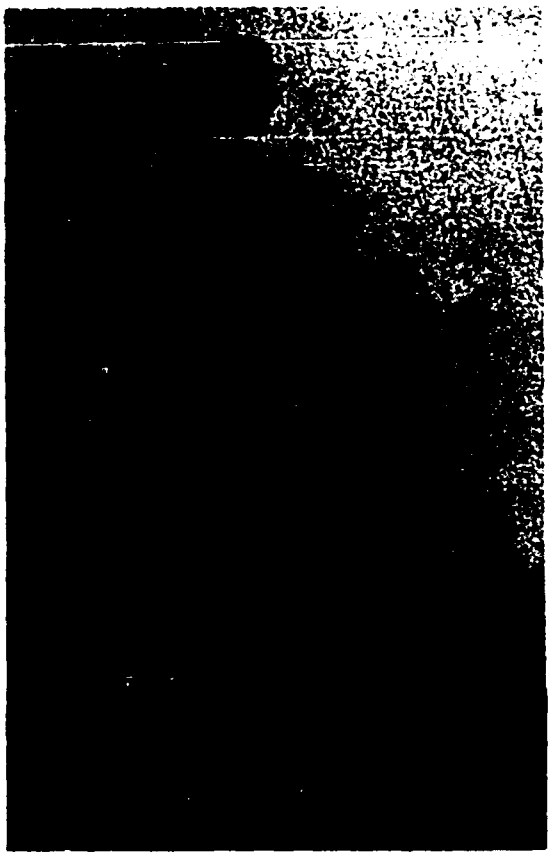


Figure 50. A Photograph of the Microprojector

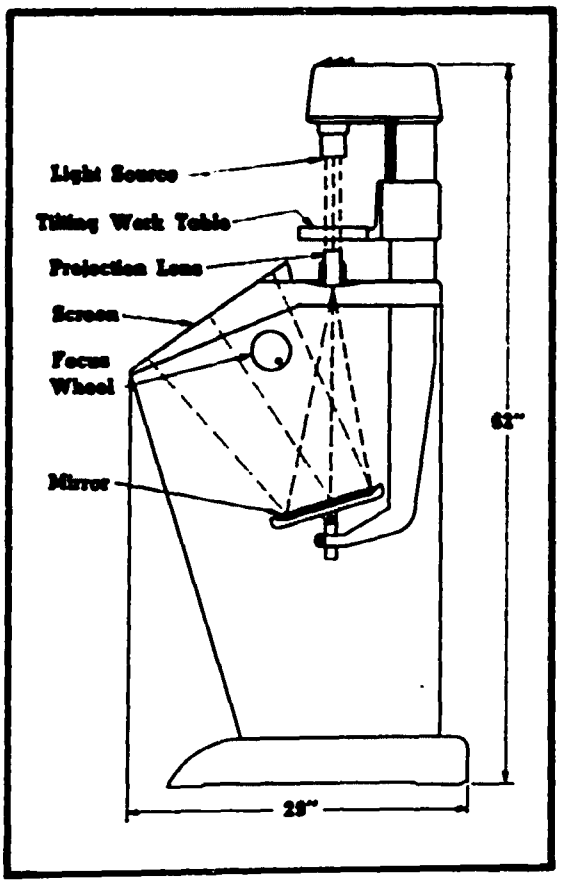


Figure 51. The Optical Arrangement of the Microprojector



Figure 52. Micrometer Cross Slide Stage

co-ordinate transformation. The projection lens was 20X. The projection screen was 14 inch, and the maximum field for viewing was 1 inch x 1 inch.

CHAPTER VI

EXPERIMENTAL RESULTS

In this chapter the results of many experiments with the previously mentioned diffusion cells are discussed. These experiments were conducted in order to demonstrate the feasibility of employing the molecular diffusion process to simulate heat conduction problems with change of phase. For this reason, only the observations and measurements which were necessary for determining the nature of mass transfer in the cell were made. In fact, the rate of movement of the interface between the phenol rich phase and the water rich phase turned out to be the only reliable measurement which can determine the nature of mass transfer at the boundary and in the cells. The concentration profile in the cell and the total flux at the boundary were not measured because these two measurements require a development program of their own. Such an undertaking is profitable only when the conditions for producing a pure diffusion mass transfer, the optimum design of the cells, and the optimum partially miscible liquid system are well specified.

The diffusion mass transfer in liquid systems is a very specialized process and quite distinct from any other

phenomena responsible for the transfer of mass in such systems. For one thing, it is extremely slow when compared with free or forced convection, or capillary rise. For another, the mass flux by diffusion for a given concentration potential is dependent on the square root of time. For example, in the case of the linear flow of mass the ratio $X(t)/\sqrt{t}$ (X is the distance between the interface and the boundary, t is time) for the phenol-water system at 55°C is less than 1.3 mm per $hr^{\frac{1}{2}}$ depending on the boundary concentration. Thus, after 81 hours $X(t) \leq 11.7$ mm, and after 100 hours $(t) \leq 13$ mm. Clearly, any disturbance of the pure diffusion field will appreciably upset the relation $X(t)/\sqrt{t} \leq 1.3$.

To facilitate recognizing, and perhaps resolving, the problems involved in the design and operation of a two-dimensional diffusion cell, a series of tests were completed with the one-dimensional cells. These tests also resulted in the integral diffusion coefficients which were needed in the study of the two-dimensional cells. The early tests with the two-dimensional cells only served to reveal several mechanical defects of the cells. These shortcomings were finally resolved to the extent that it was possible to assert that all mass transfer to and from the cell was due to either diffusion or various interfacial forces acting on the liquid film in the cell. The central problem then became the complete elimination of all interfacial forces which were responsible for the bulk flow inside the cell. The approach to this problem was strictly empirical. Although advances have been made in

the past decade in understanding the nature of liquid-liquid and solid-liquid interfacial forces, it is not as yet possible to make a precise prediction of the possible ways of reducing the sum of all these forces to a negligibly small value (say 10^{-10} dyne per cm). Only this type of prediction could have been helpful in the present work because an interfacial force as small as 10^{-5} dyne per cm can be responsible for a continuous bulk flow, which is several times larger than that obtained by diffusion.

The two-dimensional tests can be classified as follows:

1. A uniform phenol (or water) rich phase in the cell with a water (or phenol) rich phase being passed over the boundary.
2. A finely dispersed emulsion of phenol (or water) rich phase in saturated water (or phenol) rich phase in the cell with water (or phenol) solution passed over the boundary.
3. As item 1, except that here the volume of the cell was filled with a porous media (filter paper).

The objective of these tests and their results are covered below.

Determination of the Average Diffusion Coefficient from the Experimental Data of the One-Dimensional Cells

Consider a long capillary tube, Figure 53, initially filled with a phenol rich phase of concentration C_∞ moles of phenol per liter ($C_\infty \geq C_s^{II}$) and kept at a constant temperature T. Let, at time t = 0, a water rich phase with a phenol

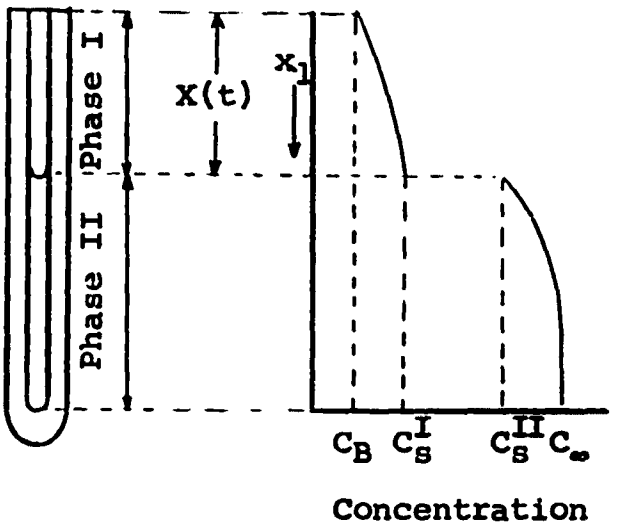


Figure 53. The Concentration Profile in a Capillary Initially Containing a Solution of Uniform Concentration, $C_\infty \geq C_s^{II}$ whose Surface x = 0.0 is kept at $C_B < C_s^I$

concentration C_B moles of phenol per liter ($C_B < C_s^I$) be passed over the open end of the capillary tube. Then an interface will form inside the capillary whose position, X(t), for the case of constant diffusion coefficients, $\tilde{D}^I$ and $\tilde{D}^{II}$, is given by the relation,

$$X(t) = 2\xi\sqrt{\tilde{D}^I t} \tag{6.1}$$

where

$$1/\chi_1(\xi) = \bar{\lambda} + \mu/\chi_2(z\xi) \tag{6.2}$$

$$\chi_1(y) = ye^{y^2}\text{erf } y$$

$$\chi_2(y) = ye^{y^2}\text{erfc } y$$

$$\mu = \frac{C_s^{II} - C_\infty}{C_s^I - C_B}$$

$$\bar{\lambda} = (C_s^{II} - C_s^I)\sqrt{\pi}/(C_s^I - C_B) \qquad (6.3)$$

$$Z = (\tilde{D}^I/\tilde{D}^{II})^{\frac{1}{2}}$$

It can be shown that when $D^I = D^I(C)$, a relation of the type (6.1) approximately holds, provided that the integral values of diffusivities,

$$\bar{D}^I = \frac{1}{C_s^I - C_B} \int_{C_s^I}^{C_B} D^I(C)\, dC$$

and (6.4)

$$\bar{D}^{II} = \frac{1}{C_s^{II} - C_\infty} \int_{C_s^{II}}^{C_\infty} D^{II}(C)\, dC$$

are used. How good this approximation is depends on the functional form of $D^I(C)$.* If, on the other hand, the experimental data confirmed that $X(t)/\sqrt{t}$ is constant, then it can be concluded that there are average values, $\tilde{D}^I$ and $\tilde{D}^{II}$, of the diffusivities such that the relation (6.1) holds. Because only these average values are needed in the present investigation, the discussion on their relations to the point diffusivities is omitted. Of course, all the above observations are still valid if the cell is filled with a water solution, and a phenol solution is passed over the boundary.

---

*See Geddes and Pontius (37) for further discussion and other methods for measuring the diffusion coefficient in binary-liquid systems.

If $\mu = 0$, that is, if $C_\infty = C_s^{II}$, then ξ does not depend on $\tilde{D}^{II}$. For this case the value of $\tilde{D}^{I}$ can be calculated from the experimental values of X(t) by using the Equation (6.1). However, for the reasons to be discussed later, it is better to plot the values of X(t) versus $\sqrt{t}$ and find the slope of the line that best fits all the points, then to calculate $\tilde{D}^{I}$ from the relation

$$\tilde{D}^{I} = \left(\frac{1}{2\xi}\, d\overline{X(t)} \,/\, d\sqrt{t}\right)^2$$

where $d\overline{X(t)}\,/d\sqrt{t}$ is the slope of this line. Using a least square method to find the best line,

$$X(t) = a\sqrt{t} + b$$

which fits all data points, one gets,

$$a = \frac{\overline{dX(t)}}{d\sqrt{t}} = \left[\sum_{i=1}^{n} t_i^{\frac{1}{2}} X_i - \frac{1}{n}\sum_{i=1}^{n} X_i \cdot \sum_{i=1}^{n} t_i^{\frac{1}{2}}\right] \Big/$$

$$\left[\sum_{i=1}^{n} t_i - \frac{1}{n}\left(\sum_{i=1}^{n} t_i^{\frac{1}{2}}\right)^2\right]$$

where n is the number of data points. This method was used to obtain the values of the average diffusivity, $\tilde{D}^{I}$, for the water-rich phase. By having phenol-saturated water in the capillary and passing a phenol-rich solution over the boundary, one can similarly get the values of the average diffusivity for the phenol-rich phase. If the value of the diffusivity for the water-rich phase is known, one

alternatively fills the cell initially with pure water and passes a phenol solution over the boundary. For this case,

$$\xi = \frac{1}{2\sqrt{\tilde{D}^I}} \cdot \frac{\overline{dX(t)}}{d\sqrt{t}}$$

$$X_2(Z\xi) = \frac{\mu X_1(\xi)}{1 - \bar{\lambda} X_1(\xi)}$$

Knowing $X_2(Z\xi)$, one can calculate $Z\xi$ and consequently

$$\tilde{D}^{II} = \tilde{D}^I / Z^2$$

The Experimental Results of the One-Dimensional Cells

As mentioned earlier, the purposes of the capillary experiments were:

1. To demonstrate that a one-dimensional cell can be used to solve many unsolved problems of linear heat conduction with change of phase.
2. To obtain the average values of the diffusivity of phenol-water system, which were necessary in the study of the two-dimensional diffusion analogs.
3. To acquire some preliminary knowledge and experience on the problems of developing a pure two-dimensional diffusion field prior to the design and construction of the two-dimensional cell.

To attain these objectives, three sets of experiments were carried out using capillary tubings of various sizes ranging

from 2mm ID to 0.5 mm ID. In the first set the solution in the capillary was water saturated phenol and the solution at the boundary was pure water. The tests were conducted at 30°, 40° and 50°C. In the second set the temperature was kept at 55°C for all tests, but a water solution of various phenol concentrations was passed over the boundary. The initial solution in the cell was a water saturated phenol at 55°C. The last set consisted of two tests having pure water as the initial solution in the cell and a phenol solution containing about 8 weight per cent water passed over the boundary.

The experimental set-up for the first test was that of Mirshamsi (57), using a scale behind the capillaries to read the position of the interface. For the second set it was that shown in Figure 32. A cathetometer was used to read the position of the interface. The set-up for the last set of tests is shown in Figures 33 and 34, with the cell mounted upside down to avoid any convection mass transfer developed by the lower density of the water phase.

The experimental data obtained from the above capillary tests, as well as their least square analysis, are covered in Appendix D. Some typical plots of X(t) versus $\sqrt{t}$ are shown in Figures 54 and 55. The average diffusivities obtained from these tests are given in Tables 3, 4 and 5. Figure 56 shows the effect of concentration driving force on the average diffusivity of a water rich phase at 55°C.

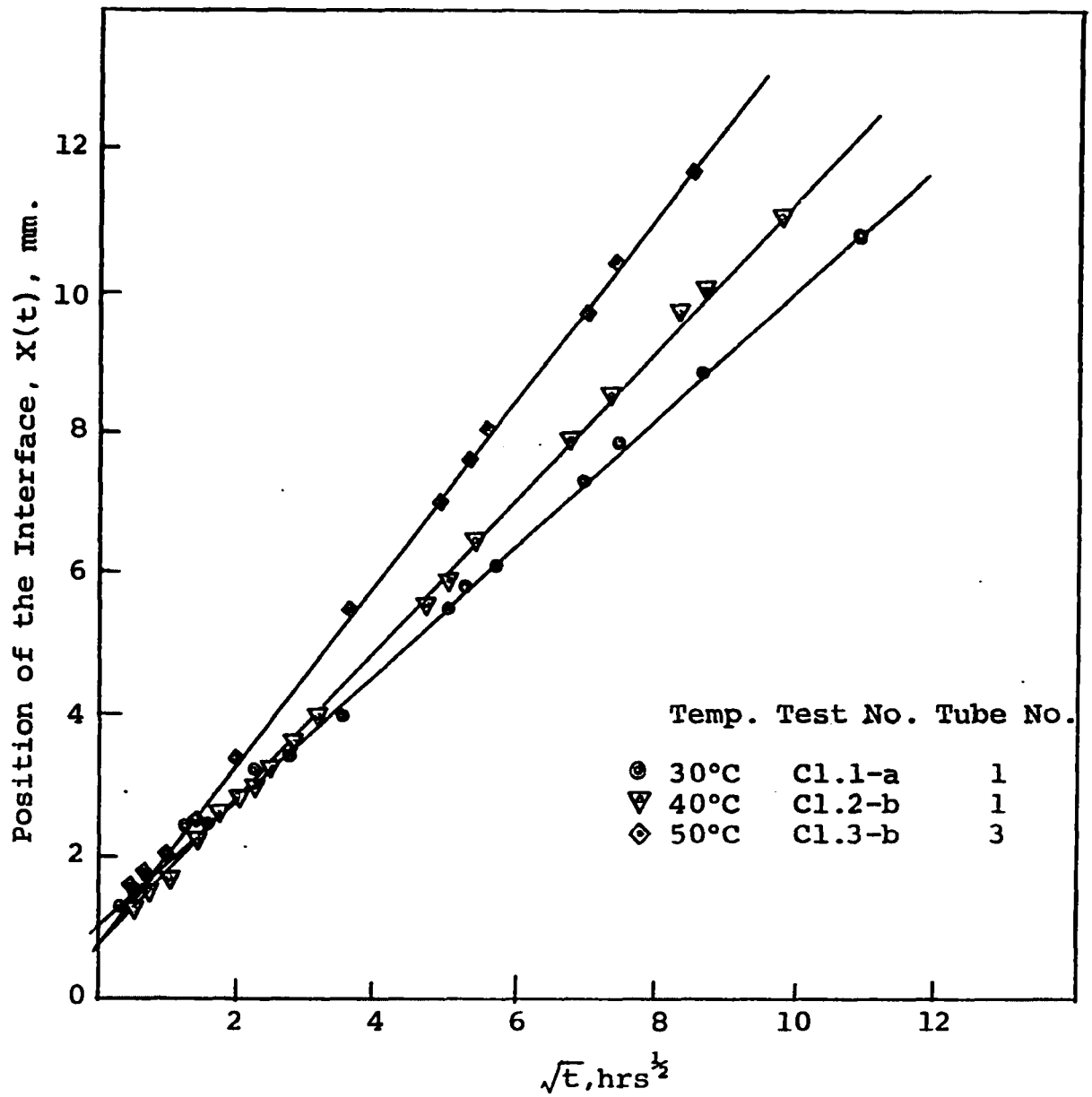


Figure 54. Growth of the Water Rich Phase in a Capillary Tube Initially Containing a Saturated Phenol Rich Phase whose Surface x = 0.0 is kept at C_B = 0.0 Moles Phenol per Liter.

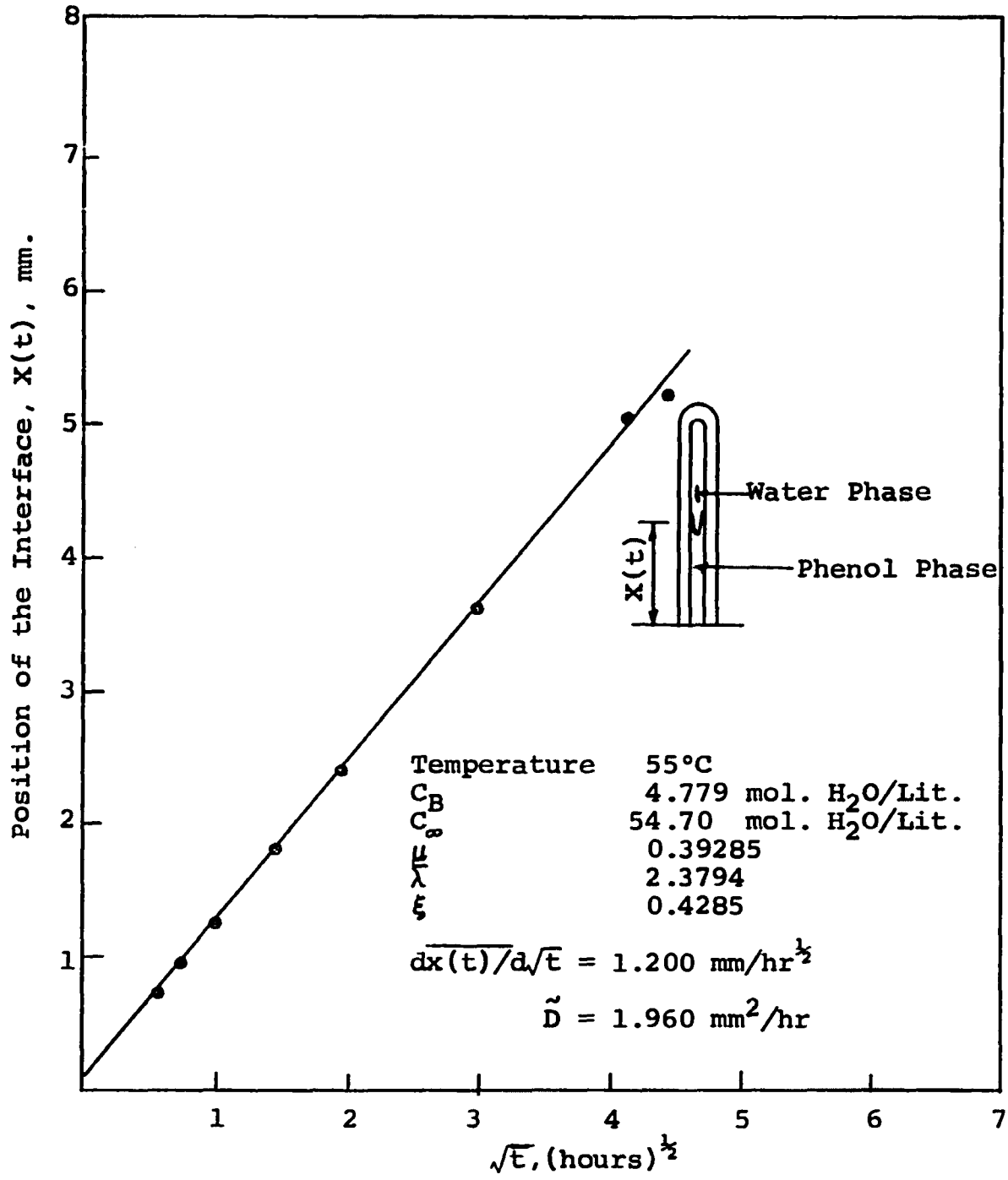


Figure 55. Determination of the Average Diffusivity of Phenol Rich Phase at 55°C from the Data on X(t).

TABLE 3

EFFECT OF TEMPERATURE ON THE AVERAGE DIFFUSION COEFFICIENT FOR THE PHENOL-WATER BINARY SYSTEM

Test No.	Temp. °C	Concentration Range Mols Phenol per Liter	$\mu = \frac{C_\infty - C_B^{II}}{C_s^I - C_B}$	$\overline{\frac{dX(t)}{d\sqrt{t}}}$	Average Diffusion Coefficient mm^2/hr	Average Diffusion Coefficient $cm^2/sec \times 10^5$
C-1.1-a	30	0.0-0.9334	0.0	0.89415	3.06	0.849
C-1.1-b	30	0.0-0.9334	0.0	0.9091	3.15	0.875
C-1.2-a	40	0.0-1.0205	0.0	1.07342	3.75	1.042
C-1.2-b	40	0.0-1.0205	0.0	1.06925	3.725	1.035
C-1.3-a	50	0.0-1.2496	0.0	1.25175	3.740	1.040
C-1.3-b	50	0.0-1.2496	0.0	1.2756	3.855	1.070

TABLE 4

EFFECT OF CONCENTRATION ON THE AVERAGE DIFFUSIVITY OF THE WATER RICH PHASE AT 55°C

Test No.	Concentration Range Mols Phenol per Liter	μ	$\overline{\frac{dX(t)}{d\sqrt{t}}}$	Average Diffusion Coefficient mm^2/hr	Average Diffusion Coefficient $cm^2/sec \times 10^5$
C-2.1	0.0 - 1.459	0.0	1.59	4.698	1.305
C-2.2	0.27 - 1.459	0.0	1.090	3.381	0.939
C-2.3	0.532 - 1.459	0.0	0.981	2.164	0.601
C-2.3	0.956 - 1.459	0.0	0.593	1.721	0.478

TABLE 5

AVERAGE DIFFUSIVITY OF THE PHENOL RICH PHASE AT 55°C

Test No.	Concentration Range Mols Water per Liter	μ	$\overline{\frac{dX(t)}{d\sqrt{t}}}$	Average Diffusivity mm^2/hr	Average Diffusivity $cm^2/sec \times 10^5$
C-3.1-a	4.78 - 23.03	0.39285	1.200	1.960	0.5546
C-3.1-b	4.66 - 23.03	0.39035	1.1445	1.814	0.5039

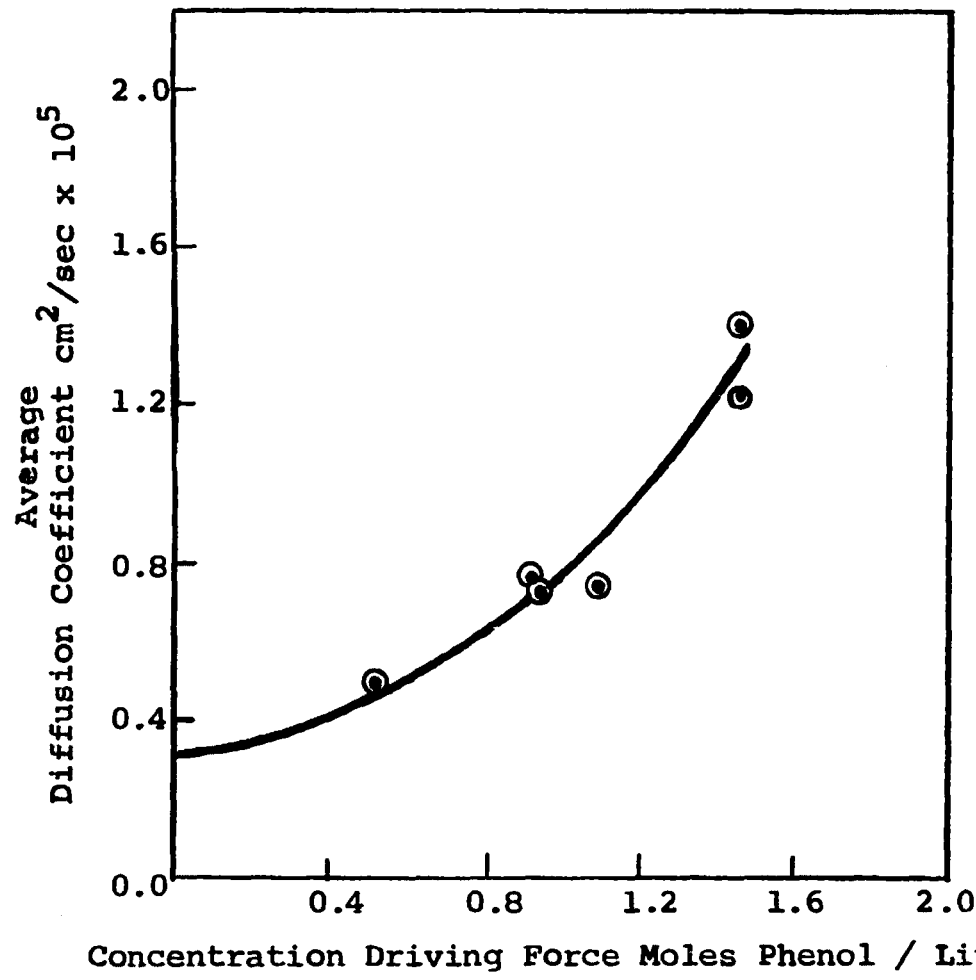


Figure 56. Effect of Concentration Driving Force, $(C_S^I - C_B)$ on the Average Diffusivity of Water.

Inspection of the plots of X(t) versus $\sqrt{t}$ shows that the best straight line which fits the data does not pass through the origin as predicted by equation (6.1). Instead, at $\sqrt{t} = 0$ most of these lines intersect the x axis at a point which is almost one-half of the diameter of the capillaries used. The reason for this behavior is essentially the formation of a concave meniscus immediately after water is brought into contact with the phenol solution in the cell as shown in Figure 57. Thus, the true mathematical boundary $X = 0$ is not the tip of the capillary but about half the diameter of the capillary inside. When the interface is moved sufficiently away from the surface, the stream lines for the solution passing over the boundary are perhaps like those shown in Figure 57. Therefore, the surface at which the boundary condition $C = C_B$ is maintained is always somewhere inside the capillary. The curvature of the meniscus depends largely on the state of the surface of the quartz glass of which the capillaries are made. Although all the necessary precautions were made in cleaning the capillaries, it varied from one capillary to another and from one test to another. To reduce this curvature, the inside surfaces of the capillary tubings were treated with "Desicote" a commercial solid surface tension reducing agent. This treatment of the capillaries and the phenol solutions was effective as far as flattening the meniscus was concerned, but, due to the phenomenon shown in Figure 57, it did not help to bring the intersection of the line X(t) versus $\sqrt{t}$ with the X(t)

axis closer to the origin. It seems that the best solution for this difficulty is the use of capillaries with a smaller inside diameter, say about 0.25 mm or less.

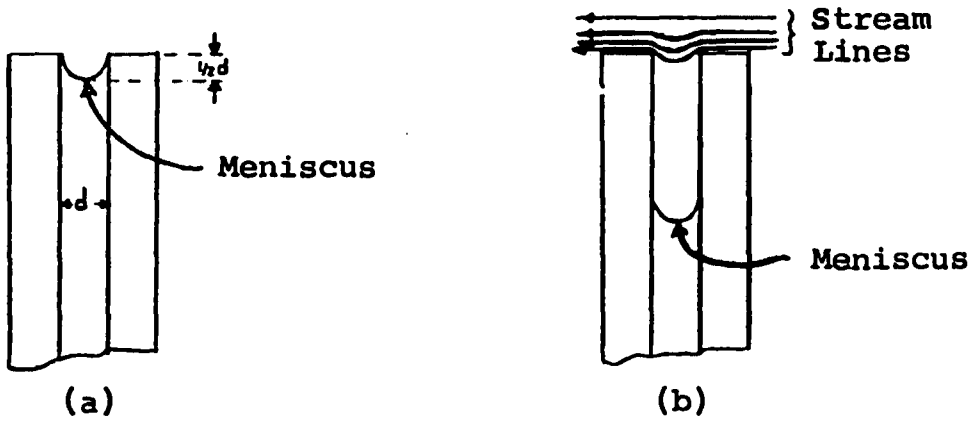


Figure 57. a) Formation of a Meniscus Immediately after Immersion of the Capillary in the Water Bath; b) Disturbance of the Concentration Field Inside a Capillary caused by the Liquid passing over its Surface.

The values of $\overline{dX(t)}/\ d\sqrt{t}$ given in Table 3 are the average values of the slope of the lines X(t) versus $\sqrt{t}$ obtained from four different capillaries used in each test. The values of the diffusivity for 30°C and 40°C are believed to be very reliable. To study the effect of the concentration range on the average diffusivity of the water rich phase, the tests reported in Table 4 were completed. Although the test set-up was further refined for these tests, the values of the diffusivity given in Table 4 are not believed to be very accurate. The two values of the diffusivity for the phenol rich phase reported in Table 5 are believed to be quite

reliable because of the much improved apparatus used to perform these tests. The only major source of error is perhaps introduced by the use of the diffusivity of the water rich phase which was obtained from the previous tests.

It should be observed that the above tests were conducted only for the purposes described before. No attempt was made to produce diffusion data suitable for general use, but rather, to get the data needed for the feasibility study of the two-dimensional diffusion cell with the least amount of effort. For this reason the experimental set-up was somewhat crude. However, when sufficiently refined, the method offers a promising possibility for obtaining the integral diffusion data for a partially miscible liquid-liquid binary system.

The Experimental Results of the Two-Dimensional Cells

The two-dimensional region under consideration for all the tests except the last demonstration tests consisted of a liquid layer of uniform thickness held between two parallel plates. The exposed boundary of this region was a rectangle subjected to a uniform, environmental concentration. The closed boundary was sufficiently away from the exposed boundary such that for all practical reasons it could have been assumed that the region simulated a semi-infinite domain bounded internally by an infinitely long parallel pipe whose surface is subjected to certain uniform conditions. The cross-section of this region is shown in Figure 58. The

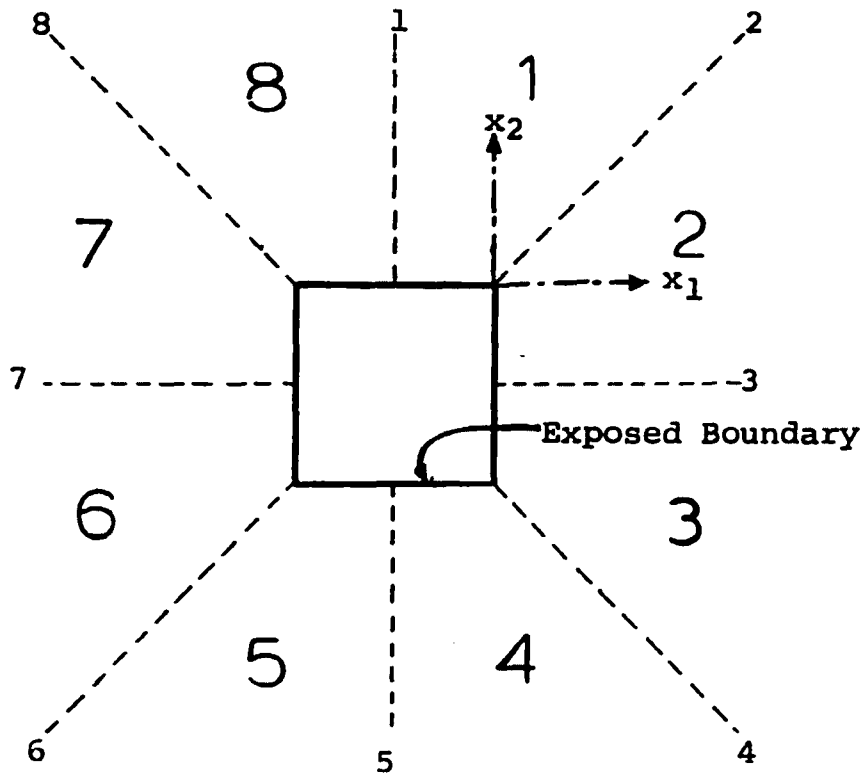


Figure 58. A Plane Region External to a Square divided into Symmetric Subregions.

dotted lines on the figure represent the lines of symmetry when the boundary concentration is uniform. The region is then divided into eight symmetrical sub-regions, such that any test represents eight sets of data. The choice of this particular region was based on the following considerations:

1. For a long, elapsed time, the concentration field close to the lines 1, 3, 5, and 7 of Figure 58 is essentially one-dimensional, therefore allowing a quick and reliable check on the existence of mass transfer by any phenomenon other than diffusion.

2. The shape of the interface formed around this region can be estimated so that the soundness of the experimental results can easily be verified. On the other hand, the boundary conditions on a sharp corner are the most difficult ones to deal with experimentally.
3. Because the experimental results can never be absolutely reproducible and exact, the eight similar regions provide an excellent way of establishing the position of the interface by plotting the best curve which averages the eight sets of curves obtained from these regions.

In the first set of tests, the region under consideration was initially made of a uniform liquid film (water rich phase or phenol rich phase). The liquid having passed over the boundary was a uniform solution of different concentration. Table 6 describes the conditions of each series of tests belonging to this category as well as their objectives and overall results. Each series of these tests consisted in turn of several tests, using various thicknesses of the liquid film in the cell (in most cases 0.125 mm, 0.25 mm and 0.5 mm) and several schemes for the distribution of flow over the boundary. All that these tests demonstrated was the impracticality of producing a pure two-dimensional diffusion field in a stationary liquid film subject to a boundary condition which is maintained by a flowing solution. The insurmountable difficulty was the bulk flow due to an uneven surface force between

TABLE 6

THE CONDITIONS AND OBJECTIVES OF THE PRELIMINARY TESTS WITH THE TWO-DIMENSIONAL CELL

Test Series	Solution in the Cell	Solution Passed over the Boundary	Objectives	Qualitative Results and Observations
1.1-	Saturated Phenol Rich Phase	Saturated Water Rich Phase	Study of Bulk Flow by Interfacial Tensions in the Absence of Chemical Diffusion	Unstable Interface Close to Boundary
1.2-	Saturated Water Rich Phase	Saturated Phenol Rich Phase		Interface very Unstable Phenol moved in the Cell Continuously, pushing Water out
1.3-	Saturated Phenol Rich Phase	Saturated Water Rich Phase γ = 40 & 35 dyne per cm	As Above	No Appreciable Change over 1.1-
1.4-	Saturated Water Rich Phase γ = 40, 35 & 30 dyne per cm	Saturated Phenol Rich Phase	As Above	No Appreciable Change over 1.2-
1.5-	Saturated Phenol Rich Phase	Distilled Water γ = 72,45,40 & 30 dyne per cm	Study of Bulk Flow by Interfacial Tensions in the Presence of Chemical Diffusion	An Interface was formed and moved in the Cell. Later on it was distorted into a very Irregular Shape. Globules of Water formed and moved inside the Cell away from the main Interface
1.6-	Pure Phenol	As Above		
1.7-	Saturated Water Rich Phase γ = 40, 35 & 30 dyne per cm	Unsaturated Phenol Solution	As Above	Same as Above, except that Phenol showed a strong Tendency to move inside the Cell and replace Water
1.8-	Distilled Water γ = 40, 35 & 30 dyne per cm	Unsaturated Phenol Solution	As Above	As Above

glass and phenol and glass and water as well as the interfacial tension between water and phenol. Every effort to resolve this difficulty was unsuccessful. These efforts included the use of several surfactants such as Leconal (liquid), Sodium Laurylsulfate (solid) and Alconox (a commercial detergent) to match the surface tension of water and phenol, as well as the use of Desicote on the glass disks to reduce their surface energy.

To eliminate completely the bulk flow due to interfacial tensions, the cell was filled with a finely dispersed emulsion of a saturated phenol solution in water. Then, by passing water over the boundary, a concentration gradiant develops in the continuous water phase, which in turn gradually dissolves the dispersed phenol solution. The reason for the absence of bulk flow due to surface forces is that here phenol is dispersed in the continuous water phase and is sustained in the cell. The water solution passing over the boundary does not form a true interface with the saturated water in the cell, so that all interfacial forces are absent. The position of what one visualizes as the interface can easily be observed by a sharp difference in the turbidity of the solution in the cell, i.e., the emulsion phase is turbid and the water phase is clear.

Use of the emulsion phase in the cell offered several advantages but also one important limitation. The limitation was that this system is only capable of solving problems of heat conduction in which the conducting medium is initially

at its transition temperature. The reason is the absence of any detectable concentration gradient in the continuous water phase in equilibrium with small phenol bubbles. Its most important advantage is in the possibility of making an emulsion of any desired overall concentration, C_{EM}, so long as the amount of dispersed phenol does not exceed the concentration required to form a stable emulsion of water in phenol. Consequently, one can simulate a wide range of latent heat parameters without changing the temperature at which the diffusion tests are conducted. In fact, for a phenol-water system, all experiments can be carried out at room temperature. The same can be said for an emulsion of water in a saturated phenol phase with a phenol solution passing over the boundary.

The early experiments with the emulsion phase were very inconclusive, but they yielded several important observations. Viewing the region close to the boundary through a magnifying (20X) telescope, it was possible to see clearly how the mechanical defects in the cell design, as well as the motion of the liquid which passed over the boundary, give rise to bulk motion in the cell. It was also observed that, even at a flow rate of about 2 cc per hour, there is a definite induced agitation in the region immediate to the boundary. A slight irregularity in the rate of pumping of the micro-pump, which was caused by excessive friction in the pump's gear box and rack, developed a pressure wave. When the pressure wave reached the boundary of the cell, it gave rise to a non-uniform pressure distribution on the boundary, which in turn

created a bulk flow from one side to another. It should be noted that the strength of such pressure waves developed in the inlet channel was indeed negligibly small. The disturbance in the cell was a result of infinitesimal pressure waves which did not reach the boundary at the same time. Consequently, there were regions of different pressure on the open boundary. To eliminate this difficulty the following steps were taken:

1. The micropump was improved to allow a much more uniform flow.
2. The boundary was separated from the flow channel by a thin belt made of filter paper so that these pressure waves could be dampened effectively.

Figure 59 shows a top view of the cell at the viscinity of the boundary with the above boundary arrangement at two different time levels. The boundary was a 2 cm x 1 cm rectangle. Pure water was passed over the boundary. The top photograph was taken after 1:35 hours. Note that distortion of the bottom side of the boundary in the photograph is caused by a surface crack on the glass disk. The boundary is exactly the same as the top side. Observe the water phase-emulsion phase interface just formed around the filter paper belt. By the shape of this interface it can be positively stated that no preferential wetting of the glass surface or interfacial force exists which could cause any bulk flow. Compare this interface with that of a large globule of phenol on the top left of the bottom photograph. Here the interface is circular, which is the equilibrium shape when there are interfacial forces.



01:35 hours



08:50 hours

Figure 59. Photographs of the Two-Dimensional Cell showing the Formation and Progress of the Interface between Water and an Emulsion of Phenol in Water.

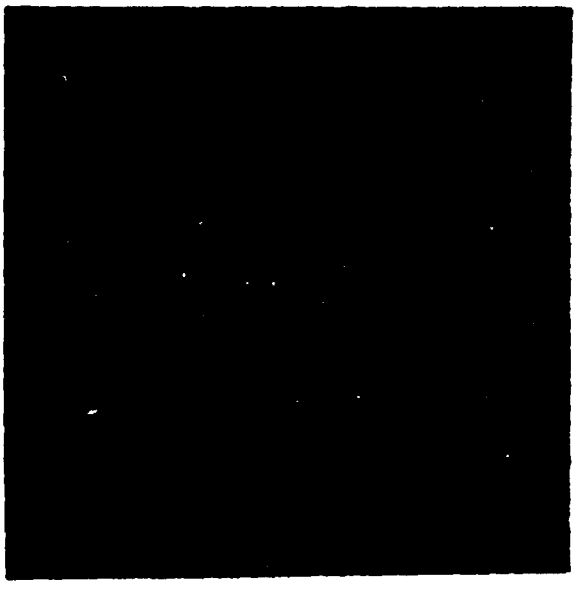
The bottom photograph in Figure 59 shows the shape of the interface after 8:50 hours. The bright spots in the clear phase are from the background. On the left side of the boundary the average rate of the movement of the interface was close to the approximate theoretical prediction. This prediction was based on the assumptions that a) the diffusion field is linear, b) the emulsion phase is uniform, and c) the concentration on the external side of the paper belt is that of pure water. With all the care taken in performing this test, there was every reason to believe that the mass flow at the boundary was strictly by chemical diffusion. The non-uniformity of the interface at the top and left sides of the boundary was believed to be caused by the variable concentration (the amount of suspended phenol phase per unit volume) in the cell and by stagnation of the boundary flow at these sides. Although the latter difficulty was overcome in the subsequent tests, the former could not be resolved.

In order to fill the cell uniformly, the emulsion has to either enter the cell through the filter paper belt and flow out for a sufficient length of time at the periphery of the glass disks to an exit tube connected to the cell's cylindrical frame, or vice versa. In each case the cell is sealed from the outside by the O-rings situated on the aluminum frame (Figure 41) which, as discussed in Chapter V, is not very desirable. When the emulsion is passed through the filter paper, the paper preferentially allows the continuous (water) phase to flow, so that it distorts the initial uniform distribution of

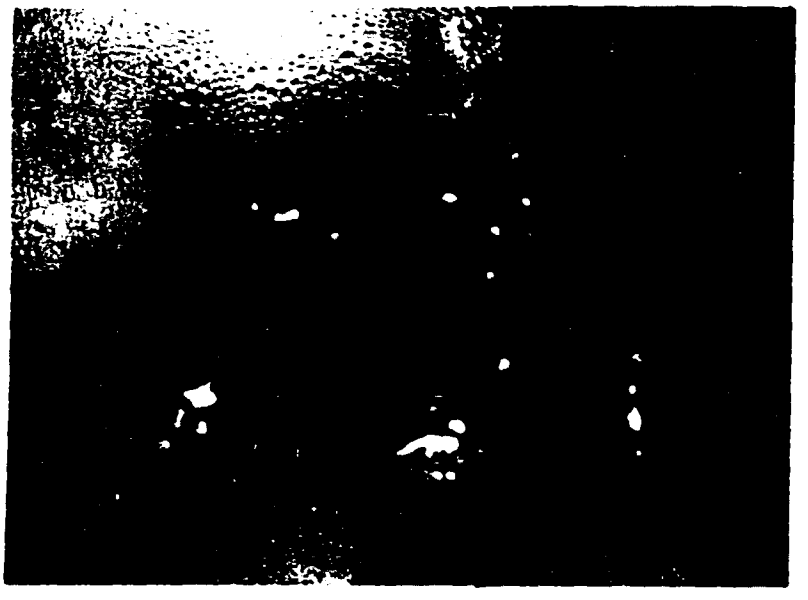
the emulsified phase. This situation is shown in the top photograph of Figure 60. Here, the emulsion entered from the periphery and left the cell through the filter paper belt. Observe the phenol bubbles of various sizes accumulated around the belt. Observe also the large phenol bubbles (the dark spots) spread all over the liquid film in the cell. These bubbles were formed by the aggregation of fine phenol bubbles while passing through the cell. The spacing between the glass disks (or the thickness of the liquid film) here was about 1/8 mm. The dark shadows (especially on the right) indicate the sparseness of the suspended phenol phase.

At a film thickness of more than 1/4 mm, a secondary aggregation of phenol particles gradually took place which gave rise to local disturbance and internal flow. The bottom photograph in Figure 60 shows this situation. The photograph was taken after 18:00 hours. This phenomena would not have occurred if the phenol-water system had made a stable emulsion. The same results were observed when the cell was initially filled with an emulsion of water in phenol. Some success was achieved in filling the cell with a uniform emulsion when the emulsion and the cell were heated to a few degrees above the complete solubility temperature prior to filling. Upon cooling, a relatively uniform emulsion was formed in the cell.

To avoid gradual aggregation of the dispersed phase, a 0.005 inch thick nylon cloth mesh was placed between the glass disks which covered the entire space in the cell. The



(a) 00:00 hours



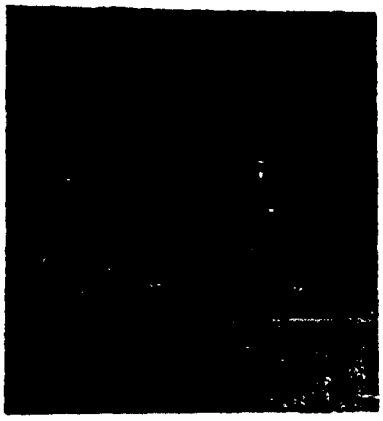
(b) 18:00 hours

Figure 60. Photographs of the Two-Dimensional Cell: (a) Immediately after Filling with an Emulsion of Phenol in Water and (b) after 18:00 Hours. The Emulsion Film Thickness was 1/8 mm in (a) and 1/4 mm in (b).

openings of the cloth were about 0.004 inch. The cell was then filled with a heated solution of phenol in water and allowed to cool down so that an emulsion phase was formed. Interestingly enough, every opening of the cloth contained a globule of phenol rich solution. The sizes of these globules were almost uniform throughout. Figure 61 shows some typical results obtained by this arrangement. The approximate position of the interface was drawn on the photographs while examining them under a microscope. Note the degree of symmetry and uniformity of the interface in photographs (b) and (c) of Figure 61, where a thin paper belt is used to separate the flowing liquid at the boundary from the stationary liquid in the cell.

The tests in which the emulsion was trapped by the nylon cloth were successful in making it possible to develop a pure two-dimensional diffusion mass transfer, but several shortcomings arose which forced these tests to be discontinued:

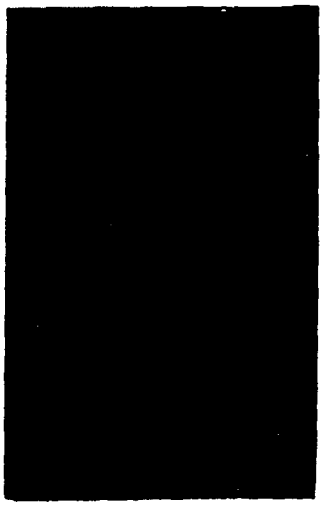
1. The presence of a finely porous filter paper between the flowing boundary solution and the stationary liquid in the cell restricted very sharply the variety of boundary conditions which could be accurately simulated.
2. It was most difficult to see the interface between the emulsion phase and the clear phase even under a suitable microscope. The lines drawn on the photographs shown in Figure 61 are only accurate to ±0.2 mm since the line of demarcation was not clear.



a



b



c

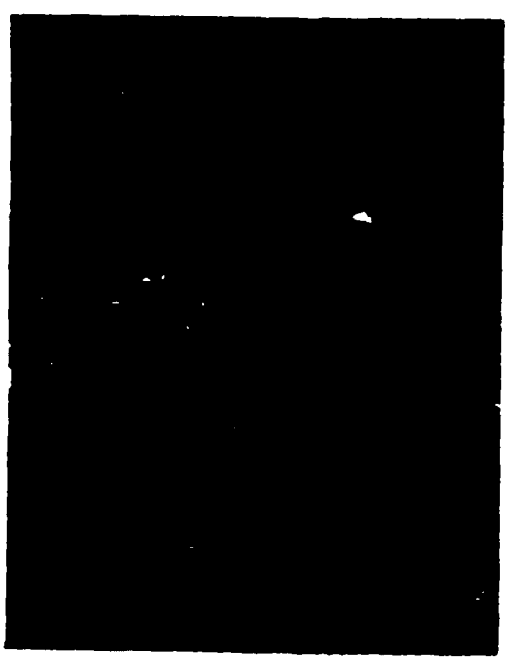
Figure 61. Photographs of the Two-Dimensional Cell Initially Filled with an Emulsion of Phenol in Water, Using a Nylon Cloth to Stop Aggregation of the Suspended Phase with and without a Filter Paper Belt.

3. The nylon cloth in the cell precluded the use of an interferometric method for measuring the concentration profile in the cell.

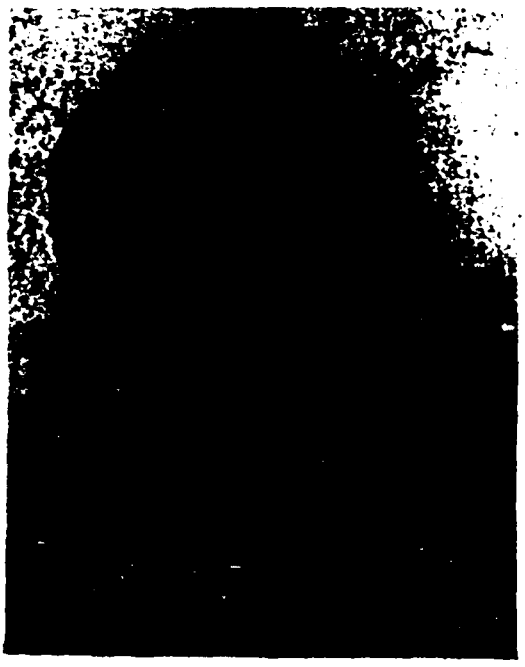
However, it should be noted that most of the above criticisms are specific to the phenol-water system. They may not apply to partially miscible liquids which form a permanent emulsion.

In all the experiments with the clear solutions in which the filter paper belt was used as a partition at the boundary, it was observed that a fine interface formed in the paper and moved outward from the rectangular boundary quite regularly. The difference between the refractive index of the water phase and the phenol phase made a distinct difference in the brightness of the filter paper so that it was possible to see the interface very clearly. For this reason a porous medium, consisting of Whatman filter paper Number 52, with a rectangular boundary cut out of the center, was used in subsequent experiments. The boundary flow distribution was as before, except that here there was no need for the filter paper belt. The boundary was directly exposed to the solution passing over it.

In the first set of tests (Runs 3.1-) the porous region in the cell was initially filled with a saturated phenol solution, and pure water was passed over the boundary. In Figure 62 the three photographs of the cell show the position of the interface at different time levels. Observe the high degree of symmetry and the well defined interface. Further examination of these photographs indicated that the



01:10 hours



05:35 hours



10:35 hours

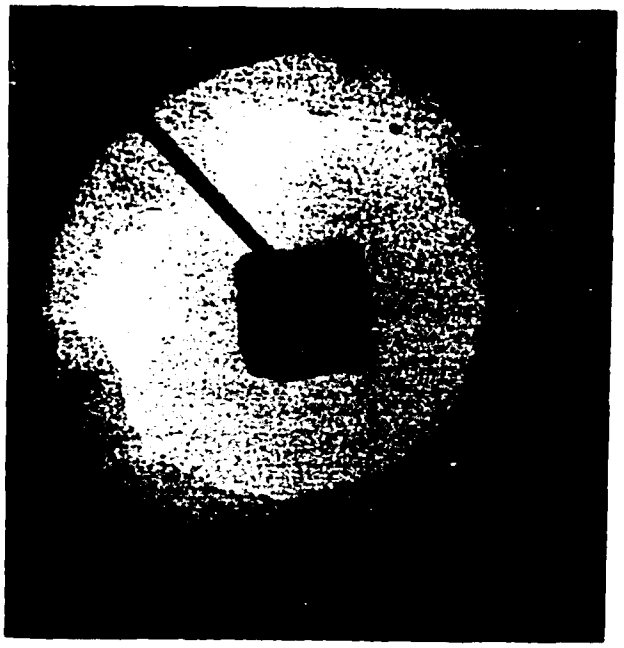
Figure 62. Test 3.1-1. The Progress of the Interface Formed by Passing Pure Water over the Rectangular Boundary of the Filter Paper Sheet Initially Saturated with a Phenol Rich Solution.

interface moved at a velocity much higher than that expected for linear diffusion in a non-porous medium. The test was repeated in order to determine the cause of this behavior. When the boundary was viewed through a 20X telescope it was observed that small globules of phenol gradually came out of the pores, and consequently water moved in by perhaps capillary action. At first it was thought that such behavior only occurs at the surface of the glass disks because of the non-uniform contact between the filter paper and glass. To correct this situation, four layers of filter paper were compressed together, and a thin sheet of polyethylene was uniformly melted over the outer surfaces to close the pores on the surface of the paper and to provide a very smooth contact surface. Figure 63 shows the interface developed in such a region after seven minutes. As before, the distance of the interface from the boundary is what one would have expected after almost one hour. Note the small phenol globules coming out to the flow channel at the bottom right corner of the boundary.

Using the same arrangements, but filling the cell initially with pure water and passing an unsaturated phenol-rich phase at the boundary, resulted in the formation of an interface which moved at a rate very close to the theoretical prediction. The interface was much sharper and smoother than that shown in Figure 63. These tests are discussed in the remainder of this chapter.

interface moved at a velocity much higher than that expected for linear diffusion in a non-porous medium. The test was repeated in order to determine the cause of this behavior. When the boundary was viewed through a 20X telescope it was observed that small globules of phenol gradually came out of the pores, and consequently water moved in by perhaps capillary action. At first it was thought that such behavior only occurs at the surface of the glass disks because of the non-uniform contact between the filter paper and glass. To correct this situation, four layers of filter paper were compressed together, and a thin sheet of polyethylene was uniformly melted over the outer surfaces to close the pores on the surface of the paper and to provide a very smooth contact surface. Figure 63 shows the interface developed in such a region after seven minutes. As before, the distance of the interface from the boundary is what one would have expected after almost one hour. Note the small phenol globules coming out to the flow channel at the bottom right corner of the boundary.

Using the same arrangements, but filling the cell initially with pure water and passing an unsaturated phenol-rich phase at the boundary, resulted in the formation of an interface which moved at a rate very close to the theoretical prediction. The interface was much sharper and smoother than that shown in Figure 63. These tests are discussed in the remainder of this chapter.



00:07 hours

Figure 63. Test 3.1-2. The Interface Formed in Whatman Filter Paper after Passing Water over the Rectangular Boundary for Seven Minutes. The Filter Paper was Initially Saturated with a Phenol Rich Phase.

Final Results

As was brought up before, it was only possible to produce a pure two-dimensional diffusion field when the porous medium in the cell was initially filled with a water rich phase, and phenol was passed over the boundary. In all the subsequent tests this condition was maintained. Having a phenol solution at the boundary, it was no longer possible to obtain the total flux at the boundary by the analysis of the exit solution. The reason was that the amount of water added to the boundary solution was very small (of the order of 10^{-4} moles per liter) compared to the water content of the

phenol solution (about 5.0 moles per liter). Consequently, the only experimental observation was the measurement of the position of the interface. A chemical analysis of the solution for finding the total flux would not have been sufficiently accurate to contribute towards the objectives of the present work. Furthermore, it was unlikely that the total flux would have been a convenient parameter for checking the validity of the experimental results.

A total of five tests were completed with a region external to a 1 cm x 1 cm boundary. All except one are reported here. The reason for rejecting one of the tests was a complete non-uniformity of the boundary on all sides of the square. The square boundary was cut out of the 2 inch filter paper disks with a sharp razor blade. There was always the danger of closing some of the pores in the process of cutting. These pores may either stay closed during the test and consequently result in a much lower rate of mass transfer at the boundary, or they may open later on to give rise to a non-uniform rate of interface movement. This problem existed in most of the tests. There was also the possibility of flow blockage on one or more sides of the boundary due to the formation of a small air bubble or the accidental movement of the flow distributor from its center position while assembling the cell. For the four tests reported here, not all the data obtained from the eight sub-regions shown in Figure 58 were assumed to be valid. Whenever there were sufficient reasons for believing that the above mentioned difficulties existed

at the boundary of one of the sub-regions, the data from that region, as well as the effected neighboring regions, were rejected. Table 7 gives the operating conditions for these tests as well as the duration of the tests and the sub-regions considered to be satisfactory.

TABLE 7

THE CONDITIONS OF TESTS 3.2-1 TO 3.2-4

Test No.	Temp.	C_B Mol./Lit. of H_2O	C_∞ Mol./Lit. of H_2O	Regions Considered	Duration of Test Hours
3.2-1	55°C	5.088	47.53	2,3,4,5,6&7	26:46
3.2-2	55°C	5.088	47.53	6,7,8&1	23:46
3.2-3	55°C	3.920	54.7	2,3,4&5	9:54
3.2-4	55°C	4.737	54.7	5,6,7&8	29:43

The photographs in Figure 64 show the progress of the interface with time for Test 3.2-2. Note the very sharp difference in thetranslucency of the filter paper at the opposite sides of the interface. The brightness of the region saturated with phenol rich phase is essentially due to the closeness of the refractive index of phenol rich solution (1.44 - 1.53) to that of filter paper. The water rich phase has a refractive index ranging between 1.3 - 1.38 depending on the composition and temperature. Figures 65 and 66 are two sets of photographs showing the progress of the interface in Test 3.2-3 and Test 3.2-4.

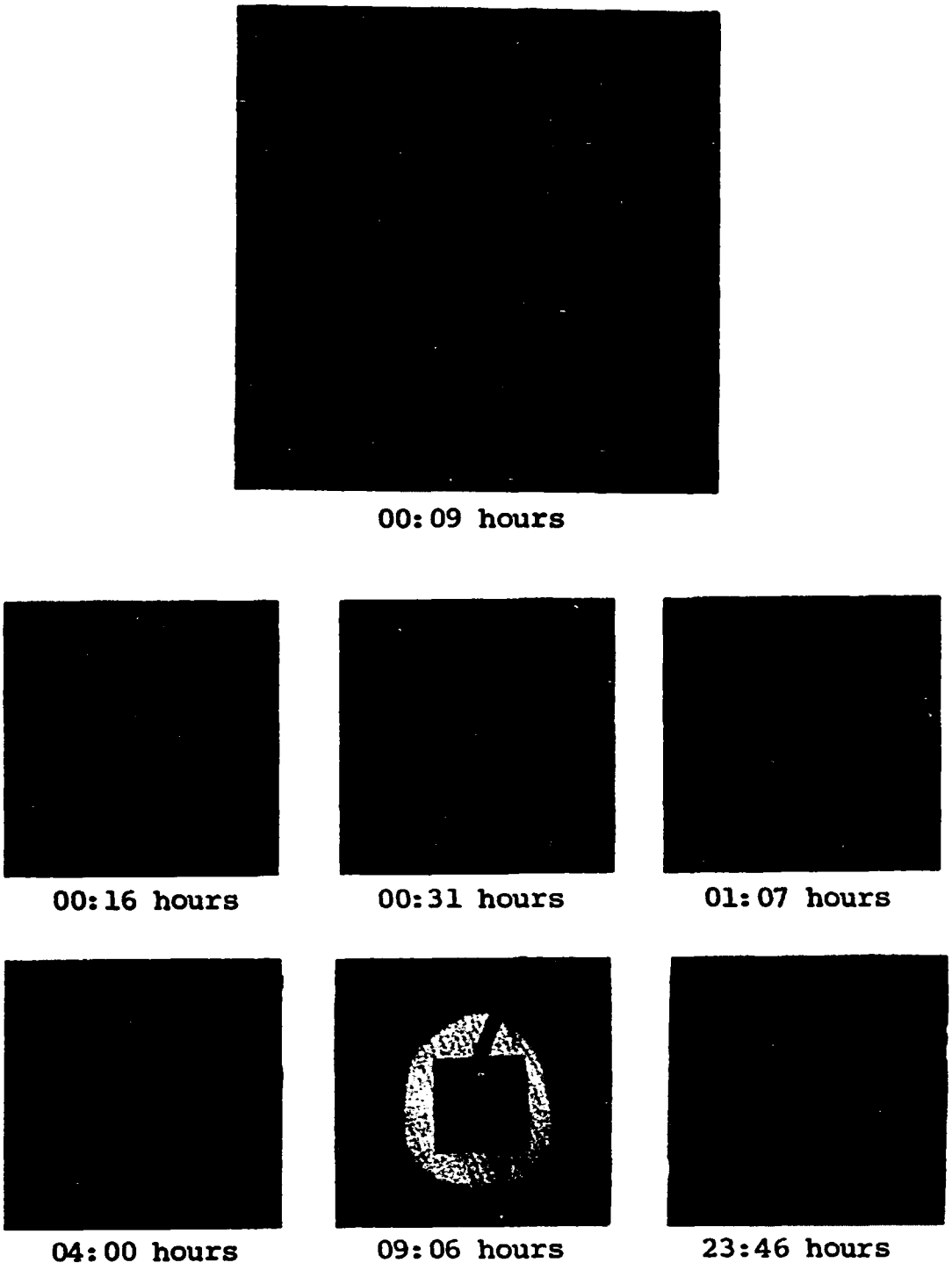
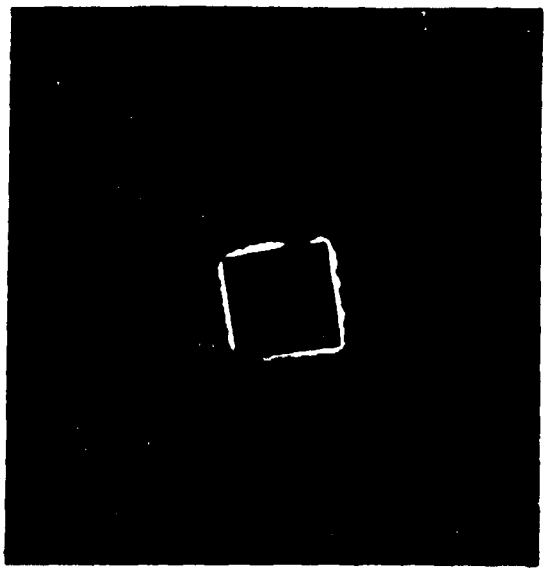
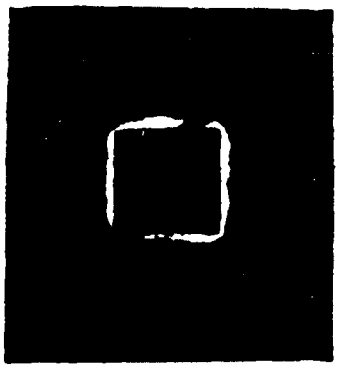


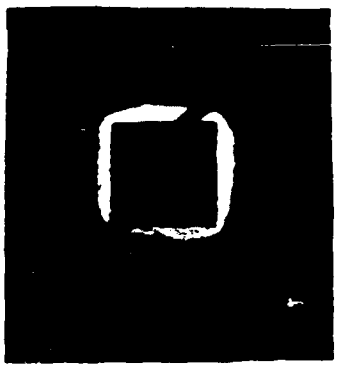
Figure 64. Test 3.2-2. Photographs of the Diffusion Cell Showing the Progress of the Interface Developed Around a 1 cm x 1 cm Square Boundary. The Cell Was Initially Filled with Water Saturated with Phenol at 55°C. A Phenol Rich Solution was Passed over the Boundary and the Temperature was kept at 55°C.



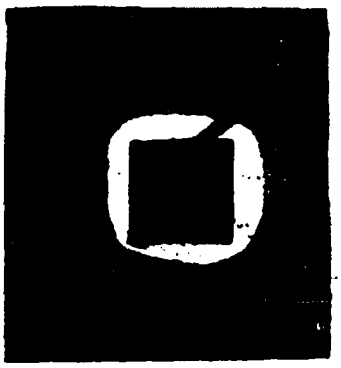
00:30 hours



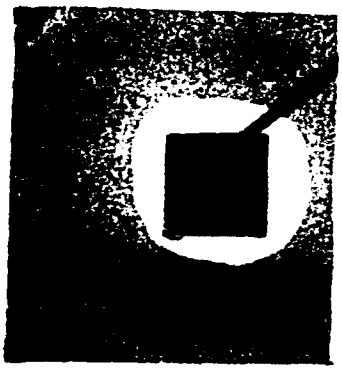
01:00 hours



02:23 hours



05:07 hours



09:54 hours

Figure 65. Test 3.2-3. Photographs of the Diffusion Cell Showing the Progress of the Interface Developed Around a Square Boundary. The Cell was Initially Filled with Pure Water. A Phenol Rich Solution was Passed over the Boundary and the Temperature was kept at 55°C.

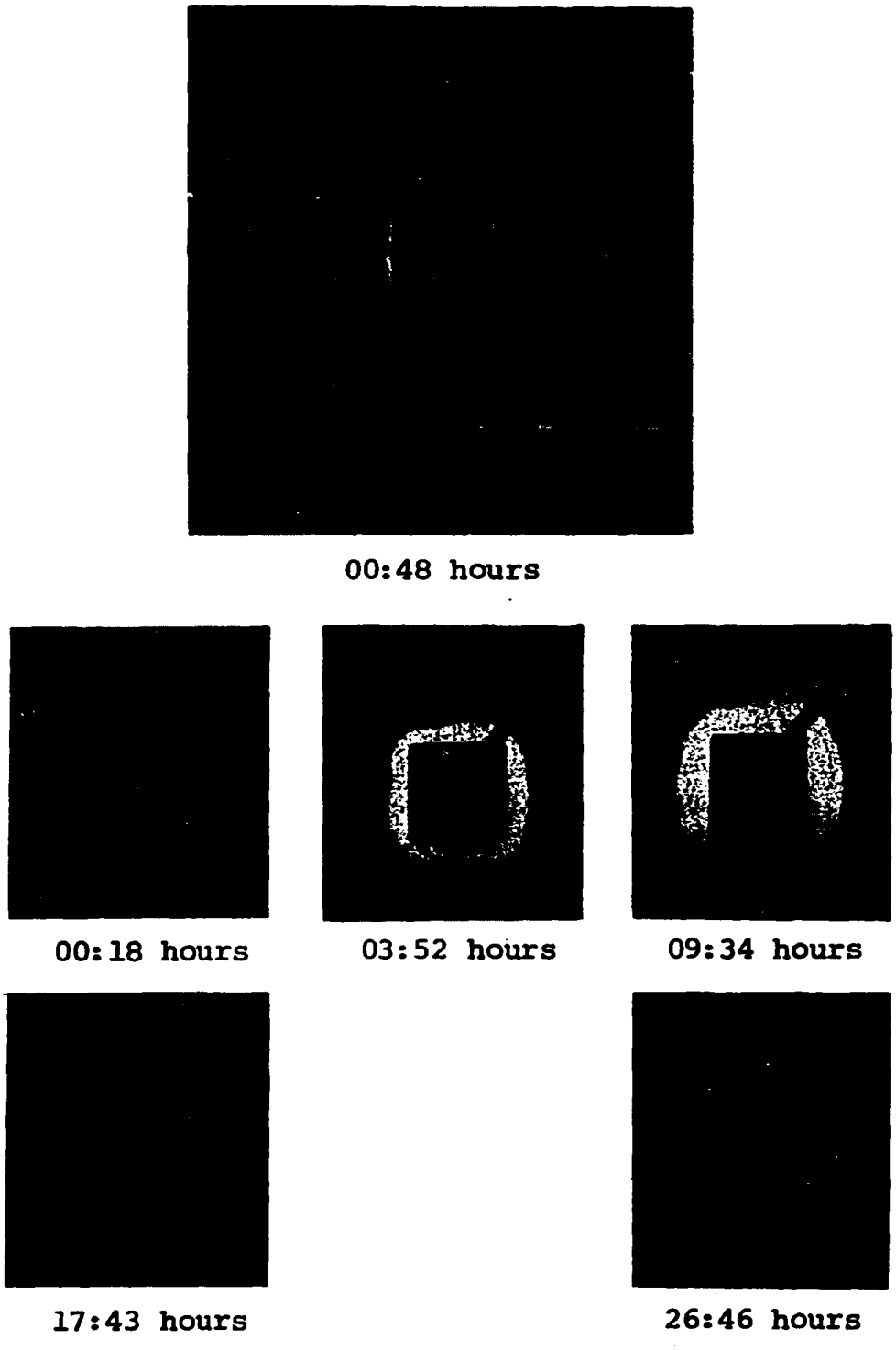


Figure 66. Test 3.2-1. Photographs of the Diffusion Cell Showing the Progress of the Interface Developed Around a 1 cm x 1 cm Square Boundary. The Cell was Initially Filled with Phenol Saturated Water. A Phenol Rich Solution was Passed over the Boundary. The Temperature was kept at 55°C.

The temperature in all these tests was 55°C which corresponds to a change of concentration of 24.5 moles of water per liter across the interface. In Tests 3.2-1 and 3.2-2, the cell was initially filled with pure water, while in Tests 3.2-3 and 3.2-4 it was filled with phenol-saturated water solution at 55°C.

Figures 67, 68, 69 and 70 are plots of the average position of the interface $X(x_1,t)$, at several time levels in the subregions considered to be satisfactory for Tests 3.2-1, 2, 3 and 4, respectively. Not all the regions are represented by an equal number of data points on these figures. The solid lines drawn among the data points are, in reality, the average of several continuous curves obtained from each photograph of the cell. They do not correspond to the best curve passing through the points shown in the above mentioned figures. In all these figures the actual distances in the direction of x_1 and x_2 are divided by one-half the length of the side of the square boundary (i.e., 5 mm). Thus, x_1 and $X(x_1,t)$ are both dimensionless. The center of the coordinates is situated at the corner. The dimensionless elapsed time, $\tau = \omega \tilde{D}^I t/a^2$, was calculated from the knowledge of the time at which the photographs were taken, the experimental values of $\tilde{D}^I$ for the phenol rich phase, and the experimental values of ω (to be described below).

Test 3.2-3 was carried on first, because of the less tedious filling procedure for pure water. Note the large departure from the average curve of the position of the

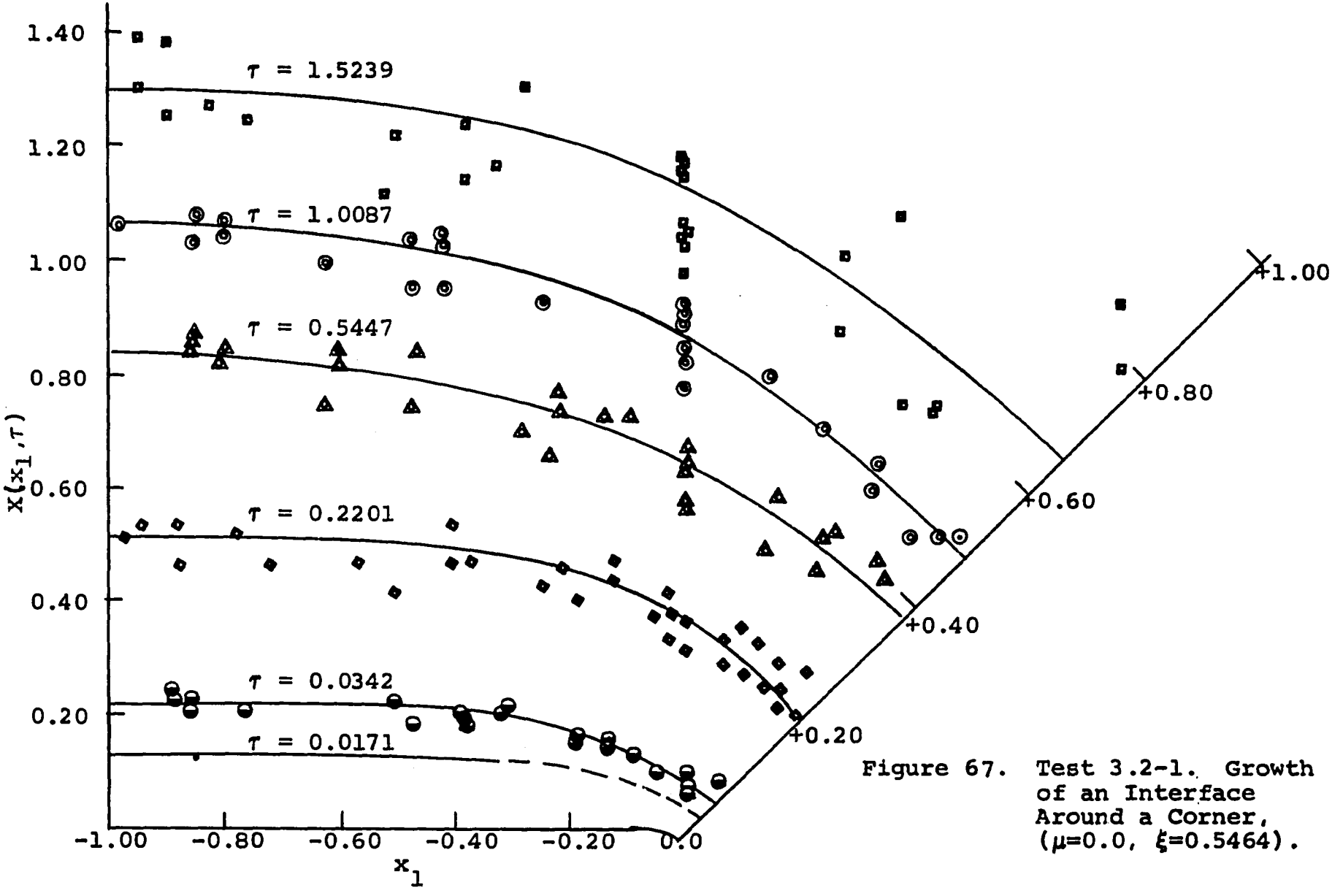


Figure 67. Test 3.2-1. Growth of an Interface Around a Corner, (μ=0.0, ξ=0.5464).

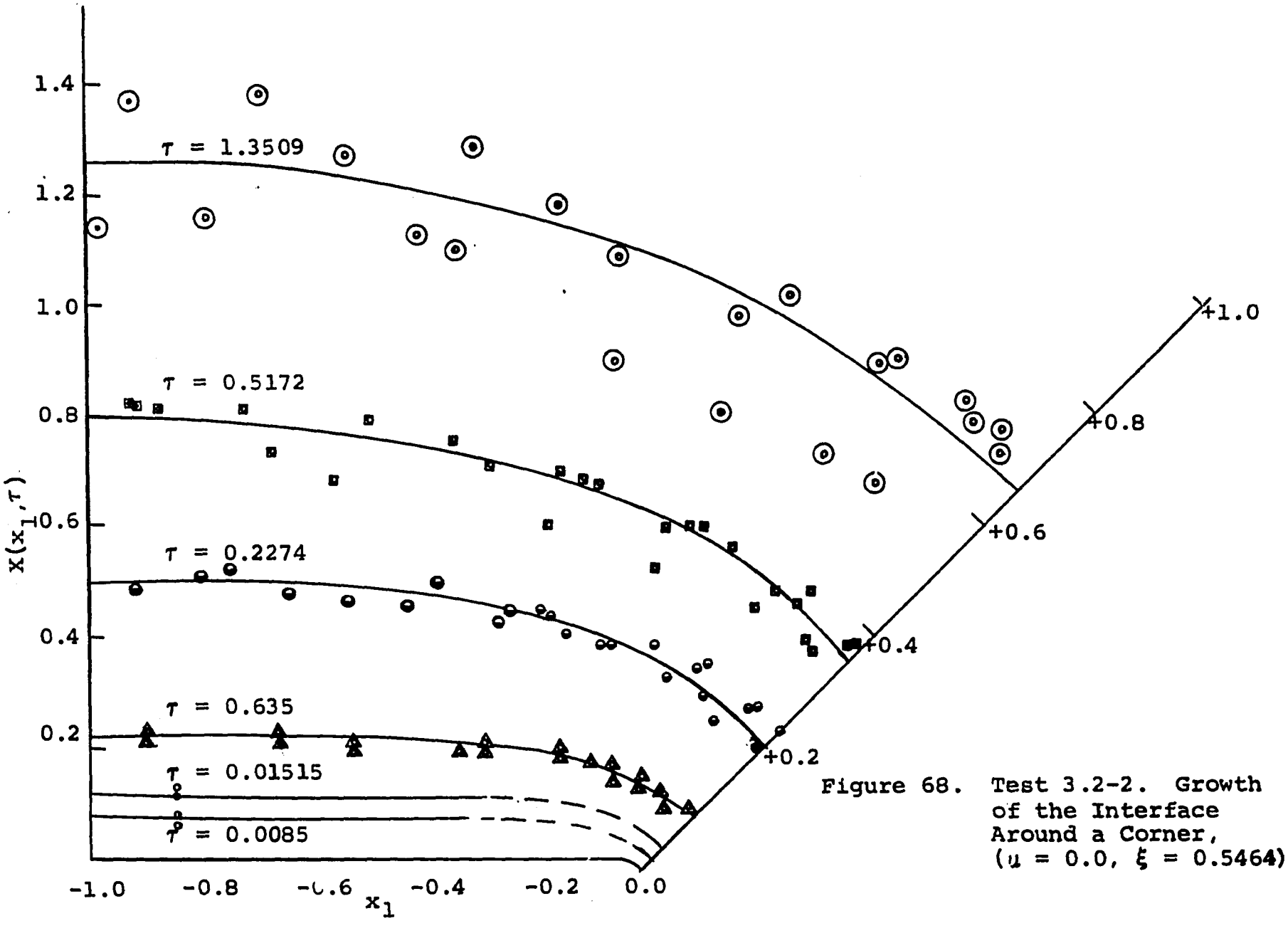


Figure 68. Test 3.2-2. Growth of the Interface Around a Corner, (μ = 0.0, ξ = 0.5464)

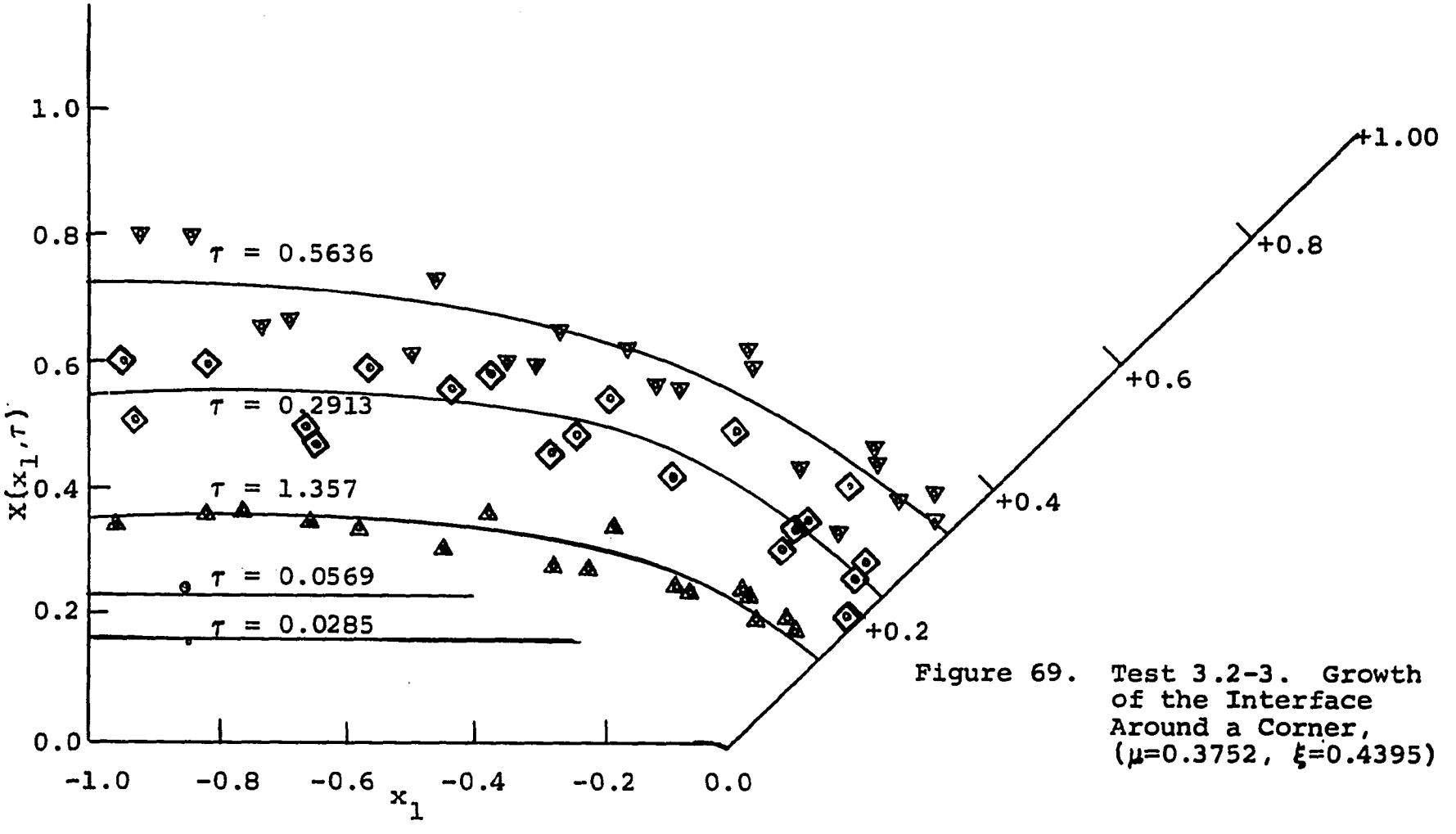


Figure 69. Test 3.2-3. Growth of the Interface Around a Corner, (μ=0.3752, ξ=0.4395)

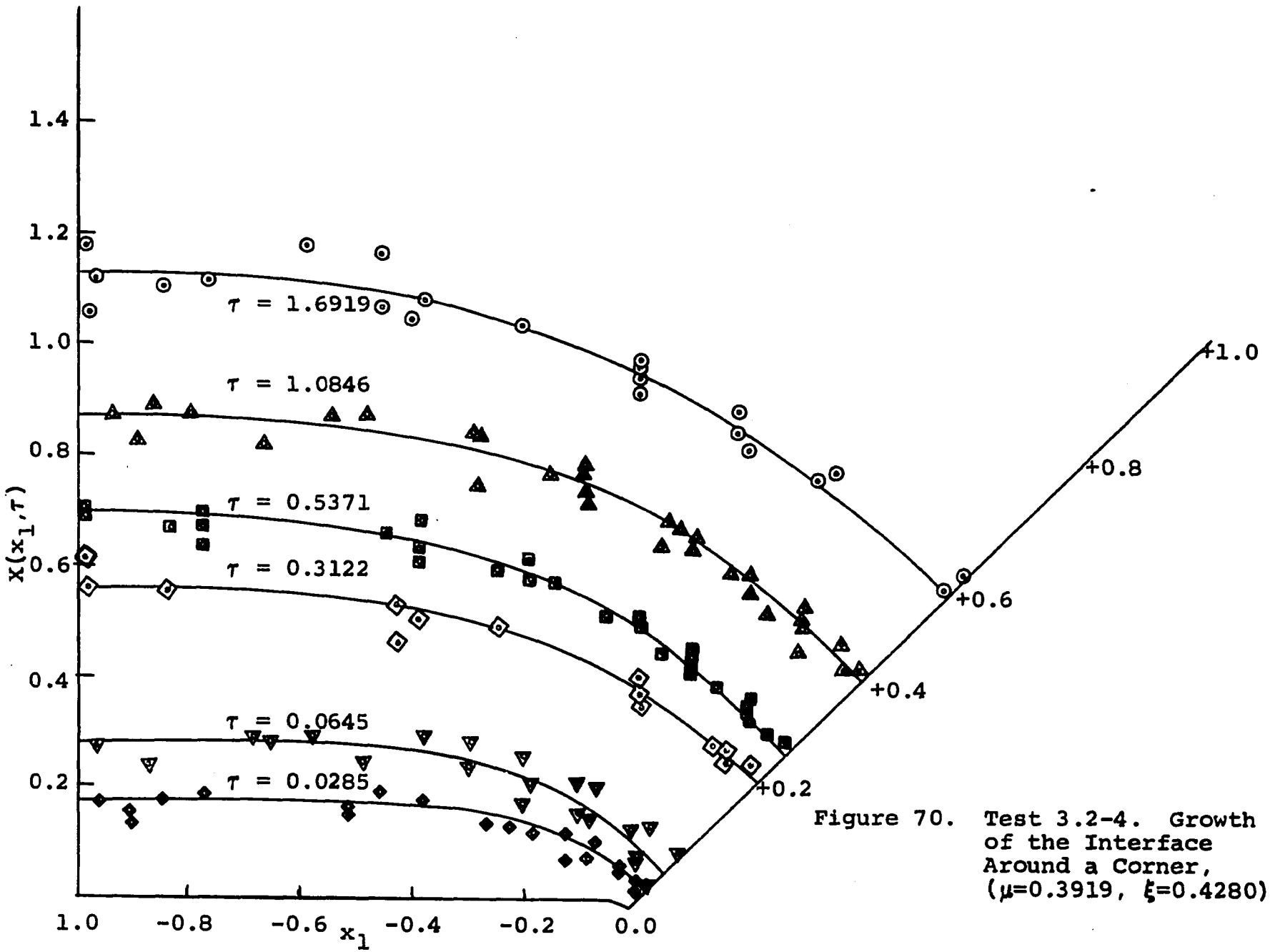


Figure 70. Test 3.2-4. Growth of the Interface Around a Corner, (μ=0.3919, ξ=0.4280)

interface in the various regions, probably due to the fact that the boundary was not properly cut. Also, one of the corners was blocked internally by absorption of silicone rubber before setting. It is interesting to see the formation of the interface behind the closed corner in Figure 65. Note also the improvement in the experimental data plotted in Figure 68, which was attained only by gaining experience in conducting these tests.

To establish that the mass transfer in the cell has been only by chemical diffusion, one observes that at the middle of each side of the square boundary the concentration field is essentially one-dimensional for a long period of time. Therefore, the vertical position of the interface on the lines 1, 3, 5 and 7, shown in Figure 54, should follow equation (6.1) i.e.,

$$X(x_1,t)\Big|_{x_1=-1} = X(-1,t) = 2\xi\sqrt{\omega\, D^I t/a^2} \qquad (6.1a)$$

where ω is defined by (2.9). It was observed in Chapter II that the value of ω for a fibrous material such as filter paper should be about 0.75. Figure 71 is a plot of $\bar{X}(-1,t)$ versus $\sqrt{t/a^2}$ for Tests 3.2-1 and 2 where $\bar{X}(-1,t)$ is the linear average of $x_2(-1,t)$ at time t for all the regions considered in these tests. The solid line on the figure is the best straight line which fits all the data points. The slope of this line was 1.30308. For the conditions of these two tests $\xi = 0.5464$ and $\tilde{D}^I = 1.887$ mm^2 per hour (from capillary

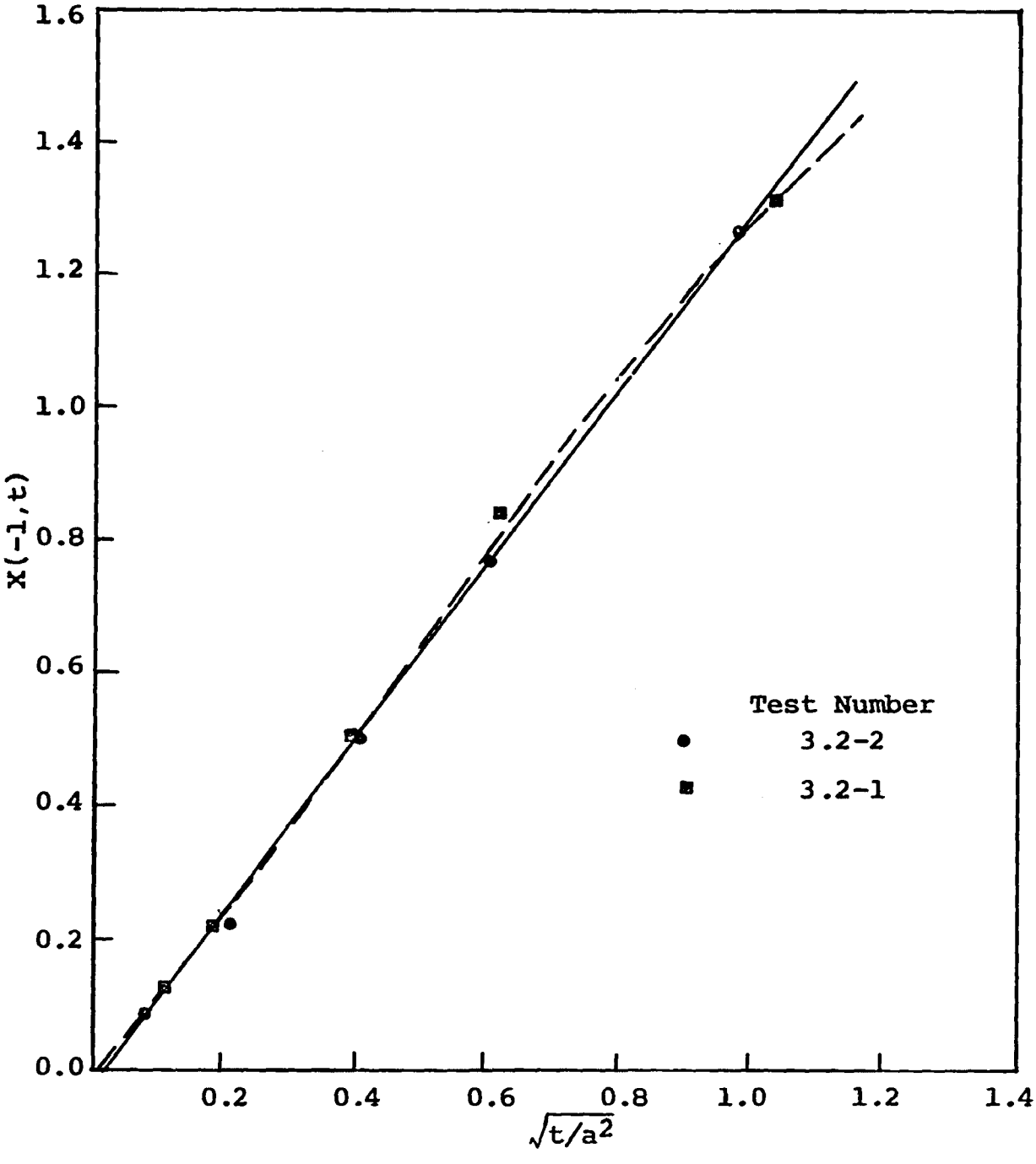


Figure 71. Variation of X(-1,t) with $\sqrt{t/a^2}$ showing the One-Dimensional Nature of the Concentration Field at $x_1 = -1.0$.

Tests C-3.1 and 2). Substituting these values in (6.1a):

$$\frac{dX(-1,t)}{d(\sqrt{t/a^2})} = 1.50\ \omega^{\frac{1}{2}} = 1.30$$

or

$$\omega = 0.75$$

which is in remarkable agreement with the expected approximate value of 0.75 for ω.

No process other than pure diffusion could have followed Equation (6.1a) so closely for such a long period of time (about 24 hours). Further proof of the pure diffusion nature of the mass transfer in the cell can be obtained by a close study of the best curve, shown as the dotted line in Figure 71, as passing through all the data points. At the beginning of the test the progress of the interface is slower than that predicted by Equation (6.1a). This result can also be concluded by noting that the least square line intersects the X axis below the origin. (Note that the intersection was always above the origin in all the one-dimensional capillary tests). The reason for this phenomenon is the impracticality of bringing the boundary concentration instantaneously to a desired value. Observing the displacement of water by phenol in the flow channel around the boundary showed that it takes about five minutes before the boundary concentration approaches that of the solution pumped into the cell.

As time goes on, and the interface gets sufficiently away from the boundary, the concentration field at $x_1 = -1$ is no longer one-dimensional. The corner effect makes the

interface move slower than that of the linear flow of heat. This trend is also shown by the data points in Figure 71.

Having evaluated ω, it is now possible to calculate the dimensionless time, $\tau = \omega \tilde{D}^{I} t/a^2$, where as before 'a' is one-half of the length of the square boundary (i.e., 5 mm in the above tests). Using the experimental values of $\tilde{D}^{I}$ and $\tilde{D}^{II}$ obtained from the one-dimensional tests, and the value of ω for the filter papers obtained from the two-dimensional saturated water tests, the linear rate of progress of the interface was predicted for the pure water tests (i.e., Tests 3.2-3 and 4 in which the cell was initially filled with pure water and there was a changing concentration field on both sides of the interface). Figure 72 shows the comparison between the position of the interface at $x_1 = -1$ predicted by Equation (6.1a) (the solid line) and the experimental values of $X(-1,\tau)$ for all the four tests. Plotted in this figure are the values of $X(-1,\tau)/(2\xi)$ versus $\sqrt{\tau}$. Considering the magnitude of the sum of all possible sources of error which would have made the results partially inconsistent, the agreement between the experimental points and the theoretical predictions based on the one-dimensional model is quite remarkable. Not only are the data points reasonably close to the line $X(-1,\tau)/(2\xi) = \sqrt{\tau}$, but they also follow the expected trends discussed before.

Figure 73 provides a comparison between the diffusion analog results and the computer solution of Example Problem 1. Plotted in this figure is $X(x_1,\tau)/2\xi$ for $x_1 = -1.0$, -0.20, 0.0,

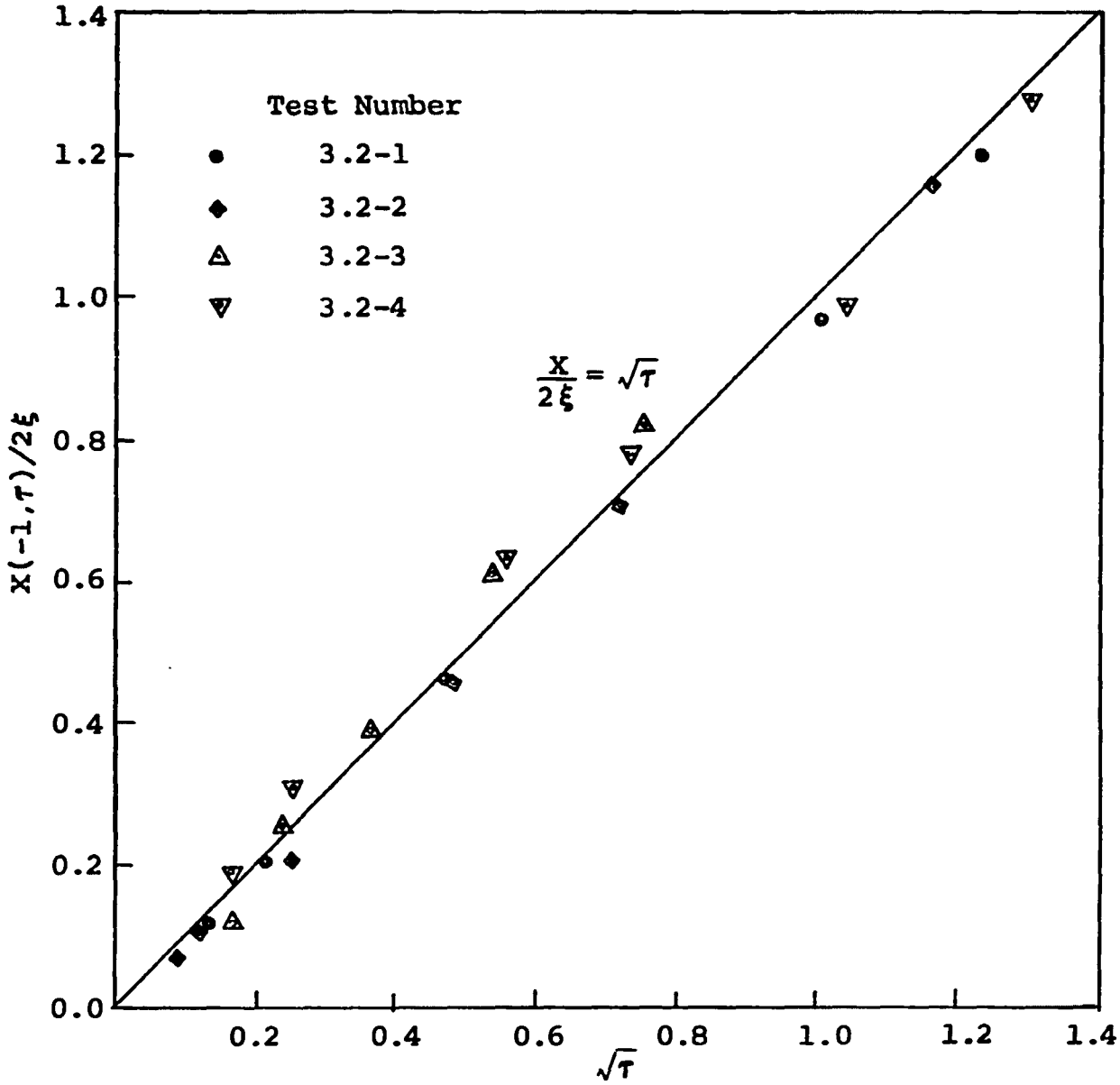


Figure 72. Comparison of the Experimental Position of the Interface at $x_1 = -1.0$ and Neumann's Solution ($X = 2\xi\sqrt{\tau}$).

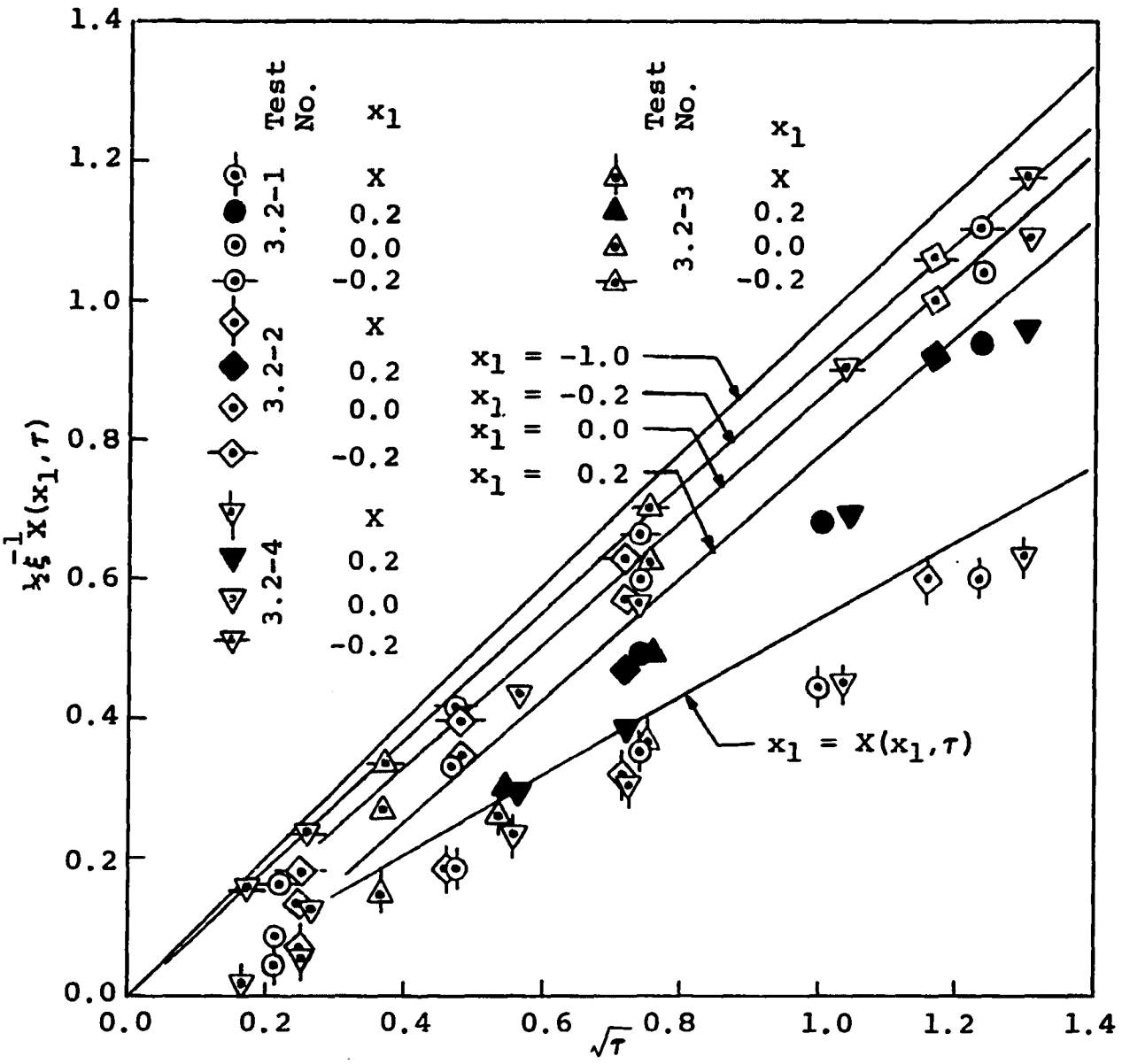


Figure 73. A Comparison of the Computed (Example Problem 1) Values of $X(x_1, \tau)$ and those of the Diffusion Cell Analog.

+0.20 and $X(x_1,\tau) = x_1$ versus $\sqrt{\tau}$. The solid lines represent the computed values of $X(x_1,\tau)$. The data points represent the diffusion analog results obtained from the average curves of Figures 67, 68, 69 and 70. The agreement between the computer solution and the analog results is somewhat poor for $X(x_1,\tau) = x_1$ because the corners were not sharp in the diffusion model and there were imperfections in the exposed boundary around the corners. Almost all the other data points in Figure 73 fall below the computed lines due to imperfections at the boundary surface which have the result of reducing the effective diffusion cross section. The lines of constant x_1 in Figure 73 are a convenient means for demonstrating the consistency of all the data obtained from a region external to a square. It is not, however, intended to provide a correlation of all the data because of the many possible sources of error in the experimental measurements. In other words, these data were considered to be unworthy of a satisfactory correlation. The sources of inaccuracy of the data were essentially:

1. The cross sectional area of the open pores at the boundary was not uniform throughout and perhaps somewhat different from that of the rest of the cell.
2. The pores of the filter papers were not sufficiently uniform throughout.
3. In all tests, four layers of filter paper, sealed by a polyethylene sheet, were used. At the contact surface of this sheet, the structure of the

pores was substantially different from that of the filter papers.

4. Around the sharp corners, there was always an almost stagnant liquid which was not flowing at the same rate as that of the flat sides of the boundary.
5. Not all four sides of the square boundary could be brought to the predetermined boundary concentration instantaneously. This deficiency introduced an error of about 2 to 3 minutes in the values of the initial time.
6. Although most photographs were read twice on the microprojector, the human errors in these readings were appreciably large.
7. The value of the diffusion coefficient for the water rich phase used to calculate ξ for Tests 3.2-1 and 2, was not very accurate.

Although all these difficulties can be resolved, they nevertheless offer some challenges to future investigators.

To demonstrate the utility of the diffusion cell in solving the complex problems of heat conduction with change of phase, two tests were completed with a wedge-like region in which a circle of 5 mm in radius was excavated, Figure 74. This region represents a symmetric section of a ring of circles in a semi-infinite plane region. The closed boundary is, of course, the sides of the wedge, and the open boundary is the internal circle. As before, four layers of Whatman

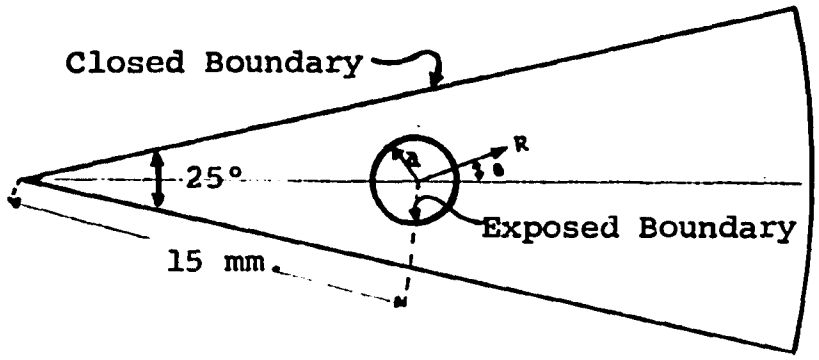
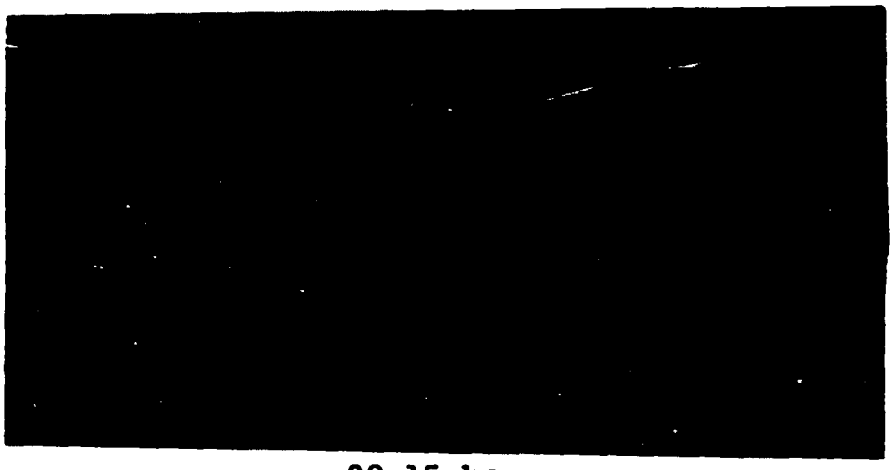
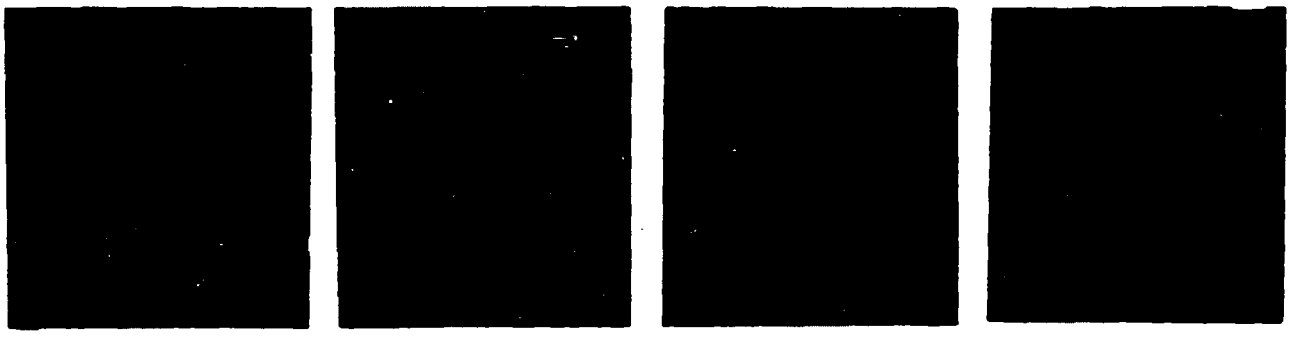


Figure 74. The Wedge-Like Region Similar to a Symmetric Section of a Ring of Circles in a large Plane Region.

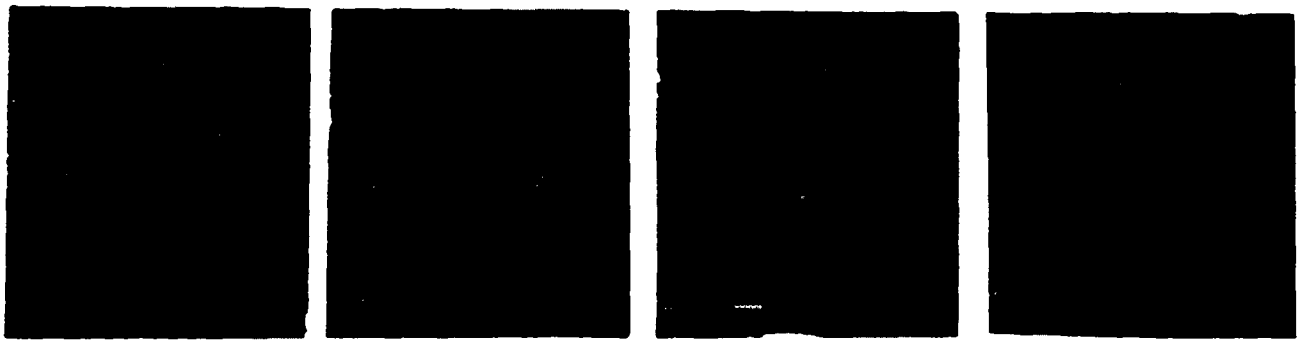
filter paper Number 52 cut in the wedge-like shape shown in Figure 74 were placed in the cell to simulate this region (see Figure 45). In the first test (Test 3.2-5) the cell was initially filled with pure water and maintained at 55°C throughout the test. A phenol solution containing 4.737 moles of water per liter was passed over the boundary. Figure 75 is a series of photographs of the cell showing the progress of the interface at several time levels. These photographs were read on the microprojector and tabulated in Table 35 of Appendix E. Figure 76 is a map of the interface at various values of the dimensionless time $\tau = \omega D^I t/a^2$ where 'a' is the radius of the boundary circle ($\approx$ 5 mm). The radial distance in Figure 76 is also dimensionless, i.e., $R = r/a$, where r is the actual radial distance in the region situated in the cell.



00:15 hours



00:31 hours | 03:13 hours | 08:46 hours | 22:33 hours



29:42 hours | 47:47 hours | 73:41 hours | 86:54 hours

Figure 75. Test 3.2-5. Progress of the Interface Around a Circular Boundary Situated in A Wedge-Shaped Region and Initially Containing Pure Water. Phenol Solution was Passed over the Circular Boundary and the Temperature was kept at 55°C.

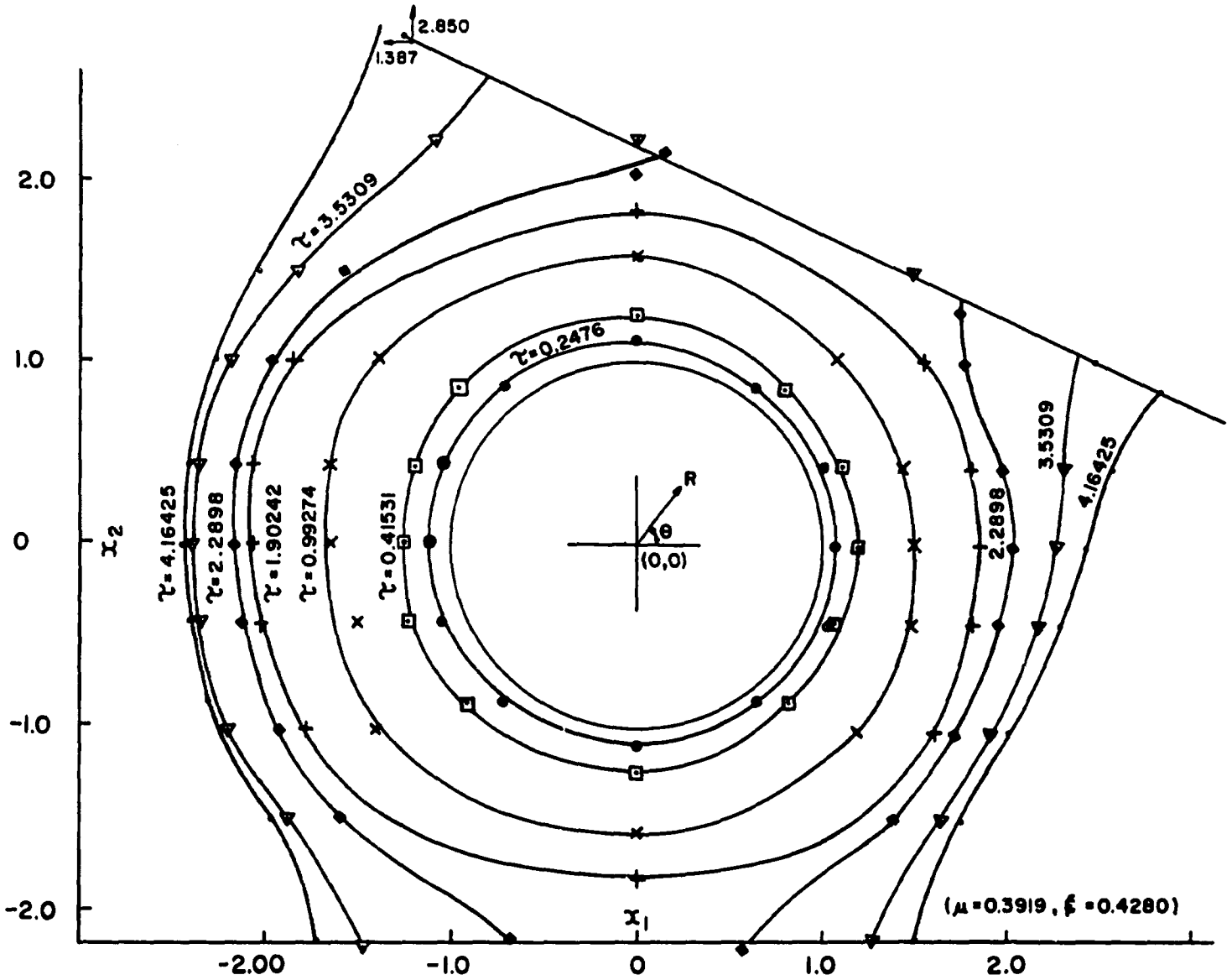


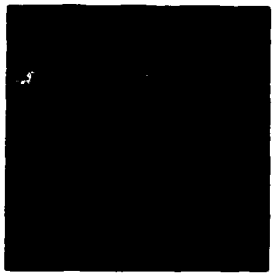
Figure 76. Growth of the Interface Around a Circle Situated in a Wedge-Like Region.

The way the interface deflects near the sides of the wedge raised some questions as to the possibility of small capillary action in the space between the filter paper and the polyethylene sheets. Note that every effort was made to bring about a direct contact between the polyethylene sheets and the filter paper around the edges. However, the effort was not 100 per cent successful. To verify what might have happened at the edges, the test was repeated with a new wedge, which had a definite clearance at the edges. The cell was initially filled with phenol saturated water at 55°C. Clearly, for this case the concentration field in the cell was strictly one-dimensional as long as the interface had not touched the sides of the wedge. The test was carried out at 55°C and the same phenol solution was passed over the boundary. The series of photographs in Figure 77 shows how the interface moved with time. When the interface touched one side of the wedge, the phenol phase was pulled into the clearance space at the side of the wedge. As a result, the water solution moved towards the circular boundary of the other sides and distorted the diffusion field. Figure 78 shows the radial position of the interface as a function of $\sqrt{\tau}$ before the capillary action on the sides took place.

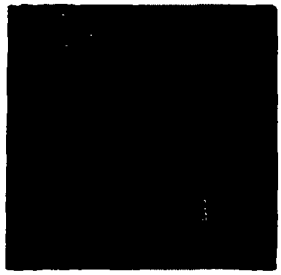
It is clear from the above experiment that the capillary effects at the sides of the wedge were very small for Test 3.2-5.



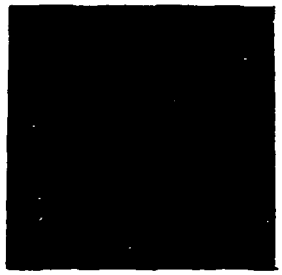
00:30 hours



00:15 hours



01:01 hours



03:04 hours



04:13 hours



18:26 hours



25:34 hours

Figure 77. Test 3.2-6. Progress of the Interface Around a Circular Boundary Situated in a Wedge-Shaped Region (Top Photo) and Initially Containing Phenol Saturated Water Phase (at 55°C). Test Temperature was 55°C.

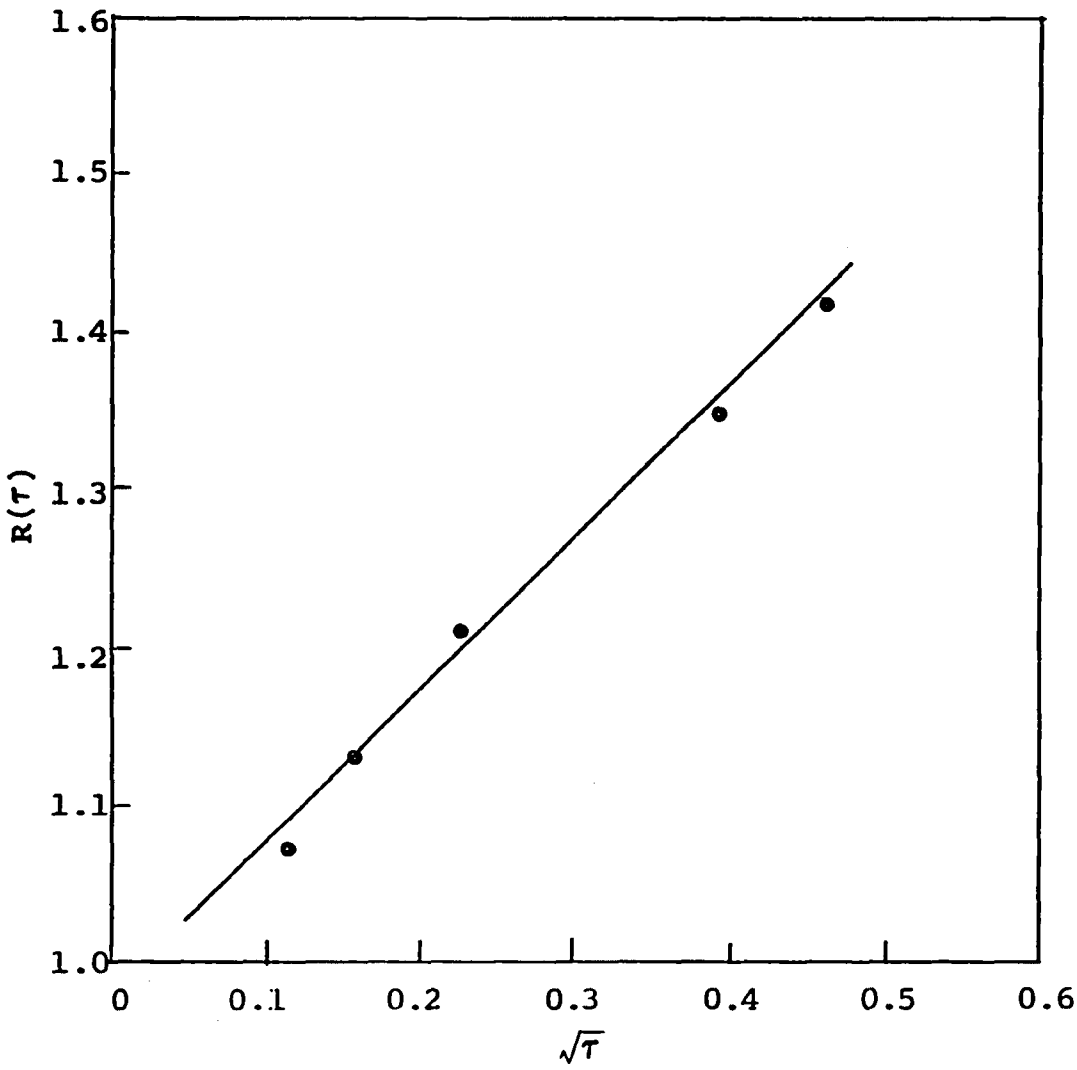


Figure 78. Radial Position of the Interface in a Region External to a Unit Circle for μ=0.0 and ξ=0.551 (Test 3.2-6).

Closing Remarks

It has been the purpose of the experimental work of this investigation to search for a diffusion cell which can simulate the problems of heat conduction with change of phase. The experiments, in most cases, were conducted with enough care to make possible qualitative observations on the nature of mass transfer in the cell. The final experiments with filter papers are accurate in as much as demonstrating that the development of a two-dimensional diffusion field is practically possible and relatively easy once a workable arrangement is found. The scattering of data shown in Figures 67, 68, 69 and 70 is essentially caused by the obstructions in the passage of diffusing molecules in the cell, or at the boundary, and by the non-uniformity of the porous medium employed for these experiments.

To overcome the destructive effect of the interfacial tensions on the diffusional mass transfer in the cell, an empirical approach was adopted. An effort to predict the conditions and environment for off-setting these forces was unsuccessful. Although it is possible to provide a satisfactory explanation for the success of the final experimental work, elaboration is not justified. Prior to performing these tests, it was not possible to predict if any particular arrangement would work since, as noted, the tests with a phenol solution in the cell were unsuccessful. Subsequent tests did not shed any further light on the nature of interfacial forces in the porous medium (used for this

investigation) to allow advancement of any particular hypothesis.

Now that a practical way of assembling a workable diffusion cell has been found, it is advisable to improve the technique used here by investigating many more binary liquid systems, as well as other porous media.

CHAPTER VII

CONCLUSIONS AND RECOMMENDATIONS FOR FUTURE WORK

The objectives of the present investigation were two fold. First, to develop a general numerical procedure for solving two-dimensional heat conduction problems in a locally isotropic medium whose state is temperature dependent (including phase transitions). Secondly, to examine the practicality of simulating the temperature field in a medium having a single transition temperature with a concentration field developed by mass transfer due to pure chemical diffusion in a suitable, partially miscible, liquid-liquid binary system. It is believed that both of these objectives were successfully attained. However, more work needs to be done in order to develop a diffusion cell analog which can compete with the efficiency and accuracy of modern, high speed digital computers.

As a result of the theoretical analysis presented in Chapter III, and the numerical results reported in Chapter IV, it can be concluded that problems of heat conduction with change of phase can be most conveniently solved by the proposed method. Except for a simple additional predictor step,

the proposed numerical solution is not different from that of solving an ordinary heat conduction problem. The proposed solution circumvents the difficult task of finding the precise position of the interface (or interfaces) while the problem is being processed in a digital computer. As a result, the location of the interface can be taken as the isotherm which represents some arbitrary stage of completion of the phase transition, preferably when it is half complete. It was shown that the proposed solution is highly stable and second order correct. The occurrence of the change of phase does not introduce any stability limitation over and above those of solving a linear parabolic partial differential equation by the ADI method. However, when the temperature field is very steep and the time steps are very large, the discretization error of the proposed solution may become much larger than that expected when the same procedure is used to solve linear parabolic differential equations. The reason is that the change of temperature between the consecutive time steps may be so large that the peaks in $\varphi(u(x_1,x_2;\tau))$ may remain unrecognized by the discrete solution.

Although many difficulties were encountered in the development of a workable two-dimensional diffusion cell analog, it can be said with reasonable assurance that such an approach is indeed feasible. The diffusion analog, when fully developed, can very well prove to be a convenient tool in determining the progress of the interface in a two-dimensional region of complex geometry subjected to strongly time

dependent boundary conditions. If an ideal binary liquid system is selected, if a suitable porous medium with known characteristics is used, and if the design of the cell allows fast filling and evacuating, the diffusion cell analog can then solve problems of melting and solidification with much less human effort than that of a well-chosen numerical solution. To appreciate this point, it suffices to state that approximately 50 man hours were spent in setting up the parameters for the very simple two-dimensional example problem solved in Chapter IV, in addition to the time spent in developing and de-bugging the computer program.

The one-dimensional diffusion cell not only proved to be a convenient tool in studying problems of melting and solidification, but it also served as a very simple and quick way of measuring the binary diffusion coefficients in partially miscible liquid-liquid binary systems.

Recommendations for Further Work

The central problems in approximating the matrix solution

$$\mathbf{v}(t_m) = \prod_{j=1}^{m} \exp(-r_j \tilde{\Phi}_j A)\ \mathbf{v}_o$$

are: a) to find a suitable operator $T(r_j)$ that best approximates $\exp(-r_j \tilde{\Phi}_j A)$, and b) to choose the set of acceleration parameters r_j, $1 \leq j \leq m$, such that $\mathbf{v}(t_m)$ can be approximated with a desired accuracy and with a minimal amount of computations.

The analysis in Chapter III covers many known approximating solution of parabolic differential equations, but not all of them. For example, multilevel approximations such as the unconditionally stable method of Du Fort and Frankel (31) need special treatment. The behavior of the three level Du Fort-Frankel approximation of the latent heat problems needs to be investigated because, with this method, there is really no need for a predictor formula, which in turn saves a substantial amount of computation.

To minimize the error of the numerical solution one has to minimize $\left\| \exp(-r_j \tilde{\Phi}_j) - T(r_j) \right\|$. It is unlikely that this quantity has a strong minimum for $r_j > 0$. The trivial solution of such a minimization problem is, of course, $r_j = 0$, which is of little help. Thus, the problem for further research is that, given a positive integer m and the variable $t_m > 0$, one must find a set of parameters

$$\mathcal{S} = (r_j \,|\, r_j > 0, \sum_{j=1}^{m} r_j = t \ , \ j = 1,2,\ldots m)$$

such that

$$\left\| \prod_{j=1}^{m} \exp(-r_j \tilde{\Phi}_j) - \prod_{j=1}^{m} T(r_j) \right\|$$

is minimized. Such a minimization problem offers a real challenge, but the solution would be most rewarding.

It was shown in Chapter IV that the recursion formulae (4.14) and (4.17) for r_j produced remarkably good numerical results, especially in the case of the

two-dimensional example problems. The maximum number of iterations, for a given δ_x, for which these recursion formulae remain useful, remains to be investigated.

It was noted before that, as required of a correct solution of the heat equation, the operator $\exp(-r_j\tilde{\Phi}_j A)$ is primitive (i.e., non-negative, irreducible and non-cyclic). One of the main problems that should be avoided when solving parabolic differential equations by any unconditionally stable numerical method is the erratic behavior of the solution that was observed here while solving the one-dimensional problem and was also observed by other investigators [e.g., Larkin (50)] in solving the two-dimensional problems with the ADI method. The author believes that such behavior is unlikely to occur so long as the operator T(r) is primitive. Thus, it is most useful to establish accurately for what values of r the operator T(r) is primitive. Varga (77) has shown that for T(r) to be primitive it is sufficient that

$$\frac{2}{r} > \min_{1\le i\le n} \{h_{ii}, v_{ii}\}$$

where h_{ii} and v_{ii} are the diagonal entries of the n x n matrices H and V, respectively. Because of the strong restriction that the above condition imposes on r, the need for a better estimate of the limits of primitivity of T(r) and also

$$\prod_{j=1}^{m} T(r_j)$$

is quite obvious.

Future work in developing the diffusion cell analog should be primarily directed towards resolving the difficulties and the sources of inaccuracy of the experimental measurements with porous media, which were discussed in Chapters V and VI. In this respect it is desired to find a porous medium which is chemically and dimensionally, very stable and has uniform pores of about 0.5 micron. Methods should be developed for cutting the exposed boundary out of such a porous medium without disturbing the pores or changing the cross-sectional area of flow. To make accurate control and measurement of the mass transfer at the boundary possible, and also to relax the stringent requirements on the dimensional stability of the cell, it is desired to increase the thickness of the porous medium used in the cell.

Along with this evaluation program, an arrangement for a more effective distribution of flow over the boundary, and a less cumbersome set-up for charging the cell, should also be designed. This development program would result in a diffusion cell capable of giving the precise position of the interface in a two-dimensional plane region subjected to any desired concentration conditions at its exposed boundary as well as giving the total flux at the boundary surface.

The measurement of the concentration profile in the cell offers a real challenge. The choice of any particular method depends almost exclusively on the choice of the pair of partially miscible liquids. There are many binary liquid systems suitable for the analog studies. A search should be

conducted to find a suitable binary liquid system for which the concentration of the solution in the cell can be most conveniently measured. Ideally, one wishes to obtain the complete concentration profile and the position of the interface on a single photograph.

One promising technique would be to measure the brightness of white diffused light transmitted through the cell. The amount transmitted depends on the concentration of the liquid retained in porous medium of the diffusion cell. If the refractive index of the material of which the porous medium is made is very close to that of one of the two liquids, then the porous medium changes from transparent to translucent, depending on the concentration of the solution contained in its pores. The extent of transparency, or translucency, may be used as a measure of the local concentration. Such measurement is not,however, very accurate, because of scattering phenomena.

Another technique is based on the change in color of the solution with concentration, in which case the concentration profile can be obtained directly by color photography. Of course, optical measurements of the concentration profile need not be limited to visible light. The wide spectrum from ultraviolet to infrared should be considered. Except for the inevitable scattering of the incident light by the media, the optical method would be the simplest and most accurate way of obtaining the concentration profile in the cell.

The widely used radioisotope techniques of measuring the binary diffusion coefficients of liquids do not appear to be very suitable because it involves tertiary diffusion instead of binary diffusion. At least for the case where only one phase transition occurs, it is not possible to establish an exact analogy between tertiary diffusion and heat conduction.

The electrical conductivity method offers another possibility for obtaining the concentration profile in the diffusion cell. In this case a solid material must be found which conducts electrical current in one direction only. This material must also have sufficient mechanical strength and other properties in order to replace one of the glass disks of the diffusion cell. If one of the disks passes the electrical current only in the direction perpendicular to its plane, and the other is a perfect conductor, then the point electrical resistivity of the solution in the cell can be measured by a variety of well known and accurate methods. The concentration at each point can then be obtained from the knowledge of the electrical resistivity. The prospects of finding a substance that has the above mentioned directional property do not seem very promising. One possibility would be to make a disk composed of extremely fine wires glued together by an efficient insulator.

The above ideas on the measurement of concentration profile in the cell have been advanced to provide a guide line for future work. Only a thorough study can establish whether any of these methods are feasible.

The one-dimensional diffusion cell is more useful in determining the diffusion coefficients than in solving the heat transfer problems. The accuracy of this method can be largely improved when capillaries with a much smaller diameter are used. Glass capillary fused arrays are available on the market (Permeonics Corporation of Southbridge, Mass.,) which have pore diameters ranging from 10 to 100 microns. The pores are parallel capillaries with a uniform diameter. Such a rod could be used for the one-dimensional test instead of the single capillary with a larger diameter.

In summary, then, future work should be directed towards:

1. Numerical methods for solving the problem by finding better acceleration parameters.
2. Study of the two-dimensional diffusion cell analog aimed essentially at improving the techniques developed in the present work, as well as developing a convenient method for measuring the concentration profile in the cell.
3. Using the one-dimensional cell for obtaining the much needed diffusion coefficients in partially miscible, liquid-liquid binary systems.

NOMENCLATURE

a_i $\quad a_{i,j}/\eta_j$

$a_{i,j}$ $\quad \delta_{i-1,j}c'_{i,j} + \delta_{i+1,j}b'_{i,j}$

$A(c)$ $\quad H(c) + V(c)$

b'_i $\quad b'_{i,j}/\eta_j$

$b'_{i,j}$ $\quad c'_{i+1,j}$ if (i,j) and $(i+1,j) \in R_h$

$b_{i,j}$ $\quad b'_{i,j}\,\sigma_{i+1,j}$

$\mathfrak{B}$ $\quad$ a Banach spare

$c(T)$ $\quad$ specific heat $= \frac{1}{\rho}(\partial E/\partial T)_\rho$

c_s, c_L $\quad$ specific heat of a solid phase, and a liquid phase, respectively

c'_i $\quad c'_{i,j}/\eta_j$

c_{ij} $\quad$ the boundary of r_{ij}

$c_{i,j}$ $\quad c'_{i,j}\,\sigma_{i-1,j}$

$c'_{i,j}$ $\quad 2kh\,P(x_i - \frac{1}{2}h_i, y_j)/[h_i(h_i+h_{i+1})]$, for $(i,j) \in R_h$

C $\quad$ a n x n positive diagonal matrix whose diagonal entries are the n values of $\tilde{\psi}_{i,j}$, $(i,j) \in R_h$ [See Equation (3.22)]

$\mathcal{C}$	the class of strongly continuous mapping from $\mathcal{G}$ into $\mathcal{R}$.
C_A	concentration of species A in moles per unit volume
C_o	initial concentration of species A in a system under consideration
C_A^B	the external boundary concentration of species A
C_s^I	saturation concentration of species A in phase I, moles per unit volume
C_s^{II}	saturation concentration of species A in phase II, moles per unit volume
d_j	$d_{i,j}/\eta_i'$
$d_{i,j}$	$\delta_{i,j-1} f_{i,j}' + \delta_{i,j+1} e_{i,j}'$
$d_{p,q}(x)$	$\sum_{k=0}^{q} \frac{(p+q-k)!p!}{(p+q)!k!(p-k)!} x^k$
$\tilde{D}^{II}$	the average binary diffusion coefficient in a phase II
$\tilde{D}^{I}$	the average binary diffusion coefficient in a phase I
$D_{AB}'(u)$, $D_{AB}(C_A)$	a concentration dependent binary diffusion coefficient of species A in an A - B binary system

$\mathcal{D}_{AB}$ $\quad \frac{\omega_1}{\eta\omega_2} D_{AB} = \omega D_{AB}$

e'_j $\quad e'_{i,j}/\eta'_i$

$e_{i,j}$ $\quad e'_{i,j}\ \sigma_{i,j+1}$

$e'_{i,j}$ $\quad f'_{i,j+1}$ if (i,j) and (i,j+1) ϵR_h

$e^{(m)}$ $\quad u(t_m) - w(t_m)$

$\tilde{e}^{(m)}$ $\quad \frac{1}{N_1} e^{(m)}$

E $\quad$ the internal energy of a unit volume element of a system

E_o $\quad$ the initial internal energy of a unit volume element of a system

E_B $\quad$ environmental internal energy defined by $\int_{T_R}^{T_B} \rho c dT$

E_F^{II} $\quad$ the internal energy of a unit volume element of Phase II at its transition temperature

E_F^{I} $\quad$ the internal energy of a unit volume of phase I at its transition temperature

$E_{p,q}(B)$ $\quad$ Pade', (p,q) approximation of e^{-B}, where B is a n x n real matrix $= d_{p,q}^{-1}(B)\ n_{p,q}(B)$, p,q = 0, 1, 2 ...

$f_1(t)$ & $f_2(t)$ $\quad$ two unknown function of t appearing in the Boley's solution [See Equations (1.13) and (1.15)]

$f(x,t)$	$(C^B-C_s^I)/(C_s^{II}-C_s^I)$ also $(E_B-E_F^I)/(E_F^{II}-E_F^I)$
f_j'	$f_{i,j}'/\eta_i'$
$f_{i,j}'$	$2khQ(x_i,y_j-\frac{1}{2}k_j)/[k_j(k_j+k_{j+1})]$, for $(i,j)\epsilon R_h$
$f_{i,j}$	$f_{i,j}'\,\sigma_{i,j-1}$
$f(t,v(t))$	$[I - \Phi^{-1}(u(t))]\,Av(t)$
F	Wachspress and Habetler conditioning matrix
g	$C^{\frac{1}{2}}g_1$
g_1	a n-dimensional vector whose entries are the n values of $u_{i,j}(o)$, $(i,j)\epsilon R_h$
$g(x)$	the initial temperature distribution in a semi-infinite slab
g_i, $1\le i\le s$	a weight function depending on the coordinates x_1, x_2 and x_3 [See Equation (1.2d)]
$G(x)$	the initial temperature (dimensionless) distribution in the region R'
h	$\max_{1\le i\le I} \{h_i\}$
$h_i(x)=h_i$	the mesh spacing in x-direction = $x_i - x_{i-1}$
H	$C^{-\frac{1}{2}}\,H^{(s)}\,C^{-\frac{1}{2}}$
$H^{(C)}$	$C^{-1}\,H^{(s)}$
$H^{(s)}$	a n x n symmetric matrix defined by Equation (3.14)

$h(E,x)$, $h(x,T)$	film coefficient of heat transfer at the boundary
$i'(j)$ & $i''(j)$	indicate that in a region R the jth vertical grid line begins at a mesh point (i',j) and ends at a mesh point (i'',j)
I	the number of horizontal grid lines passing through a plane region R, also identity matrix
$\mathcal{J}$	a finite and real interval $[0,T]$
$\mathbf{j}$	a flux vector
j_A	diffusion mass flux of species A in a binary system of species A and B
$j'(i)$ & $j''(i)$	indicate that in a region R the ith horizontal grid line be ins at a mesh point (i,j') and ends at a mesh point (i,j'')
J	the number of vertical grid lines passing through a plane region R
k	$\max_{1\leq j\leq J} \{k_j\}$
$k_j(y)=k_j$	the mesh spacing in y-direction = y_j-y_{j-1}
K(T)	a temperature dependent thermal conductivity
$K(C_A,x)$	film coefficient of mass transfer at the boundary

l	dimensionless latent heat parameter defined by Equation (1.5)
l_{ij}	dimensionless latent heat of transition from the state "i" to the state "j"
L	latent heat of transition, BTU/LB
n	$\left(\frac{2}{r_{m+1}} \tilde{\Phi}^{(m+\frac{1}{2})} - V\right) w^{(m)} + s$
n_{ij}	an outward directed normal on Γ'_{ij}
$n_{p,q}(x)$	$\sum_{k=0}^{q} \frac{(p+q-k)!q!}{(p+q)!k!(p-k)!} (-x)^k$
N_s	the number of isolate phases in region R'
o	the null vector
O	the null matrix
$P(x,y)$	$\{g_1(x,y)/[g_2(x,y)g_3(x,y)]\}(1-x)^2/(1-y)^2$
q	a local heat flux vector
q	local heat flux
Q	heat flux at the boundary of a semi-infinite slab [Chapter I]
Q_j	$\Phi_j^{-1} A$ [Chapter III]
$Q_j^{(s)}$	$\Phi_j^{-\frac{1}{2}} A \Phi_j^{-\frac{1}{2}}$ [Chapter III]
$Q(x,y)$	$[g_2(x,y)/(g_1(x,y)g_2(x,y)](1-y)^2/(1-x)^2$

$Q(\tau_m)$ cumulative heat transferred across the boundary = $\sum_{j=1}^{m} \delta Q_j$

r_j $t_j - t_{j-1}$ [Chapter III and IV]

r_{ij} a mesh region defined by $-\frac{1}{2}h_i \leq x - x_i \leq \frac{1}{2}h_{i+1}$, $-\frac{1}{2}k_j \leq y - y_j \leq \frac{1}{2}k_{j+1}$

R the mapping of R'' into $\mathfrak{R}$ under the transformation (3.1)

R' a connected three-dimensional region

R'_i, $i=1,2,\ldots$ a subregion belonging to R'

R'' a plane and connected two-dimensional region

$\mathfrak{R}''$ the plane region $x_1, x_2 \geq 0$

$\mathfrak{R}$ the plane region, $1 \geq x, y \geq 0$

R_h the union of all mesh point (i,j) contained in R

$\mathfrak{R}_h$ the union of all mesh point (i,j) contained in $\mathfrak{R}$

s dimensionless sensible heat removed in the transition interval

s' sensible heat removed in the transition interval, BTU/LB

$s_{i,j}$ $\sigma'_{i-1,j} c'_{i,j} + \sigma'_{i+1,j} b'_{i,j} + \sigma'_{i,j+1} e'_{i,j} + \sigma_{i,j-1} f'_{i,j}$ for $(i,j) \in R_h$

$\mathbf{s}(t)$ $\quad C^{-\frac{1}{2}}\,\mathbf{s}_1(t)$

$\mathbf{s}_1(t)$ $\quad C^{-1}\mathbf{s}_1(t)$

$\mathcal{S}$ $\quad (r_j \mid \ r_j > 0,\ j = 1, 2, \ldots)$

t $\quad \tau/kh$, [Chapter III]

t $\quad$ time elapsed

t_j $\quad t_o + \sum_{i=1}^{j} r_i$

T $\quad$ temperature

T_∞ $\quad$ the uniform initial temperature in a semi-infinite region

T_e $\quad$ environmental temperature

T_o $\quad$ an arbitrary reference temperature, occasionally defined as the temperature for which $K(T)/\rho c(T)$ is maximum

T_F $\quad$ a transition temperature

T_R $\quad$ an arbitrary reference temperature

$T(r_j)$ $\quad (\rho_j\tilde{\Phi}_j + V)^{-1}(\rho_j\tilde{\Phi}_j - H)\,(\rho_j\tilde{\Phi}_j + H)^{-1}(\rho_j\tilde{\Phi}_j - V)$, [Chapter III and IV]

$T_1(r_j)$ $\quad E_{1,1}(-r_j\tilde{\Phi}_j^{-1}H)\,E_{1,1}(-r_j\tilde{\Phi}_j^{-1}V)$, [Chapter III and IV]

$T_s(x,t)$ $\quad$ one-dimensional transient temperature in a solid phase

$T_L(x,t)$ one-dimensional transient temperature in a liquid phase

u a dimensionless temperature defined by Equation (1.1) or (2.8)

u_o $(E_o-E_F^I)/(E_F^{II}-E_F^I)$ also $(C_o-C_s^I)/(C_s^{II}-C_s^I)$

u_F a transition temperature (dimensionless)

$u(x;\tau)$ the transient dimensionless temperature in a region R'

$u_{i,j}(t)$ $\equiv u(x_i, y_j; t)$

$u^{(i)}(x;\tau)$ transient temperature (dimensionless) in a subregion $R_i' \epsilon R$

$u^F_{i,j}$ dimensionless transition temperature from state "i" to state "j"

$\mathbf{u}(t)$ $C^{\frac{1}{2}}\mathbf{u}_1(t)$

$\mathbf{u}_o$ $\mathbf{u}(0)$

$\mathbf{u}_1(t)$ a n-dimensional vector whose entries are the n unknown values of $u_{i,j}(t)$, $(i,j)\epsilon R_h$

$\tilde{\mathbf{u}}(t_n)$ $\bar{\mathbf{v}}(t_n) + A^{-1}\mathbf{s}(\xi)$, $t_{m-1} \le \xi \le t_m$, (a fundamental discrete solution)

$\bar{\mathbf{u}}(t_n)$ $\bar{\mathbf{v}}(t_n) + A^{-1}(\mathbf{s}(\xi) + \boldsymbol{\theta}(\xi))$, $t_{m-1} \le \xi \le t_m$

U a unitory matrix

$v(t_m)$ $\quad u(t_m) - A^{-1}s(\xi),\ t_{m-1} \leq \xi \leq t_m$

v_o $\quad v(0)$

$v_1(t_m)$ $\quad T(r_m)\ [w(t_{m-1}) - A^{-1}s(t_m - \frac{1}{2}r_m)]$

$= \prod_{j=1}^{m} T(r_j)\ v_o$ if and only if s is time independent

$\bar{v}(t_m)$ $\quad Z_j \bar{v}(t_{m-1})\ ;\ \bar{v}(t_o) = v(t_o)$

V $\quad C^{-\frac{1}{2}}\ V^{(s)} C^{-\frac{1}{2}}$

$V^{(s)}$ $\quad$ a n x n symmetric matrix defined by Equation (3.16)

$V^{(c)}$ $\quad C^{-1} V^{(c)}$

$w_{i,n}$ $\quad$ a numerical approximation of the dimensionless temperature $u(x_1, t)$ at a point $x_1 = i\Delta x$ and at a time level $t = t_n$

$w^{(m)} \equiv w(t_m)$ $\quad u(t_m) - \epsilon_1(t_m) - \epsilon_2(t_m)$

w_i $\quad (w_{i,j'}, \cdots w_{i,j'+1} \cdots w_{i,j''})$

w_j $\quad (w_{i',j}, \cdots w_{i'+r,j} \cdots w_{i'',j})$

x $\quad x_1/(1 + x_1)$ if $x_1 \geq 0$ otherwise $= x_1/(1 + |x_1|)$

$x_i,\ 1 \leq i \leq 3$ $\quad$ a co-ordinate axis in any orthogonal curvilinear co-ordinate system

$\mathbf{x}$ $\quad (x_1, x_2, x_3)$

$X(t)$ the position of the interface in a one-dimensional region

$X(x_1,\tau)$ the distance of the interface from the line $x_2 = 0$ for given values of x_1 and τ

$\dot{X}(t)$ $dX(t)/dt$

X_i $X(t_i)$

y $x_2/(1 + x_2)$ if $x_2 \geq 0$, otherwise $= x_2/(1 + |x_2|)$

z $\sqrt{\tilde{D}^I/\tilde{D}^{II}}$

$z_j, z(t_j)$ $\exp[-(t_j - t_{j-1})Q_j]$

Greek Letters

$\alpha(t)$, $\alpha(T)$, $\alpha'(u)$, α thermal diffusivity $= K/\rho c$

$\alpha(x;\tau)$ $h(x,T,T_e) \equiv h(x,E,E_B)$, $T_1 \neq T$, $x \in \Gamma'$,

α_L and α_s thermal diffusivity of a liquid phase and a solid phase, respectively

α_I and α_{II} thermal diffusivity of a phase I and a phase II, respectively

$\boldsymbol{\alpha}_j$ $\int_{t_{j-1}}^{t_j} \exp[(\eta - t_{j-1})Q_j]\beta(\eta,v)\,d\eta$

$\alpha^*(u)$ $D'_{AB}(u)/D'_{AB}(0)$, in a diffusion model

$= \alpha'(u)/\alpha'(0)$, in a heat conduction model

$\bar{\alpha}(x,y)$ $\alpha(x,y)/\beta(x,y)$

β a positive constant such that $\beta\delta_F \geq 6$

$\beta(x;\tau)$ $\dfrac{1}{T(x;\tau)-T_1}\int_{T_1}^{T(x;\tau)} K(T')dT' \qquad T_1 \neq T$

$\beta(t,v)$ $-\Sigma\, dv(t)/dt$

γ interfacial tension, dyne/cm

$\gamma(x;\tau)$ $[\alpha(x;\tau)\cdot\beta(x;\tau)]\,T_e$

$\bar{\gamma}(x,y)$ $\gamma(x,y)/\beta(x,y)$

Γ the boundary of R

Γ' the boundary surface of the region R'

Γ_h' a union of all mesh points $(i,j)\notin R_h$ such that either $(i\pm1,j)\in R_h$ or $(i,j\pm1)\in R_h$

Γ_s the interface between two co-existing phases

Γ'' the boundary of R"

Γ_{ij}' the interface between two subregions R_i' and R_j'; R_i', $R_j'\in R'$

δ_F', δ_F'' dimensionless half transition temperature intervals defined by Equation (1.6)

δ_x a constant used in the recursion formulae for the acceleration parameter r_j, $j = 1,2,\ldots.$ It is usually so chosen that $1/\delta_x$ is an integer [See Equations (4.14) and (4.17)]

$\delta_{i,j}$ a coefficient defined by Equation (3.11)

δ_j $[I - Z(r_j)]^{-1} Z(r_j) \alpha_j$

$\delta(\delta_F)$ a vector quantity whose entries are the difference between the exact values of the dimensionless temperature $u_i(\tau)$, $1 \le i \le N_1$, when $\delta_F = 0$ and that of $\delta_F \neq 0$

δq_m total heat transferred at the exposed boundary in the time interval τ_{m-1} to τ_m

δQ_m the dimensionless total heat transferred at the exposed boundary of a region in the time interval τ_{m-1} to τ_m

δT_F the transition temperature interval divided by two

ΔC_A equilibrium concentration change across the interface between two-partially miscible liquids = $(C_s^{II} - C_s^I)$

ΔE latent heat of change of state of a unit volume element of a system = $(E_F^{II} - E_F^I)$

Δx a mesh spacing along the co-ordinate x

$\Delta \tau_j$ $(t_j - t_{j-1})kh$

$\bar{\epsilon}(t_m)$ $v(t_m) - \bar{v}(t_m)$

$\tilde{\epsilon}(t_m)$ $\bar{u}(t_m) - \tilde{u}(t_m)$

$\epsilon_1(t_m)$ $\quad \sum_{i=1}^{m} \prod_{j=1}^{m} Z(r_j)\ \alpha_i + [I - \sum_{i=1}^{m} Z(r_j)]A^{-1}\theta$

$\epsilon_2(t_m)$ $\quad [\prod_{j=1}^{m} Z(r_j) - \prod_{j=1}^{m} T(r_j)]\ v_o$

η "tortuosity" or "lithologic" factor = (actual diffusion pass)/(linear path)

η_i' function of x defined by Equation (3.18)

η_j a function of y defined by Equation (3.18)

$\theta_{i,j}$ the error committed at a mesh point (i,j) because of discretization of the spacial co-ordinates

$\theta(t)$ $\quad C^{-\frac{1}{2}}\theta_1(t)$

$\theta_1(t)$ a n-dimensional vector whose entries are the n values of $\theta_{i,j}(t)$

$\theta_2(t)$ $\quad C^{-1}\theta_1(t)$

λ $\quad \frac{\beta}{\sqrt{\pi}} \int_{-\infty}^{\infty} \varphi_2(u)\ du = \beta\bar{\lambda}/\pi$

Λ_m a positive coefficient defined by Equation (3.21)

μ $\quad = (E-E_F^I)/(E_F^{II}- E_F^I)$ in a heat conduction problem

$= (C_A - C_s^I)/(C_s^{II}-C_s^I)$ in a diffusion problem

ξ the root of the transcendental Equation (1.11d)

ρ_j $\quad 2/r_j$

ρ density, mass per unit volume

$\sigma_i(B)$	the ith eigenvalue of the n x n matrix B
$\sigma_{i,j}$	1.0 if $(i,j) \epsilon \Gamma_h'$ otherwise it is zero
$\sigma'_{i,j}$	a coefficient defined by Equation (3.11)
Σ	$\tilde{\Phi}^{-1}\Phi - I$
τ	$[K(T_o)/\rho c(T_o)]t/a^2$ (where a is a scaling factor)
$\varphi_{i,j}$	$\varphi(u_{i,j})$
$\varphi_1(u)$	$\{[K(T_o)/\rho c(T_o)]/[K(T)/\rho \bar{c}_v(T)] - 1.0\}$, where $\bar{c}_v(T)$ is the specific <u>sensible</u> heat [See Equation (1.9a)]
$\varphi_2(u)$	$[K(T_o)/\rho c(T_o)]/[K(T)/\rho \bar{c}_\rho(T)]$ where $\bar{c}_\rho = \frac{1}{\rho}\left(\frac{\partial E}{\partial T}\right)_\rho - \bar{c}_v(T)$, [See Equation (1.9b)]
$\varphi(u), \varphi(T)$	$[\rho c(T_o)/K(T_o)]/[\rho c(T)/K(T)]$
Φ or $\Phi(u(t))$	a n x n positive diagonal matrix whose diagonal entries are the n values of $\varphi_{i,j} = \varphi(u_{i,j}(t))$, $(i,j) \epsilon R_h$
Φ_j	$\Phi(u(\xi))$, $t_{j-1} \leq \xi < t_j$
$\chi(t_m)$	$X(t_m)/(1 + X(t_m))$
$\varkappa$	$\alpha'(1)/\alpha(0)$ in a heat conduction model $D'_{AB}(1)/D'_{AB}(0)$ in a diffusion model

$\chi_1(\xi)$ $\xi\, e^{\xi^2}\, \mathrm{erf}\, \xi$

$\chi_2(\xi)$ $\xi\, e^{\xi^2}\, \mathrm{erfc}\, \xi$

$\psi(x,y)$ $g_1 g_2 g_3/[(1-x)(1-y)]^2$, $(x,y) \in R$

$\psi_{i,j}$ $\frac{1}{4} \iint_{r_{ij}} \psi(x,y)\, dxdy/[(h_i+h_{i+1})(k_j+k_{j+1})]$

ω $\omega_1/\eta\omega_2$

ω_1 (mean cross-sectional area open for diffusion)/(total cross-sectional area)

ω_2 effective porosity = (volume of the pores available for diffusion)/(total volume)

Special Symbols

$\mathrm{diag}(d_1,\ldots,d_n)$ a n x n diagonal matrix whose i^{th} diagonal entry is d_i, $1 \le i \le n$

erf x, or erf (x) $\frac{2}{\sqrt{\pi}} \int_0^x e^{-x^2} dx$

erfc x, or erfc (x) $\frac{2}{\sqrt{\pi}} \int_x^\infty e^{-x^2} dx = 1 - \mathrm{erf}\, x$

$\exp(tA)$ or e^{tA} $\sum_{i=0}^{\infty} \frac{(tA)^i}{i!}$, for any n x n matrix A and scaler t

$\Delta^2 x$ a finite difference operator approximating $\partial^2/\partial x^2$

∇^2 the Laplacian operator
$= \left(\prod_{i=1}^{3} g_i\right)^{-1} \sum_{\substack{1\le i,j,k\le 3 \\ i\neq j\neq k}}^{3} \tilde{a}_i^2 \frac{\partial}{\partial x_i}\left(\frac{g_i}{g_j g_k} \frac{\partial}{\partial x_i}\right)$

∇ $\left(\frac{\partial}{\partial x_1}, \frac{\partial}{\partial x_2}, \frac{\partial}{\partial x_3}\right)$ where x_1, x_2, and x_3 are the cartesian co-ordinates

$\subset$ "is a subset of", e.g., $R_i \subset R$ (reads: R_i is a subset of R)

$\cup$ "union of", e.g., $R_1 \cup R_2$ (reads: the union of R_1 and R_2)

ϵ "is an element of" e.g., $x \epsilon R$ (reads: x is and element of R)

$\notin$ "is not an element of"

$O(\ )$ "of the order of", e.g., $|x| = O(h^2)$ (reads: x is of the order of h^2, i.e., there exists a positive number M, independent of x such that $|x| \le Mh^2$ as $h \to 0$)

$\lambda_i(B)$ & $\sigma_i(B)$ the ith eigenvalue of the n x n matrix B

$\rho(B)$ the spectral radius of a n x n matrix B
$= \max_{1\le i\le n} |\sigma_i(B)|$

$\prod_{j=1}^{m} Z_j$ $Z_m Z_{m-1} \cdots Z_j \cdots Z_2 Z_1$

$\|A\|$ the spectral norm of a n x n matrix A

$\|\mathbf{x}\|$	the Euclidean norm of a n-dimensional vector $\mathbf{x}$
$\|\mathbf{x}\|_m$	$\|x_1\| + \ldots + \|x_n\|$ for any n-dimensional vector $\mathbf{x}$
$(\mathbf{y},\mathbf{x})$	$\sum_{i=1}^{n} (y_i^* x_i)$ = the inner product of two n-dimensional complex vectors $\mathbf{x}$ and $\mathbf{y}$

Superscripts

*	designates the complex conjugate of a complex variable (e.g., y*); conjugate transposed of the n-dimensional vector (e.g., $\mathbf{y}^*$); conjugate transposed of a n x n complex matrix (e.g., B*)

Subscripts

x and t	designates the first order derivative of a variable with respect to x and t, respectively, (e.g., $u_x = \partial u/\partial x$, $u_t = \partial u/\partial t$)

BIBLIOGRAPHY

1. Altman, M., "Some Aspects of the Melting Solution for a a Semi-Infinite Slab," Chem. Engr. Progress Symposium Series, 57, No. 32, 1961.

2. Bellman, R., Introduction to Matrix Analysis, McGraw Hill Book Co. Inc., New York, 1960.

3. _____, "On the Boundness of Solutions of Non-Linear Differential and Difference Equations," Trans. Amer. Math. Soc., 64, 1948, pp. 374-388.

4. Birkhoff, G. and Varga, R. S., "Implicit Alternating Direction Methods," Trans. Amer. Math. Soc., 92, 1959, pp. 13-24.

5. Birkhoff, G., Varga, R. S. and Young, D. M., Jr., "Alternating Direction Implicit Methods," Advances in Computers, 3, Academic Press, New York, 1962.

6. Bodewig, E., Matrix Calculus, Interscience Publishers Inc., New York, 1956.

7. Boley, B. A., "A Method of Heat Conduction Analysis of Melting and Solidification Problems," J. of Math. and Appl. Phys., 40, 1961, p. 300.

8. _____, "Upper and Lower Bounds for the Solution of a Melting Problem," Quart. of Appl. Math., 21, No. 1, April 1963.

9. Boley, B. A. and Weiner, J. H., Theory of Thermal Stresses, John Wiley and Son, Inc., New York, 1960.

10. Brian, P. L. T., "A Finite-Difference Method of High-Order Accuracy for the Solution of Three-Dimensional Transient Heat Conduction Problems," AIChE Journal, 7, No. 3, September 1961, pp. 367-370.

11. Carman, P. C., "Fluid Flow Through Granular Beds," Trans. Inst. Chem. Engineers, 15, 1937, p. 150.

12. Carslaw, H. S. and Jaeger, J. C., Conduction of Heat in Solids, Clarendon Press, Oxford, 1959.

13. Cesari, L., Asymptotic Behavior and Stability Problems in Ordinary Differential Equations, Springer-Verlag, Berlin, 1959

14. Churchill, S. W. and Teller, A. S., "Freezing Outside a Sphere," Paper Presented at 7th National Heat Transfer Conference, August 9, 1964, AIChE Preprint 38.

15. Churchill, S. W. and Seider, W. D., "The Effect of Insulation on Freezing Motion," Paper Presented at 7th National Heat Transfer Conference, August 9, 1964, AIChE Preprint 37.

16. Coddington, E. A. and Levinson, N., Theory of Ordinary Differential Equations, McGraw Hill Book Co. Inc., 1955.

17. Crank, J., The Mathematics of Diffusion, Oxford, 1956.

18. De Boor, C. and Rice, R. J., "Chebyshev Approximation by a $\pi(x-r_i) / (x+s_i)$ and Application to ADI Iteration," J. Soc. Indust. Appl. Math., 11, No. 1, March 1963.

19. Dewey, C. F., Jr., Schlesinger, S. I. and Sashkin, L., "Temperature Profiles in a Finite Solid with Moving Boundary," J. of Aerospace Sciences, January 1960.

20. Douglas, J., Jr., "On the Numerical Integration of $\partial^2 u/\partial x^2 + \partial^2 u/\partial y^2 = \partial u/\partial t$ by Implicit Methods," J. Soc. Indust. Appl. Math., 3, 1955, pp. 42-65.

21. _____, "On the Numerical Integration of Quasi-Linear Parabolic Differential Equations," Pacific J. Math. 6, 1956, pp. 35-42.

22. _____, "A Note on the Alternating Direction Implicit Method for the Numerical Solution of Heat Flow Problems," Proc. Amer. Math. Soc., 8, 1957, pp. 408-412.

23. _____, "Alternating Direction Method for Three Space Variables," Num. Math., 4, 1962, pp. 41-63.

24. _____, "The Application of Stability Analysis in the Numerical Solution of Quasi-Linear Parabolic Differential Equations," Trans. Amer. Math. Soc., 82, 1958, pp. 484-518.

25. _____, "A Uniqueness Theorem for the Solution of the Stefan Problem," Proc. Amer. Math. Soc., 8, 1957.

26. Douglas, J., Jr. and Gallie, T. M., Jr., "On the Numerical Integration of a Parabolic Differential Equation Subject to a Moving Boundary Condition," Duke Math. Journal, 22, 1955, pp. 557-572.

27. Douglas, J., Jr. and Gunn, J. E., "Two High-Order Correct Difference Analogs for the Equation of Multidimensional Heat Flow," Math. Comp., 17, No. 81, January 1963.

28. Douglas, J., Jr. and Jones, B. F., "On Predictor-Corrector Methods for Non-Linear Parabolic Differential Equations," J. Soc. Indust. Appl. Math., 11, No. 1, March 1963.

29. Douglas, J., Jr., Kellogg, R. B. and Varga, R. S., "Alternating Direction Iteration Methods for n Space Variables, Math. Comp., 17, No. 83, July 1963.

30. Douglas, J., Jr. and Rachford, H. H., Jr., "On the Numerical Solution of Heat Conduction Problems in Two or Three Space Variables," Trans. Amer. Math. Soc. 82, 1956, pp. 421-439.

31. Du Fort, E. C. and Frankel, S. P., "Stability Conditions in the Numerical Treatment of Parabolic Differential Equations," Math. Tables Aids Comput., 7, 1953, pp. 135-152.

32. Dullien, F. A. L. and Scott, D. S., AIChE Journal, 8, 1962, p. 113.

33. Ehrlich, L. W., "A Numerical Method of Solving a Heat Flow Problem with Moving Boundary," J. Assoc. Comput. Mach., 5, 1958, pp. 161-176.

34. Fatt, I., "Pore Structure of Sintered Glass from Diffusion and Resistance Measurements," J. Phys. Chem., 63, 1959, p. 751.

35. Friedman, A., Partial Differential Equations of Parabolic Type, Prentice-Hall, Inc., Englewood Cliffs, N.J., 1964.

36. Forsythe, G. E. and Wasow, W. R., Finite Difference Methods for Partial Differential Equations, John Wiley and Sons, Inc., New York, London, 1960.

37. Geddes, A. L. and Pontius, R. B., "Determination of Diffusivity," in Physical Methods of Organic Chemistry, Edited by A Weissberger, Interscience Publishers, New York, 1959.

38. Gould, R. F., "Critical Solution Temperatures," Advances in Chemistry Series, 31, 1961.

39. Grosh, R. J. and Sunderland, J. E., "The Transient Temperature Distribution in Semi-Infinite Solids with Melting," Final Technical Report, Office of Ordnance Research Contract No. DA-33-008 ORD-1219, Purdue University, August 1958.

40. Hamill, T. D. and Bankoff, S. G., "Maximum and Minimum Bounds on Freezing-Melting Rates with Time-Dependent Boundary Conditions," AIChE Journal, 9, No. 6, November 1963, pp. 741-744.

41. Hashemi, H. T., "On the Analytical and Approximate Solution of the Stefan Problem," Department of Chemical Engineering, University of Oklahoma, 1963, unpublished.

42. Hille, E. and Phillips, R. S., Functional Analysis and Semigroups, Rev. Ed. Amer. Math. Soc. Providence, 1957.

43. Hummel, P. M. and Seebeck, C. L., "A Generalization of Taylor's Theorem," Amer. Math. Monthly, 56, 1949, pp. 243-247.

44. Jost, W., Diffusion, Acad. Press, 1960.

45. Kellogg, R. B., "Another Alternative Direction Implicit Method," J. Soc. Indust. Appl. Math., 11, No. 4, December 1963.

46. Klinkenberg, L. J., "Analogy between Diffusion and Electrical Conductivity in Porous Rocks," Bull. Geol. Soc. Amer., 62, 1951, p. 559.

47. Kolodner, I. I., "Free Boundary Problem for Heat Equation with Applications to Problems of Change of Phase," Comm. Pure Appl. Math., 9, 1956.

48. Kyner, W. T., "An Existence and Uniqueness Theorem for a Non-Linear Stefan Problem," J. Math. and Mech., 8, 1959, pp. 483-498.

49. _____, "On Free Boundary Value Problem for the Heat Equation," Quart. Appl. Math., 17, 1959, pp. 305-310.

50. Larkin, B. K., "Some Finite Difference Methods for Problems in Transient Heat Flow," Paper Presented at 7th National Heat Transfer Conference, August 1964, AIChE Preprint 16.

51. La Salle, J. P. and Lefschetz, S., Non-Linear Differential Equations and Non-Linear Mechanics, Academic Press, New York, 1963, pp. 259-265.

52. Lax, P. D., "Weak Solutions of Non-Linear Hyperbolic Equations and their Numerical Computation," Comm. Pure Appl. Math., 7, 1954, pp. 159-193.

53. Lax, P. D. and Richtmyer, R. D., "Survey of the Stability of Linear Finite Difference Equations," Comm. Pure Appl. Math., 9, 1956, pp. 267-293.

54. Lightfoot, N. M. H., Proc. London Math. Soc., 31, No. 2, 1929, pp. 97-116.

55. Linke, W. F., Solubilities of Inorganic and Metal Organic Compounds, 1, 4th Edition, Van Nostrand Co. Inc., Princeton, New Jersey, 1958.

56. Longwell, P. A., "A Graphical Method for Solution of Freezing Problems," AIChE Journal, 4, No. 1, March 1958.

57. Mirshamsi, M., "Diffusion Phenomena in Liquid Cadmium-Lead Binary System," Ph.D. Thesis, University of Oklahoma, 1963.

58. Mitchell, A. R. and Fairweather, G., "Improved Forms of the Alternating Direction Methods of Douglas, Peaceman and Rachford for solving Parabolic and Elliptic Equations," Num. Math. 6, 1964, pp. 285-292.

59. Oleinik, O. A. "On a Method of Solving General Stefan Problems," Doklady Akad. Nauk SSSR (N.S.), 135, 1960, pp. 1054-1057.

60. Peaceman, D. W., and Rachford, H. H., Jr., "The Numerical Solution of Parabolic and Elliptic Differential Equations," J. Soc. Indust. Appl. Math., 3, No. 1, March 1955, pp. 28-41.

61. Pearcy, C. M., "On Convergence of Alternative Direction Procedures," Num. Math., 4, No. 2, 1962, p. 172.

62. Price, H. S. and Varga, R. S., Gulf Research and Development Company Report, Harmarville, Pa., 1962.

63. Riemann-Weber, Die Partiellen Differential gleichungen der Mathematischen Physik, 1912, 2, p. 121.

64. Rose, M. E., "A Method for Calculating Solutions of Parabolic Equations with a Free Boundary," Math. Comput. 14, 1960, pp. 249-256.

65. Sestini, G., "Sul problema non lineare di Stefan in uno strato piano, indefinito," Annali Mat. Pura. Appl., 51, 1960.

66. _____, "Sul problema non lineare di Stefan in strati cilindrici o sferici," Annali Mat. Pura Appl., 51, 1960, pp. 203-224.

67. Stefan, J., Ann. Phys. u. Chem. (Wiedermann), 42, 1891, pp. 269-286.

68. Stephen, H. and Stephen, T., Solubility of Inorganic and Organic Compounds, 1, Macmillan Co., New York, 1963.

69. Sunderland, J. E. and Grosh, R. J., "Transient Temperature in a Melting Solid," J. Heat Transfer, November 1961, pp. 409-414.

70. Thompson, R. J., "Difference Approximations for Inhomogenous and Quasi-linear Equations," J. Soc. Indust. Appl. Math., 12, No. 1, March 1964.

71. Thovert, Ann. der Physique, 16, No. 2, 1914, p. 369.

72. Timmermans, J., Physico-Chemical Constants of Binary Systems, 4, p. 323, Interscience Publications Inc., New York, 1960.

73. Todd, J., Survey of Numerical Analysis, McGraw-Hill Book Co. Inc., 1962.

74. Trench, W. F., "On an Explicit Method for the Solution of a Stefan Problem," J. Soc. Indust. Appl. Math., 7, No. 2, June 1959.

75. Van der Poel, C., "Effect of Lateral Diffusivity on Miscible Displacement in Horizontal Reservoirs," Soc. Pet. Engrs. Journal, December 1962, p. 317.

76. Varga, R. S., "On Higher Order Stable Implicit Methods for Solving Parabolic Partial Differential Equations," J. Math. Physics, 40, 1961, pp. 220-231.

77. _____, Matrix Iterative Analysis, Prentice-Hall, Inc., 1962.

78. Wachspress, E. L., "Extended Application of Alternating Direction Implicit Iteration Model Problem Theory," J. Soc. Indust. Appl. Math., 11, No. 4, December 1963.

79. Wachspress, E. L. and Habetler, G. J., "An Alternating-Direction-Implicit Iteration Technique," J. Soc. Indust. Appl. Math. 8, 1960, pp. 403-424.

80. Wall, H. S., Analytic Theory of Continued Fractions, D. van Nostrand, Co. Inc., Princeton, 1948.

81. Walls, H. A., "Self Diffusion Phenomena in Cadmium and Zinc Amalgams," Ph. D. Thesis, University of Oklahoma, 1962.

82. Welker, R. J., "The Unsteady Measurement of Liquid Diffusion Coefficients," Department of Chemical Engineering, University of Oklahoma, 1964, unpublished.

83. Wintner, A., "The Nonlocal Existence Problem of Ordinary Differential Equations," Amer. J. Math., 67, 1945, pp. 277-284.

84. Yoo, H. D., "Analogue Simulation of a Radial-Flow-Moving Boundary Problem," Chemical Engineering Symposium Series, 58, No. 37, 1962.

APPENDIX A

GLOSSARY AND A SUMMARY OF SOME KNOWN THEORETICAL RESULTS

APPENDIX A

Glossary

Diagonally dominant matrix

An n x n complex matrix is diagonally dominant if

$$|a_{i,j}| \leq \sum_{\substack{j=1 \\ j \neq i}}^{n} |a_{i,j}| \qquad (1)$$

for all $1 \leq i \leq n$. If in addition A is irreducible then the matrix A is irreducibly diagonally dominant. If the strict inequality in (1) is valid for all $1 \leq i \leq n$, then matrix A is strictly diagonally dominant.

Essentially Positive matrix

A real n x n matrix $A = (a_{i,j})$ is essentially positive if A is irreducible and $a_{i,j} \geq 0$ for $i \neq j$, $1 \leq i,j \leq n$.

Non-negative matrix

A real n x n matrix $A = (a_{i,j})$ is non-negative if $a_{i,j} \geq 0$ for all $1 \leq i \leq n$, and all $1 \leq j \leq n$.

Positive matrix

A real n x n matrix $A = (a_{i,j})$ is positive if $a_{i,j} > 0$ for all $1 \leq i \leq n$ and $1 \leq j \leq n$.

Positive definite matrix

An n x n matrix $A = (a_{i,j})$ is positive definite if A has n distinct and positive eigenvalues.

Spectral norm of a matrix

If $A = (a_{i,j})$ is an n x n complex matrix, then

$$\|A\| = \sup_{x \neq o} \|Ax\| / \|x\|$$

is the spectral norm of the matrix A.

Spectral radius of A matrix

Let $A = (a_{i,j})$ be an n x n complex matrix with eigenvalues λ_i, $1 \leq i \leq n$. The

$$\rho(A) \equiv \max_{1 \leq i \leq n} |\lambda_i|$$

is spectral radius of the matrix A.

Stieltje Matrix

A real n x n matrix $A = (a_{i,j})$ with $a_{i,j} \leq 0$ for all $i \neq j$ is a Stieltjes matrix if A is symmetric and positive definite.

Tridiagonal matrix

A n x n matrix $A = (a_{i,j})$ is tridiagonal if

$a_{i,j} \neq 0$ for $i-1 \geq j \geq i+1$, $1 \leq i,j \leq n$,

$a_{i,j} = 0$ otherwise.

Euclidean norm (or length) of a vector

Let x be a vector belonging to a n-dimensional

vector space over the field of complex numbers. Then,

$$\|x\| \equiv (x^*x)^{\frac{1}{2}} = \left[\sum_{i=1}^{n} |x_i|^2\right]^{\frac{1}{2}}$$

is the Euclidean norm of x.

A Summary of Some Known Theoretical Results

Lemma A-1

Let $A = (a_{i,j})$ be an n x n matrix, then

$$\|A\| = [\rho(A^*A)]^{\frac{1}{2}}$$

[Theorem 1.3. Varga (77)]

Corollary

If $A = (a_{i,j})$ is an n x n Hermitian matrix, then $\|A\| \equiv \rho(A)$. Moreover, if $g_m(x)$ is any polynomial of degree m in x, then

$$g_m(A) = \rho[g_m(A)].$$

Lemma A-2

Let $A = (a_{i,j})$ be an n x n strictly or irreducibly diagonally dominant complex matrix. Then, the matrix A is nonsingular. If all the diagonal entries of A are in addition positive real numbers, then the eigenvalues of A satisfy $\text{Re}\,|\lambda_i| > 0$, $1 \leq i \leq n$. [Theorem 1.8, Varga (77)].

Corollary

If $A = (a_{i,j})$ is Hermitian and strictly diagonally dominant or irreducibly diagonally dominant matrix with positive real diagonal entries, then A is positive definite.

Lemma A-3

Let $A = (a_{i,j})$ be an essentially positive matrix, then A has a real eigenvalue $\zeta(A)$ such that:

1. To $\zeta(A)$ there corresponds an eigenvector $x > o$.
2. If α is any other eigenvalue of A, then $\text{Re } \alpha < \zeta(A)$.
3. $\zeta(A)$ increases when any element of A is increased.

Lemma A-4

The matrix A is essentially positive, if and only if $\exp(tA) > 0$ for all values of $t > 0$. [Theorem 8.3, Varga (77)].

Lemma A-5

If A is essentially positive and $\zeta(A)$ is the eigenvalue of Lemma A-3, then

$$\exp(tA) \approx K \exp(t\zeta(A)), \quad t \to \infty$$

where K is a positive constant independent of t.

Lemma A-6 (Monotonicity Principle)

Let A and B be two real n x n symmetric matrices with eigenvalues $\alpha_1 \le \alpha_2 \le \ldots \le \alpha_n$ and $\beta_1 \le \beta_2 \le \ldots \le \beta_n$, respectively. Let the eigenvalues of $C = A + B$ be $\gamma_1 \le \gamma_2 \le \ldots \le \gamma_n$. Then

$$(\alpha_i + \beta_j) \le \gamma_k \le (\alpha_1 + \beta_m)$$

if $\quad i + j - 1 \leq k \leq 1 + m - n$

[Theorem 10.1, Birkhoff, Varga and Young, (4)].

Lemma A-7

Let $A = (a_{i,j}) \geq 0$ be an irreducible n x n matrix, and let P^* be the hyperoctant of vectors $x > o$. Then for any $x \in P^*$, either

$$\min_{1 \leq i \leq n} \left\{ \frac{\sum_{j=1}^{n} a_{i,j} x_j}{x_i} \right\} < \rho(A) < \max_{1 \leq i \leq n} \left\{ \frac{\sum_{j=1}^{n} a_{i,j} x_j}{x_i} \right\}$$

or

$$\rho(A) = \frac{\sum_{j=1}^{n} a_{i,j} x_j}{x_i} \quad \text{for all } 1 \leq i \leq n.$$

Moreover,

$$\sup_{x \in P^*} \left\{ \min_{1 \leq i \leq n} \left[\frac{\sum_{j=1}^{n} a_{i,j} x_j}{x_i} \right] \right\} = \rho(A) =$$

$$\inf_{x \in P^*} \left\{ \max_{1 \leq i \leq n} \left[\frac{\sum_{j=1}^{n} a_{i,j} x_j}{x_i} \right] \right\} .$$

APPENDIX B

THE COMPUTER RESULTS FOR THE ONE-DIMENSIONAL CASE

APPENDIX B

THE COMPUTER RESULTS FOR THE ONE-DIMENSIONAL CASE

The following computations were carried out on the University of Oklahoma IBM 1410 in order to compare the results from the proposed numerical solution with Neumann's analytical solution for the one-dimensional, latent heat problems.

TABLE 8

THE PARAMETERS EMPLOYED IN THE COMPUTER SOLUTIONS OF THE ONE-DIMENSIONAL CASE

Run No.	ξ	h	δ_x	δ_F	u_F	Tabulated Data		
						$\|e\|$	$w(x_i,\tau)$	$u(x_{1,i},\tau)-w(x_{1,i},\tau)$
1.1	0.50	0.01	0.25	0.001	0.00	*		
1.2	0.50	0.01	0.25	0.01	0.00	*		
1.3	0.50	0.01	0.25	0.1	0.00	*	*	
1.4	0.50	0.01	0.50	0.001	0.00	*		
1.5	0.50	0.01	1.00	0.001	0.00	*		
1.6	0.50	0.005	0.50	0.005	0.00	*		
1.7	0.50	0.01	1.00	0.001	0.00			*
1.8	0.50	0.01	1.00	0.05	0.00			*
1.9	0.50	0.01	1.00	0.1	0.00			*

For Run 1.1, 1.2, 1.3, 1.4 and 1.6 the original co-ordinate axis x_1 was replaced by $x = x_1/(1 + x_1)$ and

then uniform mesh spacing was used on the x axis, i.e., the mesh point i was situated at $x_i = ih$, where h is the constant mesh spacing. For Run 1.5 and 1.7 the original coordinate x_1 was used. The entries of the n x n tri-diagonal matrix H for Run 1.1, 1.2, 1.3, 1.4 and 1.6 were computed by the following formulae:

$$c_1 = (1 - 0.5h)(1 - 1.5h + h^2)$$

$$c_i = (1 - x_i + 0.5h)^2(1 - x_i)(1 - x_i + h), \quad 2 \le i \le n$$

$$b_i = c_{i+1} \quad , \quad 1 \le i \le n - 1$$

$$a_i = [(1 - x_i + 0.5h)^2 + (1 - x_i - 0.5h)^2]$$

$$(1 - x_i)(1 - x_i - h), \quad 1 \le i \le n$$

where $x_i = ih$, and $n = 1/h$. The computer program solves $\tilde{w}(x_i,\tau) = (1 - x_i)^2 \, w(x_i,\tau)$, $1 \le i \le n$. The values of $w(x_i,\tau)$ are then calculated by dividing $\tilde{w}(x_i,\tau)$ by $(1-x_i)^2$.

For Run 1.5, 1.7, 1.8 and 1.9, $c_i = +1$, $b_i = 1$ and $a_i = 2$. Equation (4.14) was used to calculate the acceleration parameter in Run 1.1, 1.2, 1.3, 1.4 and 1.6. In Run 1.5 and 1.7, Equation (4.17) was employed.

TABLE 9

COMPUTED VALUES OF THE DIMENSIONLESS TEMPERATURE $w(ih,\tau)$
($\xi = 0.5$, $\delta_x = 0.25$, $\delta_F = 0.1$ AND $u_F = 0.0$)

i	τ = 0.000102	τ = 0.000416	τ = 0.000956	τ = 0.001736	τ = 0.00277	τ = 0.01234	τ = 0.03114	τ = 0.0625	τ = 0.1111
1	0.018276	0.508555	0.673242	0.734400	0.782624	0.899266	0.937150	0.955738	0.966880
2	0.000044	0.013121	0.331087	0.480631	0.568376	0.796792	0.873117	0.910613	0.933100
3		0.000053	0.012544	0.251957	0.371815	0.692944	0.807976	0.864639	0.898658
4			0.000088	0.010668	0.211758	0.588077	0.741812	0.817836	0.863552
5				0.000130	0.009145	0.482603	0.674704	0.770229	0.827782
6					0.000165	0.377395	0.606705	0.721843	0.791349
7						0.273117	0.537875	0.672709	0.754257
8						0.169453	0.468375	0.622860	0.716512
9						0.073131	0.398509	0.572333	0.678122
10						0.008012	0.328509	0.521166	0.639094
11						0.000495	0.258210	0.469402	0.599441
12						0.000043	0.187226	0.417068	0.559177
13							0.116087	0.364164	0.518318
14							0.047266	0.310691	0.476886
15							0.008455	0.256757	0.434901
16							0.000953	0.202674	0.392382
17							0.000129	0.148785	0.349337
18							0.000015	0.094841	0.305773
19								0.039468	0.261705
20								0.009121	0.217180
21								0.001520	0.172279
22								0.000273	0.127085
23								0.000042	0.081595
24									0.035812
25									0.009746
26									0.002162
27									0.000466
28									0.000085
29									
30									

TABLE 10

THE DEPARTURE OF THE PROPOSED NUMERICAL SOLUTION FROM THE NEUMANN'S SOLUTION

$\frac{x_1}{\sqrt{4\tau}}$	$e(x_1,.0025)$			$\frac{x_1}{\sqrt{4\tau}}$	$e(x_1,0.01)$			$\frac{x_1}{\sqrt{4\tau}}$	$e(x_1,0.04)$			$\frac{x_1}{\sqrt{4\tau}}$	$e(x_1,0.09)$		
	Run 1.7	Run 1.8	Run 1.9		Run 1.7	Run 1.8	Run 1.9		Run 1.7	Run 1.8	Run 1.9		Run 1.7	Run 1.8	Run 1.9
0.1	-0.13634	-0.14089	-0.14203	0.05	+0.10064	-0.05486	-0.06051	0.025	+0.06716	-0.02284	-0.02344	0.01667	+0.04729	-0.00500	-0.00628
0.2	+0.20215	-0.28205	-0.28494	0.10	-0.10362	-0.10823	-0.11785	0.05	-0.07516	-0.04597	-0.04783	0.03333	-0.06087	-0.01067	-0.01321
0.3	-0.06080	-0.42919	-0.43284	0.15	+0.10260	-0.14961	-0.16141	0.075	+0.06745	-0.06091	-0.06592	0.05000	+0.05016	-0.00943	-0.013854
0.4	+0.17657	-0.50416	-0.50871	0.20	-0.05138	-0.23486	-0.24575	0.100	-0.45783	-0.11344	-0.12278	0.06667	-0.03961	-0.04217	-0.04859
0.5	+0.00012	-0.76436	-0.77091	0.25	+0.08803	-0.15748	-0.16488	0.125	+0.05107	-0.04539	-0.05848	0.08333	+0.03934	-0.02475	-0.01764
				0.30	-0.02867	-0.42023	-0.43190	0.150	-0.03342	-0.21454	-0.23423	0.10000	-0.03009	-0.10235	-0.11156
				0.35	+0.08541	-0.18029	-0.21009	0.175	+0.04577	-0.03000	-0.06277	0.11667	+0.03423	-0.05672	-0.03984
				0.40	-0.01226	-0.57907	-0.60592	0.200	-0.02493	-0.29858	-0.32601	0.13333	-0.02396	-0.15777	-0.16782
				0.45	+0.08614	-0.19060	-0.22928	0.225	+0.04337	-0.00897	-0.03305	0.15000	+0.03141	-0.07832	-0.07768
				0.50	+0.00012	-0.66849	-0.78172	0.250	-0.01868	-0.30480	-0.37829	0.16667	-0.01967	-0.15908	-0.18854
								0.275	+0.04225	-0.02021	-0.11595	0.18333	+0.02973	-0.08842	-0.04505
								0.300	-0.01366	-0.40153	-0.44734	0.20000	-0.01629	-0.20225	-0.20892
								0.325	+0.04185	-0.07074	-0.14630	0.21667	+0.02873	-0.08422	-0.05294
								0.350	-0.00944	-0.43908	-0.51054	0.23333	-0.01347	-0.20585	-0.22573
								0.375	+0.04186	-0.13077	-0.19880	0.25000	+0.02813	-0.04436	-0.05288
								0.400	-0.00580	-0.38696	-0.56245	0.26667	-0.01105	-0.17481	-0.21982
								0.425	+0.04208	-0.08243	-0.27283	0.28333	+0.02781	-0.07491	-0.04818
								0.450	-0.00264	-0.44838	-0.63980	0.30000	-0.00893	-0.20792	-0.22162
								0.475	+0.04240	-0.16926	-0.37811	0.31667	+0.02765	-0.03700	-0.00280
								0.500	+0.00012	-0.48841	-0.60120	0.33333	-0.00703	-0.21487	-0.19880
												0.35000	+0.02762	-0.03310	-0.01709
												0.36667	-0.00532	-0.17205	-0.21973
												0.38333	+0.02767	-0.00592	-0.04388
												0.40000	-0.00377	-0.14310	-0.16187
												0.41667	+0.02777	-0.01452	-0.05485
												0.43333	-0.00235	-0.13651	-0.18157
												0.45000	+0.02790	-0.05102	-0.06211
												0.46667	-0.00106	-0.12483	-0.15091
												0.48333	+0.02804	-0.06648	-0.08308
												0.50000	-0.00012	-0.10000	-0.12992

TABLE 11

THE EUCLIDEAN NORM OF THE DEPARTURE OF THE PROPOSED NUMERICAL SOLUTION FROM THE NEUMANN'S SOLUTION FOR $\xi = .5$, $u_F = 0.0$, AND DIFFERENT VALUES OF h, δ_F and δ_x

	Run 1.1	Run 1.2	Run 1.3	Run 1.4	Run 1.5		Run 1.6	
h	0.010	0.010	0.010	0.01	0.01		0.005	
δ_F	0.001	0.010	0.100	0.001	0.001		0.100	
δ_x	0.250	0.250	0.250	0.500	1.000		0.500	
$\tau \times 10^4$	$\|e\|$	$\|e\|$	$\|e\|$	$\|e\|$	$\tau \times 10^4$	$\|e\|$	$\tau \times 10^4$	$\|e\|$
1.0203	0.000167	0.001877	0.018252				4.0812	0.155354
4.1649	0.029618	0.030028	0.036693	0.171389	25.000	0.307135	16.6597	0.028674
9.5653	0.030096	0.030486	0.034472		100.000	0.239725	38.2612	0.116954
17.3611	0.034910	0.011262	0.023941	0.118754	225.00	0.202668	69.4444	0.111294
27.7008	0.062666	0.053168	0.035638		400.00	0.184272	110.8030	0.088548
40.7424	0.062138	0.059488	0.038730	0.230874	625.00	0.168850	162.9690	0.072950
56.6539	0.060421	0.057857	0.032993		900.00	0.156889	226.6150	0.065071
75.6143	0.058426	0.055700	0.031007	0.192721			302.4570	0.060596
97.8142	0.056455	0.053570	0.038891				391.2570	0.057484
123.4560	0.054618	0.050854	0.046325	0.168953			493.8270	0.055384
152.7580	0.052949	0.048237	0.048481				611.0330	0.053758
185.9500	0.050701	0.048561	0.047072	0.152765			743.8010	0.052203
223.2790	0.114160	0.082224	0.044437				893.1160	0.050470
265.0080	0.124222	0.110525	0.041799	0.140834			1060.0300	0.048564
311.4180	0.120807	0.111996	0.039474					
362.8110	0.116965	0.108806	0.037410	0.120647				
419.5090	0.113494	0.105358	0.035518					
481.8560	0.110377	0.102170	0.033738	0.125542				
550.2200	0.107579	0.099279	0.032080					
625.0000	0.105058	0.096661	0.030558	0.122046				
706.6170	0.102782	0.094288	0.029183					
795.5290	0.100720	0.092130	0.027939	0.118760				
892.2240	0.098847	0.090163	0.026810					
997.2290	0.097142	0.088414	0.025780	0.116239				
1111.1100	0.095589	0.086835	0.024834					
1234.4700				0.114162				

APPENDIX C

THE COMPUTER PROGRAM FOR SOLVING TWO-DIMENSIONAL PROBLEMS AND THE TABULATED SOLUTION OF THE TWO-DIMENSIONAL EXAMPLE PROBLEMS

APPENDIX C

THE COMPUTER PROGRAM FOR SOLVING TWO-DIMENSIONAL PROBLEMS AND THE TABULATED SOLUTION OF THE TWO-DIMENSIONAL EXAMPLE PROBLEMS

The Computer Program

A listing of the program based on the procedure outlined in Chapter IV and specialized for example problem numbers 3 and 4 is given in Table 12. The program was written in Fortran language. The following nomenclature was used for input and output data transmission:

1. Input Data

IROW	Number of rows in $_h$
ICOL	Number of columns in $_h$
INR	Number of rows beyond the approximate interface $X(\tau)$ or $\chi(\tau)$
IP	Number of iterations before the first print-out
INC	Number of entries of w to be printed on one line
NW	Number of entries of w fed into the computer
NP	Number of iterations between each print-out

NS	Number of entries of s fed into the computer
TIMEO	$\tau_o/(hk)^2$
TIMAX	$\tau_{max}/(hk)^2$
H	$\sqrt{hk}$
X2	$X(\tau)/\sqrt{hk}$ or $\chi(\tau)/\sqrt{hk}\,/\,(1-\chi(\tau)$
DX	δ_x
BETA	β in $\varphi(u) = 1 + \lambda \exp\,[-\beta^2(u-u_F)^2]$
UFS	u_F
DH	λ
ET	ξ
B(I,1)	e_i'
B(I,2)	b_i'
C(I,1)	f_i'
C(I,2)	c_i'
A(I,1)	$f_i' + e_i'$
A(I,2)	$c_i' + b_i'$
A2(I,1)	The first diagonal entry of the submatrix V_i
A2(J,2)	The first diagonal entry of the submatrix H_j
S(I,J)	$s_{i,j}$
CX(I)	x_i
CY(J)	y_j

2. Output Data

DQ	δ_Q
Q	Q

ERROR	$\|e_{55}(\tau)\|^2 = \|E\|^2$
TIME	$\tau/(kh)$
V(I,J)	The solution $w_{i,j}(\tau)$

The Solutions of the Example Problems

In all the four example problems solved by the computer matrices $H^{(C)}$ and $V^{(C)}$ defined by Equation (3.17) were used in the basic scheme of page 102, instead of H and V. For the case of variable mesh spacing, the entries of $H^{(C)}$ and $V^{(C)}$ and s were first computed on the IBM 1620. The results were punched on IBM cards and used as input data when solving example problems 3 and 4 on the CDC 1604. A listing of all input data for Run 2-3 is given in Table 13. For RUN 2-4 the same input data were used except for the values of DX (δ_x), X2 and TIMEO, which were respectively 0.50, 2.0, and 4.0. Table 14 gives a listing of input data for Run 2-1. The same data were used in Run 2-2 except for the values of DX, X2 and TIMEO, which were those of Run 2-4.

In all four runs $\sqrt{kh} = .01$ was used in machine computation. For this value of $\sqrt{kh}$ the dimensionless length 'a' of the exposed boundary for constant mesh spacing and variable mesh spacing becomes 0.2 and 0.25 respectively. To make the length of the exposed boundary be unity in all cases, the geometric scaling factors 5 and 4 were used for the case of constant mesh spacing and the case of variable mesh spacing respectively. The computed values of Q were then corrected by multiplying them by 25 for the first case and by 16 for the second case. The values of τ were then

computed using the following relation:

$$\tau = 0.0025\ \text{TIME} \qquad \text{for Run 2-1}$$

$$= 0.0025\ (\text{TIME} - 4) \qquad \text{for Run 2-2}$$

$$= 0.0016\ \text{TIME} \qquad \text{for Run 2-3}$$

$$= 0.0016\ (\text{TIME} - 4) \qquad \text{for Run 2-4}$$

where

$$\text{TIME} = \sum_{j=1}^{m} r_j$$

and m is the number of the predictor steps completed.

Table 15 gives the corrected values of Q and $Q/\sqrt{\tau}$ for several values of τ and for all the four runs. Table 16 is a reduced photograph of the computer output for Run 2-1. Those of Runs 2-2, 2-3 and 2-4 are given in Tables 17, 18, and 19, respectively. The values of Q and τ in these tables are the corrected values. Note that the initial value of TIMEO in Runs 2-2 and 2-4 was used only to increase the first few values of r_j, $j = 1, 2 \ldots$, by a factor larger than 2 when compared with those of Runs 2-1 and 2-3.

The last table of this appendix (Table 20) gives the position of the interface (i.e., 0.0159 isotherm) for Run 2-1 for several values of τ. The data of this table were used to compare the computer solution and the diffusion cell analog solution.

TABLE 12
A LISTING OF THE COMPUTER PROGRAM AS
SPECIALIZED FOR RUN NUMBER 2.3

```
      DIMENSION KBB(65)
      DIMENSION CX(62),CY(62),U(62),V1(62),A2(62,2),S(41,62),B(62,2)
      DIMENSION CS(62),GS(62),FEE(41,62),V(41,62),W(41,62),A(62,2)
      DIMENSION C(62,2)
 1112 FORMAT(1H )
 1995 FORMAT(70H
     1                                                          )
 1113 FORMAT(1H1)
      PRINT 1113
      READ 1995
      PRINT 1995
      READ 1995
      PRINT 1995
      READ 1995
      PRINT 1995
      PRINT 1112
      READ 1995
      PRINT 1995
      PRINT 1112
  990 FORMAT (I4,15F7.4,///)
      READ 1995
      PRINT 1995
  998 FORMAT(2I4,2F10.2,I4,F14.7)
      READ 998,IROW,ICOL,TIMEO,TIMAX,NW,H
      PRINT998,IROW,ICOL,TIMEO,TIMAX,NW,H
      ICOLM=ICOL+1
      IROWM=IROW+1
      PRINT 1112
      READ 1995
      PRINT 1995
 1998 FORMAT(5I4)
```

TABLE 12 (CONTINUED)

```
      READ  1998,NS,INC,INR,NP,IP
      PRINT 1998,NS,INC,INR,NP,IP
      PRINT 1112
  997 FORMAT(6F12.6)
      READ 1995
      PRINT 1995
      READ 997,X2,DX,BETA,UFS,DH,ET
      PRINT997,X2,DX,BETA,UFS,DH,ET
      PRINT 1112
      READ 1995
      PRINT 1995
      KROW=IROW
      KCOL=ICOL
      IN=IP
      Q=0.
      DQ=0.
      M4=1
      KK=IROW
      LL=ICOL
      WW=.0000001*.0000001*.0000001
      DO 331 I=1,IROWM
      DO 331 J=1,ICOLM
      V(I,J)=0.
      S(I,J)=0.0
      FEE(I,J)=1.
  331 W(I,J)=WW
      DO 501 N=1,NS
      READ 502,I,J,XS
      PRINT 502,I,J,XS
  501 S(I,J)=XS
  502 FORMAT(2I5,F10.6)
      PRINT 1112
      IF (NW) 3333,3334,3334
 3333 PRINT 3338
 3338 FORMAT( 22H WS ENTERED BY PROGRAM
      DO 3336 N=1,IROWM
```

TABLE 12 (CONTINUED)

```
      NK=IROWM-N+1
      DO 3336 NN=1,NK
      W(N,NN)=-1.
3336  CONTINUE
      NW=0 -NW
3334  PRINT 1112
      READ 1995
      PRINT 1995
      DO 319 N=1,NW
      READ 996,I,J,XW
      PRINT996,I,J,XW
      W(I,J)=XW
 319  CONTINUE
 996  FORMAT(2I4,F12.6)
 995  FORMAT(5F14.7)
      READ 1995
      PRINT 1995
      DO 318 I=1,IROWM
      READ 995,B(I,2),A(I,2),CX(I),C(I,2),A2(I,1)
      PRINT995,B(I,2),A(I,2),CX(I),C(I,2),A2(I,1)
 318  CONTINUE
      PRINT 1112
      READ 1995
      PRINT 1995
      DO 320 I=1,ICOLM
      READ 995,B(I,1),A(I,1),CY(I),C(I,1),A2(I,2)
      PRINT995,B(I,1),A(I,1),CY(I),C(I,1),A2(I,2)
 320  CONTINUE
      PRINT 1113
      READ 1995
      PRINT 1995
      PRINT 1112
      READ 1995
      I2=1
      SUM=TIMEO
      M=4
```

TABLE 12 (CONTINUED)

```
      II=1
  130 M=M+1
      GO TO (60,60,60,60,51),M
   51 M=1
      GO TO (53,52),M4
   52 RO=2./R
      M4=1
      GO TO 54
   53 X2=X2+DX
      IXFIX=X2
      IROW=IXFIX+INR
      R=(.5*X2/ET/(1-H*X2))**2-SUM
      SUM=SUM+R
      RO=4./R
      M4=2
      IN=IN-1
   54 DO 250 I=2,KK
      M10=1
      DO 50  J=2,LL
      IF(W(I,J)) 50,56,56
   56 GO TO (4258,4257),M10
 4258 M11=J
      M10=2
 4257 GO TO (4256,4260),M4
 4260 DQ=DQ+FEE(I,J)*(V(I,J)-W(I,J))*(CX(I+1)-CX(I-1))*(CY(J-1)-CY(J+1))
     1 /4.0
 4256 SFS=BETA*(V(I,J)-UFS)
      IF (SFS-3.) 57,58,58
   58 FEE(I,J)=1.0
      GO TO 59
   57 SFFS=SFS*SFS
      FEE(I,J)=1.+DH/EXPF(SFFS)
   59 GO TO (62,61),M4
   61 W(I,J)=V(I,J)
      GO TO 50
   62 V(I,J)=W(I,J)
```

TABLE 12 (CONTINUED)

```
   50 CONTINUE
      FEE(I,M11)=FEE(I,M11)/2.
  250 CONTINUE
      IF (IN) 60,622,60
  622 IN=NP
      Q=DQ+Q
 1111 FORMAT(5H  DQ= ,F18.6,6H   Q= ,F18.6,6H TIME=,F16.8,8H  ERROR=,F16
11111.8)
      TIME=SUM-R
      ERROR=0.
      IROWW=IROW+1-INR
      DO 4200 I=2,IROWW
      XXX=CX(I)/((4.0*TIME)**0.5)/H
      YYY=1./(1.+0.47047*XXX)
      EROR=V(I,55)+((1.- 1.1283792*(.3084284*YYY-.0849713*YYY*YYY+.66276
     198*YYY*YYY*YYY)/EXPF(XXX*XXX))/.5205)-1
 4200 ERROR=EROR*EROR+ERROR
      PRINT 1995
      PRINT 1112
      PRINT 1112
      PRINT 1111,DQ,Q,TIME,ERROR
      DQ=0.
      PRINT 1112
      DO 4001 KNB=2,LL,INC
      KNBP=KNB+INC-1
 4011 FORMAT(4X,15(4H (I,,I2,1H)))
       DO 4300 I=KNB,KNBP
 4300 KBB(I)=I
      PRINT 4011,(KBB(I),I=KNB,KNBP)
      PRINT 1112
      DO 4002 I=2,KK
      PRINT 990,I,(V(I,J),J=KNB,KNBP)
 4002 CONTINUE
      PRINT 1113
 4001 CONTINUE
      DO 6063 I=1,IROW
```

TABLE 12 (CONTINUED)

```
7320 FORMAT(E18.8)
6063 DQ=DQ
     IF(TIMAX-SUM) 252,252,60
 252 STOP
  60 DO 10 K=2,KK
     L1=0
     I1=1
     GO TO (100,101),II
 100 I=K
     I4=K
     I3=K
     GO TO 102
 101 J=K
     J2=K
     J1=K
 102 DO 20 L=2,LL
     GO TO (103,104),II
 103 J=L
     J1=L+1
     J2=L-1
     GO TO 105
 104 I=L
     I4=L+1
     I3=L-1
 105 GO TO (106,107),I1
 106 IF (W(I,J)) 108,109,109
 108 GO TO 20
 109 A1=A2(K,II)
     CS(L-1)=0.0
     GS(L-1)=0.0
     L1=L
     I1=2
     GO TO 110
 107 A1=A (L,II)
 110 GO TO (111,112),I2
 111 V1(L)=(RO*FEE(I,J)-A1)*V(I,J)+B(L,II)*V(I4,J1)+C(L,II)*V(I3,J2)
```

TABLE 12 (CONTINUED)

```
    1+S(I,J)
     GO TO 20
 112 A5=RO*FEE(I,J)+A1
     DN=A5-C(L,II)*GS(L-1)
     CS(L)=B(L,II)/DN
     GS(L)=(V(I,J)+C(L,II)*GS(L-1))/DN
 971 FORMAT(8I4,3E16.8)
  20 CONTINUE
     IF (L1) 10,10, 4750
4750 GO TO (113,114),I2
 113 DO 115 L=L1,LL
     GO TO (116,117),II
 116 J=L
     GO TO 115
 117 I=L
 115 V(I,J)=V1(L)
 981 FORMAT (2I4,E16.8)
     GO TO 10
 114 V1(LL)=GS(LL)
     L2=LL-L1
     DO 118 L3=1,L2
     L4=LL-L3
 118 V1(L4)=GS(L4)+CS(L4)*V1(L4+1)
     DO 119 L=L1,LL
     GO TO (121,120),II
 120 I=L
     GO TO 119
 121 J=L
 119 V(I,J)=V1(L)
  10 CONTINUE
     GO TO (122,123),I2
 122 I2=2
     GO TO (222,223),II
 222 II=2
     KK=ICOL
     LL=IROW
```

TABLE 12 (CONTINUED)

```
      GO TO 130
  223 II=1
      KK=IROW
      LL=ICOL
      GO TO 130
  123 I2=1
  124 GO TO 130
      END
```

TABLE 13
INPUT DATA LISTING FOR RUN NUMBER 2.3

ROWS	COLS	TIMEO	TIME MAX	NW	H
40	61	0.0	1112.0	-21	0.01

NS	INC	INR	NP	IP
20	15	5	8	3

X2	DX	BETA	UF	DH	ET
0.0	.25	30.	.0	57.154020	0.5

I	J	S(I,J)
2	61	1.9798
2	60	1.9798
2	59	1.9798
2	58	1.9798
2	57	1.9798
2	56	1.9798
2	55	1.97980
2	54	1.9798
2	53	1.9798
2	52	1.9798
2	51	1.9798
2	50	1.9798
2	49	1.9798
2	48	1.9798
2	47	1.9798
2	46	1.9798
2	45	1.9798
2	44	1.9798
2	43	1.9798
2	42	1.9798

I	J	W(I,J)
1	41	-1.
1	42	-1.
1	43	-1.
1	44	-1.
1	45	-1.
1	46	-1.
1	48	-1.
1	47	-1.
1	49	-1.
1	50	-1.
1	51	-1.
1	52	-1.
1	53	-1.
1	54	-1.
1	55	-1.
1	56	-1.
1	57	-1.
1	58	-1.
1	59	-1.
1	60	-1.
1	61	-1.

TABLE 13 (CONTINUED)

B(I,2)	A(I,2)	CX(I)	C(I,2)	A2(I,1)
0.	0.	-.0050251	0.	0.0000000
.9702007	1.9601011	.0050251	.9899003	0.9825444
.9316838	1.8824791	.0152284	.9507952	0.9507967
.8943251	1.8071856	.0256410	.9128604	0.9128605
.8581016	1.7341738	.0362694	.8760722	0.8760727
.8229894	1.6633968	.0471204	.8404073	0.8404071
.7889662	1.5948086	.0582010	.8058424	0.8058423
.7560088	1.5283638	.0695187	.7723550	.7723550
.7240950	1.4640171	.0810810	.7399221	0.7399227
.6932024	1.4017243	.0928961	.7085218	0.7085217
.6633088	1.3414402	.1049723	.6781314	0.6781305
.6343924	1.2831216	.1173184	.6487291	0.6487291
.6064323	1.2267258	.1299435	.6202935	0.6202935
.5794068	1.1722102	.1428571	.5928034	0.5928034
.5532945	1.1195317	.1560693	.5662371	0.5662371
.5280749	1.0686487	.1695906	.5405737	0.5405737
.5037275	1.0195203	.1834319	.5157928	0.5157928
.4802320	.9721059	.1976047	.4918738	0.4918738
.4575681	.9263649	.2121212	.4687967	0.4687967
.4357158	.8822570	.2269938	.4465411	0.4465411
.4146558	.8397432	.2422360	.4250874	0.4250874
.3943684	.7987845	.2578616	.4044161	0.4044161
.3748350	.7593430	.2738853	.3845080	0.3845080
.3560363	.7213807	.2903225	.3653444	0.3653444
.3379535	.6848595	.3071895	.3469060	0.3469060
.3205687	.6497432	.3245033	.3291744	0.3291744
.3038630	.6159947	.3422818	.3121316	0.3121316
.2878190	.5835779	.3605442	.2957588	0.2957588
.2724190	.5524581	.3793103	.2800391	0.2800391
.2576453	.5225997	.3986013	.2649544	0.2649544
.2434807	.4939681	.4184397	.2504873	0.2504873
.2299085	.4665296	.4388489	.2366211	0.2366211
.2169116	.4402503	.4598540	.2233387	0.2233387
.2044738	.4150972	.4814814	.2106233	0.2106233

TABLE 13 (CONTINUED)

.1925786	.3910375	.5037593	.1984589	0.1984589
.1812100	.3680390	.5267175	.1868290	0.1868290
.1703525	.3460704	.5503875	.1757179	0.1757179
.1599901	.3251000	.5748031	.1651099	0.1651099
.1501080	.3050975	.6000000	.1549895	0.1549895
.1406908	.2860326	.6260162	.1453418	0.1453418
0.0000000	0.0000000	0.0000000	0.0000000	0.0000000
B(I,1)	A(I,1)	CY(I)	C(I,1)	A2(I,2)
0.00000 0	0.0000000	0.0000000	0.0000000	0.0000000
.1361515	.2678754	.8873157	.1317239	0.1317239
.1453418	.2860326	.8604394	.1406908	.1406908
.1549895	.3050975	.8344232	.1501080	.1501080
.1651099	.3251000	.8092263	.1599901	.1599901
.1757179	.3460704	.7848108	.1703525	.1703525
.1868290	.3680390	.7611407	.1812100	.1812100
.1984589	.3910375	.7381826	.1925786	.1925786
.2106233	.4150972	.7159047	.2044738	.2044738
.2233387	.4402503	.6942772	.2169116	.2169116
.2366211	.4665296	.6732721	.2299085	.2299085
.2504873	.4939681	.6528629	.2434807	.2434807
.2649544	.5225997	.6330246	.2576453	.2576453
.2800391	.5524581	.6137335	.2724190	.2724190
.2957588	.5835779	.5949674	.2878190	.2878190
.3121316	.6159947	.5767050	.3038630	.3038630
.3291744	.6497432	.5589265	.3205687	.3205687
.3469060	.6848595	.5416127	.3379535	.3379535
.3653444	.7213807	.5247458	.3560363	.3560363
.3845080	.7593430	.5083085	.3748350	.3748350
.4044161	.7987845	.4922848	.3943684	.3943684
.4250874	.8397432	.4766592	.4146558	.4146558
.4465411	.8822570	.4614170	.4357158	.4357158
.4687967	.9263649	.4465444	.4575681	.4575681
.4918738	.9721059	.4320280	.4802320	.4802320
.5157928	1.0195203	.4178551	.5037275	.5037275
.5405737	1.0686487	.4040138	.5280749	.5280749

TABLE 13 (CONTINUED)

.5662371	1.1195317	.3904925	.5532945	.5532945
.5928034	1.1722102	.3772803	.5794068	.5794068
.6202935	1.2267258	.3643667	.6064323	.6064323
.6487291	1.2831216	.3517416	.6343924	.6343924
.6781305	1.3414390	.3393955	.6633085	.6633088
.7085217	1.4017233	.3273193	.6932016	.6932024
.7399227	1.4640182	.3155042	.7240954	.7240950
.7723550	1.5283642	.3039419	.7560092	.7560088
.8058423	1.5948084	.2926242	.7889660	.7889662
.8404071	1.6633965	.2815436	.8229894	.8229894
.8760727	1.7341743	.2706926	.8581015	.8581016
.9128605	1.8071863	.2600642	.8943257	.8943251
.9507967	1.8824809	.2496516	.9316842	.9316838
.9825444	1.9503515	.2394483	.9678071	.9702007
.9678057	1.9503496	.2293981	.9825439	2.9500014
.9316837	1.8824790	.2191948	.9507953	2.9500014
.8943244	1.8071845	.2087822	.9128601	2.9500014
.8581023	1.7341742	.1981537	.8760719	2.9500014
.8229897	1.6633981	.1873028	.8404083	2.9500014
.7889660	1.5948084	.1762221	.8058423	2.9500014
.7560082	1.5283629	.1649045	.7723546	2.9500014
.7240951	1.4640169	.1533421	.7399217	2.9500014
.6932024	1.4017245	.1415270	.7085220	2.9500014
.6633088	1.3414402	.1294508	.6781314	2.9500014
.6343924	1.2831216	.1171047	.6487291	2.9500014
.6064323	1.2267258	.1044797	.6202935	2.9500014
.5794068	1.1722102	.0915660	.5928034	2.9500014
.5532945	1.1195317	.0783538	.5662371	2.9500014
.5280749	1.0686487	.0648325	.5405737	2.9500014
.5037275	1.0195203	.0509912	.5157928	2.9500014
.4802320	.9721059	.0368184	.4918738	2.9500014
.4575681	.9263649	.0223020	.4687967	2.9500014
.4357158	.8822570	.0074293	.4465411	2.9500014
.4146558	.4250874	-.0078128	.4250874	2.9500014
0.	0.	-.0234384	0.	0.

TABLE 14
INPUT DATA LISTING FOR RUN NUMBER 2.1

ROWS	COLS	TIMEO	TIME MAX	NW	H
40	61	0.0	1112.0	-21	0.01

NS	INC	INR	NP	IP
20	15	5	8	3

X2	DX	BETA	UF	DH	ET
0.0	.25	30.	.0	57.154020	0.5

I	J	S(I,J)
2	61	2.
2	60	2.
2	59	2.
2	58	2.
2	57	2.
2	56	2.
2	55	2.
2	54	2.
2	53	2.
2	52	2.
2	51	2.
2	50	2.
2	49	2.
2	48	2.
2	47	2.
2	46	2.
2	45	2.
2	44	2.
2	43	2.
2	42	2.

I	J	W(I,J)
1	41	-1.
1	42	-1.
1	43	-1.
1	44	-1.
1	45	-1.
1	46	-1.
1	48	-1.
1	47	-1.
1	49	-1.
1	50	-1.
1	51	-1.
1	52	-1.
1	53	-1.
1	54	-1.
1	55	-1.
1	56	-1.
1	57	-1.
1	58	-1.
1	59	-1.
1	60	-1.
1	61	-1.

TABLE 14 (CONTINUED)

B(I,2)	A(I,2)	CX(I)	C(I,2)	A2(I,1)
0.	0.	-.005	0.	0.
1.	2.	.005	1.	1.
1.	2.	.015	1.	1.
1.	2.	.025	1.	1.
1.	2.	.035	1.	1.
1.	2.	.045	1.	1.
1.	2.	.055	1.	1.
1.	2.	.065	1.	1.
1.	2.	.075	1.	1.
1.	2.	.085	1.	1.
1.	2.	.095	1.	1.
1.	2.	.105	1.	1.
1.	2.	.115	1.	1.
1.	2.	.125	1.	1.
1.	2.	.135	1.	1.
1.	2.	.145	1.	1.
1.	2.	.155	1.	1.
1.	2.	.165	1.	1.
1.	2.	.175	1.	1.
1.	2.	.185	1.	1.
1.	2.	.195	1.	1.
1.	2.	.205	1.	1.
1.	2.	.215	1.	1.
1.	2.	.225	1.	1.
1.	2.	.235	1.	1.
1.	2.	.245	1.	1.
1.	2.	.255	1.	1.
1.	2.	.265	1.	1.
1.	2.	.275	1.	1.
1.	2.	.285	1.	1.
1.	2.	.295	1.	1.
1.	2.	.305	1.	1.
1.	2.	.315	1.	1.
1.	2.	.325	1.	1.

TABLE 14 (CONTINUED)

1.	2.	.335	1.	1.
1.	2.	.345	1.	1.
1.	2.	.355	1.	1.
1.	2.	.365	1.	1.
1.	2.	.375	1.	1.
1.	2.	.385	1.	1.
1.	2.	.395	1.	1.
B(I,1)	A(I,1)	CY(I)	C(I,1)	A2(I,2)
0.0000000	0.0000000	0.0000000	0.0000000	0.0000000
1.	2.	.595	1.	1.
1.	2.	.585	1.	1.
1.	2.	.575	1.	1.
1.	2.	.565	1.	1.
1.	2.	.555	1.	1.
1.	2.	.545	1.	1.
1.	2.	.535	1.	1.
1.	2.	.525	1.	1.
1.	2.	.515	1.	1.
1.	2.	.505	1.	1.
1.	2.	.495	1.	1.
1.	2.	.485	1.	1.
1.	2.	.475	1.	1.
1.	2.	.465	1.	1.
1.	2.	.455	1.	1.
1.	2.	.445	1.	1.
1.	2.	.435	1.	1.
1.	2.	.425	1.	1.
1.	2.	.415	1.	1.
1.	2.	.405	1.	1.
1.	2.	.395	1.	1.
1.	2.	.385	1.	1.
1.	2.	.375	1.	1.
1.	2.	.365	1.	1.
1.	2.	.355	1.	1.
1.	2.	.345	1.	1.

TABLE 14 (CONTINUED)

1.	2.	.335	1.	1.
1.	2.	.325	1.	1.
1.	2.	.315	1.	1.
1.	2.	.305	1.	1.
1.	2.	.295	1.	1.
1.	2.	.285	1.	1.
1.	2.	.275	1.	1.
1.	2.	.265	1.	1.
1.	2.	.255	1.	1.
1.	2.	.245	1.	1.
1.	2.	.235	1.	1.
1.	2.	.225	1.	1.
1.	2.	.215	1.	1.
1.	2.	.205	1.	1.
1.	2.	.195	1.	3.
1.	2.	.185	1.	3.
1.	2.	.175	1.	3.
1.	2.	.165	1.	3.
1.	2.	.155	1.	3.
1.	2.	.145	1.	3.
1.	2.	.135	1.	3.
1.	2.	.125	1.	3.
1.	2.	.115	1.	3.
1.	2.	.105	1.	3.
1.	2.	.095	1.	3.
1.	2.	.085	1.	3.
1.	2.	.075	1.	3.
1.	2.	.065	1.	3.
1.	2.	.055	1.	3.
1.	2.	.045	1.	3.
1.	2.	.035	1.	3.
1.	2.	.025	1.	3.
1.	2.	.015	1.	3.
1.	1.	.005	1.	3.
0.	0.	-.005	0.	0.

TABLE 15

CUMULATIVE HEAT FLOW, Q, AND $Q/\sqrt{\tau}$ FOR THE FOUR COMPUTED RUNS

Run 2-1			Run 2-2			Run 2-3			Run 2-4		
$\sqrt{\tau}$	Q	$Q/\sqrt{\tau}$	$\sqrt{\tau}$	Q	$Q/\sqrt{\tau}$	$\sqrt{\tau}$	Q	$Q/\sqrt{\tau}$	$\sqrt{\tau}$	Q	$Q/\sqrt{\tau}$
0.025	0.0249	0.9960	0.07500	0.15182	2.0243	0.02010	0.02016	1.00296	0.06476	0.13451	2.0770
0.125	0.2793	2.2144	0.20155	0.48480	2.4053	0.10256	0.22971	2.2396	0.17066	0.41730	2.4452
0.225	0.517225	2.2988	0.30923	0.76055	2.4595	0.18848	0.43235	2.2939	0.26632	0.66243	2.4872
0.325	0.76015	2.3389	0.41306	1.02972	2.4929	0.27807	0.6476		0.36286	0.91179	2.5128
0.425	1.0093	2.3748	0.51539	1.29867	2.5198	0.37148	0.87712	2.3447	0.46240	1.17211	2.5327
0.525	1.2651	2.4097	0.61696	1.57062	2.5457	0.46927	1.12338	2.3938	0.56060	1.44709	2.5813
0.625	1.5274	2.4438	0.71807	1.84727	2.5725	0.57143	1.38766	2.4284	0.67363	1.73998	2.5830
0.725	1.79645	2.4779	0.81891	2.12950	2.6004	0.67836	1.67856	2.4643	0.78633	2.05370	2.6184
0.825	2.0723	2.5119	0.91958	2.41775	2.6292	0.79042	1.97816	2.5027	0.90444	2.39110	2.6437
0.925	2.35505	2.5460	1.02011	2.71222	2.6875	0.90797	2.30891	2.5429	1.02830	2.75512	2.6793
1.025	2.64475	2.5802	1.12052	3.01312	2.6890	1.031446	2.66678	2.5855	1.15853	3.14890	2.7180
1.125	2.94145	2.6146	1.22088	3.32055	2.7198	1.161290	3.05477	2.6305			
1.225	3.2451	2.6491	1.32121	3.63462	2.7510	1.29801	3.47621	2.6781			
1.325	3.5557	2.6836	1.42145	3.95535	2.7826						
1.425	3.8734	2.7181									
1.525	4.1979	2.7527									

TABLE 16

NUMERICAL SOLUTION OF THE EXAMPLE PROBLEM NO.1 FOR VARIOUS VALUES OF τ

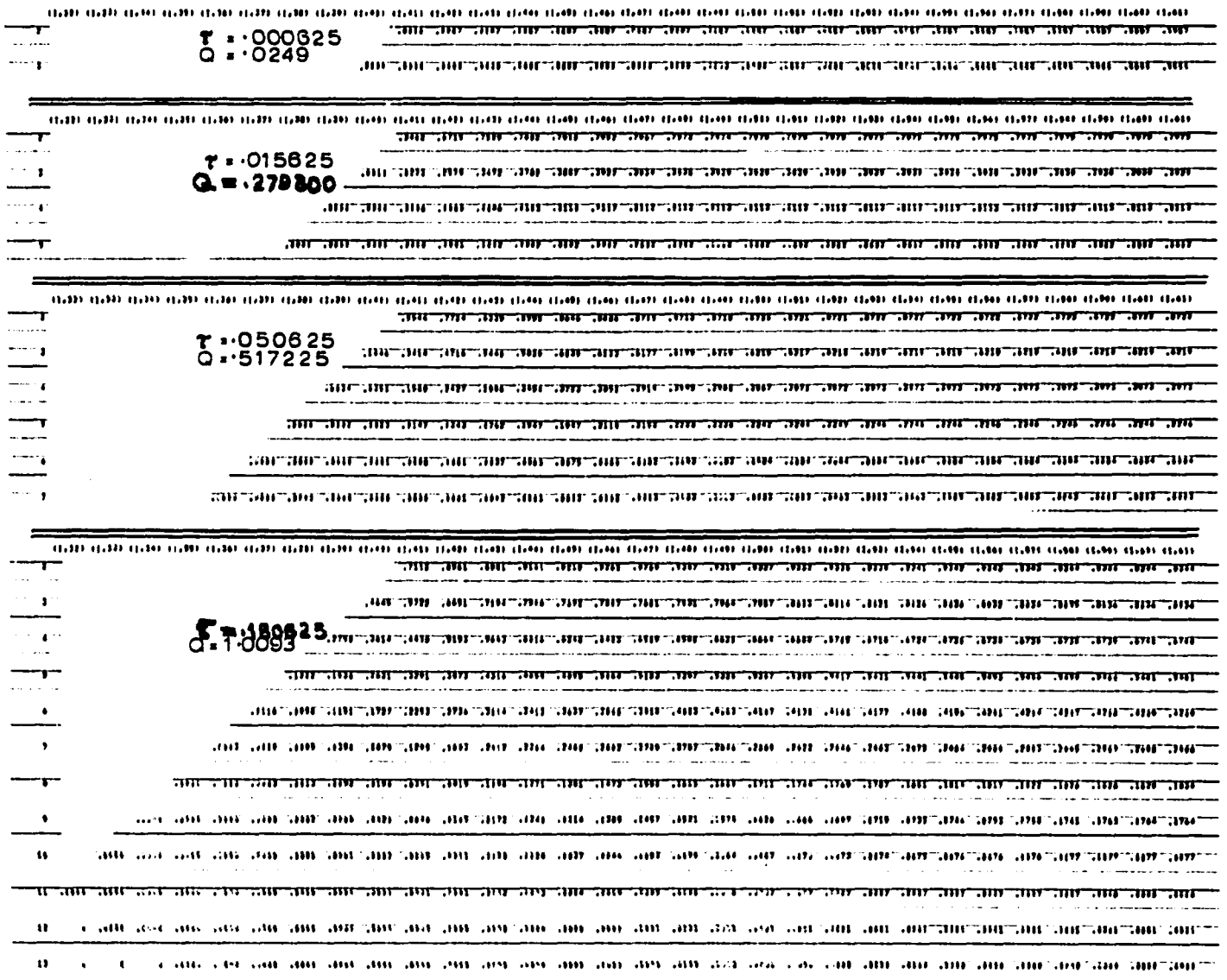


TABLE 16 (continued)

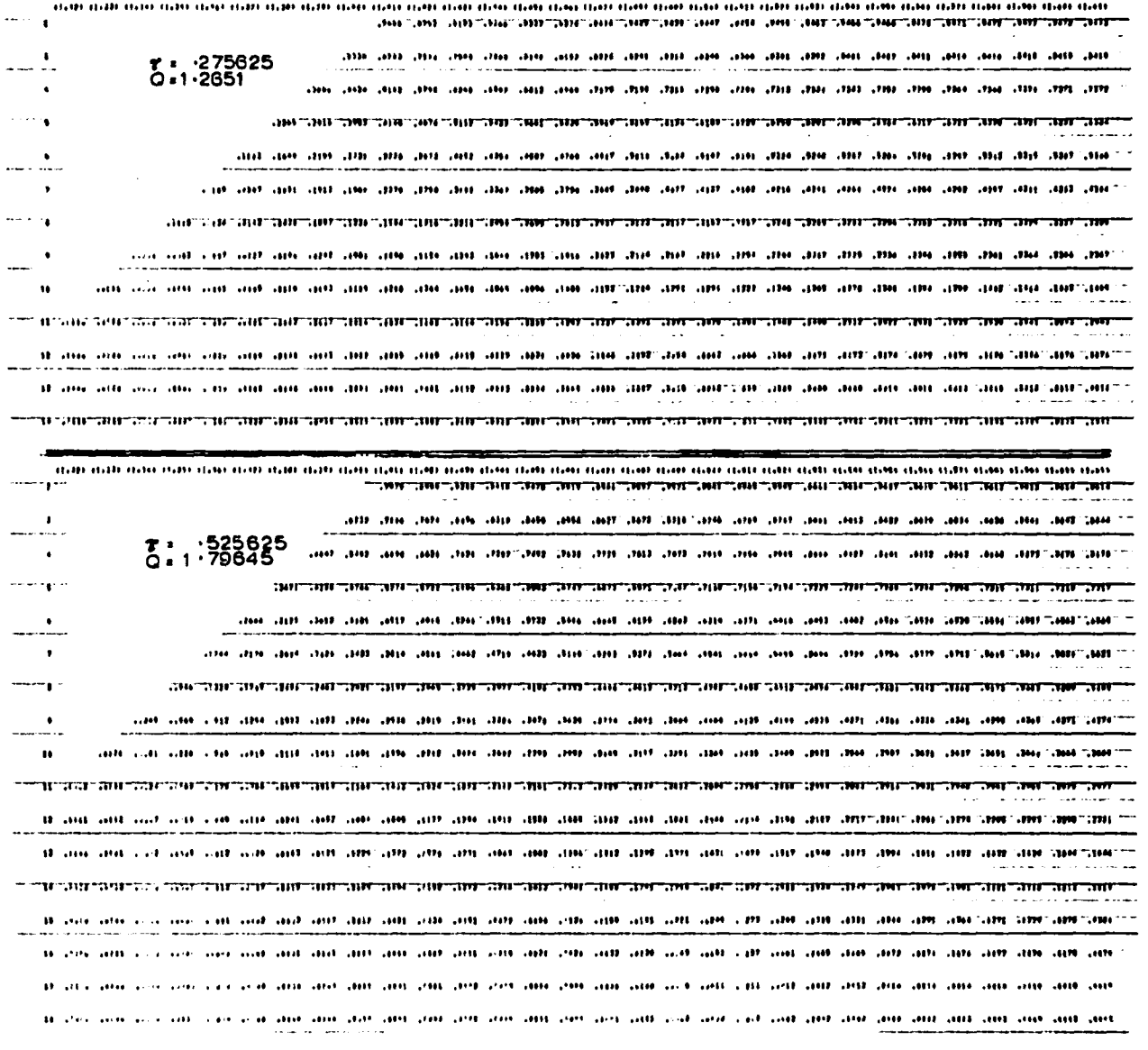


TABLE 16 (continued)

τ = ·680625
Q = 2·0723

TABLE 16 (continued)

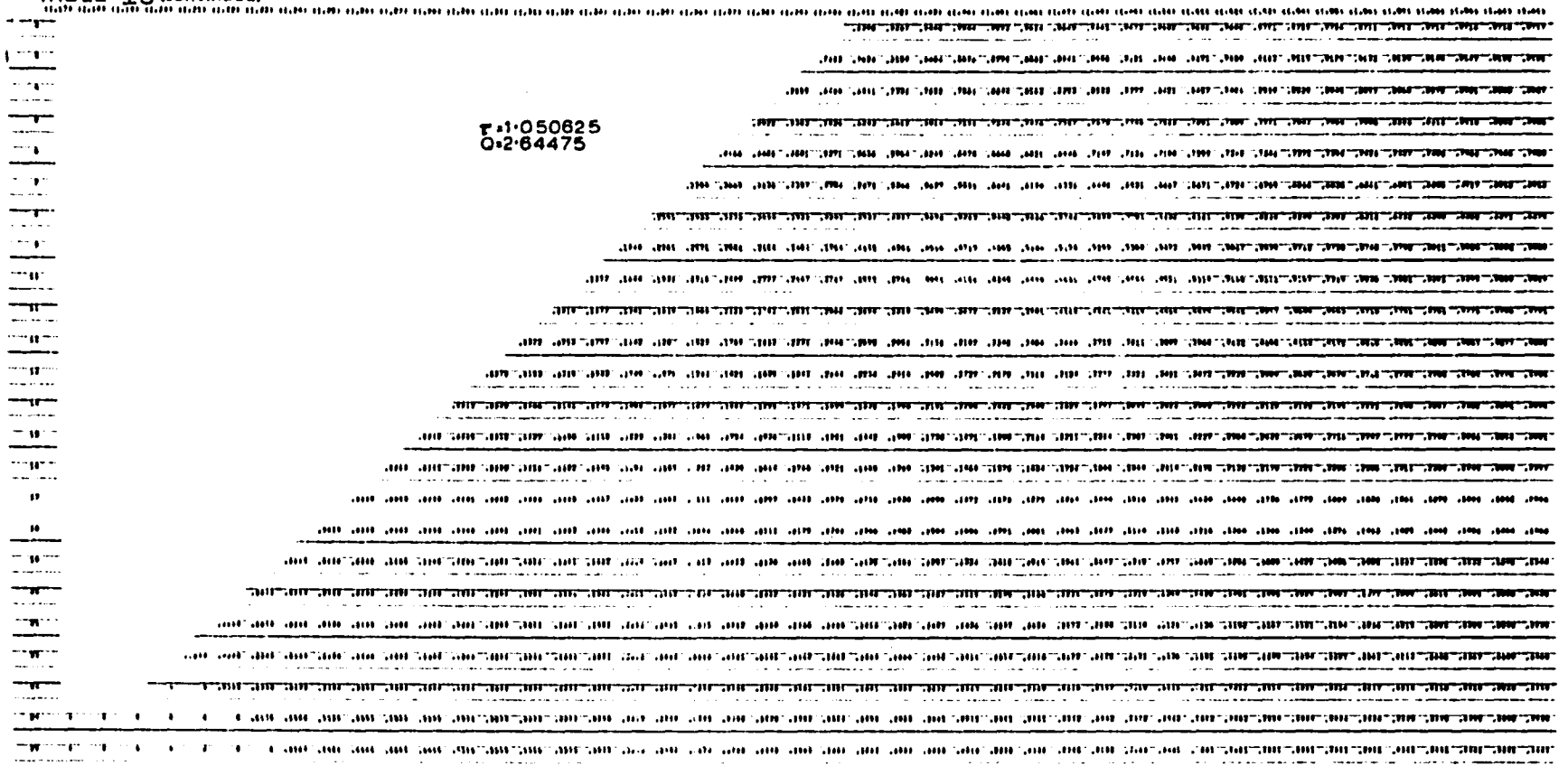


TABLE 16 (continued)

TABLE 16 (continued)

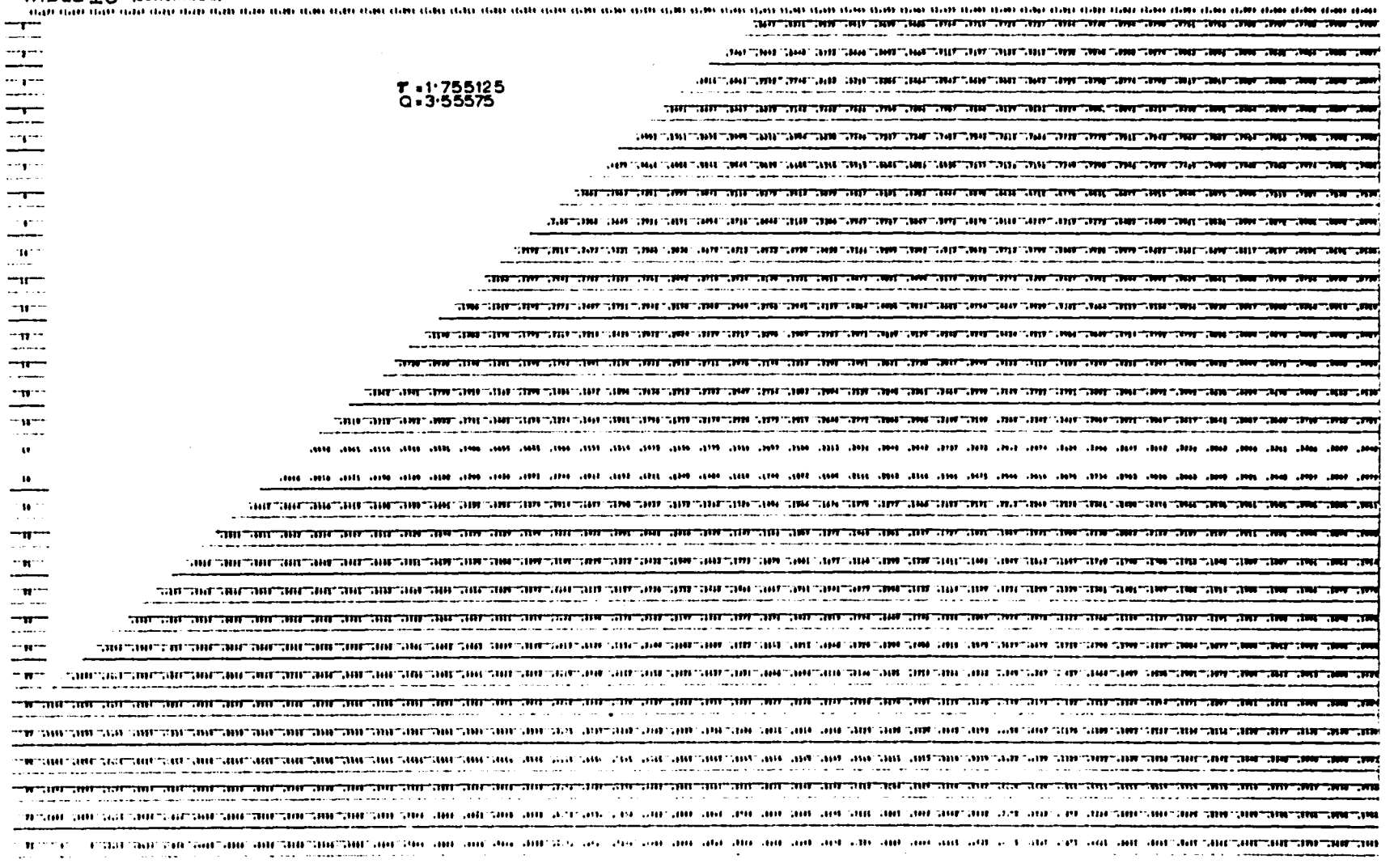


TABLE 16 (continued)

r = 2.030625
θ = 3.873375

TABLE 17

NUMERICAL SOLUTION OF THE EXAMPLE PROBLEM NO.2 FOR VARIOUS VALUES OF γ

γ = ·005625
Q = ·151825

γ = ·040625
Q = ·48480

γ = ·095625
Q = ·76055

γ = ·170625
Q = 1·029725

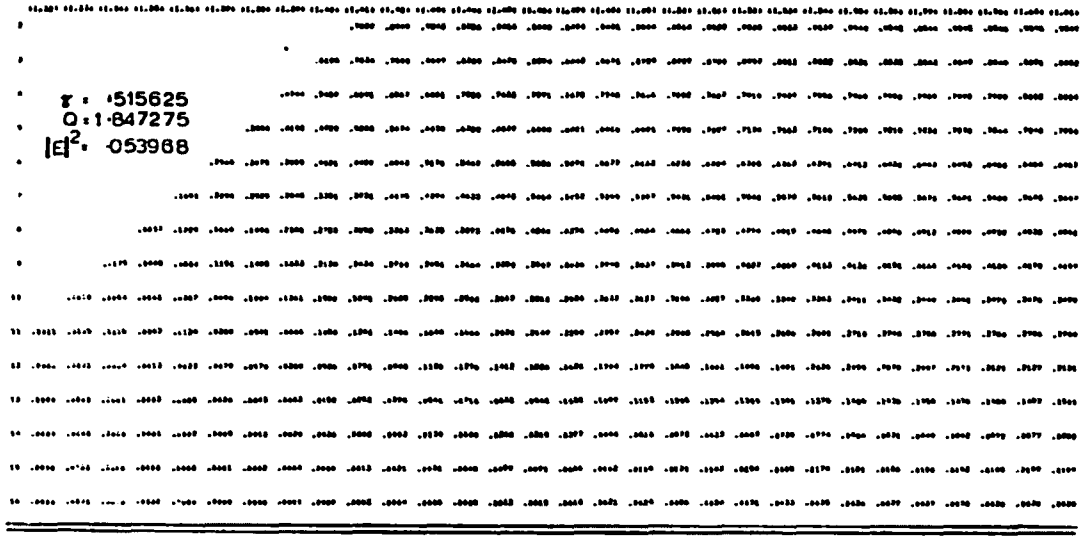
TABLE 17 (continued)

τ = ·265625
Q = 1·298675

τ = ·380625
Q = 1·570625

TABLE 17(continued)

τ = ·515625
Q = 1·847275
$|E|^2$ = ·053988



τ = ·670625
Q = 2·12950
$|E|^2$ = ·019757

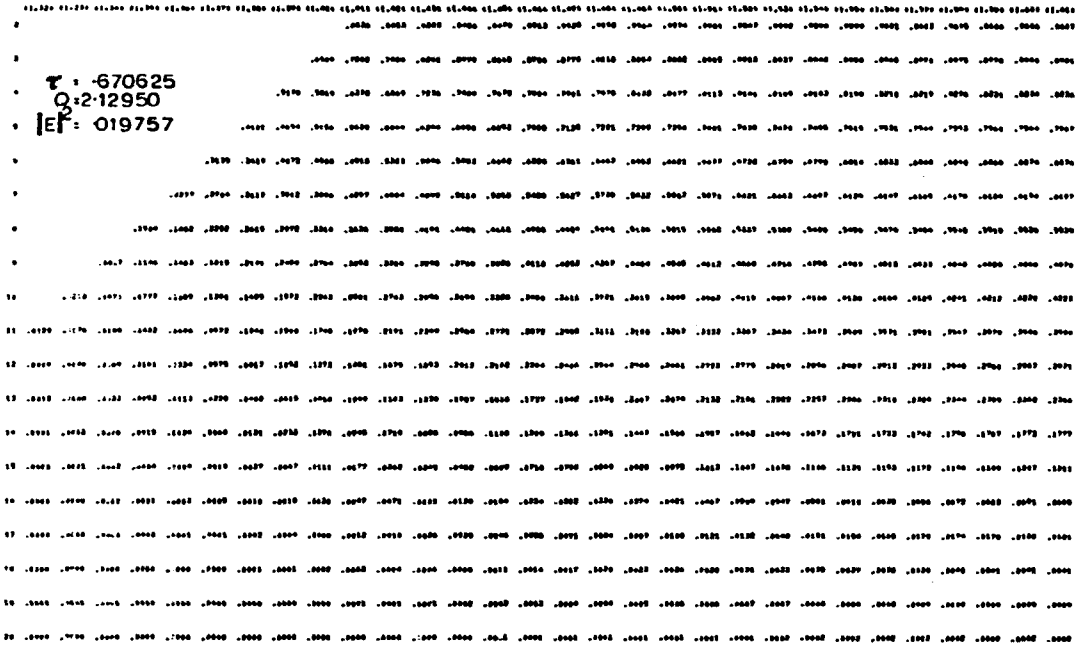


TABLE 17 (continued)

$\tau = .845625$
$Q = 2.41775$
$|E|^2 = .024953$

TABLE 17 (continued)

$\tau = 1.040625$
$Q = 2.712225$
$|E|^2 = .031842$

TABLE 17 (continued)

$\tau = 1.255625$
$Q = 3.013125$
$|E|^2 = .041396$

TABLE 17 (continued)

γ = 1·490625
Q = 3·320550
$|E|^2$ = ·054252

TABLE 17 (continued)

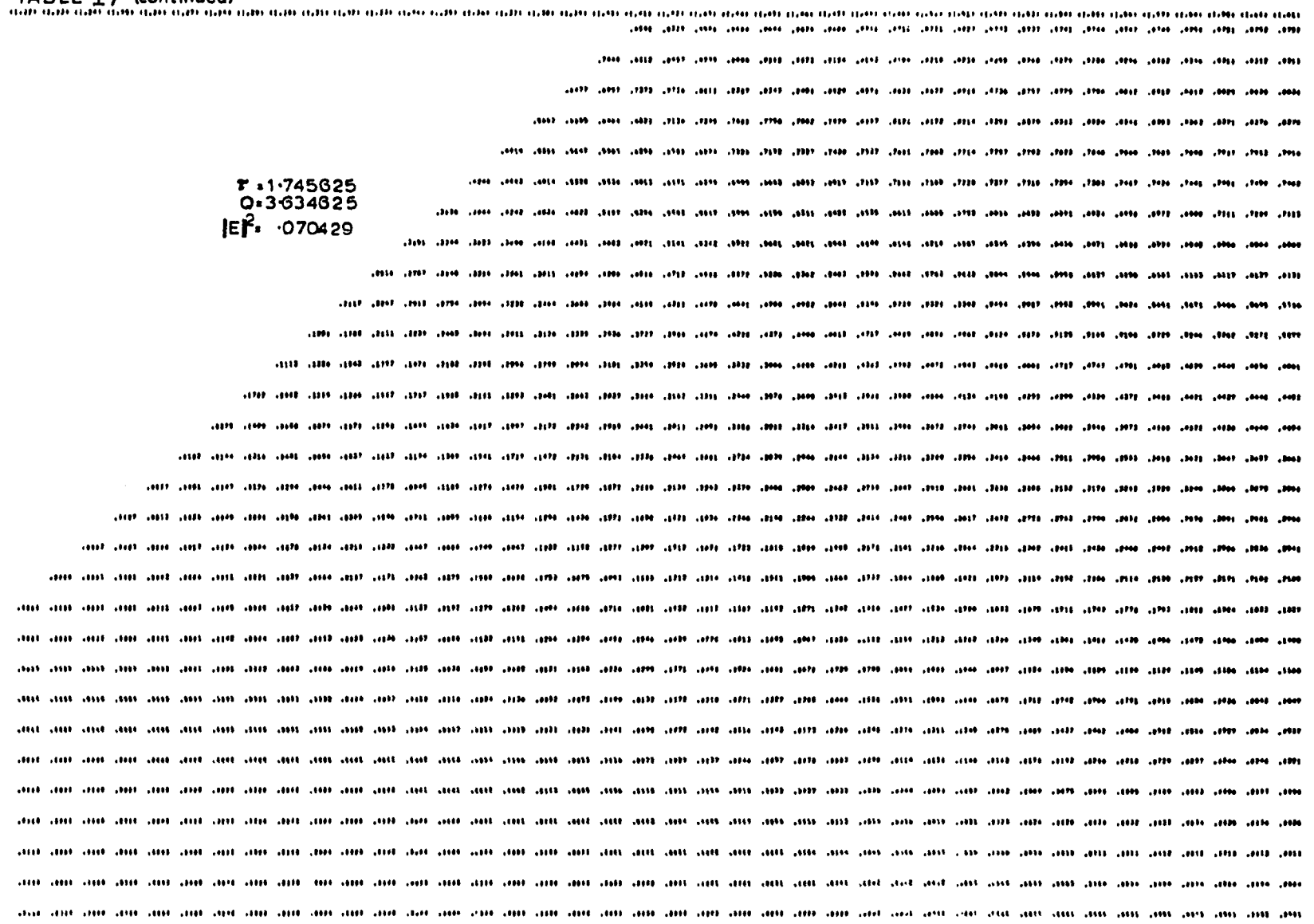


TABLE 17 (continued)

r : 2·020625
Q : 3·955350
REF. ·089860

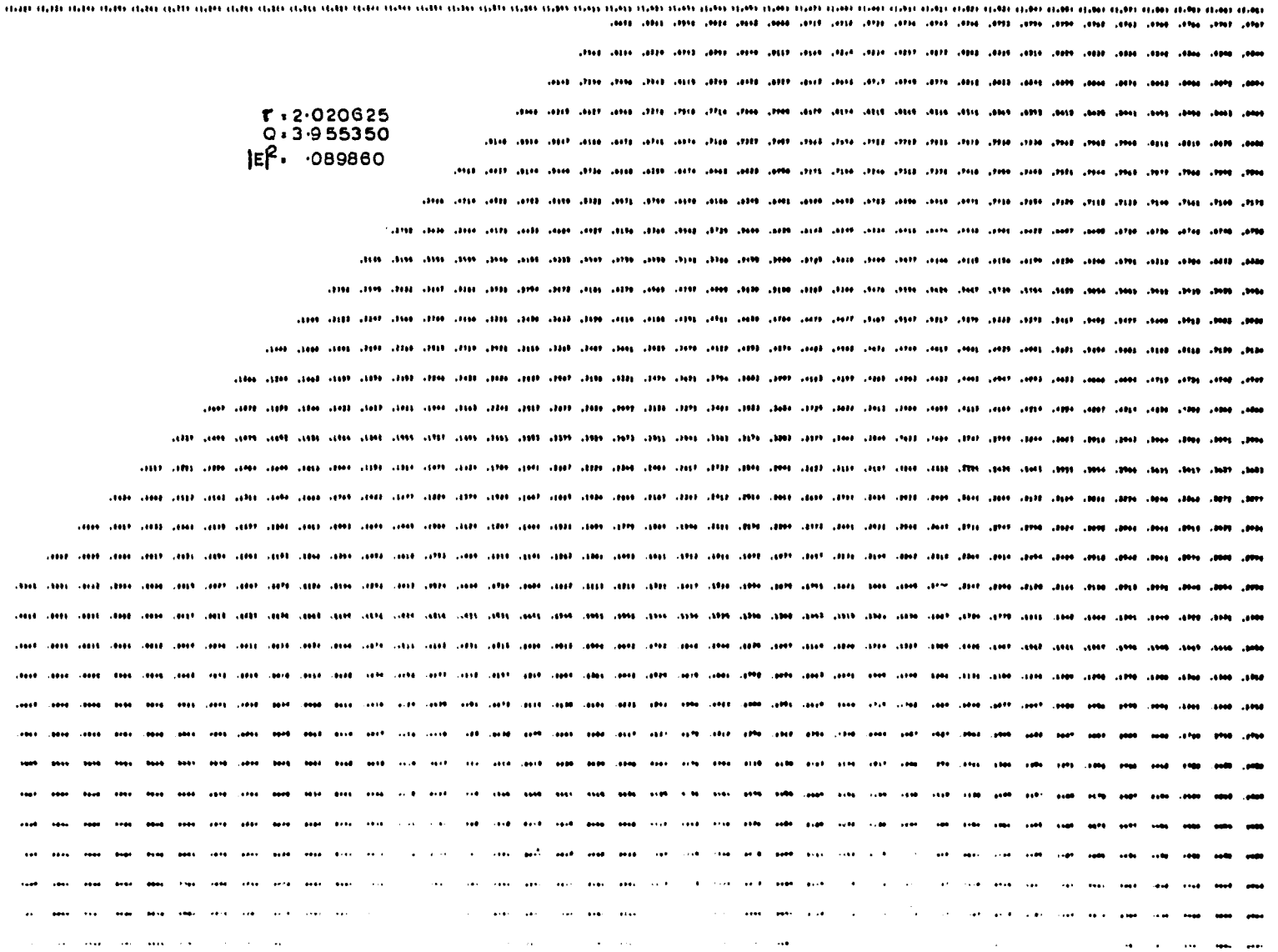


TABLE 17 (continued)

r = 2.020625
Q = 3.955350
$|\varepsilon|^2$ = .089860

TABLE 18

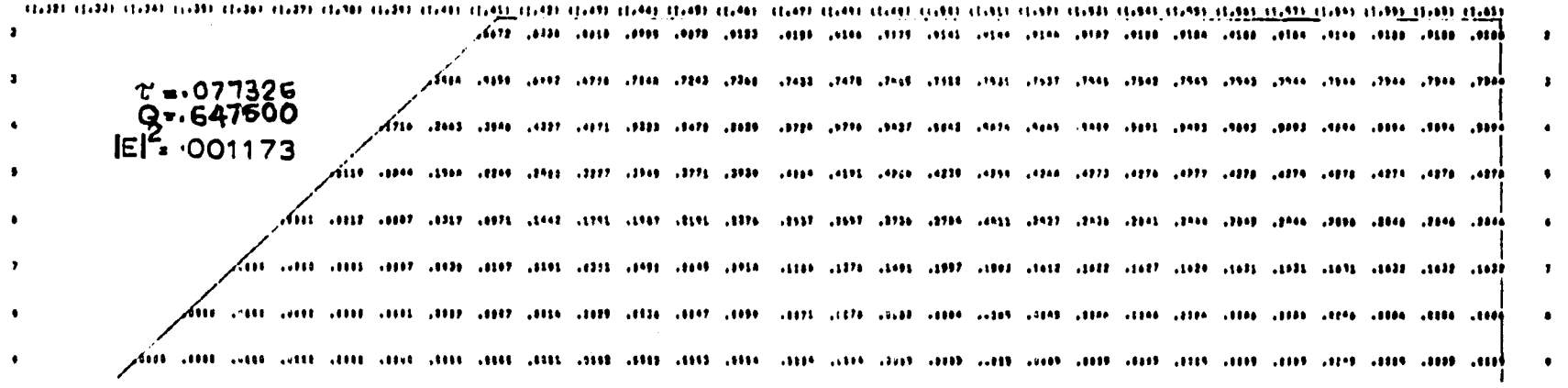
NUMERICAL SOLUTION OF THE EXAMPLE PROBLEM NO.3 FOR VARIOUS VALUES OF τ

$\tau = \cdot 000404$
$Q = \cdot 020160$
$|E|^2 = \cdot 000075$

$\tau = \cdot 010519$
$Q = \cdot 229712$
$|E|^2 = \cdot 001038$

$\tau = \cdot 035525$
$Q = \cdot 432352$
$|E|^2 = \cdot 001277$

TABLE 18 (continued)



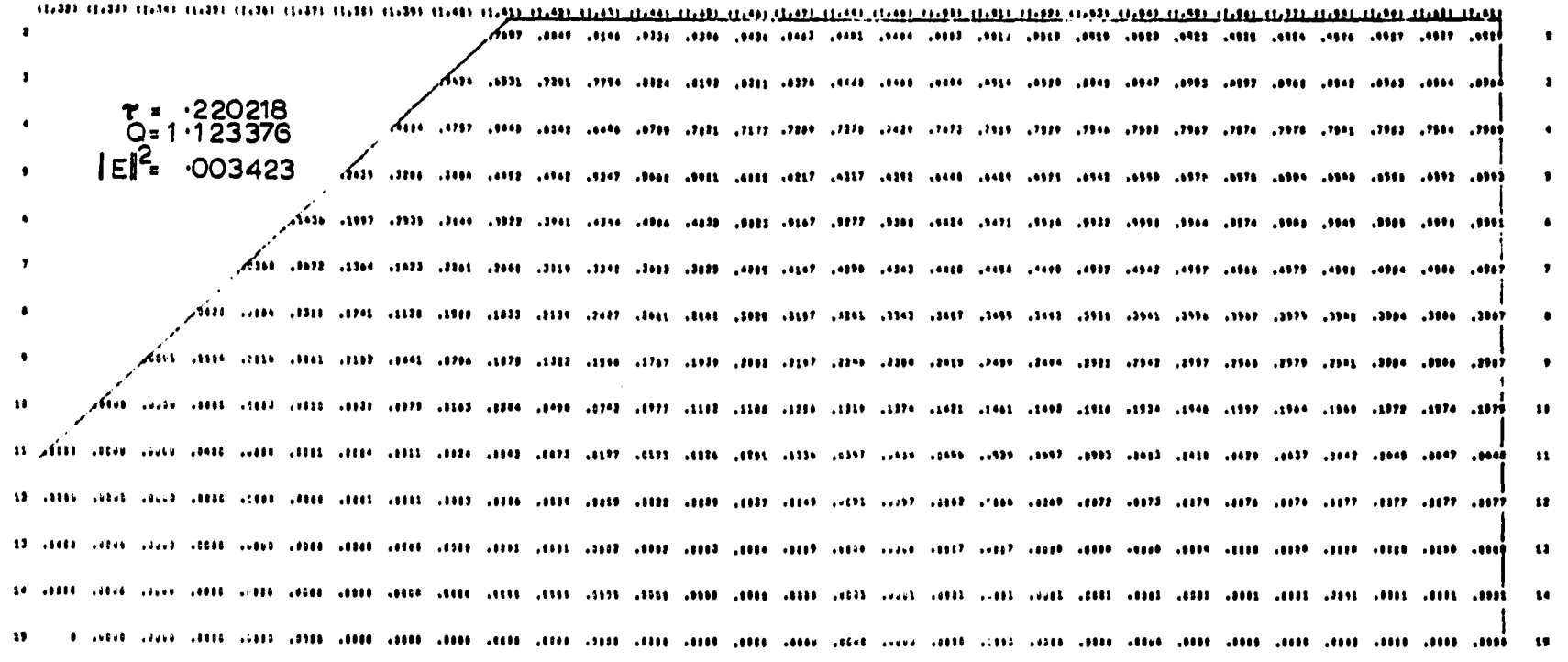


TABLE 18 (continued)

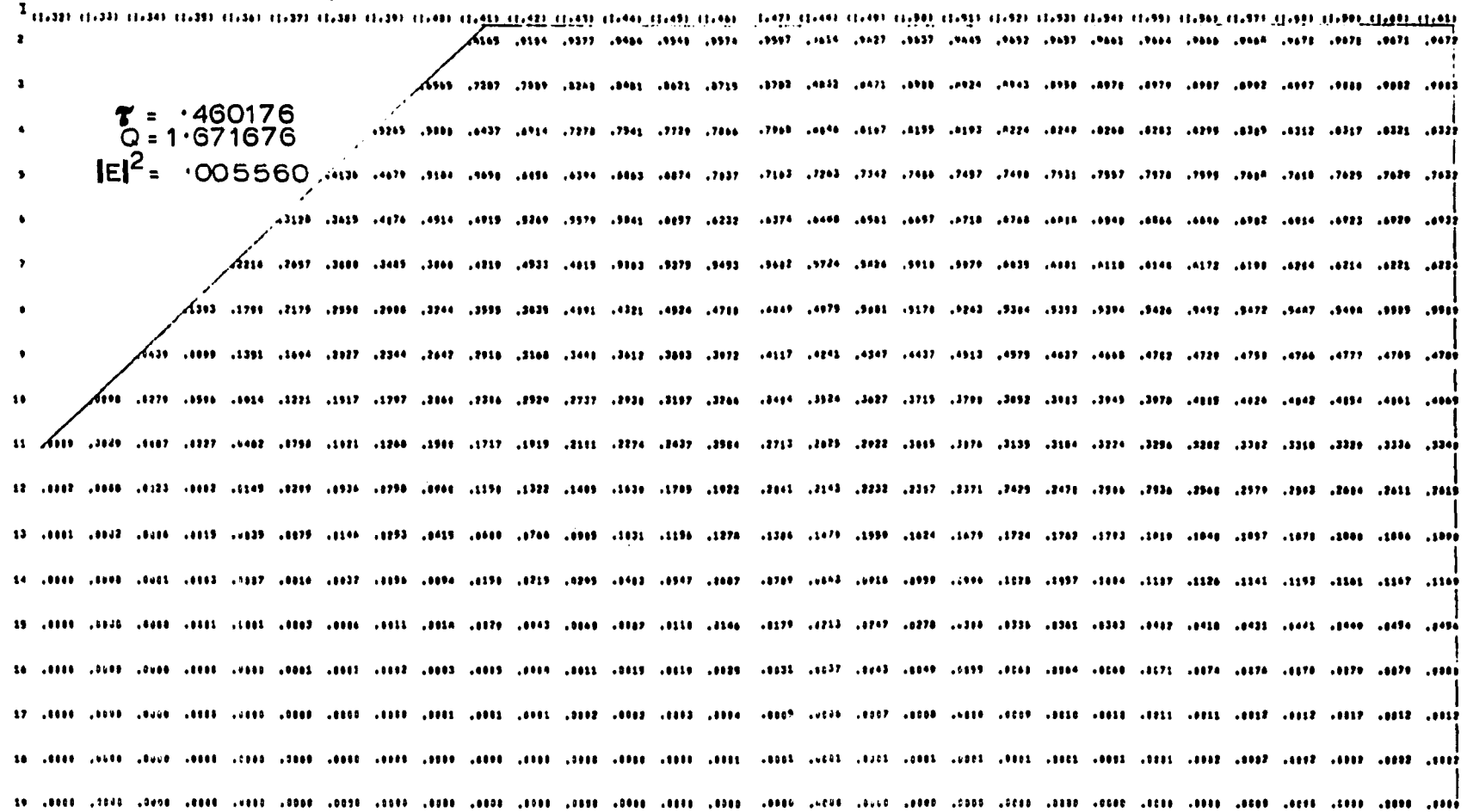


TABLE 18(continued)

τ = ·824419
Q = 2·308912
$|E|^2$ = ·014025

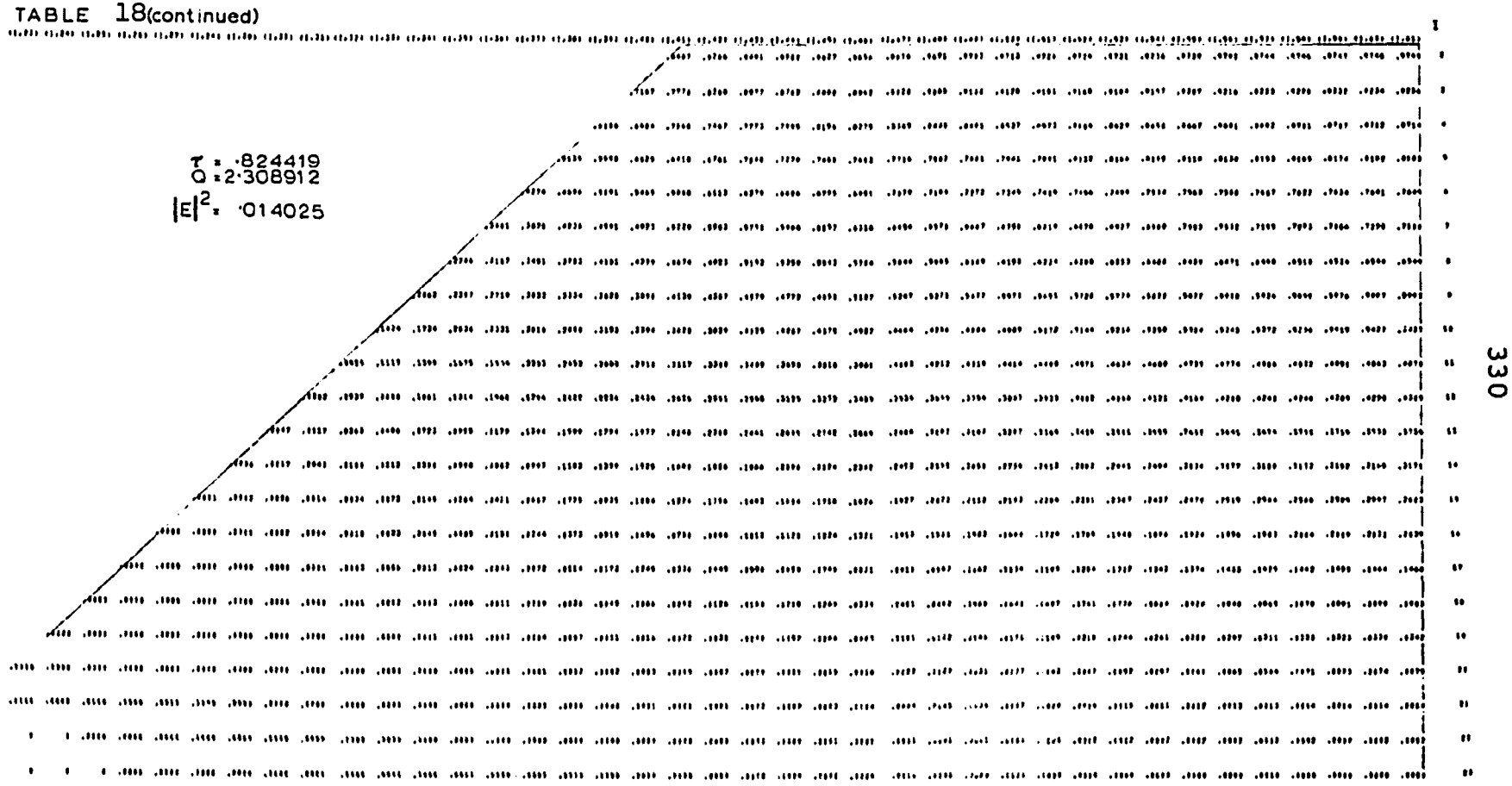


TABLE 18 (continued)

$\tau = 1.348595$
$Q = 3.054768$
$\|E\|^2 = .036302$

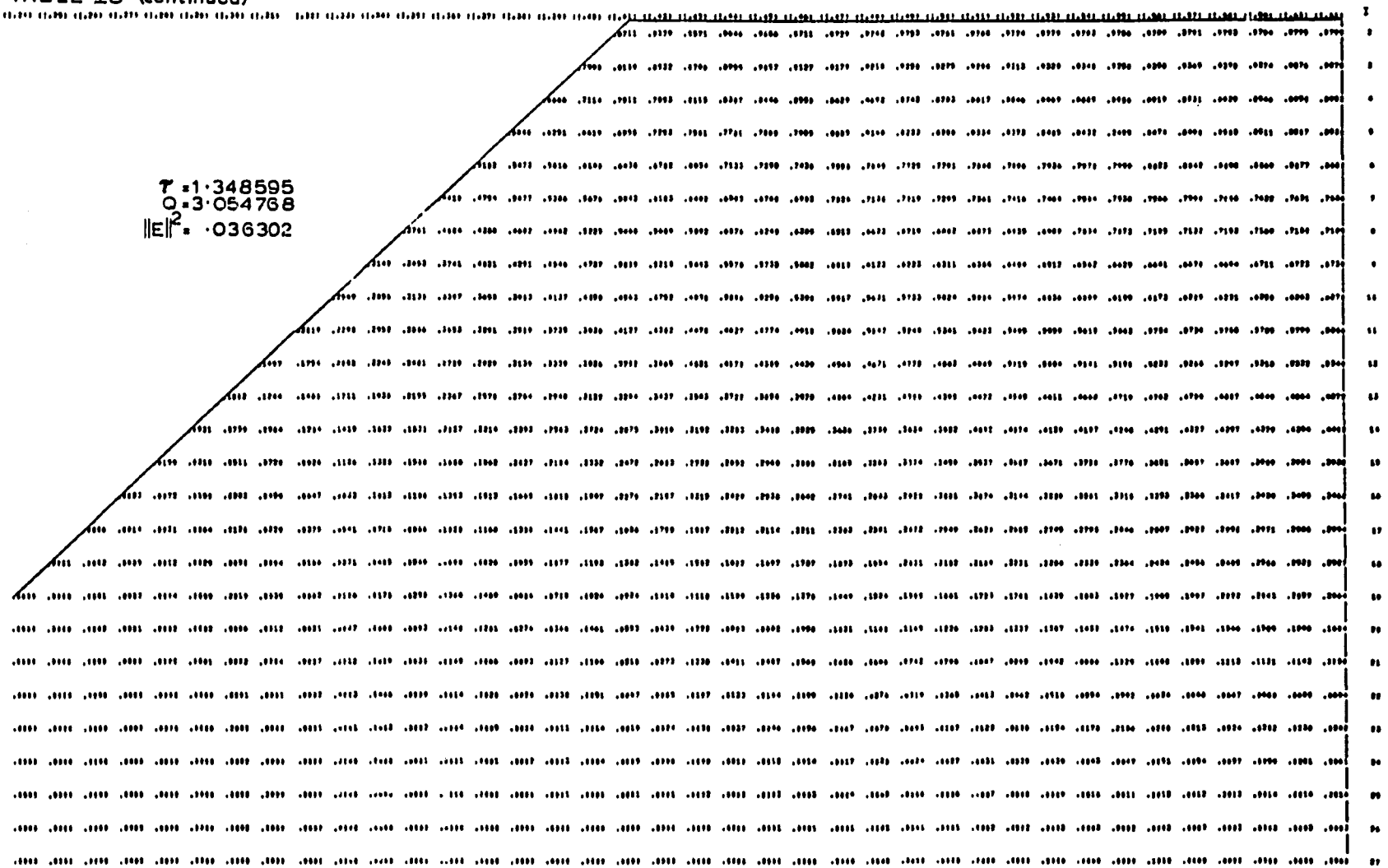


TABLE 19

NUMERICAL SOLUTION OF THE EXAMPLE PROBLEM NO. 4 FOR VARIOUS VALUES OF τ

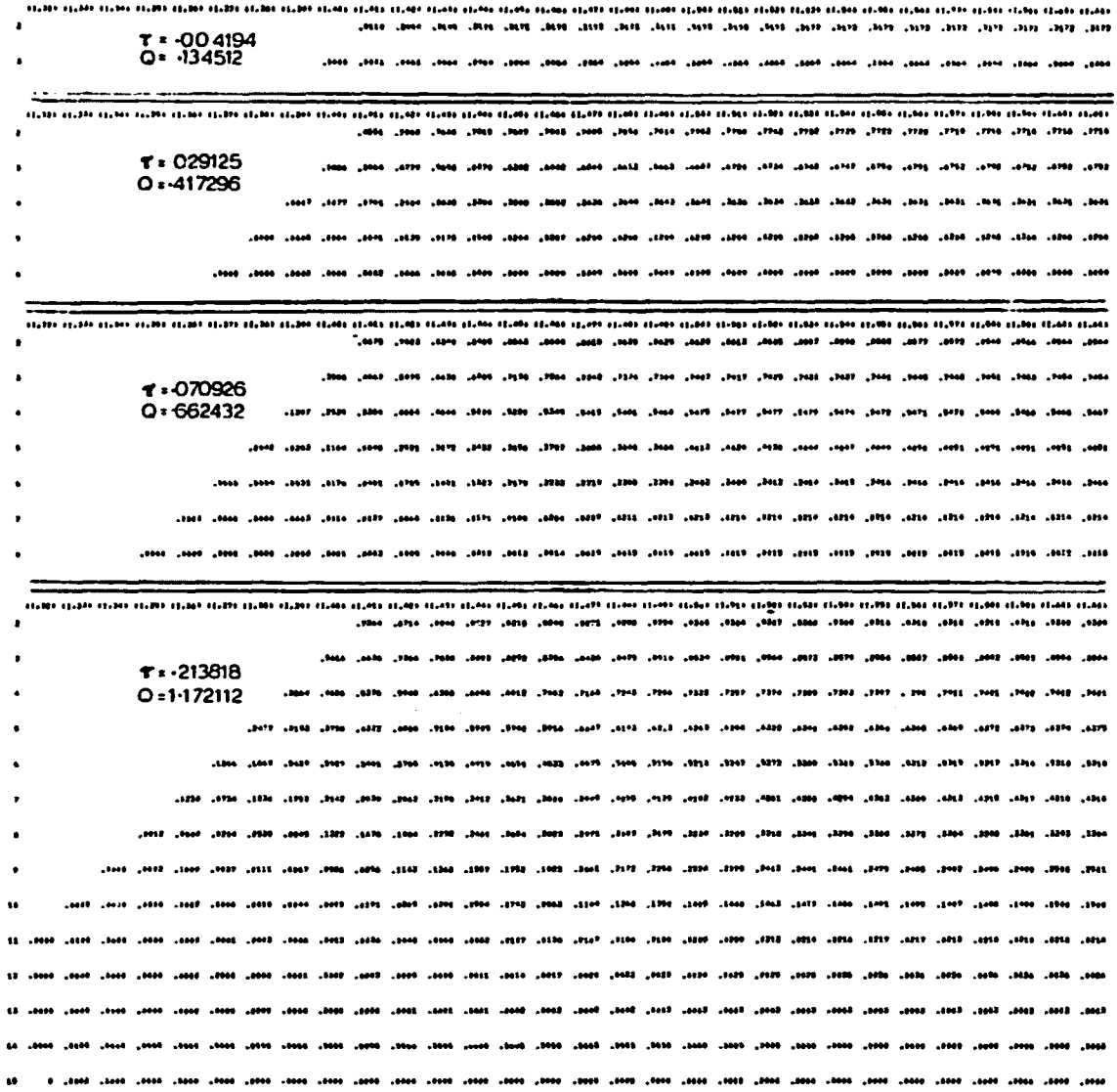


TABLE 19 (continued)

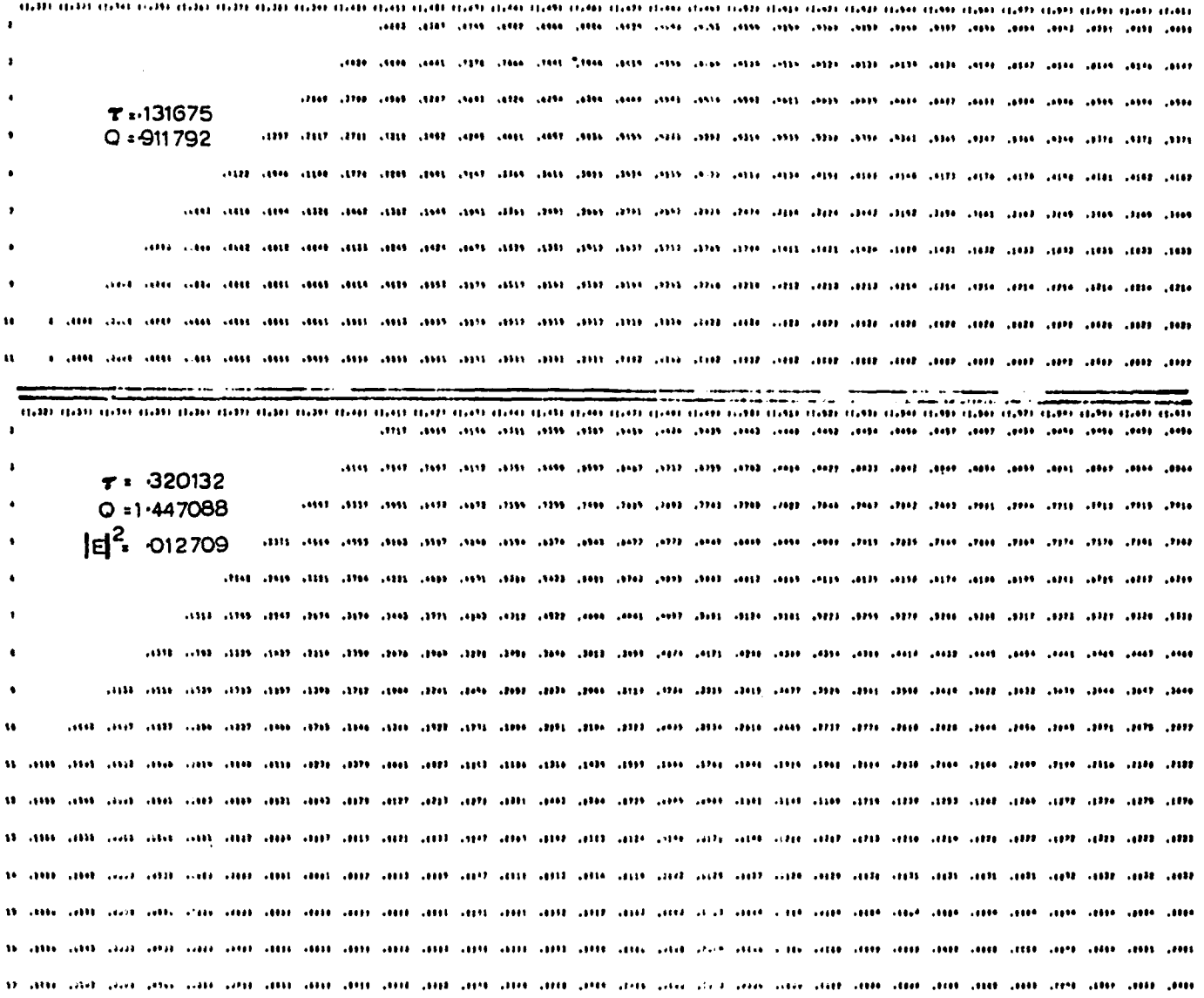


TABLE 19 (continued)

τ = .453776

O = 1.739984

$|E|^2$ = .013938

TABLE 19 (continued)

$\tau = .618362$

$Q = 2.053696$

$|E|^2 = .018155$

TABLE 19 (continued)

$\tau = 1.057482$

$Q = 2.755120$

$|E|^2 = .035543$

TABLE 19 (continued)

$\tau = 1{\cdot}342195$

$Q = 3{\cdot}148896$

$|E|^2 = {\cdot}049151$

TABLE 20

COMPUTED VALUES OF $X(x_1, \tau)$ FOR THE VARIOUS VALUES OF x_1 AND τ (RUN NUMBER 1)

τ	$\sqrt{\tau}$	$X(-1,\tau)$	$X(-0.2,\tau)$	$X(0,\tau)$	$X(0.2,\tau)$	$\frac{X(x_1,\tau)}{x_1} =$
0.105625	6.325	0.322	0.310	0.265	0.185	0.161
0.390625	0.625	0.615	0.574	0.525	0.435	0.330
0.855625	0.925	0.907	0.840	0.793	0.711	0.498
1.500625	1.225	1.175	1.100	1.043	0.980	0.665
2.323125	1.525	1.452	1.355	1.303	1.230	0.815

APPENDIX D

EXPERIMENTAL DATA AND ANALYSIS OF THE ONE-DIMENSIONAL CELL

TABLE 21

EXPERIMENTAL DETERMINATION OF THE AVERAGE BINARY DIFFUSION COEFFICIENT
FOR PHENOL-WATER SYSTEM IN WATER-RICH PHASE AT 30°C
TEST NO. C1.1-a, ξ = 0.2559

	Tube Number 1			Tube Number 2			Tube Number 3			Tube Number 4		
i	t_i hours	$t_i^{1/2}$	$X_i(t)$ mm	t_i hours	$t_i^{1/2}$	$X_i(t)$ mm	t_i hours	$t_i^{1/2}$	$X_i(t)$ mm	t_i hours	$t_i^{1/2}$	$X_i(t)$ mm
1	0.0835	0.289	0.80	0.100	0.316	0.90	0.117	0.342	1.2	0.1253	0.354	0.6
2	0.250	0.500	1.00	0.250	0.500	1.0	0.2663	0.516	1.4	0.2830	0.532	0.8
3	0.5170	0.719	1.1	0.4665	0.683	1.1	0.483	0.695	1.7	0.4998	0.707	0.9
4	1.5351	1.239	1.6	1.550	1.245	1.6	1.5006	1.225	2.3	1.515	1.231	1.5
5	2.5186	1.587	1.9	2.5313	1.591	1.8	2.5504	1.597	2.5	2.500	1.581	1.7
6	5.0176	2.240	2.5	5.0176	2.24	2.4	5.0176	2.240	3.2	5.0176	2.24	2.3
7	7.8961	2.810	2.9	7.896	2.81	3.4	7.8961	2.81	3.4	7.896	2.81	2.7
8	12.2500	3.500	3.5	12.250	3.50	3.6	12.2500	3.50	4.0	12.250	3.50	3.4
9	24.7009	4.97	4.8	24.701	4.97	5.0	24.7009	4.97	5.5	24.701	4.97	4.7
10	27.4576	5.24	5.0	27.458	5.24	5.2	27.4576	5.24	5.8	27.458	5.24	5.1
11	32.0356	5.66	5.3	32.0356	5.66	5.5	32.0356	5.66	6.1	32.0356	5.66	5.4
12	48.0249	6.93	6.7	48.025	6.93	6.9	48.0249	6.93	7.3	48.0249	6.93	6.6
13	55.056	7.42	7.1	55.056	7.42	7.4	55.056	7.42	7.8	55.056	7.42	7.1
14	73.960	8.60	8.1	73.960	8.60	8.3	73.960	8.60	8.8	73.960	8.60	8.2
15	119.902	10.95	10.0	119.902	10.95	10.2	119.902	10.95	10.8	119.902	10.95	10.0

n	15	15	15	15
ΣX_i	62.3	64.3	71.8	61.0
$\Sigma t_i^{1/2}$	62.654	62.655	62.695	62.725
Σt_i	411.205	411.198	411.216	411.224
$\Sigma X_i t_i^{1/2}$	390.846	402.934	434.494	389.534
$\frac{dX(t)}{d\sqrt{t}}$	0.8737	0.8992	0.9009	0.9028
$\tilde{D}$, mm^2/Hr	2.92	3.085	3.095	3.12
$\tilde{D}$, $cm^2/sec \times 10^{-5}$	0.811	0.857	0.8597	0.8667

TABLE 22

EXPERIMENTAL DETERMINATION OF THE AVERAGE BINARY DIFFUSION COEFFICIENT
FOR PHENOL-WATER SYSTEM IN WATER-RICH PHASE AT 30°C
TEST NO. C1.1-b, ξ = 0.2559

i	Tube Number 1			Tube Number 2			Tube Number 3			Tube Number 4		
	t_i hours	$t_i^{1/2}$	$X_i(t)$ mm	t_i hours	$t_i^{1/2}$	$X_i(t)$ mm	t_i hours	$t_i^{1/2}$	$X_i(t)$ mm	t_i hours	$t_i^{1/2}$	$X_i(t)$ mm
1	0.500	0.707	2.0	0.500	0.707	1.8	0.500	0.707	1.8	0.500	0.707	1.7
2	1.252	1.119	2.5	1.252	1.119	2.3	1.252	1.119	2.2	1.252	1.119	2.0
3	2.000	1.414	2.6	2.000	1.414	2.3	2.000	1.414	2.3	2.000	1.414	2.1
4	3.500	1.871	3.2	3.500	1.871	2.8	3.500	1.871	2.7	3.500	1.871	2.8
5	6.250	2.50	3.8	6.250	2.50	3.2	6.250	2.50	3.2	6.250	2.50	3.2
6	19.010	4.36	5.0	19.010	4.36	5.1	19.010	4.36	4.9	19.010	4.36	4.8
7	23.717	4.87	5.3	23.717	4.87	5.6	23.717	4.87	5.6	23.717	4.87	5.1
8	46.512	6.82	7.7	46.512	6.82	7.2	46.512	6.82	7.2	46.512	6.82	7.2
9	70.896	8.42	9.2	70.896	8.42	8.8	70.896	8.42	8.8	70.896	8.42	8.8
n		9			9			9			9	
Σx_i		41.3			39.1			38.7			37.7	
$\Sigma t_i^{1/2}$		32.081			32.081			32.081			32.081	
$\Sigma x_i t_i^{1/2}$		200.964			193.046			191.875			188.613	
Σt_i		173.637			173.637			173.637			173.637	
$\frac{dX(t)}{d\sqrt{t}}$, mm/Hr$^{1/2}$		0.9066			0.9054			0.9097			0.9148	
$\tilde{D}$, mm^2/Hr		3.1356			3.1284			3.1572			3.1932	
$\tilde{D}$, cm^2/sec x 10^{-5}		0.871			0.869			0.877			0.887	

TABLE 23

EXPERIMENTAL DETERMINATION OF THE AVERAGE BINARY DIFFUSION COEFFICIENT
FOR PHENOL-WATER SYSTEM IN WATER-RICH PHASE AT 40°C
TEST NO. C1.2-a, ξ = 0.2769

	Tube Number 1			Tube Number 2			Tube Number 3			Tube Number 4		
i	t_i hours	$t_i^{1/2}$	$X_i(t)$ mm	t_i hours	$t_i^{1/2}$	$X_i(t)$ mm	t_i hours	$t_i^{1/2}$	$X_i(t)$ mm	t_i hours	$t_i^{1/2}$	$X_i(t)$ mm
1	0.08	0.289	0.90	0.10	0.317	1.0	0.12	0.342	1.4	0.12	0.315	0.90
2	0.27	0.516	1.00	0.27	0.516	1.2	0.28	0.532	1.6	0.25	0.500	1.1
3	0.50	0.707	1.2	0.50	0.707	1.6	0.52	0.719	1.9	0.52	0.719	1.3
4	1.000	1.000	1.4	1.00	1.000	1.8	1.02	1.009	2.0	1.02	1.009	1.5
5	1.50	1.225	1.6	1.50	1.225	2.1	1.50	1.225	2.3	1.50	1.225	2.0
6	2.75	3.318	2.0	2.75	1.659	2.6	2.75	1.659	2.6	2.75	1.659	2.3
7	4.00	2.00	2.4	4.00	2.000	3.0	4.00	2.000	3.0	4.00	2.000	2.6
8	6.50	2.55	2.9	6.50	2.550	3.6	6.50	2.550	3.6	6.50	2.550	3.2
9	11.75	3.428	4.0	11.75	3.428	4.4	11.75	3.428	4.3	11.75	3.428	4.3
10	22.50	4.743	5.3	22.50	4.743	5.8	22.50	4.743	5.6	22.50	4.743	5.6
11	27.00	5.196	5.8	27.00	5.196	6.3	27.00	5.196	6.1	27.00	5.196	6.1
12	30.00	5.477	6.2	30.00	5.477	6.6	30.00	5.477	6.4	30.00	5.477	6.4
13	47.25	6.874	8.0	47.25	6.874	8.1	47.25	6.874	8.0	47.25	6.874	7.7
14	54.25	7.365	8.4	54.25	7.365	8.7	54.25	7.365	8.4	54.25	7.365	8.1
15	70.25	8.382	9.5	70.25	8.382	10.0	70.25	8.382	9.6	70.25	8.382	9.3
16	77.25	8.789	10.0	77.25	8.789	10.3	77.25	8.789	10.1	77.25	8.789	9.8
17	95.75	9.785	11.0	95.75	9.785	11.2	95.75	9.785	11.0	95.75	9.785	11.0
n		17			17			17			17	
ΣX_i		81.60			88.3			87.0			83.2	
$\Sigma t_i^{1/2}$		71.64			70.013			70.075			70.106	
$\Sigma X_i t_i^{1/2}$		515.473			541.101			529.786			515.275	
Σt_i		452.60			452.62			452.69			452.66	
$\frac{\overline{dX(t)}}{d\sqrt{t}}$, mm/Hr$^{1/2}$		1.13869			1.0802			1.0221			1.0527	
$\tilde{D}$, mm^2/Hr		4.228			3.80			3.40			3.61	
$\tilde{D}$, cm^2/sec x 10^{-5}		1.174			1.055			0.944			1.003	

TABLE 24

EXPERIMENTAL DETERMINATION OF THE AVERAGE BINARY DIFFUSION COEFFICIENT
FOR PHENOL-WATER SYSTEM IN WATER-RICH PHASE AT 40°C
TEST NO. C1.2-b, ξ = 0.2769

	Tube Number 1			Tube Number 2			Tube Number 3			Tube Number 4		
i	t_i hours	$t_i^{\frac{1}{2}}$	$X_i(t)$ mm	t_i hours	$t_i^{\frac{1}{2}}$	$X_i(t)$ mm	t_i hours	$t_i^{\frac{1}{2}}$	$X_i(t)$ mm	t_i hours	$t_i^{\frac{1}{2}}$	$X_i(t)$ mm
1	0.25	0.50	1.3	0.25	0.50	1.3	0.25	0.50	1.8	0.25	0.50	1.5
2	0.50	0.707	1.5	0.50	0.707	1.8	0.50	0.707	1.9	0.50	0.707	1.7
3	1.00	1.000	1.7	1.00	1.000	2.0	1.00	1.000	2.0	1.00	1.000	1.8
4	2.00	1.414	2.2	2.00	1.414	2.4	2.00	1.414	2.5	2.00	1.414	2.3
5	3.00	1.732	2.6	3.00	1.732	2.8	3.00	1.732	2.8	3.00	1.732	2.6
6	4.00	2.000	2.8	4.00	2.000	3.0	4.00	2.000	3.1	4.00	2.000	2.9
7	5.00	2.236	3.0	5.00	2.236	3.3	5.00	2.236	3.4	5.00	2.236	3.2
8	6.00	2.449	3.2	6.00	2.449	3.4	6.00	2.449	3.6	6.00	2.449	3.4
9	8.00	2.282	3.6	8.00	2.828	3.8	8.00	2.828	4.1	8.00	2.828	3.8
10	9.75	3.122	4.0	9.75	3.122	4.1	9.75	3.122	4.3	9.75	3.122	4.1
11	21.50	4.637	5.6	21.50	4.637	5.8	21.50	4.637	5.9	21.50	4.637	5.8
12	25.00	5.000	5.9	25.00	5.000	6.0	25.00	5.000	6.3	25.00	5.000	6.0
13	29.00	5.385	6.5	29.00	5.385	6.6	29.00	5.385	6.8	29.00	5.385	6.6
14	45.5	6.745	7.9	45.5	6.745	8.0	45.5	5.745	8.2	45.5	6.745	8.0
15	54.00	7.348	8.5	54.00	7.348	8.5	54.00	7.348	8.8	54.00	7.348	8.6
16	69.25	8.322	9.7	69.25	8.222	9.8	69.25	8.222	10.0	69.25	8.222	9.8
17	75.50	8.689	10.0	75.50	8.689	10.1	75.50	8.689	10.3	75.50	8.689	10.1
18	95.00	9.747	11.0	95.00	9.747	11.1	95.00	9.747	11.3	95.00	9.747	11.1
n		18			18			18			18	
ΣX_i		91.0			93.8			97.1			93.3	
$\Sigma t_i^{\frac{1}{2}}$		73.861			73.861			73.861			73.861	
Σt_i		454.25			454.25			454.25			454.25	
$\Sigma X_i t_i^{\frac{1}{2}}$		534.933			543.78			558.571			543.429	
$\frac{dX(t)}{d\sqrt{t}}$		1.068			1.088			1.059			1.062	
$\tilde{D}$, mm^2/Hr		3.719			3.860			3.657			3.677	
$\tilde{D}$, $cm^2/sec \times 10^{-5}$		1.033			1.072			1.016			1.021	

TABLE 25

EXPERIMENTAL DETERMINATION OF THE AVERAGE BINARY DIFFUSION COEFFICIENT
FOR PHENOL-WATER SYSTEM IN WATER-RICH PHASE AT 50°C
TEST NO. C1.3-a, ξ = 0.3236

	Tube Number 1			Tube Number 2			Tube Number 3			Tube Number 4		
i	t_i hours	$t_i^{1/2}$	$X_i(t)$ mm	t_i hours	$t_i^{1/2}$	$X_i(t)$ mm	t_i hours	$t_i^{1/2}$	$X_i(t)$ mm	t_i hours	$t_i^{1/2}$	$X_i(t)$ mm
1	0.25	0.500	2.2	0.25	0.500	1.3	0.25	0.500	1.4	0.25	0.500	1.8
2	0.50	0.707	2.4	0.50	0.707	1.7	0.50	0.707	1.7	0.50	0.707	2.1
3	1.00	1.000	2.6	1.00	1.000	2.0	1.00	1.000	2.0	1.00	1.000	2.5
4	2.00	1.414	3.0	2.00	1.414	2.5	2.00	1.414	2.6	2.00	1.414	2.9
5	4.00	2.000	3.8	4.00	2.000	3.3	4.00	2.000	3.3	4.00	2.000	3.7
6	6.00	2.449	4.4	6.00	2.449	3.9	6.00	2.449	3.9	6.00	2.449	4.3
7	8.50	2.828	4.8	8.00	2.828	4.5	8.00	2.828	4.5	8.00	2.828	4.9
8	10.25	3.202	5.1	10.25	3.202	4.8	10.25	3.202	4.8	10.25	3.202	5.2
9	12.00	3.464	5.5	12.00	3.464	5.2	12.00	3.464	5.0	12.00	3.464	5.6
10	25.25	5.025	7.6	25.25	5.025	7.3	25.25	5.025	7.2	25.25	5.025	7.8
11	27.50	5.244	7.8	27.50	5.244	7.6	27.50	5.244	7.50	27.50	5.244	8.0
n		11			11			11			11	
ΣX_i		49.2			44.1			43.9			48.8	
Σt_i		97.25			97.25			97.25				
$\Sigma t_i^{1/2}$		27.833			27.833			27.833				
$\Sigma X_i t_i^{1/2}$		156.064			146.183			144.655			158.027	
$\frac{dX(t)}{d\sqrt{t}}$		1.177			1.290			1.252			1.288	
$\tilde{D}$, mm^2/Hr		3.3084			3.9708			3.744			3.96	
$\tilde{D}$, $cm^2/sec \times 10^{-5}$		0.919			1.103			1.040			1.1	

TABLE 26

EXPERIMENTAL DETERMINATION OF THE AVERAGE BINARY DIFFUSION COEFFICIENT
FOR PHENOL-WATER SYSTEM IN WATER-RICH PHASE AT 50°C
TEST NO. C1.3-b, ξ = 0.3236

	Tube Number 1			Tube Number 2			Tube Number 3			Tube Number 4		
i	t_i hours	$t_i^{1/2}$	$X_i(t)$ mm	t_i hours	$t_i^{1/2}$	$X_i(t)$ mm	t_i hours	$t_i^{1/2}$	$X_i(t)$ mm	t_i hours	$t_i^{1/2}$	$X_i(t)$ mm
1	0.25	0.500	1.0	0.25	0.500	2.0	0.25	0.500	1.6	0.25	0.500	1.3
2	0.50	0.707	1.3	0.50	0.707	2.7	0.50	0.707	1.8	0.50	0.707	1.6
3	1.00	1.000	1.5	1.00	1.000	2.9	1.00	1.000	2.0	1.00	1.000	1.8
4	2.00	1.414	2.0	2.00	1.414	3.4	2.00	1.414	2.5	2.00	1.414	2.3
5	4.00	2.000	2.9	4.00	2.000	4.2	4.00	2.000	3.4	4.00	2.000	3.1
6	6.00	2.449	4.0	6.00	2.449	5.4	6.00	2.449	4.5	6.00	2.449	4.2
7	13.00	3.605	5.0	13.00	3.605	6.4	13.00	3.605	5.5	13.00	3.605	5.2
8	24.00	4.899	6.6	24.00	4.899	7.8	24.00	4.899	7.0	24.00	4.899	6.8
9	28.00	5.291	7.2	28.00	5.291	8.4	28.00	5.291	7.6	28.00	5.291	7.4
10	31.00	5.568	7.6	31.00	5.568	8.8	31.00	5.568	8.0	31.00	5.568	7.8
11	48.50	6.964	9.3	48.50	6.964	10.5	48.50	6.964	9.7	48.50	6.964	9.5
12	54.5	7.382	10.0	54.50	7.382	11.1	54.50	7.382	10.4	54.50	7.382	10.2
13	72.25	8.500	11.5	72.25	8.500	12.8	72.25	8.25	11.8	72.25	8.500	11.7
n		13			13			13			13	
ΣX_i		69.9			86.4			75.8			72.9	
$\Sigma t_i^{1/2}$		50.279			50.279			50.279			50.279	
Σt_i		285.00			285.00			285.00			285.00	
$\Sigma X_i t_i^{1/2}$		388.488			449.995			408.929			398.826	
$\overline{dX/d\sqrt{t}}$		1.305			1.257			1.279			1.262	
$\bar{D}$, mm^2/Hr		3.931			3.773			3.906			3.8021	
$\bar{D}$, $cm^2/sec \times 10^{-5}$		1.092			1.048			1.085			1.05614	

TABLE 27

EXPERIMENTAL DETERMINATION OF THE EFFECT OF CONCENTRATION ON AVERAGE BINARY DIFFUSION OF WATER-RICH PHASE AT 55°C

	Test No. C2.1-a			Test No. C2.2-a			Test No. C2.2-b			Test No. C2.3-a			Test No. C2.4-a			Test No. C2.4-b		
$(C_s^I - C_B)$	0.503 moles/Lit.			0.927 moles/Lit.			0.927 moles/Lit.			1.189 moles/Lit.			1.459 moles/Lit.			1.459 moles/Lit.		
ξ	0.220			0.2972			0.2972			0.3344			0.3671			0.3671		
i	t_i hour	$\sqrt{t_i}$ $hour^{\frac{1}{2}}$	$X_i(t)$ mm	t_i hour	$\sqrt{t_i}$	$X_i(t)$	t_i hour	$\sqrt{t_i}$	$X_i(t)$ mm	t_i hour	$\sqrt{t_i}$	$X_i(t)$	t_i hour	$\sqrt{t_i}$	$X_i(t)$ mm	t_i hour	$\sqrt{t_i}$	$X_i(t)$ mm
1	0.20	0.45	1.15	0.15	0.39	1.70	0.17	0.41	1.75	0.15	0.39	1.60	0.20	0.45	2.05	0.27	0.52	1.3
2	0.83	0.91	1.40	00.85	0.92	2.35	0.87	0.93	2.50	00.53	0.73	2.05	0.53	0.73	2.70	0.50	0.71	2.45
3	2.13	1.46	1.75	2.05	1.43	2.80	2.07	1.43	2.60	2.27	1.51	2.80	1.20	1.10	3.25	1.033	1.01	2.55
4	3.90	1.98	1.95	4.52	2.13	3.30	4.52	2.13	3.10	3.83	1.96	3.35	3.03	1.74	4.65	1.67	1.29	2.95
5	5.65	2.38	2.25	11.28	3.36	4.75	11.32	3.37	4.60	6.52	2.55	4.20	5.25	2.30	5.60	4.78	2.19	4.35
6	7.22	2.69	2.30	14.30	3.78	4.85	14.32	3.78	4.75	10.13	3.18	4.85	8.38	2.89	6.10	10.08	3.18	5.70
7	9.80	3.13	2.80	19.32	4.40	5.60	19.33	4.40	5.60	19.98	4.47	6.15	13.395	3.66	7.60	11.83	3.44	6.25
8	13.38	3.65	2.95	24.47	4.95	6.45	24.48	4.95	6.55	22.97	4.79	6.45	20.85	4.57	8.90			
9	32.22	4.82	3.65							27.17	5.21	7.15						
10	26.25	5.12	4.00							30.82	5.55	7.30						
11	30.47	5.52	4.05															
12	34.08	5.82	4.30															
n	12			8			8			10			8			7		
$\Sigma X_i(t)$	32.55			31.80			31.50			49.50			40.85			25.6		
Σ/t_i	37.95			21.36			21.40			30.34			17.44			12.34		
Σt_i	157.12			77.02			77.12			124.28			52.90			30.20		
$\Sigma X_i\sqrt{t_i}$	124.80			104.7			103.90			174.40			113.60			58.00		
$\overline{dX(t)}/d\sqrt{t}$	.593			.978			.985			1.090			1.65			1.53		
$\breve{D}$, mm^2/Hr	1.7212			2.7072			2.7461			2.656			5.053			4.343		
$\breve{D}$, $cm^2/sec \times 10^5$	0.478			0.752			0.768			0.738			1.404			1.2064		

TABLE 28

EXPERIMENTAL DETERMINATION OF THE AVERAGE BINARY DIFFUSION COEFFICIENT FOR PHENOL-WATER SYSTEM IN PHENOL-RICH PHASE

	Test No. C3.1-a			Test No. C3.1-b		
	Temperature = 55°C C_B = 4.779 Moles H_2O/Lit. $\bar{\lambda}$ = 2.3794 β = 0.39285 D^{II}= 4.698 mm^2/Hr			Temperature = 55°C C_B = 4.6620 $\bar{\lambda}$ = 2.3652 β = 0.39035 D^{II}= 4.698 mm^2/Hr		
i	t_i hours	$t_i^{\frac{1}{2}}$	$X_i(t)$ mm	t_i hours	$t_i^{\frac{1}{2}}$	$X_i(t)$ mm
1	0.30	0.5477	0.745	0.50	0.7071	1.44
2	0.533	0.7300	0.970	0.917	0.9576	1.90
3	1.000	1.000	1.290	1.70	1.3034	2.310
4	2.067	1.4380	1.825	2.30	1.516	2.535
5	3.783	1.944	2.392	3.30	1.8169	2.91
6	9.000	3.000	3.630	11.00	3.316	4.584
7	16.900	4.111	5.031	13.883	3.728	5.048
8	19.417	4.4046	5.22	15.317	3.911	5.268
9				21.167	4.604	5.968
n		8			9	
ΣX_i		21.030			31.963	
$\Sigma t_i^{\frac{1}{2}}$		17.1753			21.860	
Σt_i		53.000			70.084	
$\Sigma X_i t_i^{\frac{1}{2}}$		64.4249			97.0778	
$\overline{dX}/d\sqrt{t}$		1.2000			1.1445	
$Z = \xi\sqrt{\frac{D_I}{D_{II}}}$		0.27792			0.26384	
Ze^{Z^2}erfc Z		0.20841			0.20095	
ξe^{ξ^2}erf ξ		0.2345			0.23214	
ξ		0.428512			0.42485	
$\tilde{D}^I$, mm^2/Hr		1.9606			1.814	
$\tilde{D}^I$, cm^2/sec		0.5446×10^{-5}			0.5039×10^{-5}	

APPENDIX E

EXPERIMENTAL DATA AND ANALYSIS OF THE TWO-DIMENSIONAL CELL

APPENDIX E

ANALYSIS OF DATA

TEST NUMBERS 3.2-1 AND 3.2-2

Shape of the boundary: 1 cm x 1 cm square

Solution in the cell: Phenol-saturated water

Solution on the boundary: Phenol with 8.918 Wt% water

Temperature: 55±0.25°C

C_∞ = 47.53 moles/liter of H_2O

C_s^I = 23.03 moles/liter of H_2O

C_s^{II} = 47.53 moles/liter of H_2O

C_B = 5.088 moles/liter of H_2O

$$\bar{\lambda} = \frac{(C_s^{II} - C_s^I)\sqrt{\pi}}{(C_s^I - C_B)} = 2.4206$$

$$\mu = \frac{C_s^{II} - C_\infty}{C_s^I - C_B} = 0.000$$

$$\tilde{D}^I = 1.887 \text{ mm}^2/\text{Hr}$$

$$\chi_1^{-1}(x) = \bar{\lambda} + B/\chi_2(\xi\sqrt{\tilde{D}^I/\tilde{D}^{II}})$$

where

$$\chi_1(x) = xe^{+x^2} \text{ erf } x$$

$$\chi_2(x) = xe^{x^2} \text{ erfc } x$$

$$\chi_1^{-1}(\xi) = 2.4206$$

$$\chi_1(\xi) = 0.4172$$

$$\xi = 0.5464$$

Assuming that $X(-1,t) = 2\xi\sqrt{\omega \tilde{D}^I t/a^2}$ i.e., at $x_1 = -1$, the concentration field is essentially one dimensional, one can write,

$$\frac{d\left(\bar{X}(-1,t)\right)}{d\left(\sqrt{t/a^2}\right)} = 1.0928\ \sqrt{1.887}\ \omega^{\frac{1}{2}} = 1.5012\ \omega^{\frac{1}{2}}$$

where

$$\bar{X}(-1,t) = \frac{1}{n}\sum_{t}^{n} X_i(-1,t)$$

n = number of regions considered.

TABLE 29

EVALUATION OF THE EFFECTIVE BINARY DIFFUSION COEFFICIENT OF PHENOL-WATER SYSTEM IN WHATMAN FILTER PAPER NUMBER 52

Test Number	$\bar{X}_i(-1,t)$	$t_i^{\frac{1}{2}}/a$	t_i/a^2	$\frac{t_i^{\frac{1}{2}}}{a}\bar{X}_i(-1,t)$	i
	0.1245	0.1095	0.0120	0.01363	1
	0.2186	0.1789	0.0320	0.03911	2
	0.5034	0.3950	0.1560	0.19884	3
3.2-1	0.8387	0.6185	0.3827	0.51873	4
	1.0558	0.8416	0.7087	0.88856	5
	1.3070	1.0344	1.0707	1.35196	6
	0.0716	0.0774	0.0060	0.00554	7
	0.1175	0.1034	0.0107	0.01215	8
	0.2220	0.2114	0.0447	0.04693	9
3.2-2	0.499	0.4000	0.1600	0.19960	10
	0.7682	0.6033	0.3640	0.46345	11
	1.2656	0.9750	0.9507	1.23396	12
Σ	6.9984	5.5484	3.8981	4.97246	n=12

$$\frac{d\bar{X}(-1, t/a)}{d(\sqrt{t/a^2})} = \frac{n\sum_i (t_i^{\frac{1}{2}}/a)\bar{X}_i - \sum \bar{X}_i \sum (t_i^{\frac{1}{2}}/a)}{n\sum_i (t_i/a^2) - (\sum_i t_i^{\frac{1}{2}}/a)^2}$$

$$= \frac{59.66952 - 38.82992}{46.772 - 30.78474}$$

$$= 1.30308$$

Therefore

$$\omega^{\frac{1}{2}} = 1.30308/1.5012 = 0.8685$$

$$\omega = 0.7543$$

$$\tau = \frac{\omega \tilde{D}^I t}{a^2} = \frac{17543 \times 1.887}{25} t$$

$$= 0.056934\ t$$

TABLE 30

EXPERIMENTAL RESULTS OF TEST NUMBER 3.2-1

$\bar{\lambda}$ = 2.4206 ξ = 0.5464 τ = 0.056934 t
β = 0.000 a = 5.0 mm

Region	τ = 0.03416 t = :48 hours		τ = 0.22014 t = 3:52 hrs.		τ = 0.5447 t = 9:34 hrs.		τ = 1.0087 t = 17:43 hrs.		τ = 1.5239 t = 26:46 hrs.		τ = 0.01708 t = 00:18 hrs.	
	x_1	$X(x_1,\tau)$	x_1	$X(x_1,\tau)$	x_1	$X(x_1,\tau)$	x_1	$X(x_1,\tau)$	x_1	$X(x_1,\tau)$	x_1	$X(x_1,\tau)$
	+0.0585	0.082	+0.208	0.2787	+0.3474	0.4556	+0.4814	0.522	+0.4294	0.7487		
	+0.0360	0.1325	+0.1226	0.3269	+0.1575	0.5869	+0.3405	0.6503	+0.0000	0.9689		
2	-0.131	0.154	-0.0292	0.4161	+0.0000	0.6773	+0.000	0.8238	-0.5186	1.1306		
	-0.321	0.217	-0.1241	0.4389	-0.2221	0.7331	-0.4187	0.9529	-0.8982	1.2471	-0.8500	0.1245
	-0.511	0.231	-0.4089	0.5342	-0.6017	0.8166	-0.7984	1.0376				
	-0.891	0.2376	-0.8834	0.5353	-0.854	0.8679	-0.9882	1.0630				
	+0.000	0.106	+0.1006	0.2608	+0.2553	0.5224	+0.2847	0.8048	+0.7593	0.9225		
	-0.190	0.166	+0.0057	0.3170	+0.000	0.6382	+0.000	0.9074	+0.3796	1.0816		
3	-0.379	0.190	-0.1841	0.4180	-0.0949	0.7331	-0.4745	1.0364	+0.000	1.1834		
	-0.759	0.213	-0.3739	0.4738	-0.4746	0.8394	-0.8542	1.0750	-0.3796	1.2395		
			-0.9434	0.5353	-0.8542	0.8610			-0.7593	1.2433	-0.8500	0.1245
	-0.005	0.099	+0.1951	0.1955	+0.3326	0.4745	+0.522	0.6701	+0.7594	0.8124		
4	-0.384	0.203	+0.1640	0.2175	-0.1420	0.7316	+0.000	0.9233	+0.3796	1.0152		
	-0.764	0.203	+0.1325	0.2433	-0.4305	0.8007	-0.4271	1.0440	+0.000	1.1568	0.8500	0.1253
			-0.0573	0.3770	-0.8102	0.8208	-0.8067	1.0657	-0.3796	1.3060		
			-0.2471	0.4282			-0.9966	1.0611	-0.9491	1.3026		
			-0.7217	0.4628								
	+0.000	0.101	+0.1602	0.1955	+0.1363	0.4905	+0.3254	0.596	+0.2699	0.8804		
	-0.097	0.135	+0.0653	0.2847	+0.000	0.5774	+0.2304	0.6845	+0.000	1.0626	0.8500	0.1253
5	-0.476	0.1825	-0.0296	0.3383	-0.2433	0.6625	+0.000	0.8459	-0.4894	1.2180		
			-0.1245	0.3724								
	-0.856	0.203	-0.5042	0.4142	-0.623	0.7426	-0.2441	0.9279	-0.8269	1.2817		
			-0.8838	0.4656	-1.000	0.7927	-0.6238	0.9932				
	+0.000	0.066	+0.1006	0.2699	+0.2263	0.4210	+0.3918	0.5152	+0.3796	0.7483		
6	-0.095	0.133	+0.000	0.3690	+0.000	0.5604	+0.0000	0.7771	+0.000	1.0258		
	-0.190	0.158	-0.1898	0.4036	-0.2847	0.6970	-0.4746	0.9472	-0.3796	1.1420	0.8500	0.1238
	-0.380	0.193	-0.5695	0.4677	-0.4745	0.7445	-0.8542	1.0331	-0.9491	1.3838		
	-0.759	0.228	-0.980	0.5108	-0.8542	0.845						
	+0.000	0.0854	+0.1644	0.2441	+0.2388	0.5159	+0.4456	0.5152	+0.4320	0.7414		
7	-0.1313	0.146	+0.0695	0.3330	+0.000	0.6400	+0.3405	0.6446	+0.000	1.0490		
	-0.321	0.205	-0.0254	0.3857	-0.2221	0.7711	+0.1507	0.7972	-0.3272	1.1628	0.8500	0.1238
							+0.0000	0.8948				
	-0.511	0.231	-0.2153	0.4616	-0.6017	0.8450	-0.4187	1.0288	-0.8967	1.3838		
			-0.4051	0.4700								
	-0.891	0.227	-0.7847	0.5167			-0.7984	1.0698				
			-0.9746	0.5106								

TABLE 31

EXPERIMENTAL RESULTS OF TEST NUMBER 3.2-2

$\bar{\lambda}$ = 2.4206 ξ = 0.5464 τ = 0.05684 t
β = 0.0 a = 5.0 mm

Region	τ = 0.00854 t = 00:09 hours		τ = 0.01518 t = 00:16 hrs.		τ = 0.0664 t = 1:07 hrs.		τ = 0.22774 t = 4:00 hrs.		τ = 0.5181 t = 9:06 hrs.		τ = 1.3531 t = 23:46 hrs.	
	x_1	$X(x_1,\tau)$	x_1	$X(x_1,\tau)$	x_1	$X(x_1,\tau)$	x_1	$X(x_1,\tau)$	x_1	$X(x_1,\tau)$	x_1	$X(x_1,\tau)$
1	0.8500	0.0757	0.850	0.115	+0.0855	0.0555	+0.2431	0.1672	+0.408	0.2646	+0.6152	0.4320
					+0.0189	0.0921	+0.1110	0.2487	+0.2750	0.3924	+0.5772	0.7861
					-0.0736	0.1384	-0.0185	0.3255	+0.218	0.4856	+0.4062	0.7921
					-0.1661	0.1883	-0.0742	0.3852	+0.1243	0.561	+0.2162	1.0040
					-0.3511	0.2028	-0.2590	0.4430	+0.0277	0.5997	-0.1638	1.1850
					-0.5360	0.1986	-0.4439	0.4582	-0.1625	0.6950	-0.5438	1.276
					-0.906	0.2323	-0.8139	0.5118	-0.3525	0.7575	-0.9238	1.373
									-0.7328	0.8130		
									-0.9230	0.8210		
6	0.850	0.0633	0.850	0.120	+0.0699	0.0773	+0.1802	0.2019	+0.2852	0.3753	+0.4066	0.6750
					-0.0225	0.1443	+0.0877	0.2935	+0.1901	0.4494	+0.3116	0.7297
					-0.1150	0.1757	-0.0973	0.3833	+0.000	0.5228	-0.0684	0.9042
					-0.3000	0.1946	-0.2822	0.4263	-0.1901	0.6004	-0.4484	1.0005
					-0.6699	0.2116	-0.6522	0.478	-0.5704	0.6829	-0.8284	1.1620
7	0.850	0.0633	0.850	0.120	+0.0163	0.1095	+0.1849	0.2734	+0.2787	0.4844	+0.6263	0.7253
					-0.0765	0.1702	+0.0925	0.3510	+0.0886	0.5962	+0.5579	0.8195
					-0.1687	0.1986	+0.0000	0.3875	-0.1015	0.6740	-0.1550	0.9822
					-0.5386	0.2086	-0.1850	0.4369	-0.2916	0.7019	-0.3496	1.099
					-0.9086	0.2064	-0.5549	0.4612	-0.6719	0.7331	-0.4150	1.1305
							-0.9248	0.4844			-0.7950	1.1621
											-0.9850	1.1445
8	0.850	0.0757	0.850	0.115	+0.0672	0.0684	+0.1698	0.2704	+0.3517	0.3787	+0.6247	0.7681
					-0.0251	0.1925	+0.0773	0.3418	+0.2567	0.4643	+0.4347	0.9023
					-0.1176	0.1775	-0.0156	0.3917	+0.0665	0.5974	+0.2447	1.020
					-0.3026	0.2171	-0.2001	0.4498	-0.1236	0.6845	-0.0547	1.0921
					-0.6725	0.2382	-0.3851	0.4920	-0.5040	0.7932	-0.3177	1.2850
							-0.7550	0.5225	-0.884	0.8156	-0.6977	1.3830
											-0.9315	1.3820

TEST NUMBER 3.2-3

Temperature: 55±0.25°C

Solution in the cell: Pure water

Solution on the boundary: Phenol with 6.80 Wt% H_2O

Shape of the boundary: 10 mm x 10 mm square

C_∞ = 54.70 moles/liter of H_2O

C_s^{II} = 47.53 moles/liter of H_2O

C_s^{I} = 23.03 moles/liter of H_2O

C_B =

$\bar{\lambda}$ = 2.274

μ = 0.3752

$\tilde{D}^I$ = 1.887 mm^2/Hr

$\tilde{D}^{II}$ = 4.698 mm^2/Hr

ω = 0.7543

$(\tilde{D}^I/\tilde{D}^{II})^{\frac{1}{2}}$ = 0.63376

CALCULATE ξ

$$\chi_1^{-1}(\xi) = \bar{\lambda} + \mu\, \chi_2^{-1}\, (\xi \sqrt{D_1/D_2})$$

where

$$\chi_1(x) = x\, e^{x^2} \operatorname{erf} x$$

$$\chi_2(x) = x\, e^{x^2} \operatorname{erfc} x$$

Solving the above equation by trial and error, one gets

$$\underline{\xi = 0.4395}$$

TABLE 32

EXPERIMENTAL RESULTS OF TEST NUMBER 3.2-3

$\bar{\lambda} = 2.274$ $\sqrt{D^I/D^{II}} = 0.7273$ $\tau = 0.5684\ t$

$\beta = 0.3752$ $\xi = 0.4395$

Region	τ = .02847 t = :30 hrs.		τ = .05693 t = 1:00 hrs.		τ = .13569 t = 2:23 hrs.		τ = .29131 t = 5:07 hrs.		τ = .56365 t = 9:54 hrs.	
	x_1	$X(x_1,\tau)$	x_1	$X(x_1,\tau)$	x_1	$X(x_1,\tau)$	x_1	$X(x_1,\tau)$	x_1	$X(x_1,\tau)$
2	-0.7500	0.1579	-0.7500	0.2082	+0.0257 -0.0689 -0.2258 -0.4476 -0.8262	0.2254 0.2340 0.2685 0.3059 0.3563	+0.1813 +0.0767 -0.2513 -0.4411 -0.8208	0.1963 0.3018 0.4802 0.5573 0.5970	+0.1621 +0.1060 -0.0833 -0.2726 -0.4619 -0.8406	0.3287 0.4298 0.5615 0.6513 0.7319 0.7978
3	-0.7500	0.1579	-0.7500	0.2082	+0.0947 +0.0000 -0.1893 -0.3786 -0.7573	0.1742 0.2366 0.3404 0.3650 0.3612	+0.1898 +0.0000 -0.1896 -0.3796 -0.5695	0.4070 0.4833 0.5418 0.5865 0.5903 0.6020	+0.3112 +0.2166 +0.0273 -0.1621 -0.5407 -0.9194	0.3495 0.4631 0.6176 0.7179 0.7652 0.8016
4	-0.7500	0.1515	-0.7500	0.2427	+0.0810 +0.0129 -0.5808 -0.9595	0.1893 0.2416 0.3287 0.3408	+0.2020 +0.1120 -0.3625 -0.5524 -0.9320	0.2847 0.3462 0.3956 0.4677 0.5034	+0.2586 -0.1200 -0.3093 -0.4987 -0.6880	0.3820 0.5600 0.5952 0.6123 0.6634
5	-0.7500	0.1515	-0.7500	0.2427	+0.0326 -0.0882 -0.2775 -0.6562 -0.9600	0.1927 0.2380 0.2790 0.3461 0.3404	+0.1898 +0.0949 -0.0949 -0.2847 -0.6644	0.2619 0.3413 0.4168 0.4533 0.4935	+0.3116 +0.2170 +0.0276 -0.3510 -0.7296	0.3923 0.4343 0.5907 0.5956 0.6528

TEST NUMBER 3.2-4

Solution in the cell: Pure water

Solution on the boundary: Phenol with 8.222 Wt% H_2O

Temperature: 55±0.25°C

Shape of the boundary: 10 mm x 10 mm square

C_B = 4.7369 moles/liter of H_2O

C_s^I = 23.03 moles/liter of H_2O

C_s^{II} = 47.53 moles/liter of H_2O

C_∞ = 54.70 moles/liter of H_2O

$\bar{\lambda}$ = 2.3638

μ = 0.39186

ω = 0.7543

D^I = 1.887 mm^2/Hr

D^{II} = 4.698 mm^2/Hr

$(\tilde{D}^I/\tilde{D}^{II})^{\frac{1}{2}}$ = 0.63376

$z = \xi\sqrt{\tilde{D}^I/\tilde{D}^{II}} = 0.63376\ \xi$

CALCULATION OF ξ

Let $\chi_1(\xi) = \xi\ e^{\xi^2}\text{erf}\ \xi$

$\chi_2(z) = z\ e^{z^2}\text{erfc}\ z$

Then one can write

$$\chi_1^{-1}(\xi) = \bar{\lambda} + \mu\ \chi_2^{-1}(z)$$

For μ = 0.39186, $\bar{\lambda}$ = 2.3638 and $\sqrt{\tilde{D}^I/\tilde{D}^{II}}$ = 0.63376 one can solve the above equation graphically to get,

$$\underline{\xi = 0.4280}$$

TABLE 33

EXPERIMENTAL RESULTS OF TEST NUMBER 3.2-4

$\bar{\lambda} = 2.3638$ $\sqrt{D^I/D^{II}} = 0.7273$ $\tau = 0.056934\ t$

$\beta = 0.39186$ $\xi = 0.4280$ $a = 5.0$ mm

Region	$\tau = 0.02847$ t = 00:30 hrs.		$\tau = 0.06452$ t = 1:08 hrs.		$\tau = 0.31219$ t = 5:29 hrs.		$\tau = 0.53707$ t = 9:26 hrs.		$\tau = 1.08459$ t = 19:03 hrs.		$\tau = 1.69189$ t = 29:43 hrs.	
	x_1	$X(x_1,\tau)$	x_1	$X(x_1,\tau)$	x_1	$X(x_1,\tau)$	x_1	$X(x_1,\tau)$	x_1	$X(x_1,\tau)$	x_1	$X(x_1,\tau)$
5	-0.0361	0.0592	+0.000	0.0661	+0.1522	0.2710	+0.2596	0.2911	+0.3925	0.4169	+0.3516	0.7710
	-0.1323	0.0723	-0.1073	0.1472	+0.000	0.3765	+0.3408	0.1941	+0.2956	0.5269	+0.1746	0.8828
	-0.2284	0.1257	-0.2034	0.1726	-0.4301	0.4616	+0.0970	0.04351	+0.1600	0.5830	+0.0000	0.9637
	-0.5168	0.1511	-0.2995	0.2349	-1.0124	0.4616	+0.000	0.4898	+0.1019	0.6493	-0.4036	1.0430
	-0.9013	0.1538	-0.4917	0.2407			-0.1491	0.5748	-0.0918	0.7175	-0.9819	1.054
			-0.8762	0.2364			-0.3881	0.6059	-0.2855	0.7435		
							-0.7762	0.6031	-0.6730	0.8016		
							-1.000	0.6889				
6	-0.000	0.0346	+0.000	0.0707	+0.1941	0.2515	+0.1941	0.3648	+0.2906	0.5068	+0.5782	0.5902
	-0.0961	0.07805	-0.0961	0.1434	+0.000	0.4014	+0.0970	0.4564	+0.1937	0.5854	+0.1927	0.9121
	-0.1922	0.1188	-0.1922	0.2003	-0.3882	0.5031	+0.0000	0.5137	+0.0969	0.6656	+0.0000	0.9545
	-0.3845	0.1788	-0.3844	0.2899	-0.9705	0.5598	-0.1941	0.5783	+0.0000	0.7407	-0.3885	1.0771
	-0.7690	0.1884	-0.5767	0.2929			-0.3881	0.6326	-0.0969	0.7791	-0.7710	1.1150
	-0.9612	0.1753	-0.9611	0.2749			-0.7762	0.6710	-0.2906	0.8361	-0.9637	1.1150
									-0.6784	0.8756		
7	-0.0773	0.1023	+0.0738	0.0850	+0.1351	0.2803	+0.2317	0.3066	+0.2820	0.4490	+0.5428	0.5601
	-0.2695	0.1365	+0.0184	0.1342	+0.000	0.382	+0.1348	0.3840	+0.2278	0.5153	+0.313	0.7594
	-0.4618	0.1696	-0.0777	0.2053	-0.2531	0.4969	+0.0376	0.4488	+0.0340	0.6381	+0.000	0.9098
	-0.8463	0.1796	-0.2700	0.2537	-0.8354	0.5567	-0.0594	0.5111	-0.1596	0.7594	-0.4580	1.0636
			-0.6544	0.2780			-0.2534	0.5919	-0.5470	0.8706	-0.8435	1.0998
							-0.4475	0.6579	-0.9345	0.8706	-0.9599	1.1114
							-0.8356	0.6710				
8	-0.0134	0.0208	-0.0111	0.1276	+0.1522	0.2562	+0.1925	0.3287	+0.3584	0.4215	+0.1746	0.8438
	-0.0361	0.0519	-0.1072	0.2088	+0.000	0.3590	+0.0970	0.4110	+0.2956	0.5029	+0.0000	0.9348
	-0.1323	0.1207	-0.2034	0.2584	-0.4301	0.5330	+0.000	0.4941	+0.1987	0.5494	-0.2108	1.0327
	-0.5168	0.1619	-0.2995	0.2853	-1.000	0.6172	-0.1940	0.6123	+0.1019	0.6264	-0.5964	1.1773
	-0.9013	0.1353	-0.6839	0.2899			-0.3881	0.6846	-0.0918	0.7656	-0.9819	1.1758
							-0.7762	0.7006	-0.2855	0.8345		
									-0.4793	0.8725		
									-0.8667	0.8954		

TABLE 34

THE EXPERIMENTAL VALUES OF $\bar{X}(x_1,\tau)$ FOR $x_1 = -0.0, -0.2, 0.0, +0.2$ AND $x_1 = X(x_1,\tau)$ FOR ALL THE TESTS WITH A UNIT SQUARE BOUNDARY

Test No.	ξ	τ	$x_1 = -1.0$		$x_1 = -0.2$		$x_1 = 0.0$		$x_1 = +0.20$		$x_1 = \bar{X}(x_1,\tau)$		$\sqrt{\tau}$
			$\bar{X}(x_1,\tau)$	$\frac{\bar{X}(x_1,\tau)}{2\xi}$	$\bar{X}(x_1,\tau)$	$\frac{\bar{X}(x_1,\tau)}{2\xi}$	$\bar{X}(x_1,\tau)$	$\frac{\bar{X}(x_1,\tau)}{2\xi}$	$\bar{X}(x_1,\tau)$	$\frac{\bar{X}(x_1,\tau)}{2\xi}$	$\bar{X}(x_1,\tau)$	$\frac{\bar{X}(x_1,\tau)}{2\xi}$	
3.2-1	0.5464	0.0171	0.1245	0.1139									0.1308
		0.0342	0.2186	0.2000	0.173	0.1583	0.085	0.0778			0.050	0.0457	0.1849
		0.2201	0.5034	0.4606	0.455	0.4164	0.375	0.3431	0.200	0.1830	0.200	0.1830	0.4691
		0.5447	0.8387	0.7675	0.730	0.6680	0.645	0.5900	0.530	0.4850	0.380	0.3477	0.7380
		1.0087	1.0558	0.9661	0.957	0.8757	0.870	0.7961	0.735	0.6726	0.485	0.4438	1.0043
		1.5239	1.3070	1.1961	1.205	1.1027	1.130	1.0340	1.020	0.9334	0.655	0.5994	1.2345
3.2-2	0.5464	0.0085	0.0716	0.0655									0.0922
		0.0152	0.1175	0.1075									0.1229
		0.0664	0.2220	0.2031	0.195	0.1784	0.125	0.1144			0.075	0.0686	0.2577
		0.2277	0.4990	0.4566	0.435	0.3980	0.373	0.3413	0.200	0.1830	0.200	0.1830	0.4772
		0.5181	0.7682	0.7030	0.690	0.6314	0.622	0.5690	0.510	0.4667	0.350	0.3203	0.7198
		1.3531	1.2656	1.1581	1.160	1.0615	1.090	0.9974	1.000	0.9151	0.655	0.5994	1.1632
3.2-3	0.4395	0.0285	0.1547	0.176									0.1688
		0.0569	0.2254	0.2564									0.2385
		0.1357	0.3497	0.3978	0.300	0.3413	0.225	0.2560			0.130	0.1479	0.3684
		0.2913	0.5490	0.6246	0.496	0.5643	0.414	0.4710	0.260	0.2958	0.230	0.2617	0.5397
		0.5636	0.7289	0.8292	0.630	0.7167	0.556	0.6325	0.440	0.5006	0.330	0.3753	0.7508
3.2-4	0.428	0.0285	0.161	0.1881	0.140	0.1635	0.025	0.0292			0.0125	0.0146	0.1688
		0.0645	0.2698	0.3152	0.213	0.2488	0.100	0.1168			0.048	0.0561	0.2540
		0.3122	0.5488	0.6411	0.476	0.5561	0.380	0.4439	0.213	0.2488	0.205	0.2395	0.5585
		0.5371	0.6820	0.7078	0.585	0.6834	0.485	0.5666	0.335	0.3913	0.265	0.3096	0.7329
		1.0846	0.8610	1.0058	0.785	0.9170	0.700	0.8177	0.580	0.6776	0.395	0.4614	1.0414
		1.6919	1.1140	1.3014	1.026	1.1986	0.950	1.1098	0.835	0.9755	0.5550	0.6425	1.3007

TEST NUMBER 3.2-5

Shape of the Region (Fig. 74): 25° semi-infinite wedge

Shape of the exposed boundary: 1.09 cm diameter circle with its center 5.08 cm away from the apex

C_B = 4.7369 moles/liter of H_2O

C_s^I = 23.03 moles/liter of H_2O

C_s^{II} = 47.53 moles/liter of H_2O

C_∞ = 54.70 moles/liter of H_2O

$\bar{\lambda}$ = 2.3638

μ = 0.39186

ω = 0.7543

$\tilde{D}^I$ = 1.887 mm^2/Hr

$\tilde{D}^{II}$ = 4.698 mm^2/Hr

ξ = 0.428

$$\tau = \frac{\omega \tilde{D}^I t}{a^2} = \frac{.7543 \times 1.887\, t}{(5.45)^2} = 0.04792\, t$$

a = radius of the circle

$R(\frac{x_2}{x_1}, \tau)$ = dimensionless radial position of the interface

TABLE 35

POSITION OF THE INTERFACE IN THE WEDGE REGION EXTERNAL TO A UNIT CIRCLE
TEST NUMBER 3.2-5, $\xi = 0.425$, $\mu = 0.39186$

τ = .02476, t = 00:31 hrs.			τ = .154143, t = 3:13 hrs.			τ = .415307, t = 8:40 hrs.			τ = .99274, t = 20:43 hrs.		
x_1	x_2	$R(\frac{x_1}{x_2},\tau)$	x_1	x_2	$R(\frac{x_1}{x_2},\tau)$	x_1	x_2	$R(\frac{x_1}{x_2},\tau)$	x_1	x_2	$R(\frac{x_1}{x_2},\tau)$
-1.099	0.00	1.099	-1.201	0.00	0.191	-1.272	0.00	1.272	-1.656	0.00	1.656
-1.062	0.432	1.146	-1.068	0.432	0.145	-1.198	0.430	1.273	-1.658	0.429	1.713
-0.713	0.863	1.120	-0.887	0.864	0.184	-0.961	0.860	1.290	-1.387	1.021	1.722
0.00	1.123	1.123	0.00	1.206	0.199	0.00	1.256	1.256	0.00	1.583	1.583
0.00	2.266	2.266*	0.00	2.230	1.230*	0.00	2.279	2.279*	0.00	2.278	2.278*
0.649	0.863	1.080	0.761	0.864	0.145	0.799	0.860	1.174	1.071	1.021	1.480
1.008	0.432	1.097	1.048	0.432	0.128	1.111	0.430	1.191	1.432	0.429	1.495
1.076	0.00	1.076	1.154	0.00	0.147	1.196	0.00	1.196	1.496	0.00	1.496
1.038	-0.432	1.124	1.031	-0.432	0.112	1.060	-0.430	1.144	1.483	-0.429	1.544
0.647	-0.863	1.079	0.702	-0.864	0.199	0.824	-1.860	1.191	1.187	-1.009	1.558
0.00	-1.092	1.092	0.00	-1.197	0.189	0.00	-1.239	1.230	0.00	-1.579	1.579
-0.722	-0.863	1.125	-0.843	-0.864	0.201	-0.910	-0.860	1.252	-1.402	-1.009	1.727
-1.051	-0.432	1.137	-1.142	-0.432	0.213	-1.230	-0.430	1.303	-1.506	-0.429	1.566

τ = 1.90242, t = 39:42 hrs.			τ = 2.2898, t = 47:47 hrs.			τ = 3.5309, t = 73:41 hrs.			τ = 4.16425, t = 86:54 hrs.		
x_1	x_2	$R(\frac{x_1}{x_2},\tau)$	x_1	x_2	$R(\frac{x_1}{x_2},\tau)$	x_1	x_2	$R(\frac{x_1}{x_2},\tau)$	x_1	x_2	$R(\frac{x_1}{x_2},\tau)$
-2.069	0.00	2.069	-2.173	0.00	2.173	-2.397	0.00	2.397	-2.453	0.00	2.453
-2.067	0.428	2.096	-2.163	0.427	2.205	-2.365	0.429	2.404	-2.417	0.430	2.435
-1.853	1.016	2.113	-1.972	1.001	2.212	-2.189	1.003	2.407	-2.269	1.020	2.488
0.00	1.835	1.835	-1.576	1.496	2.173	-1.831	1.502	2.368	-2.030	1.505	2.527
0.00	2.252	2.252*	0.00	2.039	2.039	-1.096	2.225	2.480	-1.387	2.850	3.170*
1.546	1.016	1.850	0.152	2.162	2.167*	1.496	1.502	2.106*	2.477	1.020	2.679
1.811	0.428	1.861	0.00	2.249	2.249*	2.311	0.429	2.351	2.565	0.430	2.601*
1.856	0.00	1.856	1.752	1.276	2.167*	2.261	0.00	2.261	2.834	0.860	2.962
1.807	-0.428	1.857	1.763	1.001	2.027	2.170	-0.429	2.212	2.428	0.00	2.428
1.602	-1.013	1.895	1.973	0.427	2.019	1.912	-1.024	2.170	2.298	-0.430	2.338
0.00	-1.831	1.831	2.027	0.00	2.027	1.640	-1.502	2.224	2.007	-1.014	2.249
-1.782	-1.013	1.050	1.955	-0.427	2.001	1.272	-2.157	2.504*	1.749	-1.505	2.307
-2.021	-0.428	1.066	1.722	-1.022	2.002	1.474	-2.175	2.628*	1.499	-2.153	2.623*
			1.386	-1.496	2.039	-1.885	-1.502	2.410	-1.725	-2.167	2.770*
			0.577	-2.210	2.284*	-2.199	-1.024	2.426	-1.964	-1.505	2.474
			-0.687	-2.149	2.256*	-2.358	-0.429	2.397	-2.310	-0.860	2.46?
			-1.601	-1.496	2.191				-2.409	-0.430	2.447
			-1.925	-1.022	2.143						
			-2.126	-0.427	2.168						

* Position of the sides of the wedge.

TEST NUMBER 3.2-6

Shape of the region: 25° semi-infinite wedge

Shape of the boundary: 1.09 cm diameter circle with its center 5.08 cm away from the apex

C_B = 4.7369 moles/ liter of H_2O

C_s^I = 23.03 moles/ liter of H_2O

C_s^{II} = 47.53 moles/liter of H_2O

C_∞ = 47.53 moles/liter of H_2O

μ = 0.000

$\bar{\lambda}$ = 0.420517

ξ = 0.5506

a = 0.535 cm

$\tau = \frac{\omega \tilde{\Pi}^I}{a^2} t = 0.049726\ t$

TABLE 36

EXPERIMENTAL RESULTS OF TEST NUMBER 3.2-6

t hours	τ	$\sqrt{\tau}$	R_1^* mm	$\bar{R} = \bar{R}_1/a^*$
0.25	.01243	.11149	5.39	1.0729
0.50	.02486	.15767	6.04	1.1290
1.02	.05072	.22521	6.47	1.2093
3.07	.15266	.39071	7.21	1.3477
4.22	.20984	.4581	7.58	1.4168

* $\bar{R}_1$ = average radial position of the interface.

APPENDIX F

PHYSICAL PROPERTIES OF PHENOL-WATER SYSTEM

TABLE 37

SOLUBILITY TEMPERATURE (TIMMERMANS (72))

	Phenol Concentration					
	Water-Rich Phase			Phenol-Rich Phase		
Temp. °C	Wt.%	Mole %	Mole/ Lit.	Wt.%	Mole %	Mole/ Lit.
15	7.95	1.626		73.00	34.111	
20	8.20	1.681	0.8772	72.10	33.103	8.065
25	8.45	1.736		71.05	31.970	
30	8.75	1.803	0.9334	69.90	30.78	7.751
35	9.10	1.881		68.50	29.399	
40	9.60	1.917	1.0205	66.80	27.812	7.339
45	10.45	2.185		65.00	26.232	
50	11.80	2.497	1.2496	62.60	24.271	6.810
55	13.80	2.974		59.20	21.743	
60	16.80	3.722	1.7725	55.10	19.027	5.928
65	23.90	5.672	2.522	45.80	13.987	4.880
66	34.00	8.979	3.6043	34.00	8.979	3.6043

TABLE 38

DENSITY OF WATER-PHENOL SYSTEM
AT SATURATION POINT
(TIMMERMANS (72))

Temperature, °C	Grams per c.c.	
	Phenol Layer	Water Layer
20	1.0515	1.0056
30	1.0423	1.0028
40	1.0328	0.9993
50	1.0226	0.0055
60	1.0114	0.9918
62	1.0087	0.9914
64	1.0056	0.9912
66	1.0015	0.9920

TABLE 39

DENSITY OF WATER-PHENOL SYSTEM (TIMMERMANS (72))

Concentration of Phenol Wt. %	20°C	30°C	40°C	50°C	60°C	70°
0	1.9982	0.9957	0.9922	0.9881	0.9832	0.9778
2	1.0001	0.9974	0.9938	0.9894	0.9845	0.9788
4	1.0020	0.9990	0.9953	0.9908	0.9857	0.9799
6	1.0038	1.0006	0.9967	0.9921	0.9868	0.9808
8	1.0055	1.0022	0.9981	0.9934	0.9879	0.9819
10				0.9944	0.9989	0.9829
15					0.9913	
20						0.9872
30						0.9917
40						0.9962
50						1.0009
60					1.0138	1.0054
70	(1.0502)	1.0428	1.0352	1.0273	1.0191	1.0105
75	1.0539	1.0462	1.0382	1.0301	1.0218	1.0132
80	1.0576	1.0496	1.0413	1.0331	1.0248	1.0161
85	1.0615	1.0533	1.0450	1.0367	1.0280	1.0193
90	1.0655	1.0572	1.0488	1.0405	1.0319	1.0232
95	(1.0701)	1.0617	1.0532	1.0448	1.0362	1.0276
100				1.0498	1.0413	1.0325

TABLE 40

VISCOSITY OF PHENOL-WATER SOLUTION RELATIVE TO WATER (TIMMERMANS (72))

Wt. % Phenol	Temperature, °C	Viscosity
0.8	19.2	1.01
3.9	19.2	1.04
7.3	19.2	1.14
9.2	52.0	1.13
16.0	70.0	1.16
25.0	70.0	1.12
33.0	70.0	1.25
33.5	70.0	1.38
46.0	70.0	1.45
53.0	70.0	1.51
58.0	70.0	1.57
64.4	70.0	1.71
69.5	51.0	1.72
72.8	51.0	2.97
82.7	20.0	4.51
89.6	20.0	6.05
100.0	51.0	11.90

TABLE 41

DATA OF CAMPBELL, A. N., AND CAMPBELL, A. J.*
REFRACTORY INDICES OF AQUEOUS SOLUTION OF PHENOL

Concentration of Phenol Wt. %	7°C	22.5°C	25.0°C	30°C	35°C	45°C	55°C	60°C	65°C	70°C
0.905	1.3336	1.3328	1.3326	1.3321	1.3321	1.3311	1.3288	1.3288	1.3274	1.3262
3.85	1.3396	1.3389	1.3387	1.3387	1.3376	1.3376	1.3350	1.3339	1.3328	1.3321
6.95		1.3466	1.3461	1.3456	1.3456	1.3447	1.3417	1.3405	1.3402	1.3389
9.65						1.3510	1.3465	1.3465	1.3464	1.3402
14.68								1.3580	1.3570	1.3570
24.10									1.3725	1.3646
32.50										1.3890
42.30										1.4114
49.65										1.4225
51.50									1.4265	1.265
56.00							1.4370	1.4365	1.4355	1.4345
63.50						1.4545	1.4540	1.4506	1.4493	1.4486
68.50					1.4713	1.4679	1.4648	1.4616	1.4612	1.4601
75.20	1.4895	1.4843	1.4829	1.4814	1.4814	1.4815	1.4774	1.4708	1.4695	1.4689
82.00	1.5090	1.5051	1.5038	1.5024	1.5014	1.4977	1.4955	1.4921	1.4910	1.4895
90.00		1.5235	1.5225	1.5212	1.5197	1.5149	1.5149	1.5091	1.5084	1.5062
97.50						1.5323	1.5313	1.5277	1.5245	1.5223

* See Timmermans (72)

TABLE 42

DIFFUSION OF PHENOL INTO WATER
(THOVERT (71))

Temperature, °C	D x 10^5 cm^2/sec.
10.2	0.74
11.0	0.67
12.0	0.64
13.8	0.84
14.0	0.84
15.0	0.75
16.2	0.73
16.6	0.75
18.6	0.95
21.6	0.84
15.6	0.73

TABLE 43

FREEZING POINTS OF PHENOL-WATER SOLUTIONS

Paterno*		Rhodes and Marlsley*	
Wt. % Phenol	Freezing Temperature	Wt. % Phenol	Freezing Temperature
		I	
100	40.18	100	40.8
99.273	37.50	98	33.0
97.649	31.80	97	29.3
96.780	29.24	95	23.1
95.891	27.14	92	16.2
94.759	23.51	90	15.75
93.711	21.16	88	15.10
92.674	19.01	84	14.00
90.598	15.08	80	13.00
88.764	12.28	76	12.40
87.654	10.89	II	
86.115	9.23	91	14.1
84.043	7.41	88	9.3
81.293	5.51	85	6.2
77.315	3.72	80	3.1
72.272	2.26	77	2.0
		75	1.7

* See Timmermans (72) for references and the experimental results of other investigators.